

THE UNIVERSITY OF HULL

**CONFIGURATIONALLY RESTRICTED  
BIS-TETRAAZAMACROCYCLIC COMPLEXES:  
CHEMOKINE RECEPTOR ANTAGONISTS**

Being a thesis submitted for the Degree of Doctor of Philosophy in the  
University of Hull

by

Graeme Walter John McRobbie MChem (Hons)

March 2009

## **ACKNOWLEDGEMENTS**

I would like to thank my supervisor Dr Steve Archibald for his support, guidance and many scientific discussions throughout my research. The EXAFS experiments and analysis would not have been possible without the help of my second supervisor, Dr Nigel Young and station scientists Dr Bob Bilsborrow and Dr Steven Fiddy at Daresbury. Many thanks also to our collaborators Profs Peter Sadler, Erik De Clercq and Dr Tim Hubin.

I would also like to thank the friends I have made and everyone who has helped me along the way, in no particular order; Jon, Gary, Abid, Chris, Lizzie, Cheryll, Eleanor, Chris, Sushil, Aaron, Mike, Mark, Dave, Becky, Grazia, Andy, Joe, Amy, Amanda, Ruth, Tom, Antony, Carol, Bob, Cristina and my sister, Sarah. A special mention to Ryan who has helped enormously over the years.

Finally I would like to thank my parents, Ian and Elizabeth, for everything they have done for me throughout my life and without whom none of this would have been achieved.

Cheers!

## ABSTRACT

The chemokine receptor CXCR4 is a trans-membrane protein which has been implicated in many physiological and pathological processes including cancer, rheumatoid arthritis and most significantly HIV replication. CXCR4 plays a vital role in embryonic development but is not essential at the post-development stage; therefore, it has been identified as a potential therapeutic target.

Bis-macrocyclic drugs (e.g. AMD3100) bind to aspartate residues on the CXCR4 surface and inhibit HIV replication by blocking the interaction of gp120/gp41 with the protein. The incorporation of transition metals (e.g. zinc(II) and copper(II)) into the macrocyclic cavity increases anti-viral potency. The addition of a bridging ethylene unit to the macrocyclic framework locks the complex into a single configuration, potentially optimising the interaction with the receptor.

A series of configurationally restricted macrocyclic compounds have been prepared utilising bis-aminal chemistry. Characterisation by X-ray crystallography and X-ray absorption spectroscopy has confirmed that the complexes possessing an ethylene bridge between adjacent nitrogen atoms are fixed in the trans-II configuration and that complexes containing an ethylene bridge between non-adjacent nitrogen atoms adopt the cis-V configuration. In addition, solution EXAFS has been used as a model to probe the binding of the complexes to aspartate residues on the receptor surface.

The zinc(II) trans-II and copper(II) cis-V complexes reported here are more potent against HIV replication than AMD3100 ( $IC_{50}$  values against III<sub>B</sub>; 0.00208  $\mu$ M, 0.00491  $\mu$ M and 0.018  $\mu$ M respectively), confirming the importance of coordination interactions for potent binding to CXCR4 and also validating the strategy of configurationally fixing the macrocyclic unit for optimising receptor binding. It is believed that both thermodynamic and kinetic properties are important for effective binding to CXCR4.

## ABBREVIATIONS

[Ca <sup>2+</sup> ] <sub>i</sub>	Intracellular Calcium Concentration
2D HSQC	2 Dimensional Heteronuclear Single Quantum Coherence
Ala	Alanine
Asn	Asparagine
Asp	Aspartate
CCID <sub>50</sub>	Cell Culture Infectious Dose 50%
CCR5	CC Chemokine Receptor 5
CD4	Cluster of Differentiation Receptor 4
CSD	Crystal Structure Database
CXCL12 (and/or SDF-1)	CXC Chemokine Ligand 12 (Stromal Cell Derived Factor 1)
CXCR4	CXC Chemokine Receptor 4
Cyclam	1,4,8,11-tetraazacyclotetradecane
Cyclen	1,4,7,10-tetraazacyclodecane
DCM	Dichloromethane
DMF	Dimethylformamide
DMSO	Dimethylsulphoxide
DNA	Deoxyribonucleic Acid
EC <sub>50</sub>	Effective Concentration 50%
ESI	Electrospray Ionisation
EXAFS	Extended X-ray Absorption Fine Structure
FDA	Food and Drug Agency
FIV	Feline Immunodeficiency Virus
FT	Fourier Transform

gp120	Glycoprotein 120
gp41	Glycoprotein 41
GPCR	G-Protein Coupled Receptor
HAART	Highly Active Anti Retroviral Therapy
His	Histidine
HIV	Human Immunodeficiency Virus
IC <sub>50</sub>	Inhibitory Concentration 50%
mAb	Monoclonal Antibody
MJF	Multiple Juxtapositional Fixedness
MTT	3-(4,5-Dimethylthiazol-2-yl)-2,5-diphenyltetrazolium bromide
nBuLi	n-Butyl Lithium
NMR	Nuclear Magnetic Resonance Spectroscopy
NNRTI	Non-Nucleoside Reverse Transcriptase Inhibitor
NRTI	Nucleoside Reverse Transcriptase Inhibitor
NSI	Non-Syncytium Inducing
PBMCs	Peripheral Blood Mononuclear Cells
RNA	Ribonucleic Acid
SI	Syncytium Inducing
SIV	Simian Immunodeficiency Virus
SRS	Synchrotron Radiation Source
THF	Tetrahydrofuran
TLC	Thin Layer Chromatography
TM	Transmembrane
Trp	Tryptophan
UV-vis	Ultra Violet-visible Spectroscopy

XANES X-ray Absorption Near Edge Structure

XAS X-ray Absorption Spectroscopy

### Numbering of compounds

Compounds synthesised in this work are numbered from 1-26 whereas ligands from the chemical literature are numbered using the format L<sup>1</sup>-L<sup>49</sup>

A supplementary CD containing X-ray crystallographic data is included.

Some of the results presented in this thesis have been reported elsewhere in the literature:

*“Configurationaly restricted bis-macrocyclic CXCR4 receptor antagonists”*, G.C. Valks, G. McRobbie, E.A. Lewis, T.J. Hubin, T.M. Hunter, P.J. Sadler, C. Pannecouque, E. De Clercq and S.J. Archibald, *J. Med. Chem.*, 2006, **49**, 6162.

*“Probing key coordination interactions: configurationally restricted metal activated CXCR4 antagonists”*, G. McRobbie, G.C. Valks, C.J. Empson, A. Khan, J.D. Silversides, C. Pannecouque, E. De Clercq, S.G. Fiddy, A.J. Bridgeman, N.A. Young and S.J. Archibald, *Dalton Trans.*, 2007, 5008.

# CONTENTS

<b>Chapter 1. Introduction</b> .....	<b>1</b>
1.1 Chemokines & Chemokine Receptors.....	2
1.1.1 Chemokines .....	2
1.1.2 CXCL12.....	4
1.1.3 Chemokine Receptors .....	5
1.1.4 CXCR4.....	5
1.1.5 Role of Chemokines & Chemokine Receptors in Disease .....	6
1.2 Human Immunodeficiency Virus .....	9
1.2.1 HIV Cell Entry.....	11
1.3 CXCR4 Antagonists .....	13
1.3.1 Development of AMD3100 .....	13
1.3.2 Synthesis of AMD3100 .....	15
1.3.3 Binding of AMD3100 to CXCR4.....	17
1.3.4 Effect of Asp and His Mutations on CXCR4 Binding .....	18
1.3.5 Binding Model of AMD3100 .....	20
1.3.6 Binding Model of Metal Complexes of AMD3100.....	21
1.3.7 Lysozyme Adducts of AMD3100 Complexes.....	23
1.4 Therapeutic Potential of AMD3100 .....	25
1.4.1 HIV Studies.....	25

1.4.2	Clinical Studies .....	27
1.5	<sup>*</sup> Characteristics of Cyclam & Bicyclam Complexes .....	29
1.5.1	General Properties.....	29
1.5.2	Palladium(II) Complexes.....	31
1.5.3	Zinc(II) Complexes.....	33
1.6	Configurationaly Restricted Macrocycles .....	38
1.6.1	Molecular Organisation .....	38
1.6.2	The Chelate Effect .....	40
1.6.3	The Macrocyclic Effect .....	41
1.6.4	The Cryptate Effect.....	42
1.6.5	Ligand Rigidity .....	43
<b>Chapter 2.</b>	<b>Synthesis &amp; Charactersation of Piperazino Macrocyclic Complexes .....</b>	<b>45</b>
2.1	Side-bridged Tetraazamacrocycles.....	46
2.1.1	Synthetic Development of Side-bridged Cyclam .....	48
2.1.2	Metal Complexes of Side-bridged Cyclam.....	51
2.1.3	Synthetic Development of Side-bridged Cyclen .....	53
2.1.4	Metal Complexes of Side-bridged Cyclen.....	54
2.2	Synthetic Aims .....	56
2.3	Synthetic Discussion .....	58
2.3.1	Bis-aminal Precursors .....	58

2.3.2	Reductive Ring Cleavage.....	61
2.4	Configurationally Restricted Zinc(II) Complexes.....	63
2.4.1	X-ray Crystal Structure of $[\text{Zn}_2\mathbf{5}(\text{OAc}_2)]^{2+}$ .....	64
2.4.2	NMR Characterisation of $[\text{Zn}_2\mathbf{5}(\text{OAc}_2)]^{2+}$ .....	65
2.5	Configurationally Restricted Copper(II) Complexes .....	68
2.5.1	Characterisation of $[\text{Cu}_2\mathbf{5}](\text{ClO}_4)_4$ .....	68
2.5.2	Characterisation of $[\text{Cu}_2\mathbf{5}\text{Cl}_2]\text{Cl}_2$ .....	71
2.6	Side-bridged Tris-macrocycles.....	74
2.6.1	Synthesis of <b>6</b> .....	77
2.6.2	Transition Metal Complexes of <b>6</b> .....	78
2.7	Conclusions .....	80
<b>Chapter 3. Synthesis &amp; Characterisation of Cross-bridged Macrocyclic Complexes ..</b>		
	.....	<b>81</b>
3.1	Cross-bridged Tetraazamacrocycles.....	82
3.1.1	Synthetic Development of Cross-bridged Cyclam .....	83
3.1.2	Metal Complexes of Cross-bridged Cyclam.....	84
3.1.3	Synthetic Development of Cross-bridged Cyclen .....	89
3.1.4	Metal Complexes of Cross-bridged Cyclen.....	92
3.1.5	Kinetic Stability of Cross-bridged Macrocycles.....	96
3.2	Synthetic Aims .....	97

3.3	Synthetic Discussion .....	99
3.3.1	Bis-aminal Precursors .....	99
3.3.2	Reductive Ring Cleavage.....	99
3.4	Transition Metal Complexes .....	101
3.4.1	Copper(II) Complexation.....	101
3.4.2	EXAFS Analysis.....	103
3.5	Conclusions .....	104
<b>Chapter 4.</b>	<b>XAS Characterisation of Copper(II) Complexes of <b>5</b> and <b>9</b> .....</b>	<b>105</b>
4.1	Background .....	106
4.2	XAS Theory .....	109
4.2.1	X-ray Absorption .....	109
4.2.2	Data Collection .....	111
4.2.3	Data Reduction .....	112
4.2.4	Data Modelling.....	114
4.3	Aims of EXAFS Experiments .....	116
4.4	XAS Characterisation of Copper(II) Complexes of <b>5</b> .....	117
4.4.1	XAS Analysis of $[\text{Cu}_2\mathbf{5}](\text{ClO}_4)_4$ .....	117
4.4.2	XAS Analysis of $[\text{Cu}_2\mathbf{5}(\text{OAc})_2](\text{OAc})_2$ .....	123
4.4.3	XAS Analysis of $[\text{Cu}_2\mathbf{5}\text{Cl}_2](\text{PF}_6)_2$ .....	127
4.5	XAS Characterisation of Copper(II) Complexes of <b>9</b> .....	132

4.5.1	XAS Analysis of $[\text{Cu}_2\mathbf{9}(\text{OAc})_2]^{2+}$ .....	132
4.5.2	XAS Analysis of $[\text{Cu}_2\mathbf{9}\text{Cl}_2]^{2+}$ .....	134
4.5.3	Anion Displacement Experiments With $[\text{Cu}_2\mathbf{9}\text{Cl}_2]^{2+}$ .....	137
4.6	Conclusions .....	140
<b>Chapter 5. Biological Assays: Competition Binding, Anti-viral Activity and Calcium Signalling</b> .....		<b>142</b>
5.1	CXCR4 Antagonism.....	143
5.1.1	Displacement Assay.....	144
5.1.2	Competition Binding Assay.....	146
5.2	Anti-HIV Assays .....	148
5.2.1	Tetrazolium Based Colorimetric Assay.....	148
5.2.2	MTT Assay .....	149
5.2.3	Anti-viral Activity of Ligands .....	151
5.2.4	Anti-viral Activity of Copper(II) Complexes .....	152
5.2.5	Activity of $[\text{Cu}_2\mathbf{9}\text{Cl}_2](\text{PF}_6)_2$ Against AMD3100 Resistant Virus .....	153
5.2.6	Anti-viral Activity of Zinc(II) Complexes.....	155
5.2.7	Anti-viral Properties in PBMCs.....	156
5.3	CXCL12 Induced $\text{Ca}^{2+}$ Signalling.....	158
5.3.1	Measurement of Intracellular Calcium Concentration.....	158
5.3.2	Calculated $\text{IC}_{50}$ Values.....	159

5.3.3	Correlation between anti-HIV activity and Calcium Signalling.....	160
5.4	Structure Activity Relationships .....	161
5.4.1	Free Ligands .....	162
5.4.2	Copper(II) Complexes .....	164
5.4.3	Zinc(II) Complexes.....	167
5.5	Conclusions .....	170
<b>Chapter 6.</b>	<b>Towards the Synthesis of Asymmetrical Bis-macrocycles .....</b>	<b>171</b>
6.1	Background .....	172
6.1.1	Asymmetrical Bis-macrocycles .....	172
6.2	Synthetic Rationale.....	174
6.3	Synthetic Discussion .....	176
6.3.1	Attempted Preparation of <b>16</b> .....	176
6.3.2	Cross-bridged Cyclam .....	184
6.3.3	Nickel Template Reactions.....	185
6.3.4	Preparation of <b>26</b> .....	189
6.4	Conclusions .....	191
<b>Chapter 7.</b>	<b>Conclusions .....</b>	<b>192</b>
<b>Chapter 8.</b>	<b>Experimental .....</b>	<b>198</b>
8.1	General Methods .....	199
8.1.1	Solvents and Reagents .....	199

8.1.2	Analytical Techniques .....	199
8.2	Synthesis of Organic Compounds .....	202
8.2.1	Synthesis of 1,4,8,11-tetraazacyclotetradecane, cyclam, <b>1</b> .....	202
8.2.2	Synthesis of decahydro-3a,5a,8a,10a-tetraaza-pyrene, <b>3</b> .....	203
8.2.3	Synthesis of 3a-[methyl]-decahydro-3a,5a,8a,10a-tetraaza-pyrenium bromide, <b>20</b> .....	210
8.2.4	Crystal data and structural refinement for 3a-[methyl]-decahydro-3a,5a,8a,10a-tetraaza-pyrenium bromide, <b>20</b> .....	211
8.2.5	Synthesis of 3a-[phenylenemethylene benzoate]-decahydro-3a,5a,8a,10a-tetraaza-pyrenium bromide, <b>14</b> .....	214
8.2.6	Synthesis of 3a,3a'-[1,4-phenylenebis(methylene)]-bis(decahydro-3a,5a,8a,10a-tetraazapyrenium) dibromide, <b>4</b> .....	216
8.2.7	Synthesis of 5,5'-[1,4-phenylenebis(methylene)]-bis(1,5,8,12-tetraaza-bicyclo-[10.2.2]hexadecane), <b>5</b> .....	217
8.2.8	Synthesis of 1,1'-[1,4-phenylenebis(methylene)]bis[1,4,8,11-tetraazacyclotetra-decane], AMD3100, <b>2</b> .....	218
8.2.9	Synthesis of 8a,8a'-(bismethyl)-3a,3a'-[1,4-phenylenebis(methylene)]bis-(decahydro-3a,5a,8a,10a-tetraazapyrenium) dibromide, <b>8</b> .....	220
8.2.10	Synthesis of 12,12'-(bismethyl)-5,5'-[1,4-phenylenebis(methyl-ene)]bis-(1,5,8,12-tetraaza-bicyclo-[6.6.2]hexadecane).7HCl, <b>9</b> .....	221
8.2.11	Synthesis of 5-(4-phenylmethyl benzoate)-1,5,8,12-tetraazabicyclo[10.2.2]-hexadecane, <b>15</b> .....	222
8.2.12	Synthesis of 5-(methyl)-1,5,8,12-tetraaza-bicyclo[10.2.2]hexadecane, <b>21</b> (Method I) .....	224

8.2.13 Synthesis of 5-(methyl)-1,5,8,12-tetraaza-bicyclo[10.2.2]hexadecane, <b>21</b> (Method II) .....	226
8.2.14 Synthesis of 5-(phenylmethyl benzoate)-8-methyl-1,5,8,12-tetra-aza- bicyclo-[10.2.2]hexadecane, <b>16</b> .....	232
8.2.15 Synthesis of 5-(4-phenylmethyl methyl alcohol)-8-methyl-1,5,8,12- tetraaza-bicyclo[10.2.2]hexadecane, <b>17</b> .....	234
8.2.16 Synthesis of 5-(4-phenylmethyl benzyl bromide)-8-methyl-1,5,8,12- tetraaza-bicyclo[10.2.2]hexadecane, <b>10</b> .....	236
8.2.17 Synthesis of 3a,3a'3a''-[1,3,5-phenylenetris(methylene)]-tris- (decahydro-3a,5a,8a,10a-tetraazapyrenium) tribromide, <b>7</b> .....	237
8.2.18 Synthesis of 12,12',12''-(trimethyl)-5,5',5''-[1,3,5-phenylenetris- (methylene)]-tris(1,5,8,12-tetraaza-bicyclo-[6.6.2]hexadecane), <b>6</b> .....	239
<b>8.3 Synthesis of Transition Metal Complexes</b> .....	<b>241</b>
8.3.1 General Complexation Procedure .....	241
8.3.2 Synthesis of [Zn <sub>2</sub> <b>5</b> (OAc) <sub>2</sub> ](OAc) <sub>2</sub> .....	242
8.3.3 Synthesis of [Zn <sub>2</sub> <b>5</b> Cl <sub>2</sub> ](PF <sub>6</sub> ) <sub>2</sub> .....	247
8.3.4 Synthesis of [Zn <sub>2</sub> <b>5</b> ](ClO <sub>4</sub> ) <sub>4</sub> .....	247
8.3.5 Synthesis of [Cu <sub>2</sub> <b>5</b> (OAc) <sub>2</sub> ](OAc) <sub>2</sub> .....	247
8.3.6 Synthesis of [Cu <sub>2</sub> <b>5</b> ](ClO <sub>4</sub> ) <sub>4</sub> .....	248
8.3.7 Synthesis of [Cu <sub>2</sub> <b>5</b> Cl <sub>2</sub> ]Cl <sub>2</sub> .....	254
8.3.8 Synthesis of [Cu <sub>2</sub> <b>5</b> Cl <sub>2</sub> ](PF <sub>6</sub> ) <sub>2</sub> .....	259
8.3.9 Synthesis of [Ni <b>15</b> ](ClO <sub>4</sub> ) <sub>2</sub> .....	259

8.3.10	Synthesis of [Ni <sub>16</sub> ](ClO <sub>4</sub> ) <sub>2</sub> .....	260
8.3.11	Synthesis of [Ni <sub>15</sub> ](ClO <sub>4</sub> ) <sub>2</sub> .....	261
8.3.12	Synthesis of [Zn <sub>22</sub> (OAc) <sub>2</sub> ](OAc) <sub>2</sub> .....	261
8.3.13	Synthesis of [Cu <sub>22</sub> ](OAc) <sub>4</sub> .....	262
8.3.14	Synthesis of [Cu <sub>29</sub> Cl <sub>2</sub> ]Cl <sub>2</sub> .....	262
8.3.15	Synthesis of [Cu <sub>29</sub> Cl <sub>2</sub> ](PF <sub>6</sub> ) <sub>2</sub> .....	262
8.3.16	Synthesis of [Cu <sub>29</sub> (OAc) <sub>2</sub> ](OAc) <sub>2</sub> .....	263
8.3.17	Synthesis of [Zn <sub>36</sub> (OAc) <sub>3</sub> ](OAc) <sub>3</sub> .....	263
8.3.18	Synthesis of [Zn <sub>36</sub> Cl <sub>3</sub> ](PF <sub>6</sub> ) <sub>3</sub> .....	264
8.3.19	Synthesis of [Zn <sub>36</sub> ](ClO <sub>4</sub> ) <sub>6</sub> .....	264
8.3.20	Synthesis of [Cu <sub>36</sub> (OAc) <sub>3</sub> ](OAc) <sub>3</sub> .....	265
8.3.21	Synthesis of [Cu <sub>36</sub> ](ClO <sub>4</sub> ) <sub>6</sub> .....	265
8.3.22	Synthesis of [Cu <sub>36</sub> Cl <sub>3</sub> ](PF <sub>6</sub> ) <sub>3</sub> .....	265
<b>Chapter 9.</b>	<b>References .....</b>	<b>267</b>

## LIST OF FIGURES

<b>Figure 1.</b> NMR structure of CXCL12 (A). Highlighting the extended loop and $3_{10}$ helix (B), the 1 <sup>st</sup> $\beta$ -strand with a type III turn (C), the 2 <sup>nd</sup> and 3 <sup>rd</sup> $\beta$ -strands with a type I turn (D) and the type I turn and c-terminal $\alpha$ -helix (E) (reproduced from Current Medicinal Chemistry). <sup>3</sup> .....	4
<b>Figure 2.</b> Serpentine (A) and helical wheel (B) structure of CXCR4 (reproduced from the Journal of Biological Chemistry). <sup>34</sup> .....	6
<b>Figure 3.</b> HIV replication (reproduced from Nature Medicine). <sup>84</sup> .....	9
<b>Figure 4.</b> HIV cell entry involving: (A) interaction of gp120 with CD4 followed by (B) interaction of gp120 with co-receptor CXCR4 or CCR5 and (C) cell entry of gp41 (reproduced from Nature Reviews Drug Discovery). <sup>95</sup> .....	12
<b>Figure 5.</b> Structures of cyclam (1), AMD1657 ( $L^1$ ) and AMD3100 (2).....	14
<b>Figure 6.</b> Synthetic route to AMD3100 (2).....	15
<b>Figure 7.</b> Synthetic route to AMD3100 utilising bis-aminal chemistry.....	17
<b>Figure 8.</b> Competition binding experiments using AMD3100 (A) or cyclam (B) (reproduced from the Journal of Biological Chemistry). <sup>34</sup> .....	18
<b>Figure 9.</b> Effect of Asp to Asn substitution at positions 171 and 262 in CXCR4 on (A) AMD3100 and (B) cyclam competition binding for CXCL12 (SDF-1 $\alpha$ ) binding (reproduced from the Journal of Biological Chemistry). <sup>34</sup> .....	19
<b>Figure 10.</b> Effect of Asp to Asn substitution at positions 171 and 262 in CXCR4 on competition for 12G5 binding (reproduced from the Journal of Biological Chemistry). <sup>34</sup> .	20
<b>Figure 11.</b> Effect of incorporation of one (open symbols) or two (closed symbols) nickel(II) or copper(II) ions in AMD3100 on wild-type CXCR4 (reproduced from Biochemistry). <sup>114</sup> .....	21

<b>Figure 12.</b> Effect of incorporation of two zinc(II), nickel(II) or copper(II) ions in AMD3100 in competition with $^{125}\text{I}$ -12G5 mAb in mutants (A) Asp171 and (B) Asp262 CXCR4 receptor (reproduced from Biochemistry). <sup>114</sup> .....	22
<b>Figure 13.</b> Metal complexes of cyclam can adopt up to six configurations (five trans and a folded cis).....	30
<b>Figure 14.</b> X-ray crystal structures of $[\text{Pd1}](\text{ClO}_4)_2$ and $[\text{Pd1}]\text{Cl}_2$ . Both adopt the trans-III configuration. ....	31
<b>Figure 15.</b> X-ray crystal structure of $[\text{Pd}_2\text{L}^1](\text{OAc})_4$ . ....	32
<b>Figure 16.</b> X-ray crystal structure of $[\text{Zn1}(\text{OH}_2)_2](\text{OAc})_2$ . ....	33
<b>Figure 17.</b> Effect of acetate on the configuration of $[\text{Zn1Cl}_2]$ in aqueous solution (reproduced from Chemistry – A European Journal). <sup>147</sup> .....	34
<b>Figure 18.</b> Effect of acetate on the configuration of $[\text{Zn}_2\mathbf{2}](\text{ClO}_4)_4$ in aqueous solution (reproduced from Chemistry – A European Journal). <sup>147</sup> .....	35
<b>Figure 19.</b> X-ray crystal structure of $[\text{Zn}_2\mathbf{2}(\text{OAc})_2]^{2+}$ viewed from two angles.....	36
<b>Figure 20.</b> Time dependent configurational changes of $[\text{Zn}_2\mathbf{2}(\text{OAc})_2](\text{OAc})_2$ in aqueous solution (reproduced from the Journal of the American Chemical Society). <sup>146</sup> .....	36
<b>Figure 21.</b> The effect of complementarity on complex stability can only be increased to a certain level. ....	39
<b>Figure 22.</b> Effect of topology and rigidity on complex stability.....	40
<b>Figure 23.</b> Entropy in the chelate effect. ....	41
<b>Figure 24.</b> Linear and cyclic ligands used by Cabiness and Margerum.....	41
<b>Figure 25.</b> First donor dissociation in chelate vs macrocycle (reproduced from Coordination Chemistry Reviews). <sup>150</sup> .....	42

<b>Figure 26.</b> Cryptate compound, $L^6$ , studied by Lehn and Sauvage.....	43
<b>Figure 27.</b> Side-bridged macrocycle containing a piperazino moiety. Metal complexes adopt the trans-II configuration.....	46
<b>Figure 28.</b> 16-membered macrocycle, $L^7$ .....	47
<b>Figure 29.</b> Tetra-methyl ( $L^8$ ) and di-methyl ( $L^9$ ) cyclam. ....	48
<b>Figure 30.</b> Wainwright's synthesis of side-bridged cyclam, $L^{10}$ .....	49
<b>Figure 31.</b> Yamamoto and Muruoka's synthesis of side-bridged cyclam, $L^{10}$ . ....	49
<b>Figure 32.</b> Synthesis of side-bridged cyclam ( $L^{13}$ and $L^{14}$ ) incorporating a pendent arm..	50
<b>Figure 33.</b> Synthesis of a side-bridged cyclam ( $L^{17}$ ) possessing two ethyl pendent arms..	51
<b>Figure 34.</b> X-ray crystal structure of $[CuL^{15}(OH_2)]^{2+}$ . <sup>161</sup> .....	52
<b>Figure 35.</b> X-ray crystal structure of $[CuL^{17}(OH_2)]^{2+}$ . <sup>161</sup> .....	53
<b>Figure 36.</b> Synthesis of side-bridged cyclen, $L^{19}$ .....	53
<b>Figure 37.</b> Synthesis of a side-bridged bis-cyclen ligand.....	54
<b>Figure 38.</b> X-ray crystal structure of $[NiL^{19}]^{2+}$ . <sup>163</sup> .....	55
<b>Figure 39.</b> Proposed synthetic route to bis-side-bridged cyclam, <b>5</b> . ....	57
<b>Figure 40.</b> X-ray crystal structure of <b>3</b> from two different views. <sup>165</sup> .....	58
<b>Figure 41.</b> X-ray crystal structure of <b>3</b> . $2HClO_4$ . ....	59
<b>Figure 42.</b> X-ray crystal structure of <b>3</b> . $H[ZnCl_3(OH_2)]$ . ....	60
<b>Figure 43.</b> Mechanism of hydride reduction. ....	62
<b>Figure 44.</b> X-ray crystal structure of $[Zn_25(OAc)_2]^{2+}$ (A) highlighting the angle between the two macrocycles (B).....	64

<b>Figure 45.</b> 2D NMR of $[\text{Zn}_2\mathbf{5}(\text{OAc})_2]^{2+}$ .....	66
<b>Figure 46.</b> Aliphatic region of the $^1\text{H}$ NMR of $[\text{Zn}_2\mathbf{5}(\text{OAc})_2]^{2+}$ recorded at 800 MHz. ....	67
<b>Figure 47.</b> X-ray crystal structure of $[\text{Cu}_2\mathbf{5}]^{4+}$ .....	69
<b>Figure 48.</b> X-ray crystal structure of $[\text{CuL}^{13}]^{2+}$ .....	70
<b>Figure 49.</b> X-ray crystal structure of $[\text{Cu}_2\mathbf{5}]^{4+}$ highlighting the angle between the two macrocycles.....	71
<b>Figure 50.</b> X-ray crystal structure of $[\text{Cu}_2\mathbf{5Cl}_2]^{2+}$ showing one disordered position. ....	72
<b>Figure 51.</b> X-ray crystal structure of $[\text{Cu}_2\mathbf{5Cl}_2]^{2+}$ highlighting the angle between the two macrocycles.....	73
<b>Figure 52.</b> Tris-macrocycle (A), linear tris-macrocycle (B) and side-bridged derivative (C). .....	74
<b>Figure 53.</b> Synthetic route to tris-cyclam, $\text{L}^{22}$ .....	75
<b>Figure 54.</b> X-ray crystal structure of $[\text{Ni}_3\text{L}^{22}](\text{ClO}_4)_6$ . <sup>172</sup> .....	76
<b>Figure 55.</b> Proposed synthetic scheme to <b>6</b> . .....	77
<b>Figure 56.</b> Cross-bridged cyclam. Metal complexes adopt the cis-V configuration.....	82
<b>Figure 57.</b> Synthesis of the first cross-bridged cyclam, $\text{L}^{27}$ .....	83
<b>Figure 58.</b> X-ray crystal structure of $[\text{ZnL}^{28}(\text{OH}_2)(\mu\text{-Cl})\text{ZnCl}_3]$ . .....	85
<b>Figure 59.</b> X-ray crystal structure of $[\text{ZnL}^{28}(\mu\text{-Cl})_2]^{2+}$ .....	86
<b>Figure 60.</b> X-ray crystal structure of $[\text{CuL}^{29}\text{Cl}]^+$ .....	87
<b>Figure 61.</b> X-ray crystal structure of $[\text{CuL}^{29}(\text{NCCH}_3)]^{2+}$ .....	88
<b>Figure 62.</b> X-ray crystal structure of $[\text{CuL}^{27}\text{Cl}]^+$ .....	88

<b>Figure 63.</b> Synthetic route to bis-methyl cyclen, $L^{38}$ .....	90
<b>Figure 64.</b> Synthesis of cross-bridged cyclen, $L^{40}$ .....	91
<b>Figure 65.</b> Synthesis of cross-bridged bis-macrocyclic.....	92
<b>Figure 66.</b> X-ray crystal structure of $[ZnL^{40}Cl_2]$ .....	93
<b>Figure 67.</b> X-ray crystal structure of $[ZnL^{41}(OH_2)_2]^{2+}$ .....	94
<b>Figure 68.</b> X-ray crystal structure of $[CuL^{40}(NCCH_3)_2]^{2+}$ .....	95
<b>Figure 69.</b> Proposed synthetic route to cross-bridged bis-cyclam, <b>9</b> . .....	97
<b>Figure 70.</b> Mechanism for double ring expansion.....	100
<b>Figure 71.</b> Cr K-edge XAS spectrum of $CrO_2Cl_2$ at 10 K. ....	107
<b>Figure 72.</b> Schematic representation of the photo-electric effect.....	109
<b>Figure 73.</b> Schematic representation two decay mechanisms: X-ray fluorescence (A) and the Auger effect (B). .....	111
<b>Figure 74.</b> Summary of the EXAFS data reduction process. ....	113
<b>Figure 75.</b> Cr K-edge EXAFS (left) and FT (right) of $CrO_2Cl_2$ at 10 K. ....	114
<b>Figure 76.</b> $[CuL^{42}](ClO_4)_2$ was used as a starting point for the analysis of $[Cu_25](ClO_4)_4$ . .....	118
<b>Figure 77.</b> Cu K-edge XANES spectra of $[Cu_25](ClO_4)_4$ and $[Cu_36](ClO_4)_6$ in the solid state at 80 K.....	119
<b>Figure 78.</b> Cu K-edge XANES spectra of $[Cu_25](ClO_4)_4$ derivatives in solution at 80 K. ....	119
<b>Figure 79.</b> Cu K-edge EXAFS (left) and FTs (right) of solid $[Cu_25](ClO_4)_4$ (top), aqueous solution (middle) and excess acetate solution (bottom) at 80 K. ....	121

<b>Figure 80.</b> Cu K-edge XANES spectra of $[\text{Cu}_2\mathbf{5}(\text{OAc})_2](\text{OAc})_2$ and $[\text{Cu}_3\mathbf{6}(\text{OAc})_3](\text{OAc})_3$ in the solid state at 80 K. ....	123
<b>Figure 81.</b> Cu K-edge XANES spectra of $[\text{Cu}_2\mathbf{5}(\text{OAc})_2](\text{OAc})_2$ derivatives in solution at 80 K. ....	124
<b>Figure 82.</b> Cu K-edge EXAFS (left) and FTs (right) of solid $[\text{Cu}_2\mathbf{5}(\text{OAc})_2](\text{OAc})_2$ (top), aqueous solution (middle) and solution containing excess acetate (bottom) at 80 K. ....	125
<b>Figure 83.</b> Cu K-edge XANES spectrum of $[\text{Cu}_2\mathbf{5}\text{Cl}_2](\text{PF}_6)_2$ and $[\text{Cu}_3\mathbf{6}\text{Cl}_3](\text{PF}_6)_3$ in the solid state at 80 K. ....	127
<b>Figure 84.</b> Cu K-edge XANES of $[\text{Cu}_2\mathbf{5}\text{Cl}_2](\text{PF}_6)_2$ , $[\text{Cu}_2\mathbf{5}(\text{OAc})_2](\text{OAc})_2$ and $[\text{Cu}_2\mathbf{5}](\text{ClO}_4)_4$ in the solid state at 80 K. ....	128
<b>Figure 85.</b> Cu K-edge XANES of $[\text{Cu}_2\mathbf{5}\text{Cl}_2](\text{PF}_6)_2$ derivatives in solution at 80 K. ....	129
<b>Figure 86.</b> Cu K-edge EXAFS (left) and FTs (right) of solid $[\text{Cu}_2\mathbf{5}\text{Cl}_2](\text{PF}_6)_2$ (top) aqueous solution (middle) and solution containing excess acetate (bottom). ....	130
<b>Figure 87.</b> Cu K-edge EXAFS (left) and FT (right) of $[\text{Cu}_2\mathbf{9}(\text{OAc})_2]^{2+}$ in the solid state at 80 K. ....	132
<b>Figure 88.</b> Cu K-edge EXAFS (left) and FT (right) of $[\text{Cu}_2\mathbf{9}(\text{OAc})_2]^{2+}$ in aqueous solution at 80 K. ....	133
<b>Figure 89.</b> Cu K-edge EXAFS (left) and FT (right) of $[\text{Cu}_2\mathbf{9}\text{Cl}_2](\text{PF}_6)_2$ in the solid state at 80 K. ....	134
<b>Figure 90.</b> Cu K-edge XANES of $[\text{Cu}_2\mathbf{9}\text{Cl}_2]^{2+}$ and $[\text{Cu}_2\mathbf{9}(\text{OAc})_2]^{2+}$ in the solid state at 80 K. ....	136
<b>Figure 91.</b> Cu K-edge EXAFS (left) and FT (right) of $[\text{Cu}_2\mathbf{9}\text{Cl}_2]\text{Cl}_2$ in aqueous solution at 80 K. ....	137

<b>Figure 92.</b> Cu K-edge EXAFS (left) and FT (right) of $[\text{Cu}_2\mathbf{9}\text{Cl}_2](\text{PF}_6)_2$ in aqueous solution at 80 K with acetate added. ....	138
<b>Figure 93.</b> Cu K-edge EXAFS (left) and FT (right) of $[\text{Cu}_2\mathbf{9}\text{Cl}_2](\text{PF}_6)_2$ in aqueous solution at 80 K with silver(II) acetate added. ....	139
<b>Figure 94.</b> Typical flow cytometry plot showing negative control (purple), positive control (red) and two different antagonists (blue and green). ....	145
<b>Figure 95.</b> Summary of mAb 12G5 binding to CXCR4 in the presence of bound antagonists. ....	146
<b>Figure 96.</b> Reduction of MTT to formazan. ....	149
<b>Figure 97.</b> Inhibition of AMD3100 resistant HIV replication at varying concentrations of both $[\text{Cu}_2\mathbf{9}\text{Cl}_2](\text{PF}_6)_2$ and AMD3100. ....	154
<b>Figure 98.</b> Correlation between $\text{IC}_{50}$ anti-HIV activity vs $\text{IC}_{50}$ calcium signalling excluding $[\text{Zn}_2\mathbf{9}]\text{Cl}_4$ . ....	160
<b>Figure 99.</b> Ability of bis-macrocyclic ligands to H-bond to CXCR4. ....	163
<b>Figure 100.</b> Schematic representation of copper(II) coordination environments in $[\text{Cu}_2\mathbf{5}\text{Cl}_2]^{2+}$ (A) and $[\text{Cu}_2\mathbf{9}\text{Cl}_2]^{2+}$ (B). ....	166
<b>Figure 101.</b> Cross-bridged ligand, $\text{L}^{43}$ . ....	168
<b>Figure 102.</b> Schematic representation of the zinc(II) coordination environment in $[\text{Zn}_2\mathbf{5}(\text{OAc})_2]^{2+}$ (A) and $[\text{Zn}_2\mathbf{9}(\text{OAc})_2]^{2+}$ (B). ....	169
<b>Figure 103.</b> Synthesis of asymmetrical bis-macrocyclic, $\text{L}^{46}$ . ....	173
<b>Figure 104.</b> Proposed synthetic route to an asymmetrical bis-macrocyclic. ....	174
<b>Figure 105.</b> Proposed synthetic route to <b>10</b> . ....	175
<b>Figure 106.</b> Summary of the attempted preparation of <b>16</b> . ....	176

<b>Figure 107.</b> Alkylation of <b>15</b> .....	177
<b>Figure 108.</b> Alkylation of <b>L<sup>47</sup></b> results in the unexpected compound, <b>L<sup>49</sup></b> .....	178
<b>Figure 109.</b> Reductive amination of <b>15</b> .....	179
<b>Figure 110.</b> Acylation of <b>15</b> and subsequent reduction of intermediate <b>18</b> . ....	180
<b>Figure 111.</b> Proposed alternative synthetic route to <b>16</b> .....	181
<b>Figure 112.</b> X-ray crystal structure of <b>20</b> . ....	182
<b>Figure 113.</b> X-ray crystal structure of <b>21</b> . ....	183
<b>Figure 114.</b> Proposed synthetic route to <b>25</b> .....	184
<b>Figure 115.</b> Kaden's synthesis of <b>L<sup>15</sup></b> . ....	186
<b>Figure 116.</b> Proposed synthetic route to <b>16</b> .....	187
<b>Figure 117.</b> Synthesis of asymmetrical bis-macrocyclic, <b>26</b> .....	190
<b>Figure 118.</b> Proposed bis-macrocyclic compound, <b>27</b> ; transition metal complexes should adopt a trans-IV configuration. ....	196
<b>Figure 119.</b> Two examples of asymmetrical bis-macrocyclic compounds. ....	197
<b>Figure 120.</b> ORTEP representation of <b>3.2HClO<sub>4</sub></b> .....	205
<b>Figure 121.</b> ORTEP representation of <b>3.H[ZnCl<sub>3</sub>(OH<sub>2</sub>)]</b> .....	208
<b>Figure 122.</b> ORTEP representation of <b>20</b> .....	2121
<b>Figure 123.</b> ORTEP representation of <b>21.2H<sub>2</sub>O</b> .....	229
<b>Figure 124.</b> ORTEP representation of <b>[Zn<sub>2</sub>5(OAc)<sub>2</sub>]<sup>2+</sup></b> . Symmetry transformations used to generate equivalent atoms: -x,-y+1,-z.....	245
<b>Figure 125.</b> ORTEP representation of <b>[Cu<sub>2</sub>5](ClO<sub>4</sub>)<sub>4</sub></b> . ....	250

**Figure 126.** ORTEP representation of  $[\text{Cu}_2\text{5Cl}_2]^{2+}$  showing the two alternative disordered ring positions. Symmetry transformations used to generate equivalent atoms:  $-x, y, -z+1$ .  
..... 256

## LIST OF TABLES

<b>Table 1.</b> Chemokine receptors and their major activity. DARC and CCR1 are included for completeness but are not as well characterised. <sup>3</sup> .....	3
<b>Table 2.</b> Currently approved anti-viral drugs. <sup>85</sup> .....	10
<b>Table 3.</b> AMD3100 inhibition of various HIV strains. <sup>129</sup> .....	27
<b>Table 4.</b> Selected bond lengths and angles for $3.2\text{HClO}_4$ . .....	59
<b>Table 5.</b> Selected bond lengths and angles for $3.\text{H}[\text{ZnCl}_3(\text{OH}_2)]$ . .....	61
<b>Table 6.</b> Selected bond lengths and angles for $[\text{Zn}_2\mathbf{5}(\text{OAc})_2]^{2+}$ . .....	65
<b>Table 7.</b> Selected bond lengths and angles for $[\text{Cu}_2\mathbf{5}]^{4+}$ .....	69
<b>Table 8.</b> Selected bond lengths and angles for $[\text{Cu}_2\mathbf{5}\text{Cl}_2]^{2+}$ .....	73
<b>Table 9.</b> Refined EXAFS parameters for $[\text{Cu}_2\mathbf{5}](\text{ClO}_4)_4$ in the solid state, aqueous solution and acetate solution. ....	122
<b>Table 10.</b> Refined EXAFS parameters for $[\text{Cu}_2\mathbf{5}(\text{OAc})_2](\text{OAc})_2$ in the solid state and aqueous solution. ....	126
<b>Table 11.</b> Refined EXAFS parameters for $[\text{Cu}_2\mathbf{5}\text{Cl}_2](\text{PF}_6)_2$ in the solid state, aqueous solution and with excess acetate. ....	131
<b>Table 12.</b> Refined EXAFS parameters for $[\text{Cu}_2\mathbf{9}(\text{OAc})_2]^{2+}$ in the solid state and aqueous solution. ....	133

<b>Table 13.</b> Refined EXAFS parameters for $[\text{Cu}_2\mathbf{9}\text{Cl}_2](\text{PF}_6)_2$ in the solid state and aqueous solution.....	135
<b>Table 14.</b> Summary of EXAFS parameters for $[\text{Cu}_2\mathbf{9}(\text{OAc})_2]^{2+}$ and $[\text{Cu}_2\mathbf{9}\text{Cl}_2]^{2+}$ derivatives in the solid state and various aqueous solutions. ....	139
<b>Table 15.</b> $\text{IC}_{50}$ and $\text{IC}_{90}$ values of compounds tested.....	147
<b>Table 16.</b> Anti-HIV activity of ligands in MT-4 cells.....	151
<b>Table 17.</b> Anti-HIV activity of copper(II) complexes in MT-4 cells. ....	152
<b>Table 18.</b> Anti-HIV activity of zinc(II) complexes in MT-4 cells. ....	155
<b>Table 19.</b> Anti-HIV activity of selected compounds in PMBCs. ....	157
<b>Table 20.</b> Calcium signalling $\text{IC}_{50\text{s}}$ for a selection of compounds. ....	159
<b>Table 21.</b> Bond lengths ( $\text{\AA}$ ) and angles ( $^\circ$ ) for $3.2\text{HClO}_4$ .....	206
<b>Table 22.</b> Bond lengths ( $\text{\AA}$ ) and angles ( $^\circ$ ) for $3.\text{H}[\text{ZnCl}_3(\text{OH}_2)]$ . ....	209
<b>Table 23.</b> Bond lengths ( $\text{\AA}$ ) and angles ( $^\circ$ ) for 3a-[methyl]-decahydro-3a,5a,8a,10a-tetraaza-pyrenium bromide. ....	212
<b>Table 24.</b> Bond lengths ( $\text{\AA}$ ) and angles ( $^\circ$ ) for 5-(methyl)-1,5,8,12-tetraaza-bicyclo[10.2.2]hexadecane.....	230
<b>Table 25.</b> Bond lengths ( $\text{\AA}$ ) and angles ( $^\circ$ ) for $[\text{Zn}_2\mathbf{5}(\text{OAc})_2]^{2+}$ . ....	246
<b>Table 26.</b> Bond lengths ( $\text{\AA}$ ) for $[\text{Cu}_2\mathbf{5}](\text{ClO}_4)_4$ .....	251

**Table 27.** Bond angles ( $^{\circ}$ ) for  $[\text{Cu}_2\mathbf{5}](\text{ClO}_4)_4$ . ..... 252

**Table 28.** Bond lengths ( $\text{\AA}$ ) and angles ( $^{\circ}$ ) for  $[\text{Cu}_2\mathbf{5}\text{Cl}_2]\text{Cl}_2$ . ..... 257

# **Chapter 1. INTRODUCTION**

## **1.1 Chemokines & Chemokine Receptors**

Chemokines are involved in the regulation of the immune system cell network and are primarily responsible for the migration of cells and directing leukocytes to sites of inflammation. They exert their biological effect by binding to and activating chemokine receptors. These receptors have been identified as potential therapeutic targets and one example of a chemokine receptor antagonist, Maraviroc, has recently been granted FDA approval as an anti-viral drug. The following section introduces chemokines and their receptors, particularly highlighting the CXCL12 and CXCR4 pair as they are relevant to this work.

### **1.1.1 Chemokines**

Chemokines are a group of small (8-10 kDa) proteins which are divided into four sub-groups depending on the orientation of the first two conserved cysteine residues.<sup>1,2</sup> The CXC and CC sub-groups comprise the majority of the chemokines, of which over 40 have been presently identified (Table 1).<sup>1-3</sup>

Receptor	Selective ligands	Principal biological function
<b>CC family</b>		
CCR1	CCL14	Anti-viral response
CCR2	CCL2	Macrophage recruitment
CCR3	CCL11 CCL24	Parasite response, Th <sup>2</sup> recruitment
CCR4	CCL17 CCL22	Skin homing, Th <sup>2</sup> recruitment
CCR5	CCL3 CCL4	Th <sup>2</sup> and macrophage recruitment
CCR6	CCL20	Dendritic cell homing
CCR7	CCL19 CCL21	Secondary lymphoid tissue homing of T, B and dendritic cells NK cell recruitment
CCR8	CCL1	Th <sup>2</sup> recruitment
CCR9	CCL25	Intestinal homing, thymocyte migration
CCR10	CCL27 CCL28	Skin homing of T cells
CCR11	CCL2 CCL19	Macrophage recruitment
DARC	Many CC	Does not signal-chemokine sink, malaria receptor
<b>CXC family</b>		
CXCR1	CXCL8	Neutrophil chemotaxis and deregulation
CXCR2	CXCL1 CXCL5 CXCL7 CXCL8	Neutrophil chemotaxis and deregulation
CXCR3	CXCL9 CXCL10 CXCL11	T cell responses
CXCR4	CXCL12	B cell responses, stem cell homing
CXCR5	CXCL13	B cell responses
CXCR6	CXCL16	Activated T cells
<b>CX3C family</b>		
CX3CR1	CX3CL1	Inflammation
<b>C family</b>		
XCR1	XCL1 XCL2	Inflammation

**Table 1. Chemokine receptors and their major activity. DARC and CCR1 are included for completeness but are not as well characterised.<sup>3</sup>**

Originally identified as immune cell traffickers, the actual role of chemokines in nature goes much further. They have been shown to be involved in embryonic development, hematopoiesis, growth regulation and angiogenesis.<sup>4-7</sup> Given the crucial role chemokines play in nature, it is not difficult to imagine the consequences of a breakdown in

the regulation of the chemokine system. For example, chemokines have been proven to play an important role in many disease states including multiple sclerosis, rheumatoid arthritis, asthma and diabetes.<sup>8-13</sup>

### 1.1.2 CXCL12

CXCL12 is a unique chemokine as it has a sole receptor, CXCR4, whereas all of the other chemokines found to date are promiscuous in their nature.<sup>5</sup> It is a distant relative of the CXC chemokine family and was originally identified as a product from bone marrow stromal cells, hence its common alternative name, stromal-cell derived factor one (SDF-1).<sup>14-16</sup> The structure of the 67 residue, highly basic protein has been determined by NMR and is shown in Figure 1.<sup>17</sup>

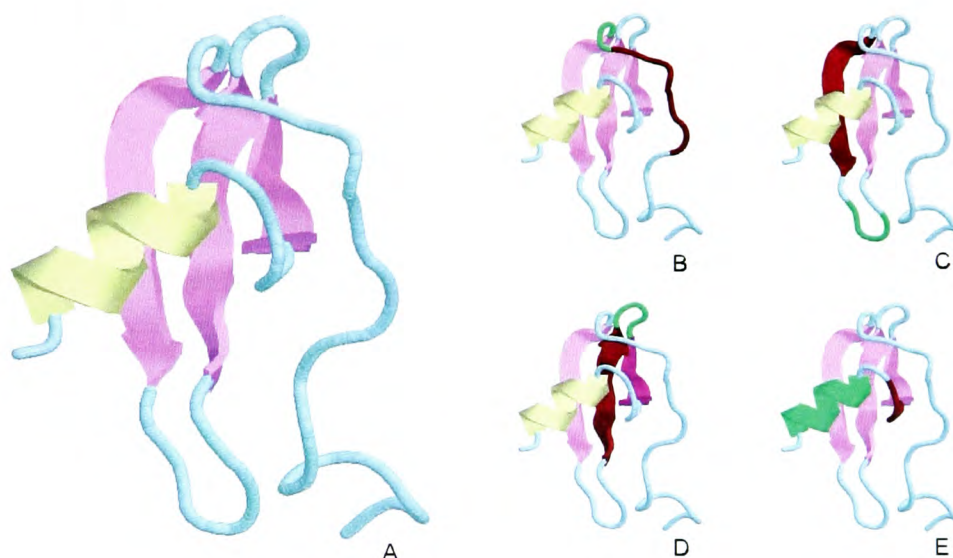


**Figure 1. NMR structure of CXCL12 (A). Highlighting the extended loop and  $3_{10}$  helix (B), the 1<sup>st</sup>  $\beta$ -strand with a type III turn (C), the 2<sup>nd</sup> and 3<sup>rd</sup>  $\beta$ -strands with a type I turn (D) and the type I turn and c-terminal  $\alpha$ -helix (E) (reproduced from Current Medicinal Chemistry).<sup>3</sup>**

The first and second  $\beta$  strands contain regions of positive charge on their surface, whereas the  $\alpha$ -helix presents a negative surface charge.<sup>17</sup> These electrostatic properties are important in the receptor binding mechanism of CXCL12 to CXCR4. CXCL12 is produced by stromal cells in the bone marrow but is also expressed and secreted by other organs including the brain, liver, lung and lymph nodes.<sup>18-22</sup> CXCL12 gene knockout mice experience developmental defects of the immune, haematopoietic, circulatory, cardiac and central nervous systems at the embryonic stage and eventually die.<sup>23-25</sup>

### **1.1.3 Chemokine Receptors**

Chemokine receptors belong to the G-protein coupled receptor (GPCR) superfamily and are 340-370 amino acids in length.<sup>26</sup> They are seven transmembrane serpentine receptors and are expressed on many different types of leukocytes and non-hematopoietic cells.<sup>27</sup> Their role in nature is primarily involved in leukocyte chemotaxis and inflammation.<sup>28, 29</sup> The identification of chemokine receptors as a class of GPCR was met with enthusiasm as most of the drugs currently on the market exploit this receptor type. The majority of chemokine receptors bind multiple ligands under a variety of conditions; however, CXCR4 has only one natural ligand, CXCL12.<sup>2</sup>

### **1.1.4 CXCR4**

CXCR4 (Figure 2) is expressed on hematopoietic cells and, to a lesser extent, on vascular endothelial cells, neurons and astrocytes.<sup>30-33</sup> The protein is important in embryonic and cardiac development and also hematopoiesis in the gastrointestinal tract.<sup>23</sup> In addition, the disruption of CXCR4 is embryologically lethal and results in serious developmental effects in the immune, circulatory and central nervous systems.<sup>24, 25</sup> The

similarity of the defects between CXCL12 and CXCR4 knockouts reflects the monogamous relationship between the pair.

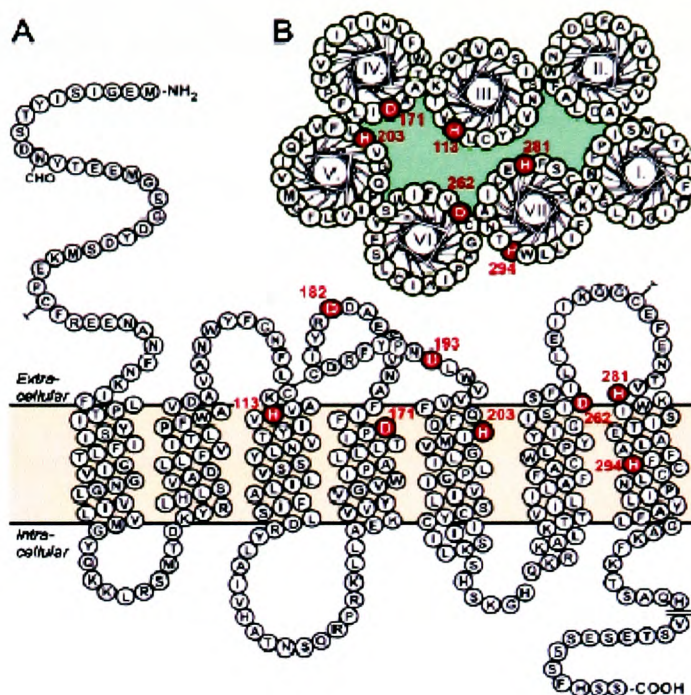


**Figure 2. Serpentine (A) and helical wheel (B) structure of CXCR4 (reproduced from the Journal of Biological Chemistry).<sup>34</sup>**

### 1.1.5 Role of Chemokines & Chemokine Receptors in Disease

Over the last decade, there has been an increase in the understanding of the association between chemokine receptors and several human diseases. In addition to their role in inflammation, chemokine receptors have been found to be required by HIV for leukocyte infection.<sup>35-37</sup> Furthermore, tumour metastasis can be influenced by the over-expression of chemokine receptors on tumour cells.<sup>1, 20, 38-43</sup>

CXCR4 and its ligand CXCL12 have specifically been implicated in rheumatoid arthritis, inflammatory liver disease, several cancers and HIV.<sup>7, 13, 41, 43-49</sup> The role of

CXCR4 in rheumatoid arthritis has been revealed due to the fact that receptor antagonists reduce the severity of arthritis in a collagen-induced mouse model.<sup>41</sup> Most of the leukocytes obtained from the inflamed joints were found to express CXCR4, showing that CXCL12 plays a central role in the pathogenesis of murine collagen-induced arthritis by attracting CXCR4(+) leukocytes to the site of inflammation. In addition, CXCR4 and CXCL12 have both been found in the synovium and articular cartilage of rheumatoid arthritis patients.<sup>50</sup> Levels of CXCL12 are found to be higher than normal in patients with inflammatory liver disease.<sup>51</sup> Antagonising CXCR4 in a murine model of airway inflammation had not only a therapeutic effect, but also a protective effect against metacholine-induced airway hyper-responsiveness and inflammation in allergic mice.<sup>52</sup>

The literature highlighting the link between tumour growth, survival, metastasis and CXCR4/CXCL12 is ever increasing. For example, the over-expression of CXCR4 has been reported in numerous epithelial, mesenchymal and haemopoietic cancers.<sup>45, 53-59</sup> The role of CXCL12 in breast cancer has been described.<sup>20, 60, 61</sup> CXCR4(+) tumour cells migrate to sites rich in CXCL12 such as bone, liver and lung.<sup>45, 62</sup> Furthermore, CXCR4 is highly expressed and has been implicated in lung, cervical, colorectal, prostate and pancreatic cancers.<sup>54, 58, 63-71</sup> Samples of pancreatic cancer tissues constitutively express CXCL12 which enables migration of cancer cells to other sites. In the presence of a CXCR4 antagonist, cell migration was inhibited, suggesting potential for prevention of growth and spread of tumour.<sup>68</sup> CXCR4/CXCL12 also play a role in certain brain tumours as CXCR4 has been found to be over-expressed on malignant cells in comparison to normal neuronal cells.<sup>72, 73</sup>

The expanding knowledge of the involvement of CXCR4 and CXCL12 in several diseases, in addition to successful receptor blocking results, suggests an immense therapeutic potential in targeting the CXCR4/CXCL12 axis.<sup>43, 44, 74-82</sup> The majority of the literature has concentrated on the role of CXCR4 in HIV infection and this is discussed in detail in the following section.

## 1.2 Human Immunodeficiency Virus

HIV first appeared in 1981 and was identified in 1983 by Montagnier and co-workers.<sup>83</sup> Montagnier was rewarded with a share of the Nobel Prize for medicine in 2008 for his work in this area. There are two known strains of the virus, HIV-1 and HIV-2. The virus contains a single stranded RNA genome, which is replicated through a double stranded DNA intermediate. The viral DNA becomes integrated into the genome of the host cell and viral genes are transcribed only when they have been integrated into the host cell. The HIV replication cycle is shown in Figure 3.<sup>84</sup>

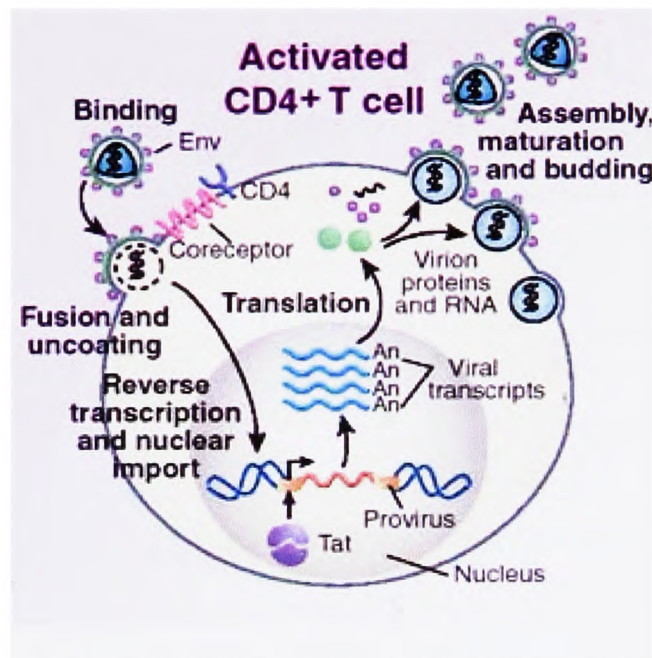


**Figure 3. HIV replication (reproduced from Nature Medicine).<sup>84</sup>**

The cycle can be summarised in five major steps: binding, reverse transcription, integration, transcription and translation. Each stage in the cycle can be targeted for treatment and over twenty anti-viral drugs have been approved over the past two decades (Table 2).<sup>85-87</sup>

Product	Generic name	Manufacturer	Year approved
<b>Nucleoside/nucleotide reverse transcriptase inhibitors</b>			
Retrovir	Zidovudine (AZT)	GSK	1987
Videx	Didanosine (ddI)	Bristol-Myers Squibb	1991
Zerit	Stavudine (d4T)	Bristol-Myers Squibb	1994
Epivir	Lamivudine (3TC)	GSK	1995
Combivir	Lamivudine, zidovudine	GSK	1997
Ziagen	Abacavir	GSK	1998
Trizivir	Abacavir, zidovudine, lamivudine	GSK	2000
Viread	Tenofovir	Gilead Sciences	2001
Emtriva	Emtricitabine	Gilead Sciences	2003
Epzicom	Abacavir, lamivudine	GSK	2004
Truvada	Tenofovir, emtricitabine	Gilead Sciences	2004
<b>Non-nucleoside reverse transcriptase inhibitors</b>			
Viramune	Nevirapine	Boehringer Ingelheim	1996
Rescriptor	Delavirdine	Pfizer	1997
Sustiva	Efavirenz	Bristol-Myers Squibb	1998
Intelence	Etravirine	Tibotec	2008
<b>Protease inhibitors</b>			
Invirase	Saquinavir	Roche	1995
Crixivan	Indinavir	Merck	1996
Norvir	Ritonavir	Abbott Laboratories	1996
Viracept	Nelfinavir	Agoron Pharmaceuticals/Pfizer/Roche	1997
Kaletra	Lopinavir, ritonavir	Abbott Laboratories	2000
Lexiva	Fosamprenavir	GSK	2003
Reyataz	Atazanavir	Bristol-Myers Squibb	2003
Aptivus	Tipranavir	Boehringer Ingelheim	2005
Prezista	Darunavir	Tibotec	2006
<b>Entry and fusion inhibitors</b>			
Fuzeon	Enfuvirtide	Roche/Trimeris	2003
Selzentry	Maraviroc	Pfizer	2007
<b>Integrase inhibitors</b>			
Isentress	Raltegravir	Merck	2007
<b>Multiclass combination</b>			
Atripla	Efavirenz, emtricitabine, tenofovir,	Gilead Sciences/Bristol-Myers Squibb	2006

**Table 2. Currently approved anti-viral drugs.<sup>85</sup>**

The earliest compounds were nucleoside/nucleotide reverse transcriptase inhibitors (NRTIs) such as AZT and d4T.<sup>88</sup> Once tri-phosphorylated, these compounds inhibit the reverse transcription process which converts viral RNA into DNA. The development of non-nucleoside reverse transcriptase (NNRTIs) and protease inhibitors resulted in the possibility of highly-active antiretroviral therapy (HAART).<sup>89-91</sup> This involves the simultaneous treatment with different classes of anti-viral compound, the typical combination being two NRTIs with either an NNRTI or a protease inhibitor. Provided the patient continues to take the drugs as prescribed, HAART has proven to be successful in reducing the viral load to undetectable levels in the bloodstream.<sup>92</sup>

Entry inhibitors have been developed which prevent HIV merging with host cells.<sup>93, 94</sup> For example, the peptidic drug Fuzeon acts at the fusion/uncoating stage and Maraviroc acts at an earlier binding stage. The initial binding step involves the interaction of HIV with one of two co-receptors, either CCR5 or CXCR4. Maraviroc acts by blocking the interaction with CCR5.

### 1.2.1 HIV Cell Entry

Binding of HIV to a host cell is summarised in Figure 4.<sup>95</sup> Initially, the viral envelope glycoprotein gp120 interacts with the CD4 receptor on the cell surface (Figure 4a). Once cell bound, the gp120 interacts with either CXCR4 (in X4 strains) or CCR5 (in R5 strains) (Figure 4b). Gp120 and gp41 are non-covalently associated and form a trimer on the virus surface.<sup>96</sup> The interaction of gp120 and the respective co-receptor leads to a conformational change within the gp120-gp41 trimer, allowing gp41 to finally enter the cell (Figure 4c).<sup>97-</sup>

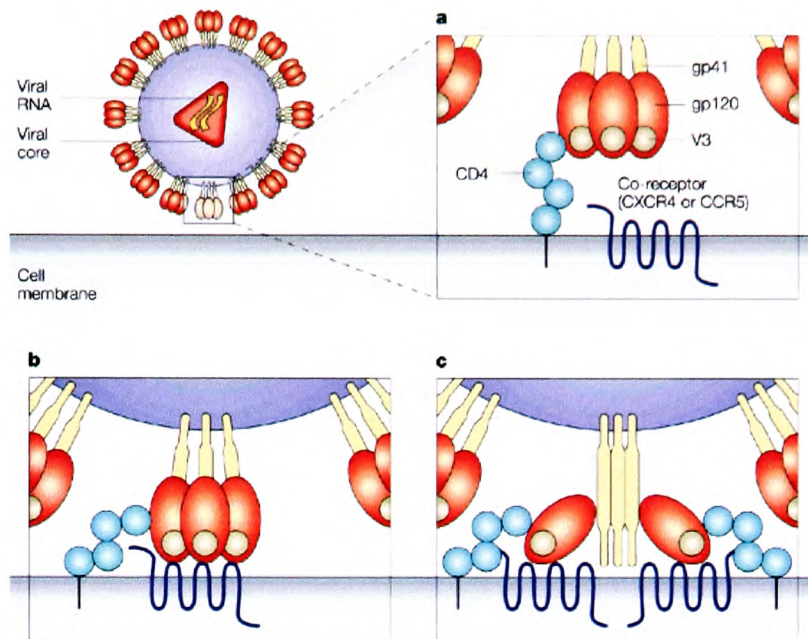


**Figure 4. HIV cell entry involving: (A) interaction of gp120 with CD4 followed by (B) interaction of gp120 with co-receptor CXCR4 or CCR5 and (C) cell entry of gp41 (reproduced from Nature Reviews Drug Discovery).<sup>95</sup>**

### 1.3 CXCR4 Antagonists

There have been numerous compounds developed to antagonise CXCR4 due to the potential for targeting the receptor as a drug target. The bicyclam class of compounds represent the most thoroughly investigated CXCR4 antagonists and are discussed here describing the development of the prototype bicyclam, AMD3100.

#### 1.3.1 Development of AMD3100

The bicyclam class of compounds was first reported in the late 1980s but were only considered as pharmaceutical candidates in the late 1990s.<sup>100-102</sup> Several batches of commercial cyclam (1,4,8,11-tetraazacyclotetradecane, **1**) were tested for their anti-HIV activity and they were found to be poor inhibitors of HIV replication in MT-4 cells. However, one sample showed a ten-fold increase in its antiviral activity compared to the other cyclam samples. This was the result of an impurity in the sample which was eventually identified as the bicyclam AMD1657, **L**<sup>1</sup> (Figure 5). This compound has an EC<sub>50</sub> value of 0.1-0.2 µg/mL and a selectivity index of > 5,000.<sup>95</sup> The selectivity index is a ratio of 50% cytotoxic concentration (CC<sub>50</sub>) to 50% antiviral effective concentration (EC<sub>50</sub>). As a comparison, AZT, a current clinical drug used for HIV treatment has a selectivity index of > 1,000.<sup>103</sup>

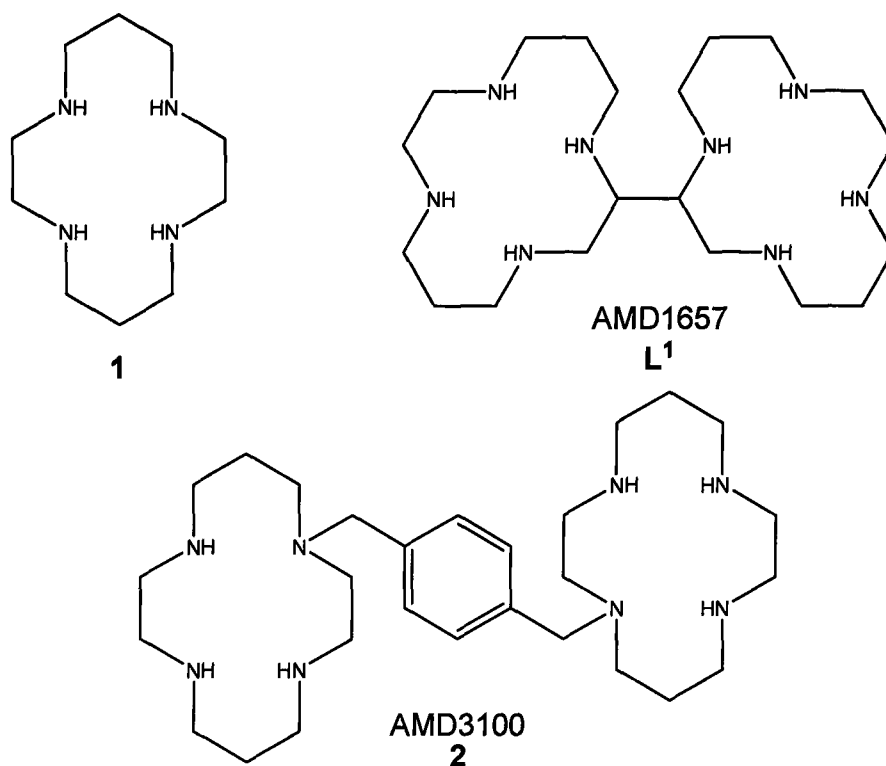


**Figure 5. Structures of cyclam (1), AMD1657 (L<sup>1</sup>) and AMD3100 (2).**

AMD1657 proved impossible to resynthesise at that time and so the synthesis of other derivatives was pursued. Notably however, a search of the literature for this report revealed a synthetic route to this compound in very low yield by Barefield *et al.*<sup>104</sup> Through the systematic preparation of analogues of AMD1657, AMD3100 (Figure 5) was eventually synthesised.

AMD3100 is a bicyclam composed of two cyclam rings tethered via an aromatic linker. It was originally developed by AnorMED and taken into clinical trials for HIV treatment. After AnorMED was taken over by Genzyme in 2006, AMD3100 was recently successfully trialled for stem cell mobilisation and was granted FDA approval under the tradename Plerixafor.<sup>105, 106</sup>

### 1.3.2 Synthesis of AMD3100

AMD3100, as it would be later named, was originally synthesised by Fabrizzi and co-workers in order to investigate the potentially interesting redox properties of its transition metal complexes.<sup>100</sup> The original synthesis (Figure 6) employs protection-deprotection chemistry resulting in a relatively low overall yield when starting from cyclam. More recently, higher yielding and hence more economical synthetic routes to AMD3100 have been reported in the literature and are also discussed here.

Fabrizzi and co-workers' synthetic route (Figure 6) begins with the preparation of compound **L**<sup>2</sup> in moderate yield (56%) from the direct reaction of **1** with toluene sulphonyl chloride. Subsequent N-alkylation of the secondary amine with  $\alpha$ - $\alpha'$ -*p*-xylenedibromide gave the tris-N protected bicyclam **L**<sup>3</sup>, which can be deprotected with H<sub>2</sub>SO<sub>4</sub> to give AMD3100, **2**. The overall yield for this synthetic route is approximately 30%.

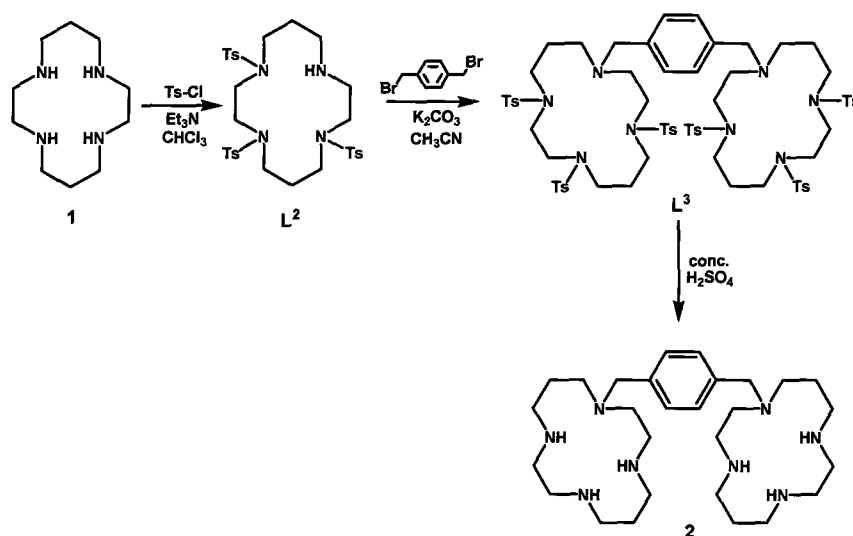
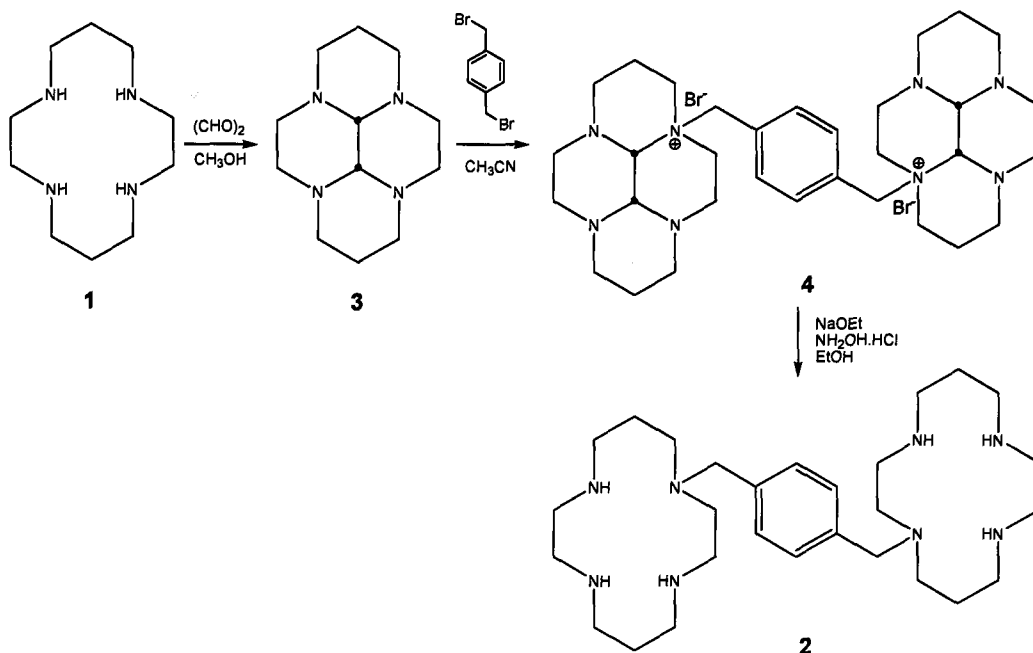


Figure 6. Synthetic route to AMD3100 (2).

An almost identical route to that shown in Figure 6 has been reported by Yang *et al.* who have used a trifluoroacetyl protecting group in preference to tosyl.<sup>107</sup> This method reports an improved yield of over 90% for the tris-protected equivalent of L<sup>3</sup>. The N-alkylation step with  $\alpha$ - $\alpha'$ -*p*-xylenedibromide is exactly the same as in Figure 6; however, deprotection is achieved with sodium hydroxide. The reported overall yield of over 70% is approximately 2-fold greater than the original synthesis.

Handel and co-workers have reported a facile route to AMD3100 which exploits bis-aminal chemistry (Figure 7).<sup>108</sup> The *cis* product of bis-aminal **3** is prepared in quantitative yield and can be selectively mono-N-alkylated with an appropriate electrophile, such as  $\alpha$ - $\alpha'$ -*p*-xylenedibromide in acetonitrile. This elegant route relies on the fact that the ammonium salt **4** precipitates out of solution once formed, which negates the possibility of any oligomer formation. Finally, the bis-aminal bridge is cleaved using a combination of hydroxylamine hydrochloride and sodium ethoxide, resulting in a total yield for the three step process of over 80%, which improves on the two previously discussed routes. In addition, this route has the advantage over those previously discussed in that it does not require any time consuming purification steps.



**Figure 7. Synthetic route to AMD3100 utilising bis-aminal chemistry.**

### 1.3.3 Binding of AMD3100 to CXCR4

Bicyclams inhibit HIV replication by binding to CXCR4, the co-receptor used by X4 strains for cell entry. De Clercq *et al.* and Bridger *et al.* have studied the structure-activity relationship of the bicyclams in detail and have concluded that two azamacrocyclic rings tethered by a para-substituted aromatic linker result in extremely potent anti-viral activity.<sup>101, 102, 109, 110</sup> Schwartz *et al.* have studied the molecular interactions of AMD3100 with CXCR4 in order to understand which residues are important for receptor binding.<sup>34</sup>

AMD3100 binding to CXCR4 in competition with <sup>125</sup>I-Met-CXCL12 in COS-7 cells showed an affinity of 74  $\mu$ M and also competed against <sup>125</sup>I-12G5 binding (Figure 8). In contrast to this, cyclam achieved an affinity of only 13  $\mu$ M and was unable to displace <sup>125</sup>I-12G5, even at mM concentrations.

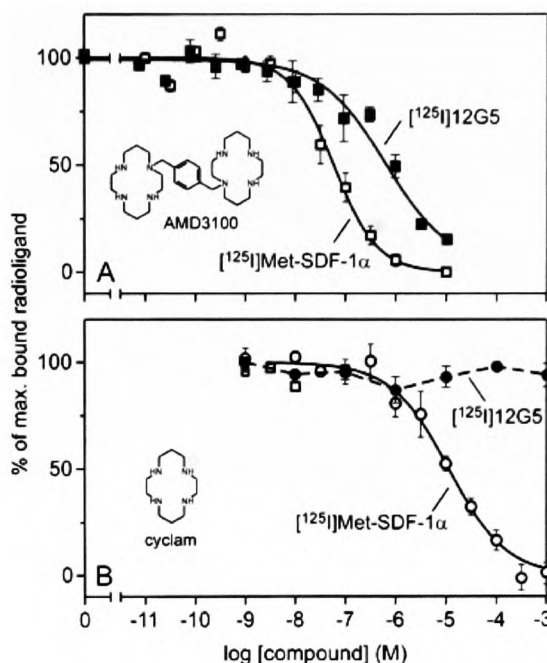


**Figure 8. Competition binding experiments using AMD3100 (A) or cyclam (B) (reproduced from the Journal of Biological Chemistry).<sup>34</sup>**

### 1.3.4 Effect of Asp and His Mutations on CXCR4 Binding

Receptor mutagenesis studies of histidine (His) and aspartate (Asp) residues in CXCR4 have been used to determine the main binding site in the CXCR4 receptor.<sup>34</sup> Histidine and aspartate residues were chosen based on the assumption that each cyclam ring was doubly protonated under physiological conditions and could interact via hydrogen bonding or electrostatic attraction. Therefore, His113, His203, His281 and His294 were individually mutated to alanine (Ala) and Asp171, Asp182, Asp193 and Asp262 were individually mutated to asparagine (Asn).

The affinity of cyclam determined in competition for <sup>125</sup>I-Met-CXCL12 binding was unaffected by each mutation except in the case of Asp171, located in the extracellular

region of TM-IV (Figure 2, section 1.1.4). This mutation led to a 30-fold decrease in the binding of cyclam (Figure 9b).

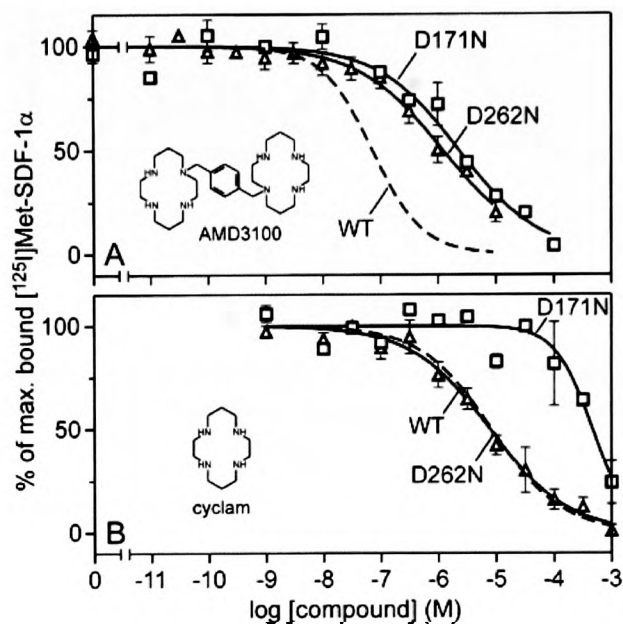


**Figure 9. Effect of Asp to Asn substitution at positions 171 and 262 in CXCR4 on (A) AMD3100 and (B) cyclam competition binding for CXCL12 (SDF-1 $\alpha$ ) binding (reproduced from the Journal of Biological Chemistry).<sup>34</sup>**

AMD3100 binding was affected by the mutation of both Asp171 and Asp262, located in the extracellular region of TM-VI, but not significantly by any other mutation (Figure 9a). In addition, AMD3100, like cyclam, was unable to compete for <sup>125</sup>I-12G5 binding (Figure 10).

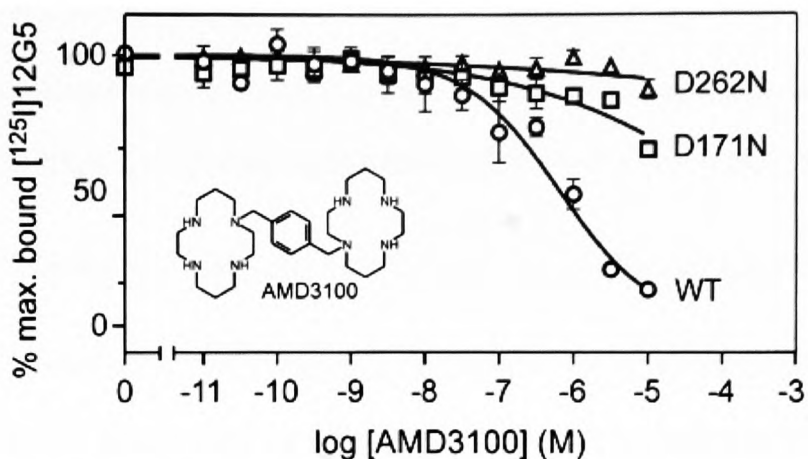


**Figure 10. Effect of Asp to Asn substitution at positions 171 and 262 in CXCR4 on competition for 12G5 binding (reproduced from the Journal of Biological Chemistry).<sup>34</sup>**

### 1.3.5 Binding Model of AMD3100

The 'free' cyclam ring has an overall 2+ charge under physiological conditions.<sup>111</sup> It has also been reported that the protonated cyclam can form direct, hydrogen-bonded stabilised complexes with carboxylate groups.<sup>112</sup> As previously mentioned, Asp171 is important for cyclam and AMD3100 competition binding with CXCL12 for the CXCR4 receptor. AMD3100 binding to CXCR4 was also dependent on Asp262. Cyclam could bind to Asp262 but with very low affinity relative to Asp171. When Asp171 is eliminated (in the D171N mutation) the affinity decreases to 400  $\mu$ M, which could represent the affinity of cyclam to Asp262. However, this could not be confirmed as the expression level of the D171N/D262N double mutation was too low.

In conclusion, given the fact that AMD3100 binding is dependent on both Asp171 and Asp262 and can interact with carboxylate groups it is thought that one cyclam ring binds to Asp171 and another one to Asp262.

### 1.3.6 Binding Model of Metal Complexes of AMD3100

Este *et al.* have shown that the incorporation of one or more transition metal ions into the macrocyclic rings of AMD3100 alters binding affinity to CXCR4 in the order:



Although other studies have suggested that the free ligand of AMD3100 has a higher binding affinity than its copper(II) complex, the zinc(II) complex increases binding affinity by between 6 to 36-fold depending on the radiolabelled ligand used.<sup>34, 114</sup> Additionally, it has been suggested that the increased binding affinity of transition metal complexes could arise from a direct coordination interaction from only one macrocyclic ring with Asp262 (Figure 11).<sup>114</sup>

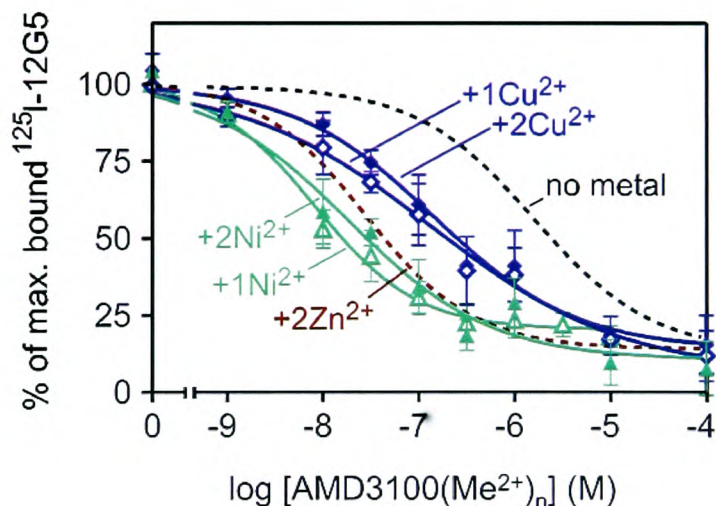


**Figure 11. Effect of incorporation of one (open symbols) or two (closed symbols) nickel(II) or copper(II) ions in AMD3100 on wild-type CXCR4 (reproduced from Biochemistry).<sup>114</sup>**

This is supported by the data presented in Figure 12, which shows that the metal enhancement can be eliminated by Asp262 mutation. Together, these data confirm that Asp262 is essential for binding but the interaction with Asp171 is less well defined. It is possible that the receptor binding pocket may only allow the optimisation of one coordination interaction. Alternatively, hydrogen bonding interactions with the secondary amine nitrogen atoms of the metal complex may also be important. For example, a trans-III configuration can potentially form up to three hydrogen bonds with carboxylate oxygen atoms.<sup>115</sup>

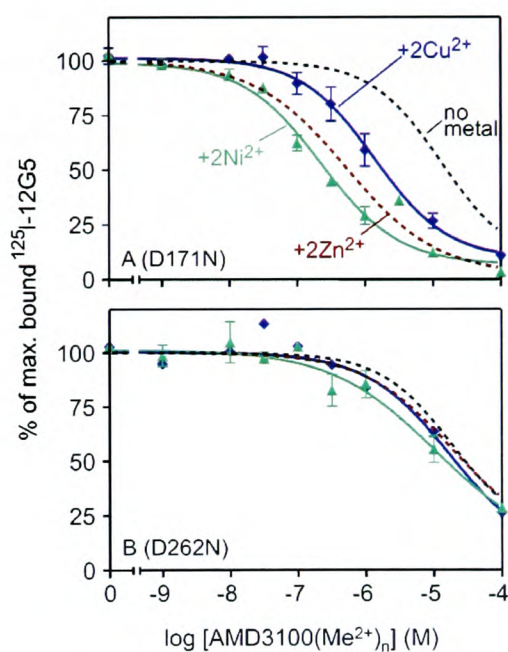


**Figure 12. Effect of incorporation of two zinc(II), nickel(II) or copper(II) ions in AMD3100 in competition with  $^{125}\text{I}$ -12G5 mAb in mutants (a) Asp171 and (b) Asp262 CXCR4 receptor (reproduced from Biochemistry).<sup>114</sup>**

### 1.3.7 Lysozyme Adducts of AMD3100 Complexes

Sadler and co-workers have reported solid state structures of protein adducts of AMD3100 complexes with copper(II) and nickel(II) respectively.<sup>116, 117</sup> The CXCR4 receptor has yet to be crystallised, and therefore lysozyme was used as a model. Lysozyme was chosen as it is readily crystallised and the active site contains carboxylates which are important residues in the binding of macrocyclic complexes to CXCR4.

$[\text{Cu}_2\mathbf{2}]^{4+}$  binds to lysozyme in two different sites with both macrocycles adopting trans configurations.<sup>116</sup> In one of the binding sites, both direct coordination (Cu-O 2.70 Å) to Asp101 and hydrophobic interactions to Trp62 and Trp63 residues are important. In the second binding site, hydrophobic interactions towards Trp123 dominate. Interestingly, no electron density was observed for the aromatic linker in the crystal structure, indicating that the two cyclam units identified in the two binding sites come from two separate molecules.

In a similar fashion to  $[\text{Cu}_2\mathbf{2}]^{4+}$ , the nickel(II) complex of AMD3100 has the two same binding sites on lysozyme as found in the copper(II) adduct.<sup>117</sup> In the first binding site, the nickel(II) coordinates directly to Asp101 and the macrocycle adopts a trans configuration which is close to Trp62 and Trp63. The macrocycle in the second binding site again adopts a trans configuration which interacts via hydrophobic stacking to Trp123. There was also evidence of a third binding site which was due to uncomplexed nickel(II) binding to Asp52. The free nickel(II) was proposed to arise due to the low pH (4.5) of the medium.

As a result of these studies, it has been suggested that tryptophan residues could also be important in the binding of metal complexes of AMD3100 to CXCR4 as they are involved in their binding to lysozyme.

## 1.4 Therapeutic Potential of AMD3100

The role of the CXCR4/CXCL12 axis in the pathogenesis and aetiology of several diseases has been previously discussed (section 1.1). As a result, AMD3100 has been evaluated for its therapeutic effect against HIV, inflammatory conditions, a range of cancers as well as a stem cell mobiliser for transplant patients undergoing chemoradiotherapy.<sup>41, 52, 118-122</sup>

### 1.4.1 HIV Studies

Time of addition experiments, where anti-viral drugs are added at different times after infection, have been used to determine which stage of the virus replicative cycle is affected by AMD3100.<sup>123</sup> A stage between virus adsorption and reverse transcription was found to be affected by AMD3100. Therefore, AMD3100 must act at HIV fusion-uncoating and does not affect the binding of the virus to the CD4 receptor. AMD3100 works by blocking viral entry once the virus has become cell bound. Este *et al.* suggested that the viral envelope gp120 was important in the anti-HIV activity of AMD3100.<sup>124</sup> In order to confirm this, viral resistance to AMD3100 was developed by repeated passages of the virus in the presence of AMD3100. The resistant virus would be expected to show several mutations across the gp120, if it was indeed important in the cell entry process. It took more than sixty passages (300 days) in MT-4 cells for the virus to become 400-fold resistant to AMD3100. Analysis of the resistant virus showed several mutations over the whole of the gp120 but mostly in the V3 loop. Substitution of amino acids close to the disulphide bridges of the V3 and V4 loops have shown that the whole of the gp120 (as opposed to



certain amino acids in its 3D structure) is responsible for the resistance and sensitivity profile of HIV strains to AMD3100.<sup>125</sup>

AMD3100 was developed over a decade ago as a potent, selective inhibitor of HIV but not simian immunodeficiency virus (SIV) replication. This was initially surprising until it was discovered that SIV solely uses CCR5 to infect host cells.<sup>126</sup> AMD3100 is potent in the nanomolar (1-10 nM) concentration range against HIV, showing a selectivity index of > 100,000.<sup>123</sup> In addition, AMD3100 is non-toxic up to 500  $\mu$ M and shows activity against a variety of X4 but not R5 viral strains.<sup>127, 128</sup> Furthermore, AMD3100 has been found to be active against some R5/X4 viral strains, which can use either receptor for cell entry.<sup>129-132</sup>

AMD3100 has proven to be active against X4 strains such as III<sub>B</sub> (IC<sub>50</sub> 0.02  $\mu$ M) and ROD, but is totally ineffective against R5 strains (Table 3).<sup>129</sup> This shows the specificity of AMD3100 to CXCR4. In addition to these data, AMD3100 has also been shown to reduce syncytia formation in HeLa cells infected with feline immunodeficiency virus (FIV) at a concentration of 0.1  $\mu$ M.<sup>133</sup> In another report, AMD3100 blocked syncytium formation and single-cell apoptosis in a dose dependent manner. The IC<sub>50</sub> values were in the range 0.009 to 0.24  $\mu$ g/mL (data not presented).<sup>134</sup>

HIV-strain	Co-receptor used	IC <sub>50</sub> / ng/mL	
		AMD3100	CXCL12
HIV-1 III <sub>B</sub>	CXCR4	2	20
HIV-1 RF	CXCR4	5	50
HIV-1 NL4-3	CXCR4	3	100
HIV-2 ROD	CXCR4	7	55
HIV-1 BaL	CCR5	> 25000	> 1000
HIV-1 SF-162	CCR5	> 25000	> 1000
HIV-1 ADA	CCR5 (CCR2b, CCR3)	> 25000	> 1000
HIV-1 JR-FL	CCR5 (CCR2b, CCR3)	> 25000	> 1000

**Table 3. AMD3100 inhibition of various HIV strains.**<sup>129</sup>

Moreover, [Zn<sub>2</sub>]<sup>4+</sup> displays an activity 6-fold greater than AMD3100 as an anti-HIV agent. A further study found that the zinc(II) and nickel(II) complexes of AMD3100 reduced syncytia formation in FIV infected cells with an IC<sub>50</sub> of 0.007 µg/mL and 0.03 µg/mL respectively (AMD3100 0.055 µg/mL).<sup>133</sup> Therefore, [Zn<sub>2</sub>]<sup>4+</sup> was up to 8-fold more potent than AMD3100.

#### 1.4.2 Clinical Studies

The first human study with AMD3100 was conducted in order to determine the safety, bioavailability and single dose pharmacokinetics of AMD3100 from 1-160 µg/kg in healthy volunteers.<sup>135</sup> The drug was well tolerated in all patients with 50% of individuals having mild side effects of a gastrointestinal nature. AMD3100 was well absorbed following subcutaneous injection (87% bioavailability); however, no drug was detectable in the blood stream following oral dose. Pharmacokinetic profiles were found to be dose dependent with an estimated half-life of 3.6 hours. In addition, it was observed that most patients experienced a transient, dose dependent increase in the white blood cell count within six hours of infusion. It was later confirmed that AMD3100 dose-dependently mobilised stem cells from the bone marrow.<sup>2</sup>

Phase II clinical trials were carried out to evaluate AMD3100 for its safety, pharmacokinetics and anti-viral activity in HIV patients.<sup>136</sup> Forty patients with a high viral load ( $> 5000$  copies/mL) of HIV RNA were enrolled with different HIV-phenotypes (30% SI, NSI 45% and 25% unknown). The drug was injected in doses over ten days by continuous intravenous infusion, with doses increasing from an initial  $2.5 \mu\text{gkg}^{-1}\text{h}^{-1}$  to a maximum of  $160 \mu\text{gkg}^{-1}\text{h}^{-1}$ . Most patients who received the higher dose ( $80\text{-}160 \mu\text{gkg}^{-1}\text{h}^{-1}$ ) had paresthesias and one patient ( $5 \mu\text{gkg}^{-1}\text{h}^{-1}$ ) suffered serious, possibly drug related thrombocytopenia. In addition, two patients ( $40 \mu\text{gkg}^{-1}\text{h}^{-1}$  and  $160 \mu\text{gkg}^{-1}\text{h}^{-1}$ ) had unexpected (but not serious) premature ventricular contractions; however, it was later determined that these patients had had previous cardiac complications.

Overall, only one patient receiving the highest dose ( $160 \mu\text{gkg}^{-1}\text{h}^{-1}$ ) had a significant ( $0.9 \log_{10}$  copies/mL) HIV RNA decrease after day eleven. It was subsequently found out that this patient had the X4 viral strain and was years into his HIV infection. This finding shows that in future, more stringent examination of past medical records, virus strain and time into infection needs to be carried out in order to correctly determine the efficacy and effectiveness of anti-HIV drugs. Moreover, at the time of the clinical trials, the mode of action of AMD3100 was not fully understood. Further testing of AMD3100 as an anti-HIV drug was discontinued in favour of orally available alternatives such as AMD070.<sup>137</sup>

## 1.5 Characteristics of Cyclam & Bicyclam Complexes

The role that cyclam complexes play in medicine has been reviewed by Liang and Sadler.<sup>138</sup> This section introduces some of the properties and characteristics of metal-cyclam and metal-bicyclam complexes, concentrating particularly on palladium(II) and zinc(II) complexes as the palladium(II) complexes have proven to be totally ineffective against HIV replication, whereas the zinc(II) complexes are some of the most potent anti-HIV candidates tested to date.<sup>139</sup>

### 1.5.1 General Properties

Cyclam is known to form highly stable metal complexes with the majority of the first row transition metals, for example, its nickel(II) complex has a demetallation half-life of around 30 years in acidic media.<sup>140</sup> The flexibility of the macrocycle means that it can adopt the most thermodynamically stable configuration for a chosen metal ion. Metal ions with an ionic radius of less than 0.75 Å afford the best fit into the macrocyclic cavity (e.g. first row transition metals).<sup>138, 141</sup> Once the metal is bound, each nitrogen atom becomes chiral, giving rise to six possible configurations that the macrocycle can adopt (Figure 13).<sup>142</sup>

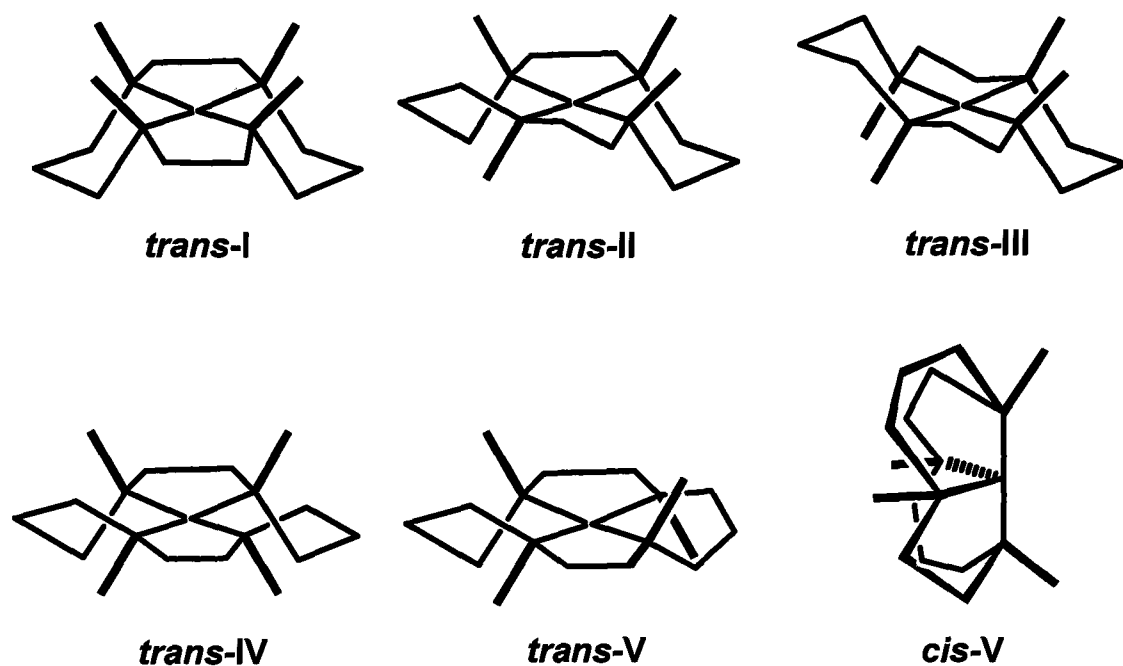


**Figure 13. Metal complexes of cyclam can adopt up to six configurations (five trans and a folded cis).**

The six-membered chelate rings adopt either chair or twist boat conformations and the five-membered rings are either gauche or eclipsed. The trans-III configuration has the lowest energy, but trans-I becomes increasingly favourable as the metal coordination number decreases from six to five to four respectively.<sup>143</sup> The trans-IV and trans-V configurations are the least stable as a result of the twist boat conformation of their six membered rings. However, the trans-V can fold along its N-N diagonal to give the cis-V configuration, where the six membered rings adopt the lower energy chair conformation. The configuration adopted by a complex will depend greatly on the coordination number and donor preference of the metal ion and also on the presence of any additional donor groups on the macrocyclic moiety.

### 1.5.2 Palladium(II) Complexes

Three palladium(II) complexes of cyclam,  $[\text{Pd1}](\text{ClO}_4)_2$ ,  $[\text{Pd1}]\text{Cl}_2$  and  $[\text{Pd}_2\text{1}](\text{OAc})_4$  have been reported by Sadler and co-workers.<sup>144</sup> They all adopt the most stable trans-III macrocyclic configuration in the solid state, with each palladium(II) ion being square planar (Figure 14).  $[\text{Pd1}]\text{Cl}_2$  solely adopts trans-III configuration in solution.

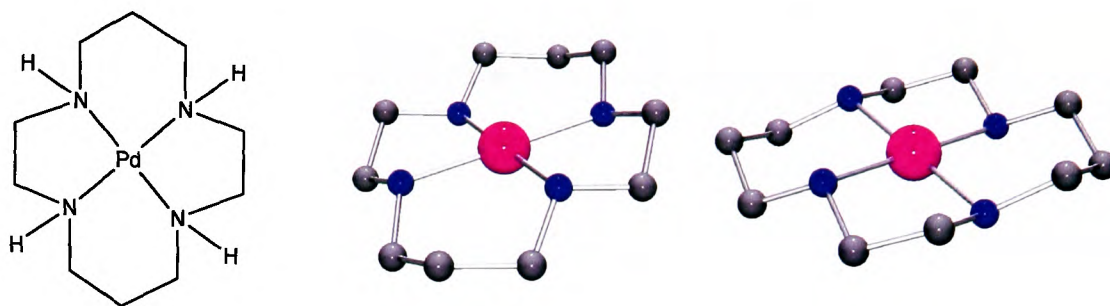


**Figure 14. Crystal structures of  $[\text{Pd1}](\text{ClO}_4)_2$  and  $[\text{Pd1}]\text{Cl}_2$ . Both adopt the trans-III configuration.**

In contrast to the previous two complexes,  $[\text{Pd1}](\text{OAc})_2$  exhibits weak hydrogen bonding between a macrocyclic amine proton and an acetate counter ion; however, there is no direct interaction between acetate and the metal ion itself, the shortest Pd–O distance being 4.0 Å.

The structure of  $[\text{Pd}_2\text{L}^1](\text{OAc})_4$  has also been reported (Figure 15).<sup>144</sup> This was serendipitously synthesised and contains two macrocycles linked via a carbon-carbon bond. The free chelator of this complex was the original bicyclam AMD1657, which proved to be an effective inhibitor of HIV viral replication. The macrocyclic rings both adopt the trans-III configuration in the solid state. The nickel(II) complex of this ligand is also known.<sup>104</sup>

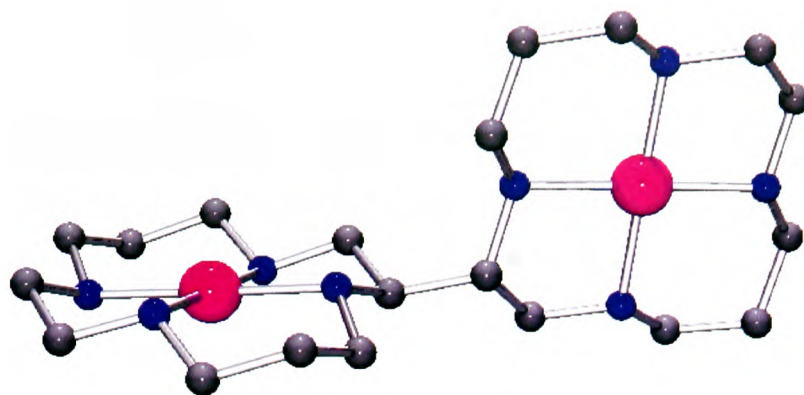


**Figure 15. Crystal structure of  $[\text{Pd}_2\text{L}^1](\text{OAc})_4$ .**

The fact that palladium(II) complexes of cyclam only adopt the trans-III configuration in the solid state and do not appear to change configuration in solution could explain their lack of anti-HIV activity. In addition, the preferred square planar geometry of the palladium(II) complexes would not allow binding to aspartate residues in the CXCR4 receptor, as this would involve the coordination number of the metal ion increasing from four to either five or six.

### 1.5.3 Zinc(II) Complexes

Sadler and co-workers have reported that cyclam selectively binds zinc(II) in preference to other metal ions under physiological conditions.<sup>145</sup> As the blood plasma concentration of free zinc(II) ions is relatively high (20  $\mu\text{M}$ ), it is not unreasonable to assume that the zinc(II) complex of AMD3100 can exist *in vivo*.<sup>146</sup> In this regard, AMD3100 can be thought of as a pro-drug where it is injected into the body as the free chelator, binds to zinc(II) in the blood stream and then interacts with CXCR4 as the metal complex.

Sadler and co-workers have studied the solid state and solution behaviour of a range of zinc(II) complexes of cyclam and AMD3100.<sup>146, 147</sup> The crystal structure of  $[\text{Zn1}(\text{OH}_2)_2]^{2+}$  (Figure 16) reveals an octahedral coordination environment with four equatorial zinc–nitrogen bonds (2.08–2.12 Å) and two axial zinc–oxygen bonds (2.27 Å). The macrocycle adopts the trans-III configuration in the solid state.

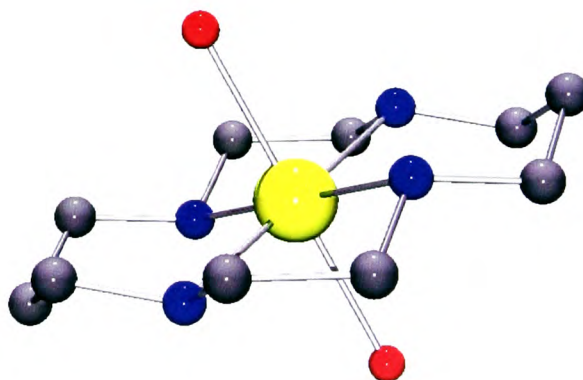


**Figure 16. X-ray crystal structure of  $[\text{Zn1}(\text{OH}_2)_2](\text{OAc})_2$ .**

However, in solution the trans-I, trans-III and cis-V configurations are all observed by proton NMR. Initially only trans-III is detected but over time, the cis-V and trans-I

configurations increase at the expense of *trans*-III. The equilibrium mixture consists of 45.3% *trans*-III, 42.8% *cis*-V and 11.9% *trans*-I. Altering the pH of the solution also affects the proton NMR spectrum of  $[\text{Zn1}(\text{OH}_2)_2]^{2+}$ . Increasing the pH leads to an increase in *trans*-I and a reduction in *cis*-V. *Trans*-III remains unchanged and is therefore not affected by pH.

Aqueous solutions of  $[\text{Zn1Cl}_2]$  have an equilibrium mixture of 11.2% *trans*-I, 79.6% *trans*-III and 9.2% *cis*-V. On addition of acetate, the amount of *trans*-III decreases and *cis*-V increases but *trans*-I stays constant as shown in Figure 17.

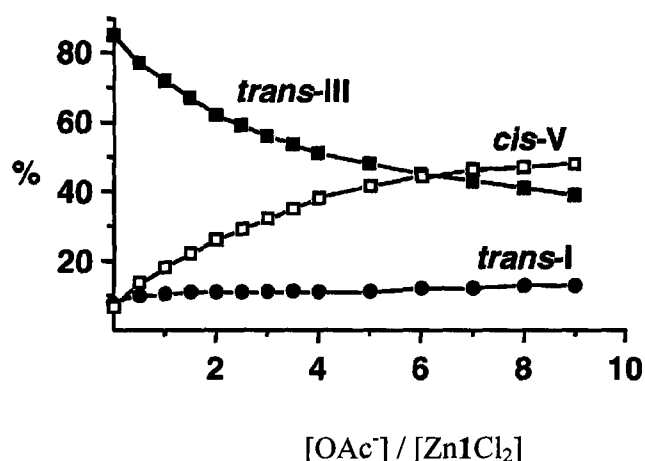


**Figure 17. Effect of acetate on the configuration of  $[\text{Zn1Cl}_2]$  in aqueous solution (reproduced from Chemistry - A European Journal).<sup>147</sup>**

The structure of  $[\text{Zn}_2\mathbf{2}](\text{ClO}_4)_4$  in the solid state has not been determined but in solution, the equilibrium mixture consists of 34% *trans*-III, 45% *trans*-I and 21% *cis*-V. Furthermore, the *cis*-V/*trans*-I configuration predominates. Addition of acetate to  $[\text{Zn}_2\mathbf{2}](\text{ClO}_4)_4$  changes the proton NMR spectrum. The effect of adding acetate is shown in Figure 18. The proportion of the *cis*-V/*cis*-V configuration increased from 0% to almost

19% on addition of four molar equivalents of acetate. The proportion of the cis-V/trans-I configuration increased from 26% to 38%.

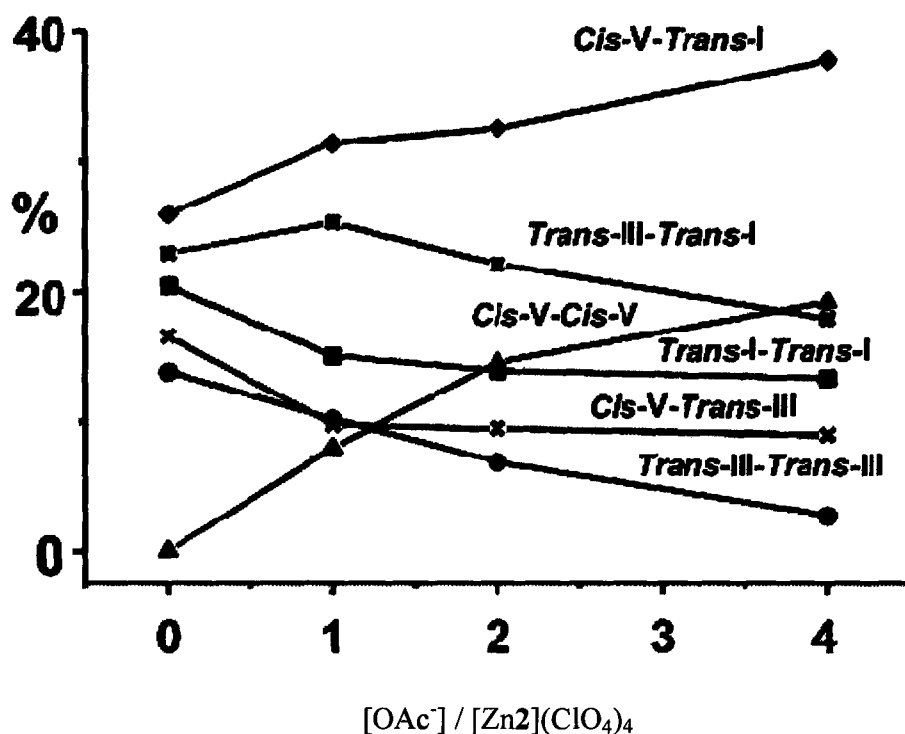


**Figure 18.** Effect of acetate on the configuration of  $[\text{Zn}_2\text{2}](\text{ClO}_4)_4$  in aqueous solution (reproduced from Chemistry - A European Journal).<sup>147</sup>

The crystal structure of  $[\text{Zn}_2\text{2}(\text{OAc})_2]^{2+}$  (Figure 19), the zinc(II) complex of AMD3100 has been reported.<sup>146</sup> The two macrocyclic rings adopt a cis-V configuration and are symmetrical with respect to the aromatic linker. The zinc(II) metal ion has a distorted octahedral geometry composed of two axial and two equatorial nitrogen atoms. Two bidentate acetate oxygen atoms also occupy equatorial coordination sites, completing the distorted octahedral geometry.

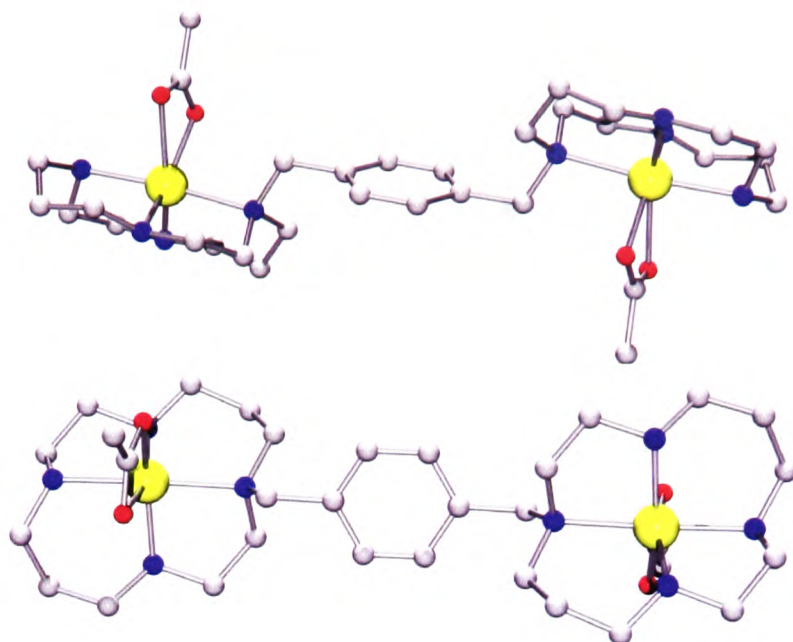


**Figure 19. X-ray crystal structure of  $[\text{Zn}_2(\text{OAc})_2]^{2+}$  viewed from two angles.**

On dissolution in aqueous solvent, the equilibrium mixture of  $[\text{Zn}_2(\text{OAc})_2]^{2+}$  is composed of 58% cis-V, 35% trans-I and 7% trans-III (cis-V/trans-I 44%, cis-V/cis-V 29%) (Figure 20).

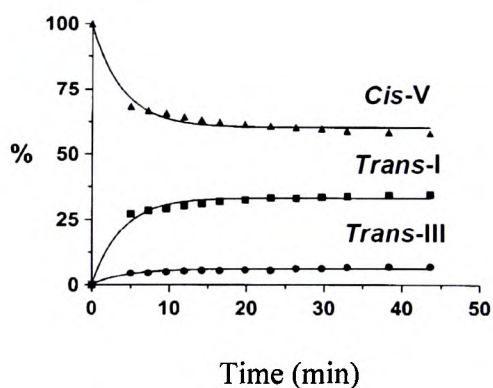


**Figure 20. Time dependent configurational changes of  $[\text{Zn}_2(\text{OAc})_2](\text{OAc})_2$  in aqueous solution (reproduced from the Journal of the American Chemical Society).<sup>146</sup>**

In conclusion, zinc(II) complexes of both cyclam and AMD3100 can adopt a variety of macrocyclic configurations in the solid state and in solution. The configuration of the macrocycle could play a vital role in the anti-HIV activity of AMD3100. For example, the ability of the macrocycle to adopt a cis-V configuration seems to improve antiviral potency; therefore, a possible reason why  $[\text{Zn}_2\text{2}(\text{OAc})_2]^{2+}$  is a potent anti-HIV agent is that it can adopt the cis-V configuration in solution.

The zinc(II) complexes discussed in this section bind strongly to acetate in order to complete a six-coordinate geometry, which could explain their impressive antiviral potency, as they would be expected to readily bind to aspartate residues in the CXCR4 receptor. However, if acetate binding were crucial to receptor binding, the cobalt(III) complex of AMD3100 would be expected to be more effective than  $[\text{Zn}_2\text{2}(\text{OAc})_2]^{2+}$  as it is known that cobalt(III) binds to acetate more effectively than zinc(II).<sup>39</sup> A plausible explanation of why the cobalt(III) complex of AMD3100 is not as effective as  $[\text{Zn}_2\text{2}(\text{OAc})_2]^{2+}$  is that cobalt(III) complexes are kinetically inert and therefore may not be able to adopt the cis-V configuration in solution. Alternatively, the ligand exchange could occur sufficiently rapidly to display any significant protein binding.

## 1.6 Configurationally Restricted Macrocycles

The previous section highlighted the importance of the configuration of the macrocyclic rings in relation to receptor binding. Configurationally restricted bis-macrocycles could be more potent in binding to CXCR4 when compared to AMD3100 as they would only present one shape to the binding site. In addition, the ability of the macrocycle to retain its metal ion will be important for *in vivo* studies as demetallation could have serious side effects due to the toxicity of the metal ion. Therefore, complexes possessing increased kinetic stability would be desirable.

Two configurationally restricted ligands have been used in this work and are discussed in later chapters (two and three respectively). An introduction to the chemistry which has been developed in order to prepare configurationally rigid transition metal complexes with increased kinetic stability is presented here.

### 1.6.1 Molecular Organisation

Macrocycles are important in transition metal coordination chemistry for two reasons. Firstly, they can mimic biological ligands and secondly they can increase the thermodynamic and kinetic stabilities of metal complexes. The factors leading to the stability of metal complexes containing macrocyclic ligands can be grouped together under the title ‘molecular organisation’.<sup>148</sup> Molecular organisation can be broken into two parts; *complementarity* and *constraint*.

Complementarity concerns the size, geometry and electronics between a metal centre and a ligand and has been defined by Lehn as “*a congruence of shape and size factors and*

*energetic or electronic compatibility between receptor and receptee, host and guest, or central atom and ligand*".<sup>149</sup> Complementarity is first order for complex stability; it is always present in stable complexes but has a maximum value and can only be improved upon so much (Figure 21).

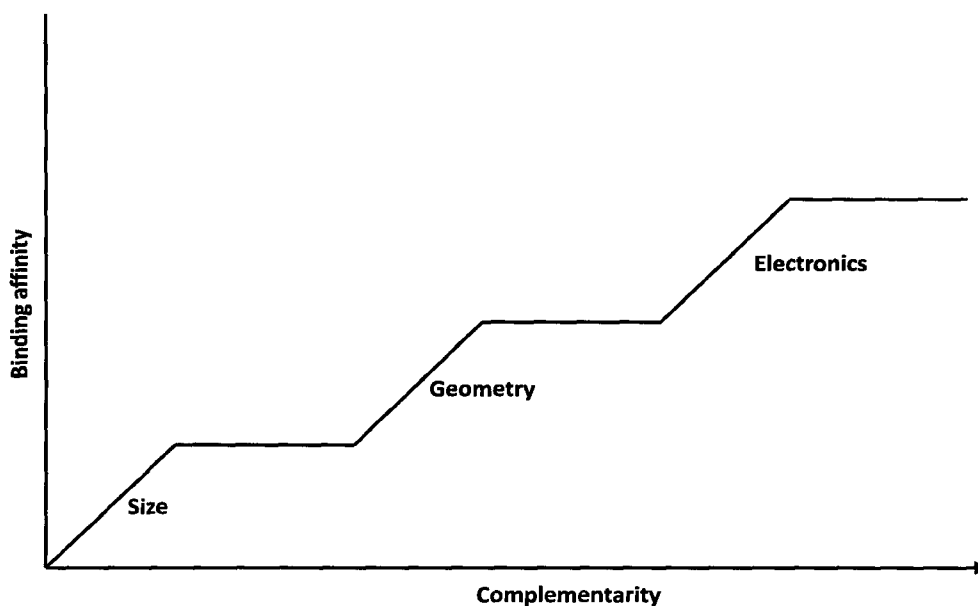


**Figure 21. The effect of complementarity on complex stability can only be increased to a certain level.**

Constraint deals with *topology* and *rigidity*. Constraint is said to be second order as it can be increased almost infinitely (Figure 22); constraint factors are the design factors that are employed in order to increase metal-ligand stability, provided that complementarity factors are maintained.<sup>150</sup> Topology concerns the interconnectedness of ligand donor atoms and can be explained by the chelate, macrocyclic and cryptate effects which are discussed in the following sections.<sup>151-153</sup>

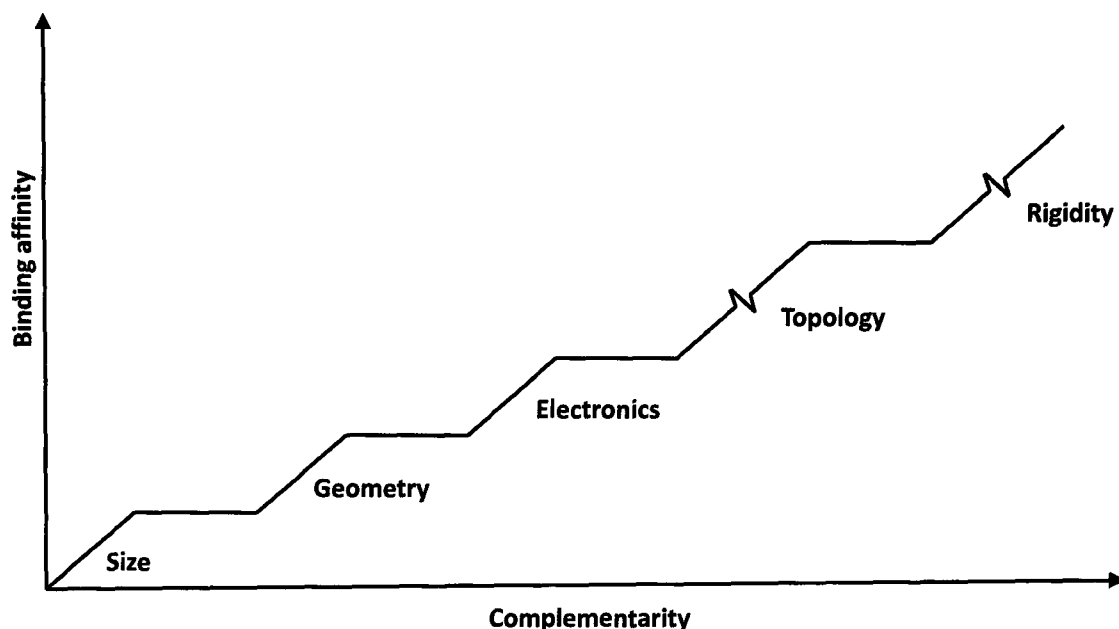


**Figure 22. Effect of topology and rigidity on complex stability.**

### 1.6.2 The Chelate Effect

The chelate effect was originally reported by Schwarzenbach.<sup>153</sup> A model system was used to explain that compounds containing a chelate ring are more stable than compounds with separate donor groups. The chelate effect can be dealt with thermodynamically by considering entropy. A chelated complex is higher in binding entropy compared to the binding entropy of separate donor atoms. This can be seen in Figure 23 where on the right hand side there are three components including the chelated complex and on the left hand side there are only two components including the mono-dentate amino ligand.

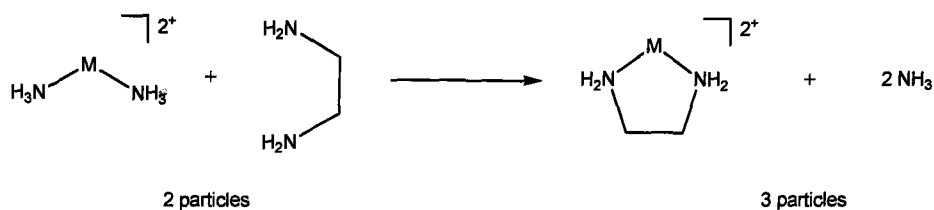


**Figure 23. Entropy in the chelate effect.**

### 1.6.3 The Macrocyclic Effect

The macrocyclic effect was reported by Cabbiness and Margerum.<sup>151</sup> They made copper(II) complexes of  $L^4$  and  $L^5$  (Figure 24) and found that the stability was much greater in the macrocyclic ligand compared to the linear ligand.

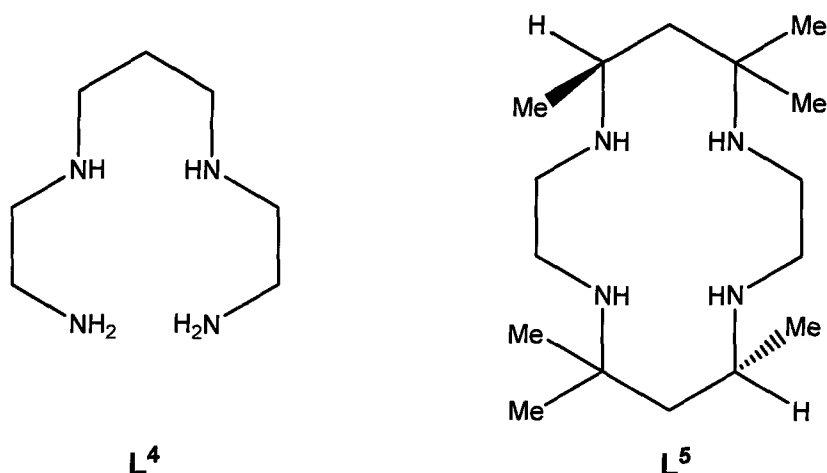


**Figure 24. Linear and cyclic ligands used by Cabbiness and Margerum.**

The macrocyclic effect can be explained by the dissociation of the first donor atom from a metal centre. In a polydentate ligand, the terminal donor atom dissociates from the metal in an  $S_N^1$  mechanism. This is not possible in macrocyclic ligands because the ring does not possess an end and therefore has no 'end donor group'. Therefore a more

complicated mechanism of dissociation must occur. The macrocyclic ligand rearranges itself and, in the process, weakens one of the metal-donor atom bonds (Figure 25).

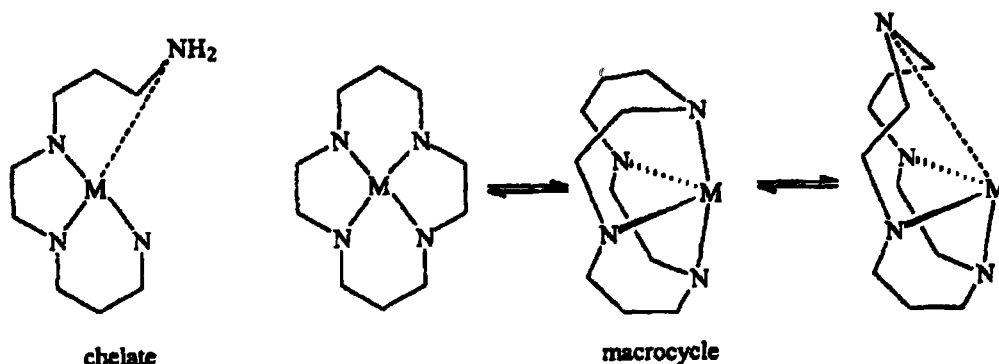


**Figure 25. First donor dissociation in chelate vs macrocycle (reproduced from Coordination Chemistry Reviews).<sup>150</sup>**

Ligand dissociation can then take place but the energy used in the rearrangement step means that dissociation is slow. The macrocyclic effect is due to the dissociation step, which is more hindered than binding. This stabilising effect is in addition to the previously mentioned chelate effect.

#### 1.6.4 The Cryptate Effect

The cryptate effect was reported by Lehn and Sauvage.<sup>152</sup> They had been working with [2]-cryptates, a class of macrobicyclic ligands containing alkali and alkaline earth metal centres. It was found that the potassium complex of  $L^6$  (Figure 26) was several orders of magnitude more stable than that of many organic ligands.

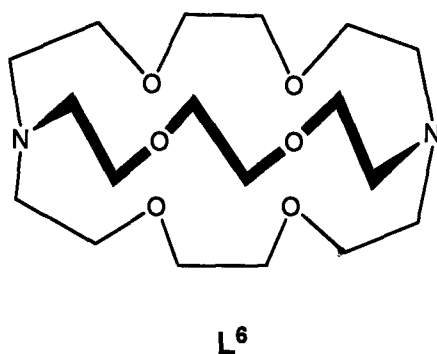


**Figure 26. Cryptate compound, L<sup>6</sup>, studied by Lehn and Sauvage.**

The addition of a second ring to a macrocycle enhances the stability more than if a second macrocycle was added to a complex. The origin of the cryptate effect has not yet been agreed but it is generally accepted that both entropic and enthalpic issues are the key to understanding this phenomenon.

### 1.6.5 Ligand Rigidity

Rigidity also plays a vital role in the three effects previously mentioned. However, the stabilising effects due to rigidity factors have not been well treated, either theoretically or experimentally. Two concepts have been developed in order to describe rigidity; *multiple juxtapositional fixedness* and *preorganisation*.<sup>154, 155</sup>

Multiple juxtapositional fixedness (MJF) was reported by Busch.<sup>154</sup> This theory addressed the rigidity of the ligand structure (i.e. donor fixedness) in the overall stability of complexes. MJF arises from the fact that stepwise donor atom dissociations from the metal centre are much slower in topologically complex ligands due to the lack of end groups.

The theory of preorganisation was developed by Cram *et al.* and describes the fact that ligands which are preformed in a size and geometry that are complementary to the

metal ion are more stable than ligands which are not.<sup>155</sup> If a ligand does not change its conformation upon metal binding it is said to be preorganised. Preorganisation is important as it increases the overall free energy of complexation. The entropic costs of complexation are said to be prepaid, as the preorganised ligand does not reorganise itself during complexation.

This prepayment of entropy in complexation explains why topologically more complex ligands form more stable complexes, provided that complementarity is maintained. Ligand rigidity is part and parcel of MJF and preorganisation and can be increased in order to get more stable complexes.

Ligands benefitting from the chelate, macrocyclic and cryptate effects are known and others have been synthesised in this work. The rigidity of the cyclam backbone can be increased by the addition of an ethylene linker. The kinetic stability imparted by the rigidity of their ligands should enable their transition metal complexes to remain intact *in vivo*, which is of great importance should the compounds ever be used in clinical studies. The synthesis and characterisation of the ligands used in this work is the subject of the following two chapters.

**Chapter 2. SYNTHESIS &  
CHARACTERISATION OF PIPERAZINO  
MACROCYCLIC COMPLEXES**

## 2.1 Side-bridged Tetraazamacrocycles

There are several methods that have been used in order to alter the structural characteristics of tetraazamacrocycles and their metal complexes. Here the structural effects of ring size, coordinating pendent arms and chemically modified macrocycles are introduced, concentrating particularly on rigidified macrocycles. The incorporation of an ethylene bridging moiety to the cyclam backbone can result in complexes of exceptional kinetic stability. The ethylene bridge can take two forms; firstly between two adjacent nitrogen atoms leading to a “side” bridge containing a piperazino unit (Figure 27) and secondly between non-adjacent nitrogen atoms which results in a “cross” bridge (chapter three).

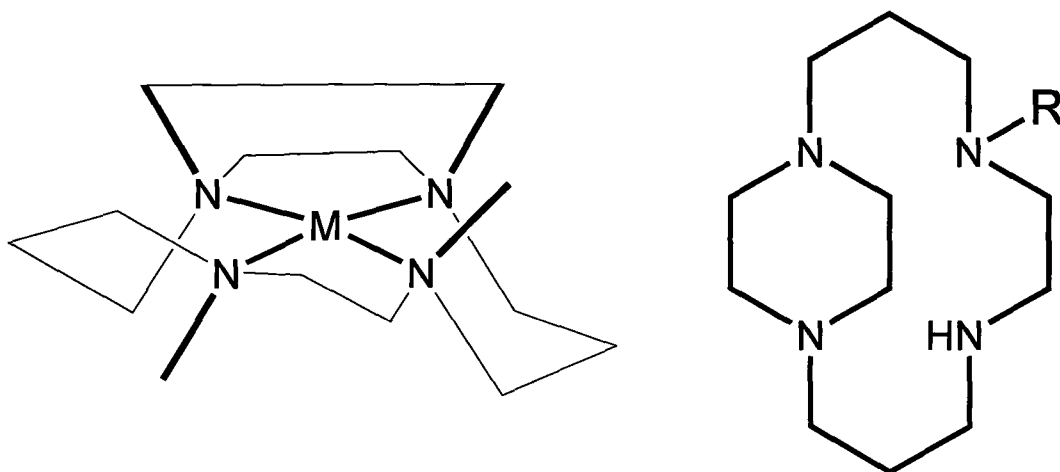


**Figure 27. Side-bridged macrocycle containing a piperazino moiety. Metal complexes adopt the trans-II configuration.**

The historical development of “side” bridged piperazino derivatives of cyclam and cyclen and a selection of their transition metal complexes are presented here. The synthetic methodology which has been used in order to incorporate these structurally modified

compounds into bis-macrocyclic metal complexes will also be discussed in detail along with their transition metal complexes. Finally, this methodology has additionally been applied to tris-macrocyclic compounds and the synthesis of a series of copper(II) and zinc(II) complexes of these ligands will also be presented.

Changing the ring size of a macrocyclic unit can result in a significant change in stereochemistry and coordination geometry. For example, the majority of metal cyclam complexes adopt the most thermodynamically stable trans-III configuration with an octahedral metal ion, whereas the 16 membered-macrocycle,  $L^7$ , allows the metal ion to be held in a tetrahedral geometry as a result of the more flexible macrocyclic cavity (Figure 28).<sup>156</sup>

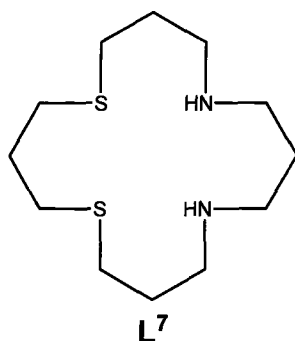


**Figure 28. 16-membered macrocycle,  $L^7$ .**

The degree of substitution at the coordinating amine also affects the structure of macrocyclic complexes. For example,  $[CuL^8]^{2+}$  assumes pentacoordinate geometry in aqueous solution but the less substituted  $[CuL^9]^{2+}$  is square planar (Figure 29).<sup>157</sup> The addition of pendent arms can also affect the structural properties of macrocyclic metal complexes.

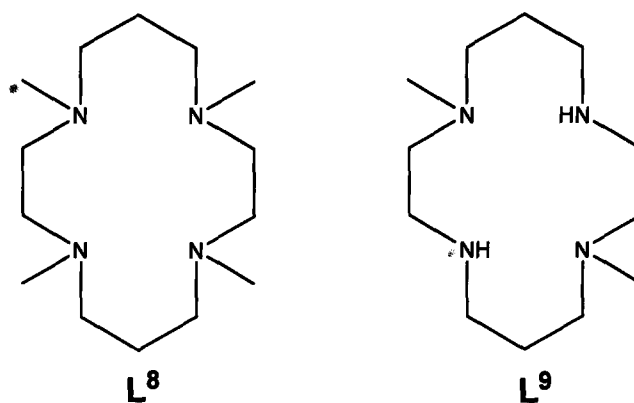


**Figure 29. Tetra-methyl ( $L^8$ ) and di-methyl ( $L^9$ ) cyclam.**

A further factor which can be employed in order to affect the structure of macrocyclic complexes is the addition of a bridging unit between two of the nitrogen atoms. This bridging unit can also impart structural rigidity to the complex and results in so-called configurationally “reinforced” macrocycles.

### 2.1.1 Synthetic Development of Side-bridged Cyclam

The first side-bridged derivative of cyclam was synthesised by Wainwright nearly 30 years ago.<sup>158</sup> This low yielding method involved the direct reaction of cyclam with dibromoethane (Figure 30). The yield and purity of this reaction were both poor due to the fact that the reaction is self-limiting. The acid formed after substitution protonates the unreacted amine and results in quarternisation.

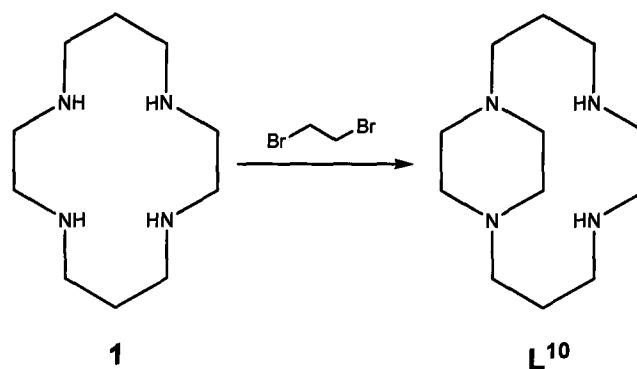


**Figure 30. Wainwright's synthesis of side-bridged cyclam,  $L^{10}$ .**

Another route to  $L^{10}$  was developed by Yamamoto and Maruoka.<sup>159</sup> They made use of the glyoxal condensate of cyclam, **3**, and reduced this using diisobutyl aluminium hydride (DIBAL) (Figure 31). This proved to be a much cleaner route together with a more satisfactory yield compared to Wainwright's original synthesis.

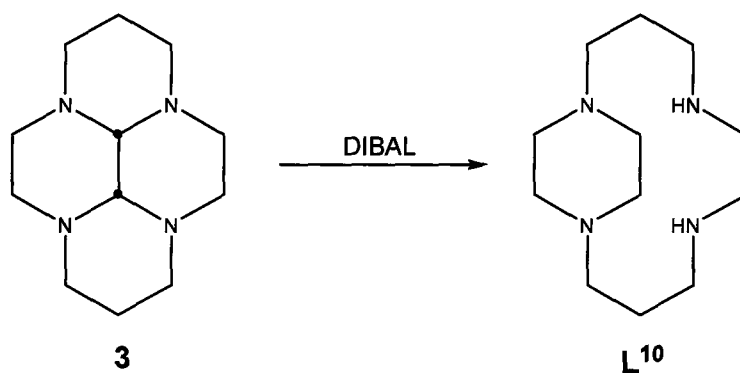


**Figure 31. Yamamoto and Maruoka's synthesis of side-bridged cyclam,  $L^{10}$**

One of the drawbacks of the synthetic strategies covered so far is that they cannot easily be adapted to give macrocycles containing pendent arms. Pendent arms can change the properties of metal complexes and they are also a necessary precursor in the synthesis of bis-macrocyclic compounds, such as AMD3100. This problem was solved by Kolinski who appended **3** with both methyl and benzyl pendent arms (Figure 32), where the

respective ammonium salt precipitates out of acetone with acceptable yields of around 60%.<sup>160</sup>

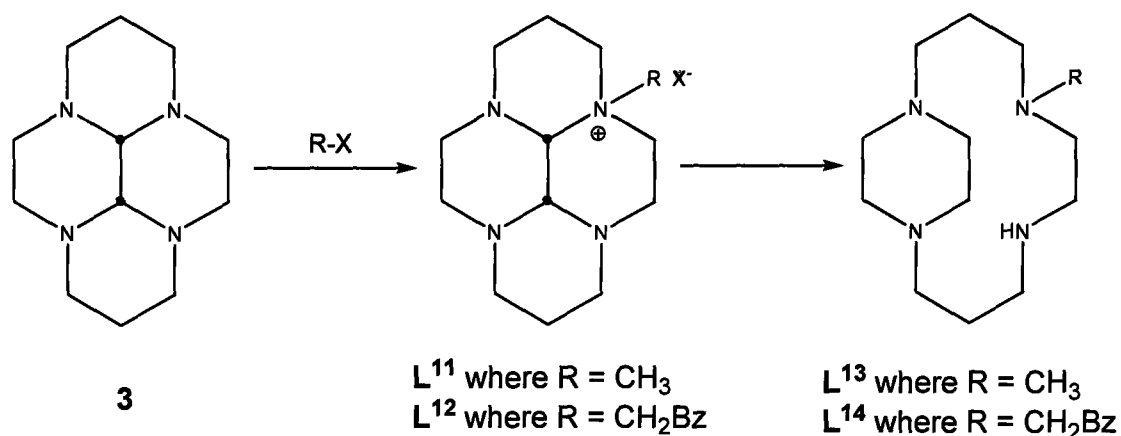


**Figure 32. Synthesis of side-bridged cyclam ( $\text{L}^{13}$  and  $\text{L}^{14}$ ) incorporating a pendent arm.**

Subsequent reduction of the ammonium salt with sodium borohydride results in the reinforced macrocycles  $\text{L}^{13}$  and  $\text{L}^{14}$ . Interestingly, the trans conformer of **3** does not react at all with sodium borohydride.

Kolinski also prepared the first side-bridged cyclam containing two pendent arms when he formylated the secondary amine of  $\text{L}^{13}$  under reductive amination conditions to give  $\text{L}^{15}$  (Figure 34).<sup>160</sup> Kaden expanded on this work and has made copper(II) and nickel(II) complexes of Kolinski's compounds as well as a further example of a bis-alkylated side-bridged macrocycle,  $\text{L}^{17}$  (Figure 33).<sup>161</sup> This route involved the reaction of cyclam with diethyl oxalate to give the bis-amide  $\text{L}^{16}$ . Subsequent acylation followed by reduction leads to  $\text{L}^{17}$  which contains only tertiary amine groups.

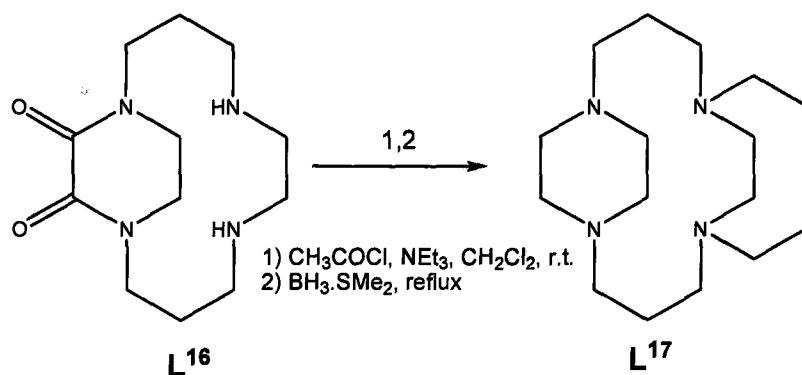


**Figure 33.** Synthesis of a side-bridged cyclam ( $\text{L}^{17}$ ) possessing two ethyl pendent arms.

### 2.1.2 Metal Complexes of Side-bridged Cyclam

Although there are examples of several cyclam ligands containing side bridges, there are relatively few structures of their transition metal complexes in the literature. A search of the CSD reveals that fourteen complexes have been reported in total consisting of eleven copper(II) complexes, two chromium(III) complexes and a sole zinc(II) complex. Three of the copper(II) complexes have been reported by Kaden and co-workers.<sup>161</sup> They have crystallised the copper(II) perchlorate complexes of ligands  $\text{L}^{15}$  and  $\text{L}^{17}$ , which are either four or five-coordinate including the coordination of a water molecule.

A wide library of side-bridged metal complexes containing a variety of pendent arms has been synthesised by the Archibald group following modifications of Kolinski's procedure. It is interesting to note that the alkylation pattern has an influence on the configuration of the macrocyclic backbone. For example, a mono-alkylated ligand (e.g.  $\text{L}^{13}$ ) gives the trans-II configuration whereas the bis-alkylated ligand (e.g.  $\text{L}^{17}$ ) results in the macrocycle adopting the unusual trans-IV configuration.

The copper(II) perchlorate complexes of  $L^{15}$  and  $L^{17}$  are both pentacoordinate, bonding to the four nitrogen atoms as well as an axial water molecule. The macrocyclic nitrogen atoms form almost perfect planes in both and the copper(II) centre sits out of the plane by 0.33 and 0.34 Å, respectively. The macrocycle takes up a trans-IV configuration where the two alkyl arms can be described as being cis to each other.

The copper(II)-nitrogen bond lengths in  $[CuL^{15}(OH_2)]^{2+}$  are in the range 1.94(1) to 2.09(1) Å. The fifth donor site is occupied by a solvent water molecule with a copper(II)-oxygen bond distance of 2.235(5) Å (Figure 34).

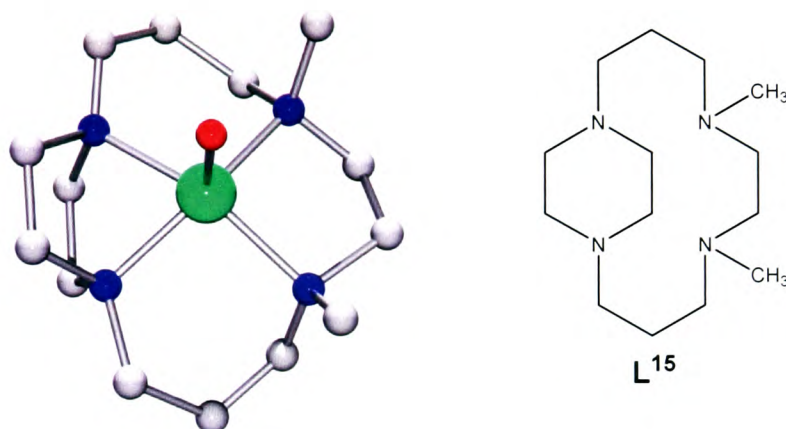


**Figure 34. X-ray crystal structure of  $[CuL^{15}(OH_2)]^{2+}$  <sup>161</sup>**

In the second example,  $[CuL^{17}(OH_2)]^{2+}$ , the copper(II)-nitrogen bond lengths are almost identical to the previous structure (2.034(2)-2.047(2) Å) as is the copper(II)-oxygen distance at 2.226(2) Å (Figure 35).

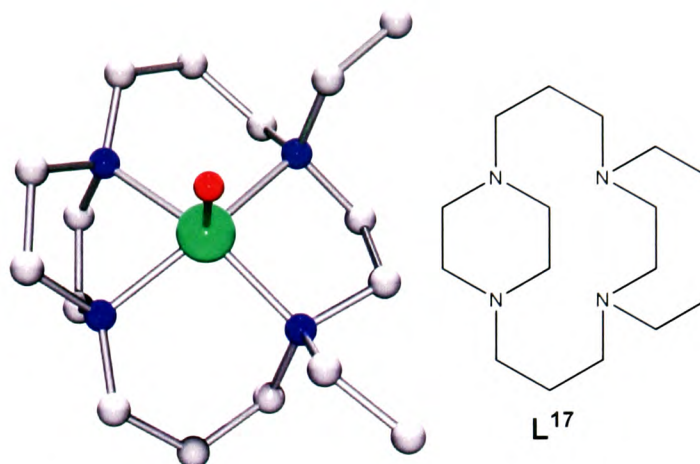


Figure 35. X-ray crystal structure of  $[\text{CuL}^{17}(\text{OH}_2)]^{2+}$ .<sup>161</sup>

### 2.1.3 Synthetic Development of Side-bridged Cyclen

Following the original preparation of side-bridged cyclam, the first cross-bridged example of the smaller macrocycle cyclen,  $\text{L}^{18}$ , was reported by Ramasubbu and Wainwright.<sup>162</sup> In an analogous manner to the synthesis of  $\text{L}^{10}$ , they reacted  $\text{L}^{18}$  directly with 1,2-dibromoethane with potassium hydroxide in benzene (Figure 36).

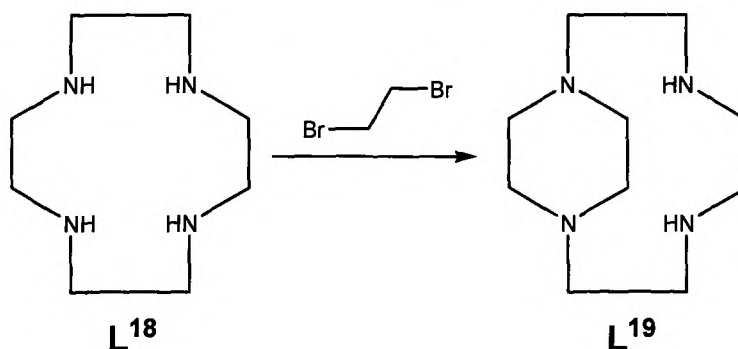
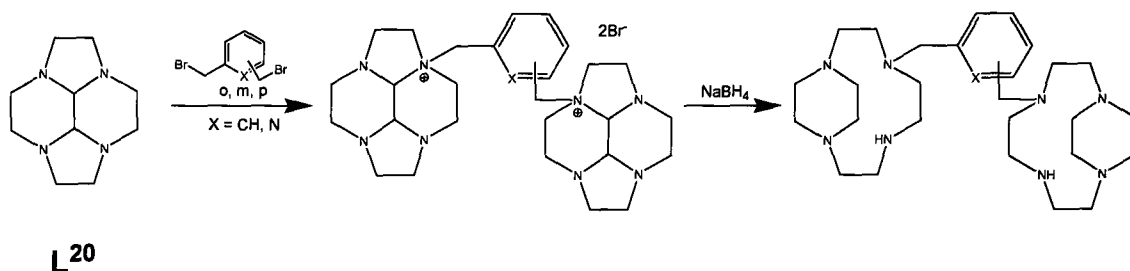


Figure 36. Synthesis of side-bridged cyclen,  $\text{L}^{19}$ .

Although no reaction yields are reported,  $\text{L}^{19}$  is the major product, in addition to a small amount of the di-bridged derivative.  $\text{L}^{19}$  could be separated from the minor impurity

by fractional sublimation. The ratio of 1,2-dibromoethane to cyclen had no effect on the product obtained. In contrast to the several side-bridged cyclam compounds, this remains the only side-bridged mono-cyclen compound in the literature, although there has been a bis-macrocyclic derivative reported recently.

Handel and co-workers have reported the synthesis of a range of bis-macrocyclic compounds containing side-bridged cyclen (Figure 37).<sup>108</sup>



**Figure 37. Synthesis of a side-bridged bis-cyclen ligand.**

This preparation provides a further indication of the utility of bis-aminal methodology in the synthesis of tetraazamacrocycles. The two step procedure starting from **L<sup>20</sup>** proceeds in overall yields ranging from 54% with the pyridine linker group upto 78% with the meta substituted aromatic linker.

#### 2.1.4 Metal Complexes of Side-bridged Cyclen

Although the preparations of copper(II), zinc(II), cadmium(II) and lead(II) complexes of **L<sup>19</sup>** have been claimed, it is only a single nickel(II) complex which has received any discussion in the literature.<sup>163</sup> Given the number of metal complexes of ethylene bridged cyclam ligands, it is surprising that these compounds have not attracted the same level of attention. The nickel(II) perchlorate complex of **L<sup>19</sup>** was initially prepared by Ramasubbu

and Wainwright although the crystal structure was reported later by Hancock *et al.*<sup>162, 163</sup> No reaction yields<sup>o</sup> were reported for the complexation, although the UV-vis spectrum consisted of a spectral band centred at approximately 400 nm, indicating a square planar coordination geometry in aqueous solution. The single crystal X-ray structure of  $[\text{NiL}^{19}]^{2+}$  confirms the square plane with nickel(II)-nitrogen bond lengths in the range 1.852(7) to 1.877(7) Å (Figure 38). In addition, the nickel(II) centre sits out of the mean nitrogen plane by 0.2 Å. A further interesting aspect to note is that the piperazino unit adopts an almost perfect boat conformation in the solid state.

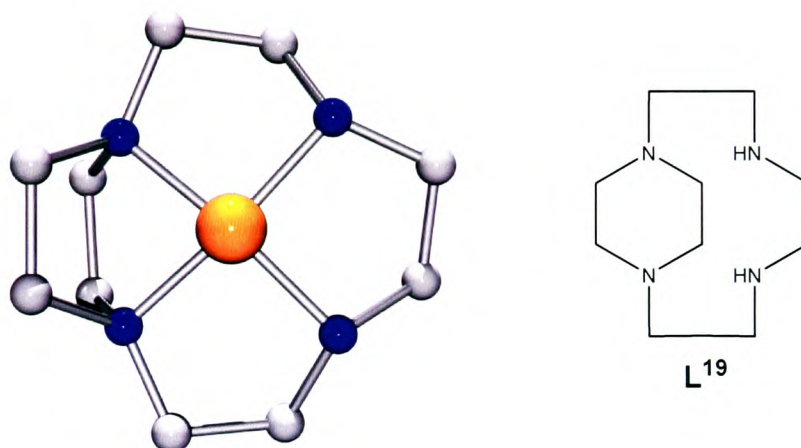


**Figure 38. X-ray crystal structure of  $[\text{NiL}^{19}]^{2+}$ .**<sup>163</sup>

## 2.2 Synthetic Aims

The prior synthesis of side-bridged macrocycles by other research groups has been discussed but these methods had not been applied to bis-macrocycles, although the bis-cyclen compound has since been reported (2006).<sup>108</sup> It has been known since the mid 1990s that bis-macrocyclic compounds (such as AMD3100) are effective antagonists of the CXCR4 receptor. However, the bis-macrocycles reported in the literature contain cyclam rings and are therefore not configurationally restricted. They can adopt a number of configurations in solution depending on factors such as pH and acetate concentration.<sup>146</sup> Therefore, a configurationally restricted bis-macrocycle could prove to have beneficial properties with regards to receptor binding as it would only present a single shape to the receptor binding site.

In order to synthesise configurationally restricted bis-macrocycles, a modification of the synthetic route reported by Handel (chapter one, section 1.3.2) was proposed (Figure 39). The proposed route makes use of the *cis* conformer of glyoxal cyclam and Kolinski's sodium borohydride reduction.

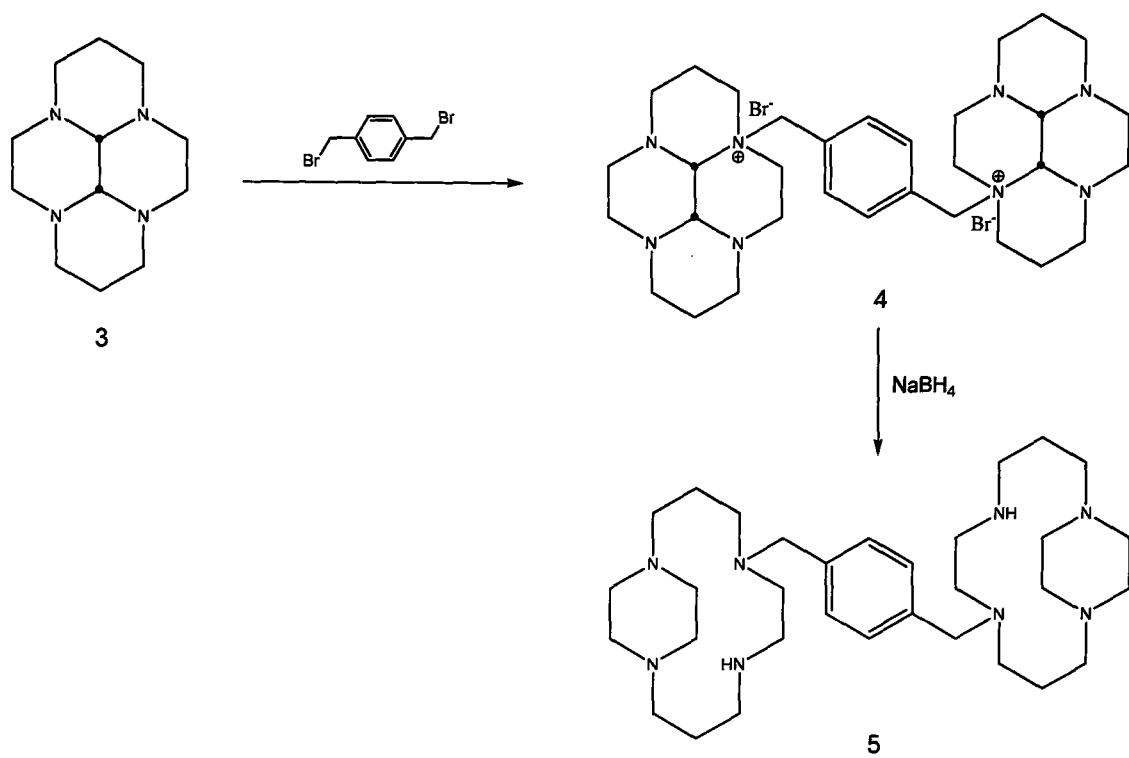


**Figure 39. Proposed synthetic route to bis-side-bridged cyclam, 5.**

This route has proved to be both successful and more importantly repeatable. The synthetic route proceeds in overall yields of around 50% for the two step process and is the subject of the next section.

## 2.3 Synthetic Discussion

### 2.3.1 Bis-aminal Precursors

The glyoxal condensate of cyclam, **3**, was prepared according to literature methods and proceeds in a quantitative yield.<sup>164</sup> The reaction is carried out at relatively low temperature ( $-10^{\circ}\text{C}$ ) to prevent the formation of oligomers. A crystal structure of **3** has previously been reported (Figure 40).<sup>165</sup> The rigid bis-aminal bridging moiety fixes the geometry of the macrocycle with the aminal protons located *cis* to each other. This results in the folded geometry of the macrocycle where each ring system adopts a chair conformation. Therefore, there are two endo nitrogen lone pair of electrons which face into the ligand fold and two exo nitrogen lone pairs of electrons which face out of the ligand fold (Figure 40). Consequently, the exo lone pairs are reactive towards electrophilic attack whereas the endo lone pairs are unreactive as they are protected by the cavity of the ring system.

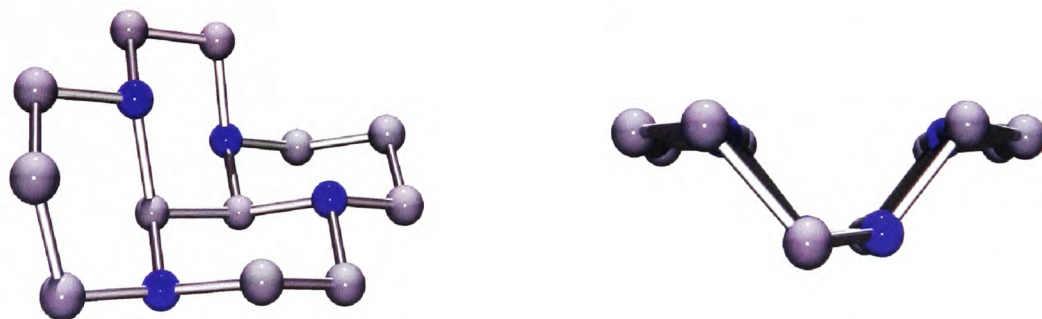


**Figure 40. X-ray crystal structure of **3** from two different views.**<sup>165</sup>

Single crystals of protonated **3** with two different counteranions have been grown during this work. The first example containing a perchlorate anion is shown in Figure 41.

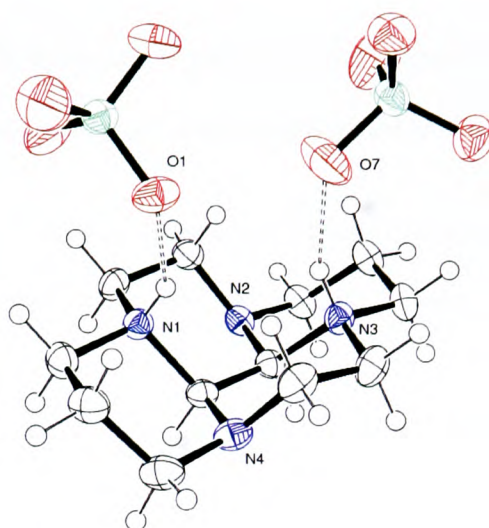


**Figure 41. X-ray crystal structure of 3.2HClO<sub>4</sub>.**

In accord with the previously reported structure, each six membered ring adopts a chair conformation and the aminal hydrogens are located cis to each other.<sup>165</sup> The protonated nitrogen atoms form two separate hydrogen bonds with perchlorate counter anions. The average N–H $\cdots$ O distance is 2.795 Å and the average O $\cdots$ H distance is 1.986 Å.

	Bond length / Å		Bond angle / °		Bond angle / °
C(1)-N(1)	1.504(2)	N(1)-C(1)-C(2)	108.51(13)	C(1)-N(1)-C(10)	111.99(13)
C(7)-N(4)	1.467(3)	N(4)-C(7)-C(6)	109.08(15)	C(1)-N(1)-C(11)	111.09(12)
C(8)-N(4)	1.468(3)	N(4)-C(8)-C(9)	113.01(17)	C(10)-N(1)-C(11)	109.05(14)
C(10)-N(1)	1.508(2)	N(1)-C(10)-C(9)	109.86(15)	C(11)-N(4)-C(7)	113.93(16)
C(11)-N(4)	1.424(2)	N(4)-C(11)-C(12)	112.75(14)	C(11)-N(4)-C(8)	112.02(15)
C(11)-N(1)	1.538(2)	N(4)-C(11)-N(1)	112.35(13)	C(7)-N(4)-C(8)	114.78(15)

**Table 4. Selected bond lengths and angles for 3.2HClO<sub>4</sub>.**

The second example with a zinc(II) chloride anion was grown via slow diffusion from methanol (Figure 42). The unit cell reveals one cyclam unit together with a zinc(II) chloride counterion. The zinc(II) centre adopts a tetrahedral geometry with a coordinated water molecule completing the tetrahedron. Additionally, the water forms a hydrogen bond with one of the nitrogen atoms in the macrocycle, the O–H $\cdots$ N distance being 2.748 Å (O $\cdots$ H

distance 1.874 Å, Table 5). The two aminal hydrogen atoms are located cis to each other which is in agreement with the structure published by Gluzinski *et al.*<sup>165</sup> As expected, each of the four 6-membered rings adopt the chair conformation in the solid state.

The major difference between the two protonated crystal structures appears to be that the first one is di-protonated whereas the second is only mono-protonated with a  $[\text{ZnCl}_3(\text{OH}_2)]^-$  counter anion.

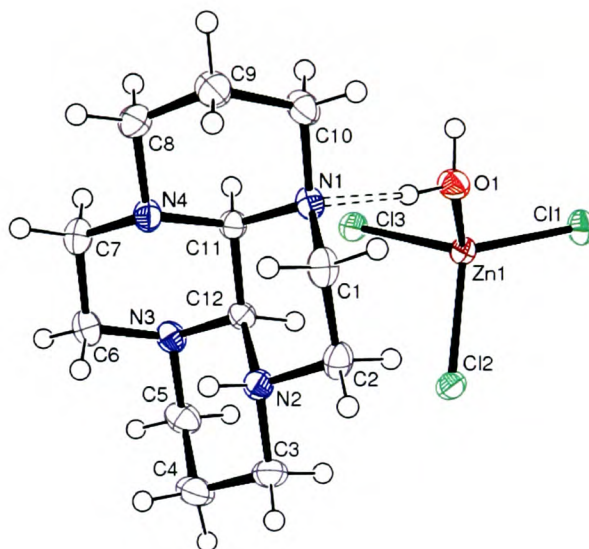


**Figure 42. X-ray crystal structure of 3.H[ZnCl<sub>3</sub>(OH<sub>2</sub>)].**

	Bond length / Å		Bond angle / °		Bond angle / °
C(1)-N(1)	1.477(2)	N(1)-C(1)-C(2)	109.44(15)	C(11)-N(4)-C(8)	108.91(16)
C(7)-N(4)	1.462(3)	N(4)-C(7)-C(6)	110.59(16)	C(7)-N(4)-C(8)	110.10(14)
C(8)-N(4)	1.477(2)	N(4)-C(8)-C(9)	111.26(17)	O(1)-Zn(1)-Cl(1)	110.03(4)
C(10)-N(1)	1.484(2)	N(1)-C(10)-C(9)	111.30(15)	O(1)-Zn(1)-Cl(3)	107.44(5)
C(11)-N(1)	1.467(2)	N(4)-C(11)-C(12)	112.39(15)	Cl(1)-Zn(1)-Cl(3)	117.34(2)
C(11)-N(4)	1.472(2)	N(4)-C(11)-N(1)	110.21(14)	O(1)-Zn(1)-Cl(2)	103.01(4)
Zn(1)-O(1)	2.0009(15)	C(1)-N(1)-C(10)	112.17(14)	Cl(1)-Zn(1)-Cl(2)	112.284(18)
Zn(1)-Cl(1)	2.2227(5)	C(1)-N(1)-C(11)	109.50(15)	Cl(3)-Zn(1)-Cl(2)	105.65(2)
Zn(1)-Cl(3)	2.2574(5)	C(10)-N(1)-C(11)	111.31(16)		
Zn(1)-Cl(2)	2.2873(5)	C(11)-N(4)-C(7)	109.52(15)		

**Table 5. Selected bond lengths and angles for 3.H[ZnCl<sub>3</sub>(OH<sub>2</sub>)].**

Alkylation with para-xylene dibromide in a 2:1 ratio was then carried out in either dry acetonitrile or dry THF. The choice between these two solvents has no significant impact on the reaction yield as long as they have been freshly dried. Literature reaction times for this reaction are seven days; however, we have found that no reduction in yield (90%) is observed if the reaction is stopped and worked up after three days.<sup>164</sup> The bis-ammonium salt, **4**, precipitates out of solution and can be filtered off and washed with diethyl ether.

### 2.3.2 Reductive Ring Cleavage

Compound **4** can be reduced following Kolinski's route for mono-macrocycles.<sup>160</sup> The success of this reaction depends on the quality and the amount of hydride reducing agent employed. Optimum results were obtained when twenty molar equivalents of sodium borohydride were used per macrocycle. Compound **5** is symmetrical in nature as indicated by the aromatic region of the proton NMR spectrum where there is only a singlet peak present. A mechanism for the reduction has been proposed by Kolinski and is shown in Figure 43.<sup>160</sup> Cleavage of the quaternary nitrogen to carbon bond results in the formation of

a highly unstable tricyclic aminal,  $L^{20}$ , which is either reductively cleaved or hydrolysed on aqueous work up.

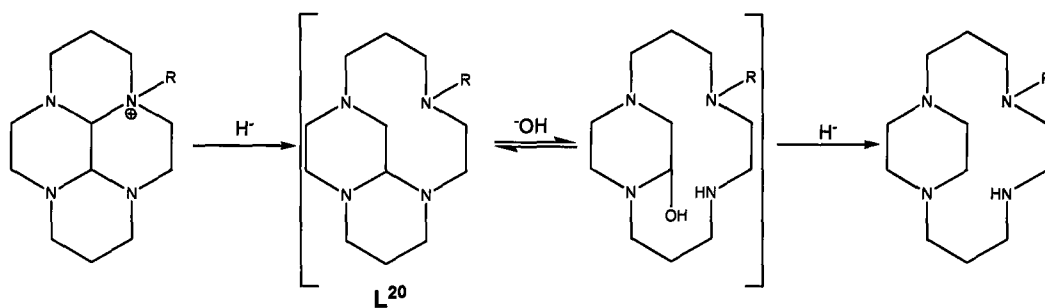


**Figure 43. Mechanism of hydride reduction.**

## 2.4 Configurationally Restricted Zinc(II) Complexes

Three zinc(II) complexes of **5** have been prepared in reasonable yields. The choice of counterion was dictated by the following factors; (1) acetate is a strongly coordinating anion and, in addition, could potentially mimic the interaction with CXCR4 aspartate residues, (2) chloride has different coordinating properties compared to acetate (which was important for proposed EXAFS characterisation) and finally, (3) perchlorate was chosen as these anions are weakly coordinating and also have crystal packing properties which could be beneficial for single crystal growth.

Complexes were prepared by mixing a methanolic solution of ligand and a slight excess of metal salt. The chloride and perchlorate salts of the ligand precipitated out of solution and were collected via filtration, whereas the acetate salt remained in solution and was purified by size exclusion chromatography. One of the overriding concerns of the synthesis of the metal complexes was sample purity and therefore the precipitates were rigorously washed. As a result, the yields are relatively low (~ 55%), however, literature yields for the complexations of related mono-macrocycles are also in the range 50-70%.<sup>161</sup>

Single crystals of  $[\text{Zn}_2\mathbf{5}(\text{OAc}_2)]^{2+}$  were obtained by slow evaporation from a methanolic solution, however, attempts to crystallise the chloride and perchlorate complexes were not successful. The following section describes the characterisation of  $[\text{Zn}_2\mathbf{5}(\text{OAc}_2)]^{2+}$  in both the solid state (X-ray crystallography) and aqueous solution (NMR).

### 2.4.1 X-ray Crystal Structure of $[\text{Zn}_2\mathbf{5}(\text{OAc}_2)]^{2+}$

The X-ray crystal structure of  $[\text{Zn}_2\mathbf{5}(\text{OAc}_2)]^{2+}$  (Figure 44) has an asymmetric unit containing only one macrocyclic ring. The two zinc(II) atoms are identical and are related by crystallographic symmetry with the macrocyclic framework adopting the equivalent of a trans-II configuration. The zinc(II) ion is six-coordinate, adopting a distorted octahedral geometry composed of four nitrogens from the macrocycle and two oxygens from the acetate counterion. Acetate oxygen atoms are bound in an anisobidentate manner; one bond being 2.112(3) Å with a longer interaction at 2.407(4) Å. The distorted octahedral geometry is completed by the four nitrogen atoms from the rigid macrocyclic backbone which have bond lengths in the range of 2.091(3) to 2.228(3) Å (Table 6).

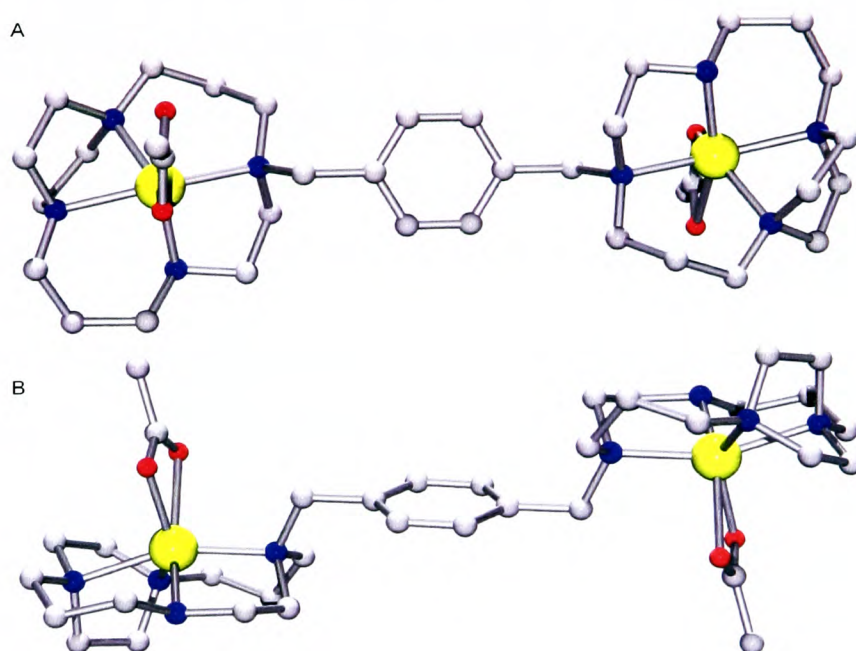


**Figure 44.** X-ray crystal structure of  $[\text{Zn}_2\mathbf{5}(\text{OAc}_2)]^{2+}$  (A) highlighting the angle between the two macrocycles (B).

Although there are no previous examples of zinc(II) complexes of side-bridged cyclams, the Zn–N bond lengths are within the expected range for cyclam type compounds.<sup>166</sup> The  $[\text{Zn}_2\mathbf{2}]^{4+}$  equivalent structure has Zn–N bond lengths of 2.071(2) to 2.252(2) Å.<sup>146</sup> Unbound acetate anions are present in disordered positions in the asymmetric unit, which show no interaction with the macrocyclic cation.

	Bond length / Å		Bond angle / °		Bond angle / °
Zn(1)-N(4)	2.091(3)	N(4)-Zn(1)-N(2)	117.91(12)	O(1)-Zn(1)-N(3)	94.58(11)
Zn(1)-N(2)	2.106(3)	N(4)-Zn(1)-O(1)	133.57(12)	N(1)-Zn(1)-N(3)	158.40(10)
Zn(1)-O(1)	2.112(3)	N(2)-Zn(1)-O(1)	102.38(13)	N(4)-Zn(1)-O(2)	85.97(13)
Zn(1)-N(1)	2.166(2)	N(4)-Zn(1)-N(1)	100.10(11)	N(2)-Zn(1)-O(2)	156.11(13)
Zn(1)-N(3)	2.228(3)	N(2)-Zn(1)-N(1)	84.86(11)	O(1)-Zn(1)-O(2)	56.31(14)
Zn(1)-O(2)	2.407(4)	O(1)-Zn(1)-N(1)	105.82(11)	N(1)-Zn(1)-O(2)	90.74(11)
		N(4)-Zn(1)-N(3)	69.44(12)	N(3)-Zn(1)-O(2)	106.79(12)
		N(2)-Zn(1)-N(3)	83.85(12)		

**Table 6. Selected bond lengths and angles for  $[\text{Zn}_2\mathbf{5}(\text{OAc})_2]^{2+}$ .**

The coordination of the acetate anion corresponds to the proposed interaction of each of the macrocyclic units with the CXCR4 receptor (Asp171 and Asp262). Interestingly, the zinc(II) ion is significantly displaced from the plane of the four nitrogen atoms (0.74 Å) and protrudes from the cavity, thus enhancing the interaction with the bound acetate.

The fact that the zinc(II) ion sticks out of the cavity and readily binds to acetate in the solid state could be a key factor in the interaction with CXCR4. This hypothesis depends on the macrocyclic configuration being maintained in aqueous solution. To assess the configuration in solution it was necessary to undertake high field NMR studies.

#### 2.4.2 NMR Characterisation of $[\text{Zn}_2\mathbf{5}(\text{OAc})_2]^{2+}$

The restricted nature of the macrocycle complicates the proton NMR spectrum of  $[\text{Zn}_2\mathbf{5}(\text{OAc})_2]^{2+}$  due to an increased number of inequivalent protons, resulting in a series of

overlapping peaks which necessitated the use of high field NMR techniques to fully assign the spectrum. This work was carried out in collaboration with Prof. Peter Sadler (University of Warwick), making use of a variety of NMR techniques, including 2D HSQC NMR.

The  $[^1\text{H}, ^{15}\text{N}]$  HSQC NMR spectrum of  $[\text{Zn}_2\mathbf{5}(\text{OAc}_2)]^{2+}$  at room temperature (Figure 45) reveals only a single peak which corresponds to the secondary amine in each macrocycle and indicates that only a single configuration exists in aqueous solution. In contrast to these data, the equivalent zinc(II) complex of AMD3100 shows multiple peaks due to there being several macrocyclic configurations and NH environments present in the equilibrium.<sup>146</sup> This equilibrium can be altered by varying the concentration of acetate present.

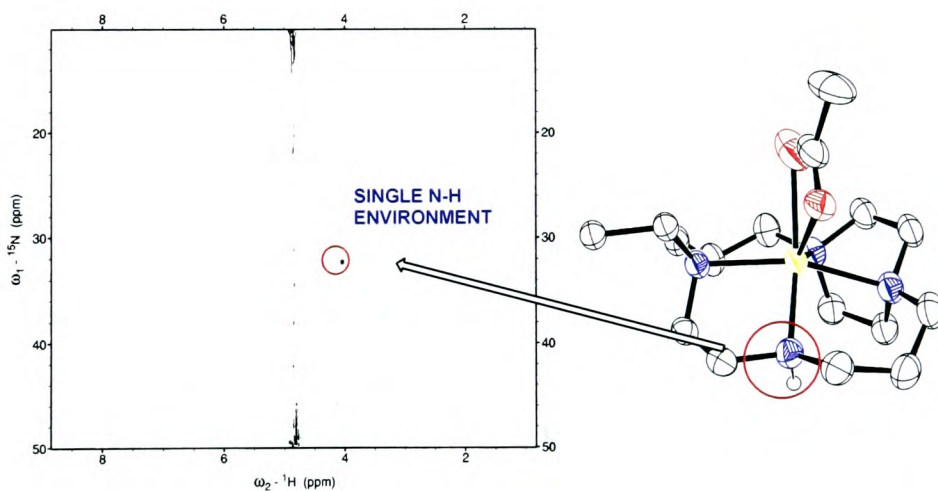


**Figure 45. 2D NMR of  $[\text{Zn}_2\mathbf{5}(\text{OAc}_2)]^{2+}$ .**

However, this is not the case with  $[\text{Zn}_2\mathbf{5}(\text{OAc}_2)]^{2+}$ , where there were no observable changes to the NMR spectrum when the counterion was varied. The NMR data (Figure 46), together with the single crystal X-ray structure, appear to be consistent with both

macrocyclic units uniquely adopting the trans-II configuration in the solid state and in solution.

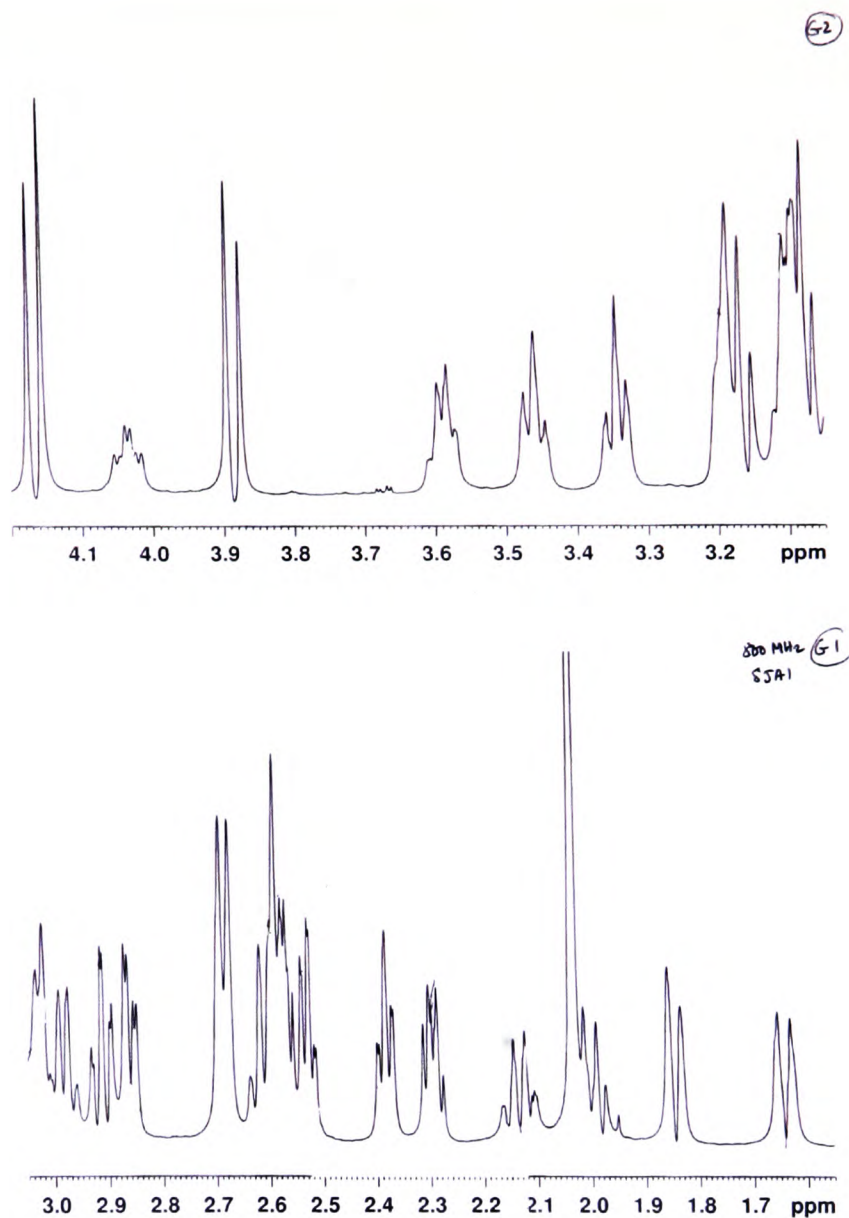


**Figure 46.** Aliphatic region of the <sup>1</sup>H NMR of [Zn<sub>25</sub>(OAc)<sub>2</sub>]<sup>2+</sup> recorded at 800 MHz.

## 2.5 Configurationally Restricted Copper(II) Complexes

Three copper(II) complexes of **5** have been prepared in a similar fashion to the zinc(II) complexes discussed previously. Complexes were prepared by mixing a methanolic solution of ligand and a slight excess of metal salt.  $[\text{Cu}_2\mathbf{5}(\text{OAc})_2]^{2+}$  was purified by size exclusion chromatography as was  $[\text{Cu}_2\mathbf{5}\text{Cl}_2]\text{Cl}_2$  after firstly filtering off trace impurities. The chromatographic purification of the copper(II) complexes was much easier in comparison to the zinc(II) complexes due to the simple fact that the compounds are coloured and can be seen running down the column. In contrast,  $[\text{Cu}_2\mathbf{5}](\text{ClO}_4)_4$  precipitated out of solution and was collected via filtration. Again, the desire for highly pure complexes meant that yields of the complexes were lower (60-70%) than anticipated, however, these are comparable to literature yields on similar, mono-macrocyclic ligands.<sup>161</sup>

Single crystals of both  $[\text{Cu}_2\mathbf{5}](\text{ClO}_4)_4$  and  $[\text{Cu}_2\mathbf{5}\text{Cl}_2]^{2+}$  were grown via ether diffusion into a methanolic solution. The following section describes the characterisation of these two complexes in the solid state.

### 2.5.1 Characterisation of $[\text{Cu}_2\mathbf{5}](\text{ClO}_4)_4$

The single crystal structure of  $[\text{Cu}_2\mathbf{5}]^{4+}$  (Figure 47) contains two macrocyclic units, and like  $[\text{Zn}_2\mathbf{5}(\text{OAc})_2]^{2+}$ , the macrocyclic framework is in a trans-II configuration. In contrast to  $[\text{Zn}_2\mathbf{5}(\text{OAc})_2]^{2+}$ , however, the copper(II) ions in each ring are not crystallographically equivalent to each other but their environments are very similar. They both adopt a tetrahedrally distorted square planar geometry, with Cu–N bond lengths ranging from 1.855(11) to 2.048(14) Å in one ring and 1.849(11) to 2.266(11) Å in the second (Table 7).

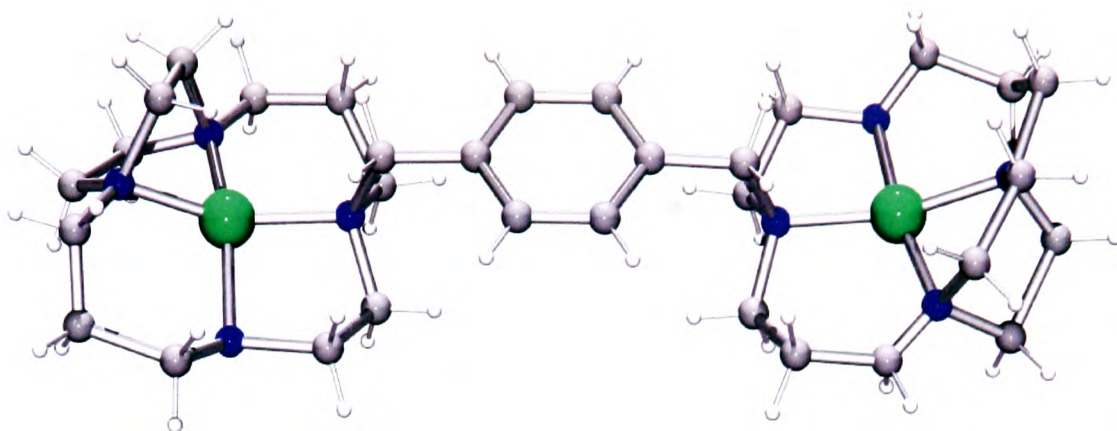


Figure 47. X-ray crystal structure of [Cu<sub>25</sub>]<sup>4+</sup>.

	Bond Length / Å		Bond Angle / °
Cu(1)-N(4)	1.855(11)	N(4)-Cu(1)-N(3)	81.4(6)
Cu(1)-N(3)	1.885(9)	N(4)-Cu(1)-N(1)	99.4(4)
Cu(1)-N(1)	2.002(5)	N(3)-Cu(1)-N(1)	154.1(5)
Cu(1)-N(2)	2.048(14)	N(4)-Cu(1)-N(2)	160.9(5)
		N(3)-Cu(1)-N(2)	97.1(6)
		N(1)-Cu(1)-N(2)	90.3(4)
Cu(2)-N(8)	1.849(11)	N(8)-Cu(2)-N(7)	79.1(6)
Cu(2)-N(7)	1.950(7)	N(8)-Cu(2)-N(5)	104.9(5)
Cu(2)-N(5)	1.988(5)	N(7)-Cu(2)-N(5)	160.3(3)
Cu(2)-N(6)	2.266(11)	N(8)-Cu(2)-N(6)	162.8(4)
		N(7)-Cu(2)-N(6)	97.4(4)
		N(5)-Cu(2)-N(6)	84.1(3)

Table 7. Selected bond lengths and angles for [Cu<sub>25</sub>]<sup>4+</sup>.

An example of a mono-side-bridged copper(II) complex reported by Kaden and co-workers, [CuL<sup>13</sup>]<sup>2+</sup>, also has two independent copper(II) environments in the asymmetric unit.<sup>161</sup> The Cu–N bond lengths are similar to [Cu<sub>25</sub>]<sup>4+</sup>, being in the range 1.979(4) to 2.016(4) Å in one ring and 1.980(3) to 2.010(3) Å in the second. Analogous to [Cu<sub>25</sub>]<sup>4+</sup>, the copper(II) is also four-coordinate in the solid state (Figure 48). The macrocyclic framework is in a trans-II configuration, where the methyl and hydrogen arms are sitting trans to each

other. The copper(II) ion sits in the plane of the four nitrogen atoms, the deviation from the best plane being 0.070 and 0.007 Å respectively.

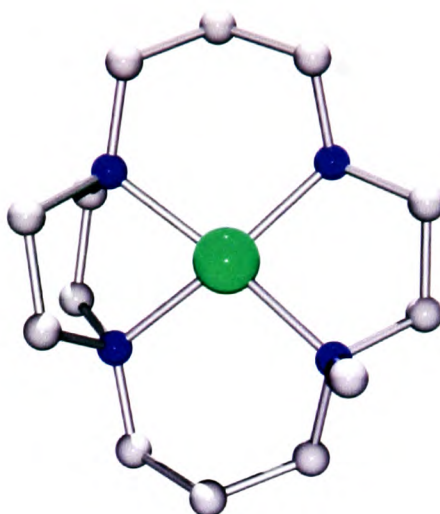


**Figure 48. X-ray crystal structure of [CuL<sup>13</sup>]<sup>2+</sup>.**

The metal-nitrogen bond lengths in [Cu<sub>2</sub>5]<sup>4+</sup> are, as expected, somewhat shorter than in [Zn<sub>2</sub>5(OAc)<sub>2</sub>]<sup>2+</sup> and, in addition, there is no significant interaction between the copper(II) centre and the counter anion. A further interesting comparison between [Cu<sub>2</sub>5]<sup>4+</sup> and [Zn<sub>2</sub>5(OAc)<sub>2</sub>]<sup>2+</sup> is the degree to which the macrocyclic units are rotated from each other. The macrocyclic rings in [Zn<sub>2</sub>5(OAc)<sub>2</sub>]<sup>2+</sup> could be described as being trans to each other, whereas in [Cu<sub>2</sub>5]<sup>4+</sup> they could be described as being cis to each other. This is demonstrated by the difference in metal-metal distance, which is 11.6584(10) Å in [Zn<sub>2</sub>5(OAc)<sub>2</sub>]<sup>2+</sup> but closer at 10.9121(17) Å in [Cu<sub>2</sub>5]<sup>4+</sup>. This can be explained further by considering the bond angle between the two nitrogen-carbon bonds next to the aromatic linker (Figure 49). In [Zn<sub>2</sub>5(OAc)<sub>2</sub>]<sup>2+</sup> this angle is 180.00(55)° whereas in [Cu<sub>2</sub>5]<sup>4+</sup> it is 1.80(77)°. These angles are created by defining three planes through the crystal structure. Two of the planes are taken through the centre of the carbon-nitrogen bonds in each macrocyclic unit respectively

and the third is taken as the plane of the phenyl linker. The angle between the plane of the carbon-nitrogen bond and the plane of the phenyl moiety is  $87.80(23)^\circ$  in  $[\text{Zn}_2\mathbf{5}(\text{OAc})_2]^{2+}$  crystal and  $89.47(61)^\circ$  in the  $[\text{Cu}_2\mathbf{5}]^{4+}$  structure.

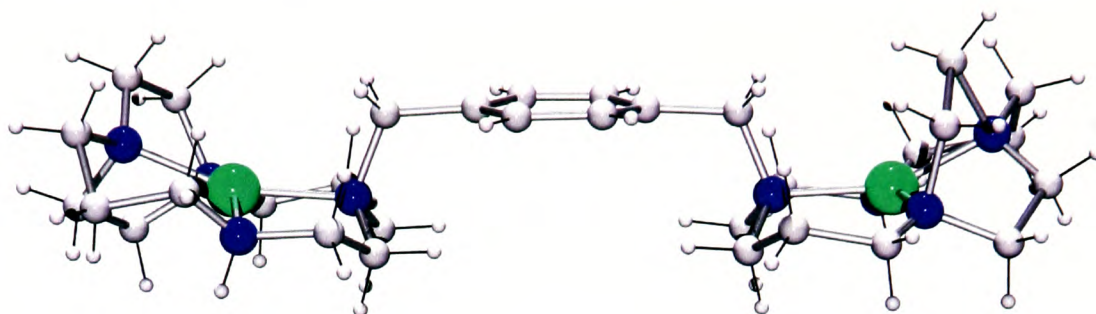


**Figure 49. X-ray crystal structure of  $[\text{Cu}_2\mathbf{5}]^{4+}$  highlighting the angle between the two macrocycles.**

The UV-vis of  $[\text{Cu}_2\mathbf{5}]^{4+}$  shows a broad band at 554 nm. This is a higher value than is usually observed for square planar copper(II) cyclam complexes, which can be attributed to the tetragonal distortion of the copper(II) centre. A more appropriate comparison is with  $[\text{CuL}^{13}]^{2+}$  which has an absorption maximum at 556 nm in aqueous solution.<sup>161</sup> Five-coordinate copper(II) complexes are known to exhibit a band at around 600 nm.<sup>167</sup> There was no shift in the band at 554 nm on addition of sodium acetate. For example, dissolution in a 2 M solution of sodium acetate showed only a marginal shift to 560 nm. Although the UV-vis data suggests a four-coordinate copper(II) species in solution, no firm conclusions can be drawn from these experiments.

### 2.5.2 Characterisation of $[\text{Cu}_2\mathbf{5Cl}_2]\text{Cl}_2$

Unlike the previous metal complexes, this X-ray structure suffered from disorder in the unit cell. Two symmetry independent structural types occupying the same space in the

asymmetric unit were determined. In contrast to the four-coordinate  $[\text{Cu}_2\mathbf{5}]^{4+}$ , the copper(II) centre is five-coordinate and is best described as being in a square-based pyramidal coordination environment, the base consisting of the four macrocyclic nitrogen atoms with a bound chloride counter anion in the apical position (Figure 50).

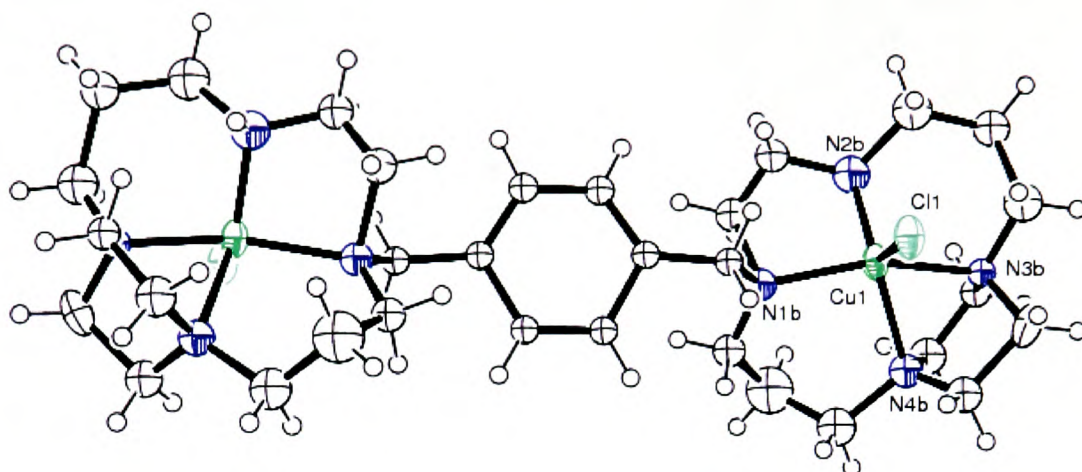


**Figure 50.** X-ray crystal structure of  $[\text{Cu}_2\mathbf{5}\text{Cl}_2]^{2+}$  showing one disordered position.

The copper(II)-nitrogen bond lengths are in the range 1.891(15) to 2.139(16) Å (Table 8) which is in agreement with  $[\text{Cu}_2\mathbf{5}]^{4+}$ . Again, the macrocycle adopts the equivalent of a trans-II configuration in the solid state. The metal-metal distance of 11.5705(16) Å is, as expected, longer than in  $[\text{Cu}_2\mathbf{5}]^{4+}$  as the two macrocycles are located in the equivalent of a trans position relative to each other (Figure 51). This distance is similar to that found in  $[\text{Zn}_2\mathbf{5}(\text{OAc})_2]^{2+}$ . As with the previous two crystal structures, the angle between the two macrocycles can be determined. The same three planes are defined and result in an angle of ca. 180°, similar to  $[\text{Zn}_2\mathbf{5}(\text{OAc})_2]^{2+}$ , with any deviation being attributed to the disorder in the structure. The angle between the plane of the carbon-nitrogen bond and the plane of the phenyl moiety is 88.200(99)°, which is similar to the two previously discussed complexes.

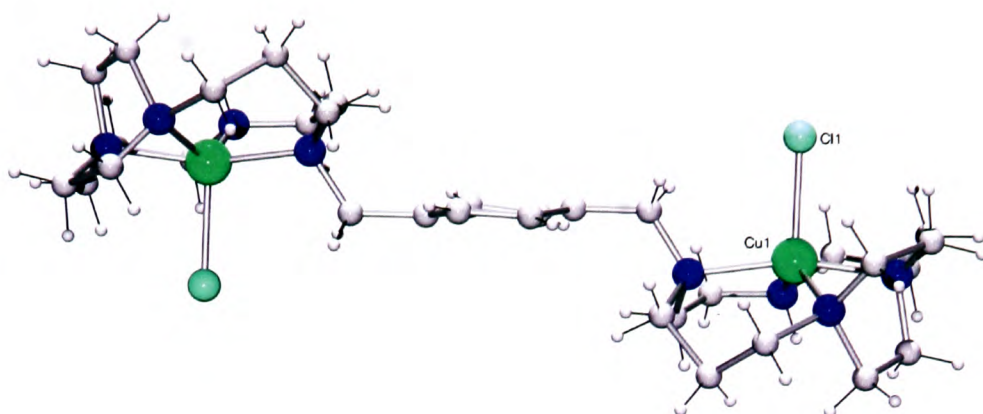


Figure 51. X-ray crystal structure of  $[\text{Cu}_25\text{Cl}_2]^{2+}$  highlighting the angle between the two macrocycles.

	Bond length / Å		Bond angle / °
<b>Cu(1)-N(2b)</b>	1.891(15)	<b>N(2)-Cu(1)-N(3)</b>	98.0(5)
<b>Cu(1)-N(3b)</b>	2.004(11)	<b>N(2)-Cu(1)-N(1)</b>	88.1(4)
<b>Cu(1)-N(1b)</b>	2.089(14)	<b>N(3)-Cu(1)-N(1)</b>	164.8(4)
<b>Cu(1)-N(4b)</b>	2.136(15)	<b>N(2)-Cu(1)-N(4)</b>	132.3(5)
		<b>N(3)-Cu(1)-N(4)</b>	68.5(5)
<b>Cu(1)-N(2)</b>	1.999(11)	<b>N(1)-Cu(1)-N(4)</b>	97.2(5)
<b>Cu(1)-N(3)</b>	2.088(11)	<b>N(2)-Cu(1)-Cl(1)</b>	108.9(3)
<b>Cu(1)-N(1)</b>	2.112(9)	<b>N(3)-Cu(1)-Cl(1)</b>	90.5(3)
<b>Cu(1)-N(4)</b>	2.139(16)	<b>N(1)-Cu(1)-Cl(1)</b>	100.8(2)
<b>Cu(1)-Cl(1)</b>	2.4131(11)	<b>N(4)-Cu(1)-Cl(1)</b>	116.5(4)

Table 8. Selected bond lengths and angles for  $[\text{Cu}_25\text{Cl}_2]^{2+}$ .

## 2.6 Side-bridged Tris-macrocycles

The bis-macrocycles which have been discussed previously could be extended to a tris-macrocylic ligand (Figure 52). The three ringed derivative can take one of two forms, either a linear combination containing two aromatic linker groups or a single aromatic linker in a 1,3,5-substituted framework (Figure 52). The cyclam derivatives of  $L^{21}$  and  $L^{22}$  have been reported by Lindoy and co-workers, although  $L^{21}$  was originally synthesised by Sun *et al.*<sup>168-170</sup>

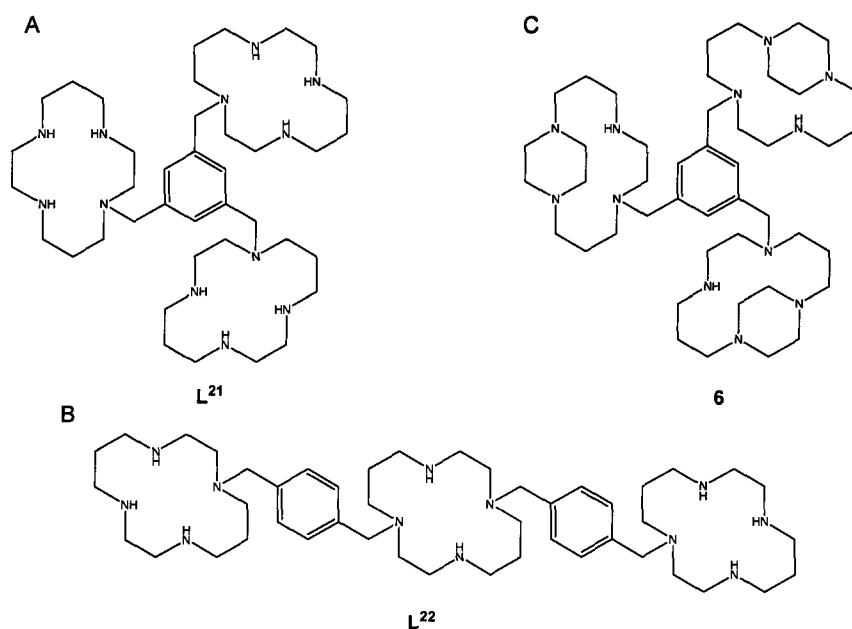


**Figure 52.** Tris-macrocycle (A), linear tris-macrocycle (B) and side-bridged derivative (C).

Sun *et al.* prepared ligand  $L^{21}$  in a three step synthesis starting from cyclam. They protected the macrocycle with tosyl chloride according to a method reported by Parker and co-workers.<sup>171</sup> The tris-protected macrocycle,  $L^2$ , is then reacted with the 1,3,5-tris-benzyl derivative,  $L^{23}$ , (Figure 53) to give  $L^{24}$  which can be purified via column chromatography.

The final step is the deprotection of the tosyl groups with HBr in acetic acid. The pure final product,  $L^{21}$ , is obtained following work up with an ion exchange column. Yields for individual reactions are not available although the overall yield has been reported to be 34%.

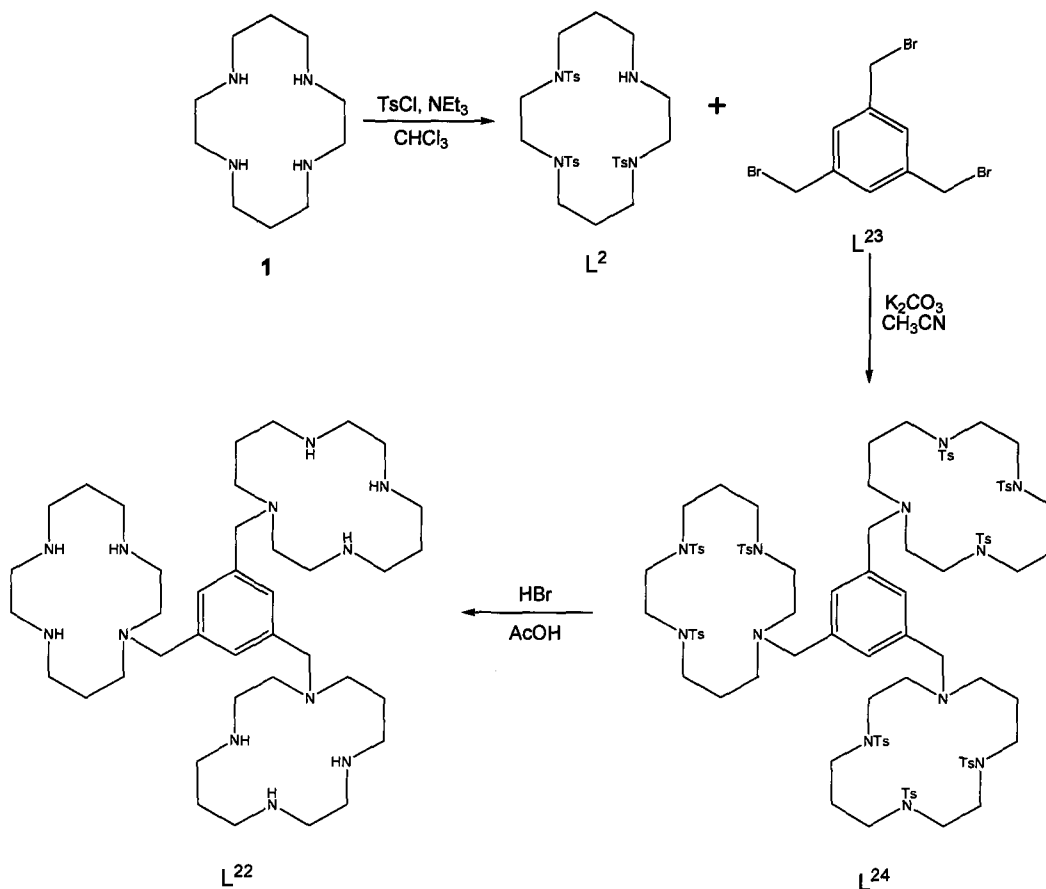


**Figure 53. Synthetic route to tris-cyclam,  $L^{22}$ .**

Copper(II), zinc(II) and palladium(II) complexes of  $L^{22}$  are known, but are prepared in relatively low yield (54% for Cu, 30% for Zn and 35% for Pd), although the only reported crystal structure is of a nickel(II) complex.<sup>168, 172</sup> The single crystal structure of  $[Ni_3L^{22}](ClO_4)_6$  is of relatively poor quality as a result of crystal degradation in the synchrotron X-ray source. The nickel(II) ion adopts an essentially square planar geometry

(Figure 54) although there is some long range interaction with perchlorate resulting in a pseudo-octahedral environment in the solid state. This long range interaction is broken down in solution, as evidenced by the UV-vis spectrum, which reveals a four-coordinate geometry ( $\lambda_{\text{max}}$  463 nm) in aqueous solution.

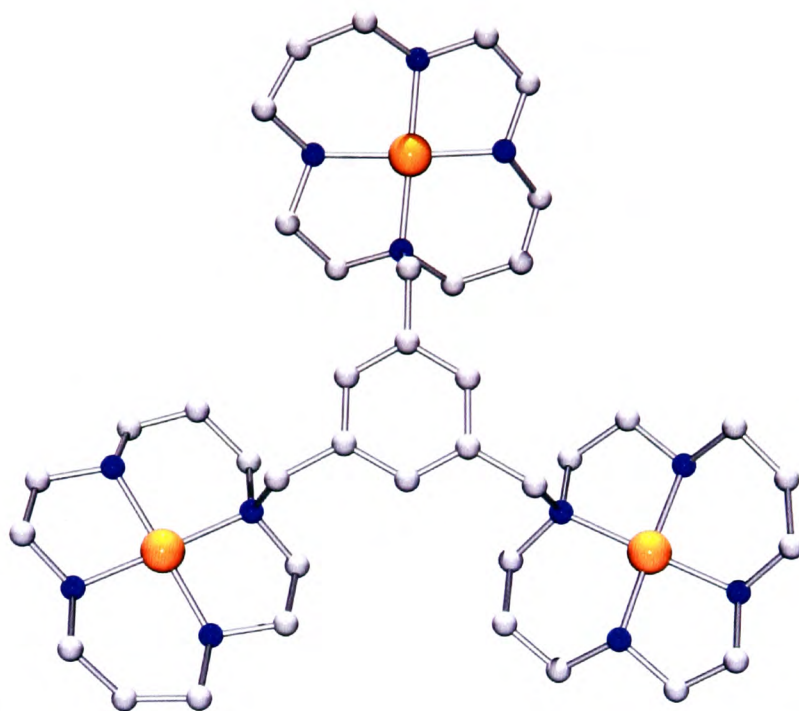


**Figure 54.** X-ray crystal structure of  $[\text{Ni}_3\text{L}^{22}](\text{ClO}_4)_6$ .<sup>172</sup>

These tris-compounds have not been further developed into configurationally restricted ligands. In this work, an example of a tris-macrocyclic containing an ethylene side bridge, **6**, has been synthesised and copper(II) and zinc(II) complexes produced.

## 2.6.1 Synthesis of 6

The proposed synthetic route to **6** involves a similar strategy to that which has proven to be successful for the previously discussed bis-macrocycles (Figure 55). The precursor to the desired ligand is the 1,3,5-tris bromo compound **L<sup>23</sup>**, which was supplied by Dr Steve Archibald.

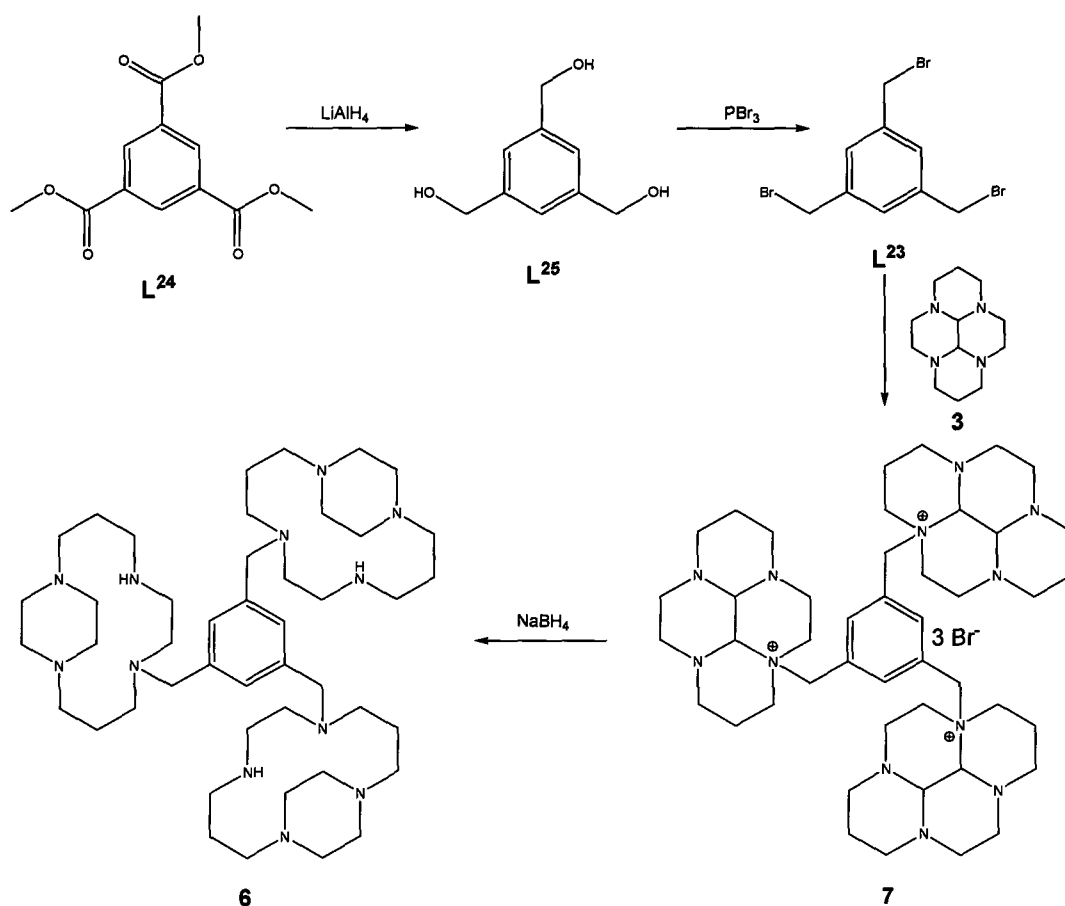


Figure 55. Proposed synthetic scheme to **6**.

The addition of **3** to **L**<sup>23</sup> was carried out in an identical manner to the respective bis-macrocycle with the combination of the two reagents in dry acetonitrile over a five day period. The isolated reaction yield is 90% which was the same as was observed for the bis-compound. The reduction of **7** with sodium borohydride results in an oily yellow product in an impressive yield of over 75%. Although the proton NMR spectrum of **6** is quite difficult to interpret fully, the aromatic region consists of a multiplet which integrates to the expected three protons. A further indication that the reduction has proceeded smoothly is the loss of the doublets at approximately 5 ppm, which are due to the diastereotopic N<sup>+</sup>-CH<sub>2</sub> protons. Carbon NMR and the mass spectrum of **6** are more informative and suggest that the reduction had worked as expected. The carbon NMR spectrum reveals fifteen carbon environments, which can be split into two aromatic carbons, eleven N- $\alpha$ -carbons and two N- $\beta$ -carbons as expected.

### 2.6.2 Transition Metal Complexes of **6**

A series of zinc(II) and copper(II) complexes of ligand **6** has been prepared in an analogous fashion to the complexes of **5** discussed previously. The zinc(II) complexations proceed in similar reaction yields of between 70 and 80%, whereas the copper(II) complexations proceed in lower yields of between 60 and 70%. The NMR spectra of the three zinc(II) complexes were difficult to interpret at 400 MHz but were essentially identical to each other. The aromatic region of the spectrum contained a singlet which integrated to three protons. This is expected of a 1,3,5-linked aromatic system and suggests that the complexation procedure had a purifying effect. In addition, the diastereotopic N-CH<sub>2</sub> protons reappear at ca. 5 ppm as a result of the rigidity imparted by the zinc(II) complexation.

Three copper(II) complexes were prepared and in the absence of any suitable single crystals have been characterised by EXAFS. This is covered in greater detail in chapter four but the complexes are either four or five-coordinate in the solid state and adopt essentially the same coordination environment as the related bis-complexes. The UV-vis studies on the copper(II) complexes of **6** were also identical to those recorded for the copper(II) complexes of **5**. For example,  $[\text{Cu}_3\mathbf{6}](\text{ClO}_4)_6$  shows a broad transition centred at 555 nm in aqueous solution.

## 2.7 Conclusions

A synthetic route to a bis-macrocyclic compound containing a piperazino or a side bridge, **5**, has been developed. This route has proven to be reproducible in approximately 50% yield for the three step procedure. This is the first example of a bis-macrocyclic cyclam based compound incorporating a piperazino unit to be reported, although a similar cyclen based compound has been independently synthesised by another group.

The X-ray crystal structure of  $[\text{Zn}_2\mathbf{5}(\text{OAc})_2]^{2+}$  is the first example of a trans-II configurationally restricted macrocyclic complex to be reported. Additionally, it is also the first example of a configurationally restricted bis-macrocyclic transition metal complex in the literature. Furthermore, NMR studies on  $[\text{Zn}_2\mathbf{5}(\text{OAc})_2]^{2+}$  confirm that the trans-II configuration is maintained in aqueous solution.

The X-ray crystal structures of  $[\text{Cu}_2\mathbf{5}\text{Cl}_2]^{2+}$  and  $[\text{Cu}_2\mathbf{5}](\text{ClO}_4)_4$  reported here are the first examples of copper(II) bis-macrocyclic complexes. The two complexes are significantly different from each other, for example  $[\text{Cu}_2\mathbf{5}\text{Cl}_2]^{2+}$  adopts a five-coordinate, square-based pyramidal geometry, whereas  $[\text{Cu}_2\mathbf{5}](\text{ClO}_4)_4$  adopts a four-coordinate, square planar geometry. The two structures reported here reflect the rich coordination chemistry of copper(II) and expand the current knowledge of copper(II) macrocyclic complexes.

The synthetic route to **5** has been extended to include the synthesis of **6**. This is the first example of a tris-macrocyclic compound incorporating a piperazino moiety. Copper(II) and zinc(II) complexes of **6** have been prepared and appear to have similar coordination environments to their bis-macrocyclic relatives.

**Chapter 3. SYNTHESIS &  
CHARACTERISATION OF CROSS-BRIDGED  
MACROCYCLIC COMPLEXES**

### 3.1 Cross-bridged Tetraazamacrocycles

An alternative to the “side” bridged piperazino macrocycles discussed in the previous chapter are the “cross” bridged cyclam derivatives which contain an ethylene bridge between non-adjacent nitrogen atoms. These compounds have been termed “adamanzanes” and have received attention primarily due to their potential as radiopharmaceutical chelators due to the extreme kinetic stability displayed by their copper(II) complexes. One drawback of these systems compared to their side-bridged counterparts is the length of time of their syntheses. The reductive ring cleavage step for the “cross” bridged analogue takes fourteen days compared to a couple of hours for its “side” bridged relative.

The framework of the cross-bridged cyclam results in the four nitrogen lone pairs converging into the macrocyclic cavity and thus making them suitable ligands for complexes adopting a folded cis-V configuration (Figure 56).

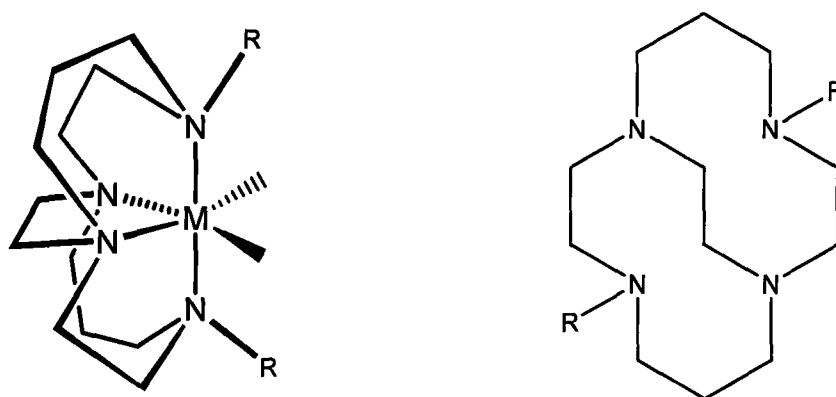


**Figure 56. Cross-bridged cyclam. Metal complexes adopt the cis-V configuration.**

There are numerous examples of cross-bridged cyclam ligands in the literature containing a variety of pendent arms; however, they have yet to be applied to bis-

macrocycles. This chapter introduces the synthesis of cross-bridged cyclams, focusing on examples possessing methyl and/or benzyl pendent arms, their transition metal complexes and also the methodology used to incorporate these systems into novel bis-macrocycles.

### 3.1.1 Synthetic Development of Cross-bridged Cyclam

The first example of a cross-bridged cyclam derivative was reported by Weisman *et al.* (Figure 57) in 1990 who exploited the regio-selectivity of the bis-aminal, **3**, which has been previously discussed (chapter two, section 2.3).<sup>173</sup> The bis-methyl salt, **L**<sup>26</sup>, is formed in 85% yield based on the addition of methyl iodide. The addition of the first methyl group proceeds rapidly, however, the second addition is relatively slow and requires longer reaction times. Subsequent reduction with sodium borohydride over a fourteen day period results in the cross-bridged ligand, **L**<sup>27</sup>, in an impressive 90% yield. The overall yield for the three stage process is around 60% which is comparable to the previously discussed side-bridged ligands.

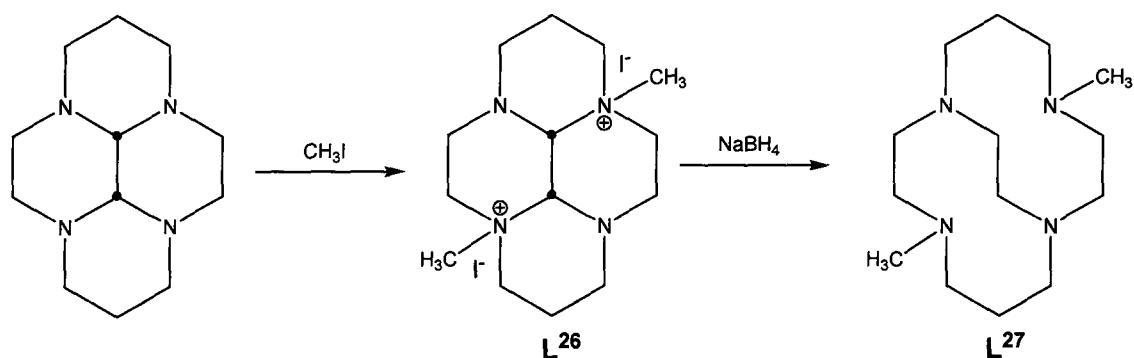


Figure 57. Synthesis of the first cross-bridged cyclam, **L**<sup>27</sup>.

This synthetic route has been expanded to cover ligands which contain two benzyl arms.<sup>174</sup> The reaction scheme is identical to Figure 57, except that benzyl bromide is used instead of methyl iodide. The debenylation step proceeds in yields ranging from 75-93% with the reduction yield being comparable to that of L<sup>27</sup> (83-96%). One advantage of preparing the di-benzyl species is that it can be debenzylated via hydrogenolysis to leave a cross-bridged cyclam with two secondary amine sites (e.g. L<sup>28</sup>, Figures 58 and 59) which can be further reacted. This methodology has proven to be successful for incorporating a variety of pendent arms, including *tert*-butyl bromoacetate. These compounds have found use as synthetic precursors for bifunctional chelators and also complexing radioactive copper(II).<sup>175</sup>

### 3.1.2 Metal Complexes of Cross-bridged Cyclam

In contrast to the relatively few transition metal complexes of side-bridged cyclam ligands, there have been numerous reported complexes of cross-bridged ligands, mainly by the groups of Weisman, Busch and Hubin and each one has revealed the expected *cis*-V configuration.<sup>150, 174</sup> This section highlights the structures of the known zinc(II) and copper(II) complexes of cross-bridged cyclams, again focusing on the examples containing either methyl or benzyl pendent arms.

A search of the CSD reveals that there are 25 reported crystal structures of cross-bridged cyclam complexes possessing methyl, benzyl or no pendent arms. These can be broken down into six copper(II), five manganese(III), two nickel(II), two zinc(II), two manganese(II), two iron(II) complexes and one each of palladium(II), gallium(III), cadmium(II), mercury(II), cobalt(II) and copper(I).

Niu *et al.* have reported the only two crystal structures of zinc(II) cross-bridged cyclam complexes.<sup>176</sup> The zinc(II) ion in the first structure,  $[\text{ZnL}^{28}(\text{OH}_2)(\mu\text{-Cl})\text{ZnCl}_3]$  is in a distorted octahedral geometry, with bonds to the four macrocyclic nitrogen atoms and a solvent water molecule (Figure 58). The octahedron is completed by a bridging chloride from a  $[\text{ZnCl}_4]^{2-}$  counter anion. The zinc(II)-nitrogen bonds are in the range 2.119(6) to 2.170(5) Å and a long range zinc(II)-chloride bond is observed at 2.629(2) Å.

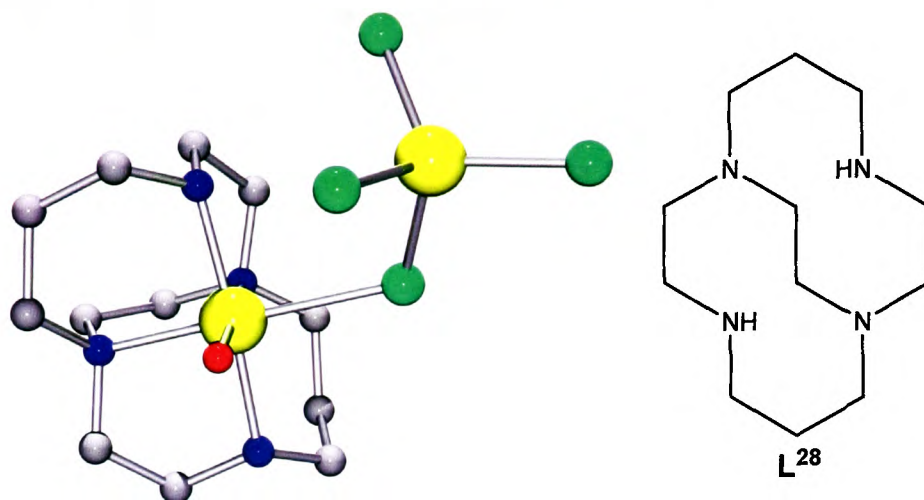


**Figure 58.** X-ray crystal structure of  $[\text{ZnL}^{28}(\text{OH}_2)(\mu\text{-Cl})\text{ZnCl}_3]$ .

The second example is also of  $\text{L}^{28}$  but the crystal structure reveals a dimer with two bridging chloride counter anions present (Figure 59). The zinc(II) ion again adopts a distorted octahedral coordination environment with zinc(II)-nitrogen bond lengths in the range 2.133(5) to 2.185(4) Å. The two bridging chlorides both have zinc(II)-chloride distances of 2.527(1) Å.

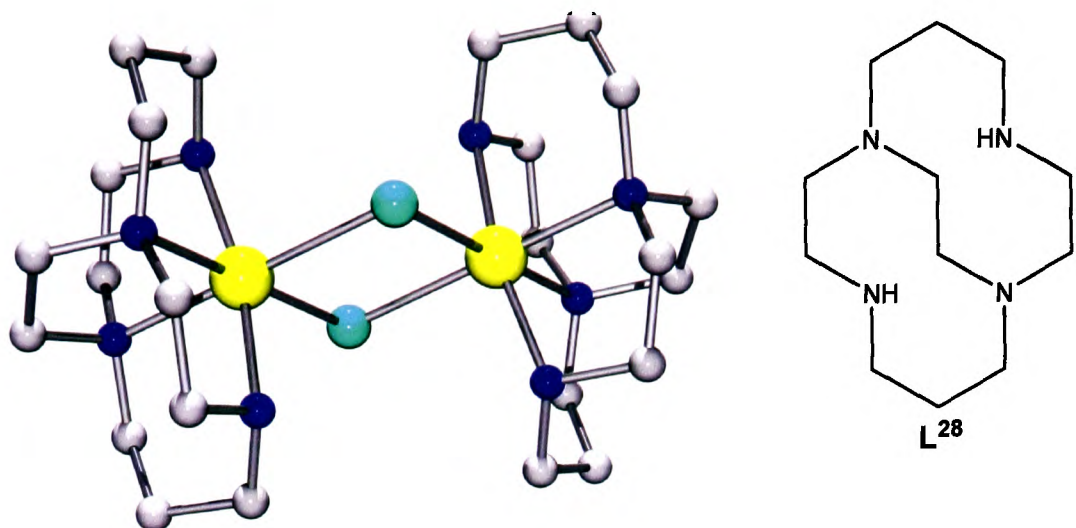


**Figure 59. X-ray crystal structure of  $[\text{ZnL}^{28}(\mu\text{-Cl})_2]^{2+}$ .**

Three copper(II) complexes of cross-bridged cyclam derivatives possessing methyl or benzyl arms are known, with the metal centre adopting either a square-based pyramidal or distorted octahedral geometry. The copper(II) complex  $[\text{CuL}^{29}\text{Cl}]^+$  was prepared by Weisman *et al.* over a decade ago (Figure 60).<sup>177</sup> The five-coordinate geometry is composed of the four macrocyclic nitrogens (Cu-N bond lengths 2.082(3)-2.188(3) Å) and one bound chloride counter anion (Cu-Cl distance 2.296(1) Å). Interestingly, there is an agostic interaction with an ortho-hydrogen from one of the benzyl arms with a bond distance of 2.74 Å.

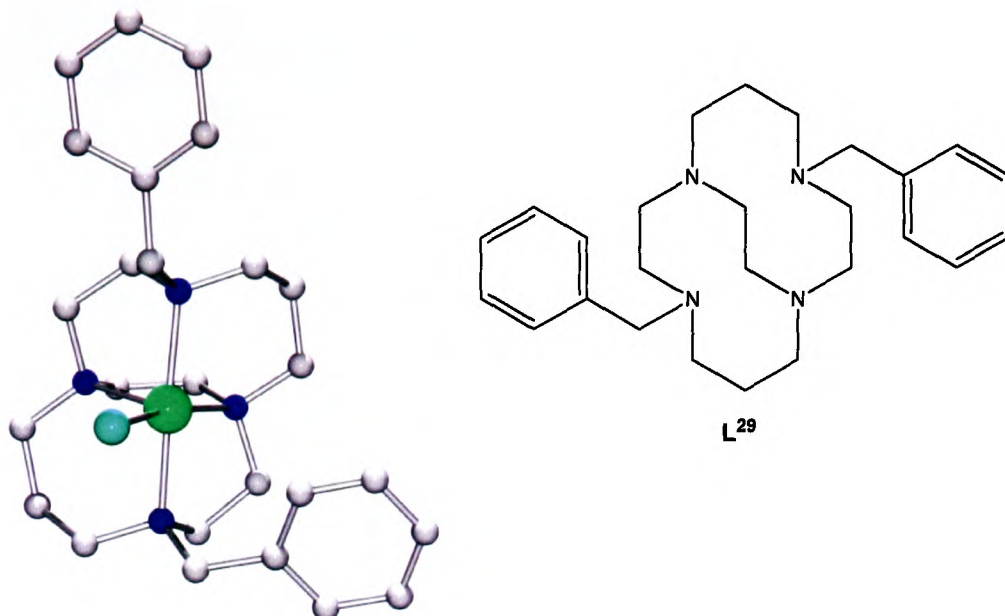


**Figure 60. X-ray crystal structure of  $[\text{CuL}^{29}\text{Cl}]^+$ .**

Hubin and co-workers have reported the copper(II) hexafluorophosphate complex of  $\text{L}^{29}$  (Figure 61).<sup>178</sup> In contrast to the previous structure, this complex adopts a square-based pyramidal geometry, where the base consists of three nitrogens and a bound acetonitrile solvent molecule. Sitting at the apex of the pyramid is the fourth macrocyclic nitrogen atom. The copper(II)-nitrogen bond lengths are in the range 2.049(3) to 2.142(3) Å. The flexible benzyl arms are folded in order to accommodate the acetonitrile molecule which completes the five-coordinate geometry in the absence of a coordinating counter anion.

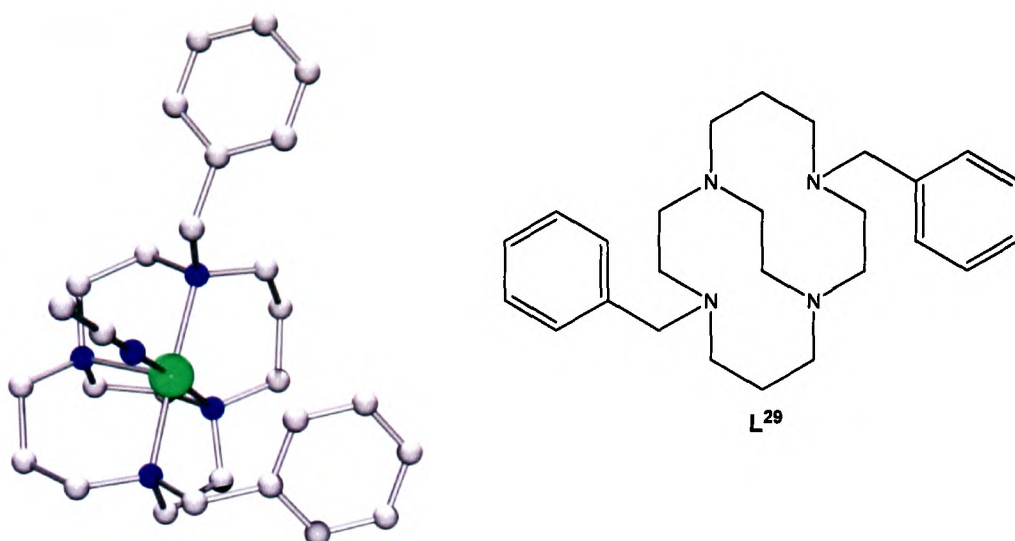


**Figure 61. X-ray crystal structure of  $[\text{CuL}^{29}(\text{NCCH}_3)]^{2+}$ .**

The bis-methyl copper(II) chloride complex,  $[\text{CuL}^{27}\text{Cl}]^+$ , adopts a similar coordination geometry to  $[\text{CuL}^{29}(\text{NCCH}_3)]^{2+}$  except that the acetonitrile is replaced with a chloride counter anion (Figure 62).<sup>179</sup> Again, the axial position is occupied by a macrocyclic nitrogen atom.

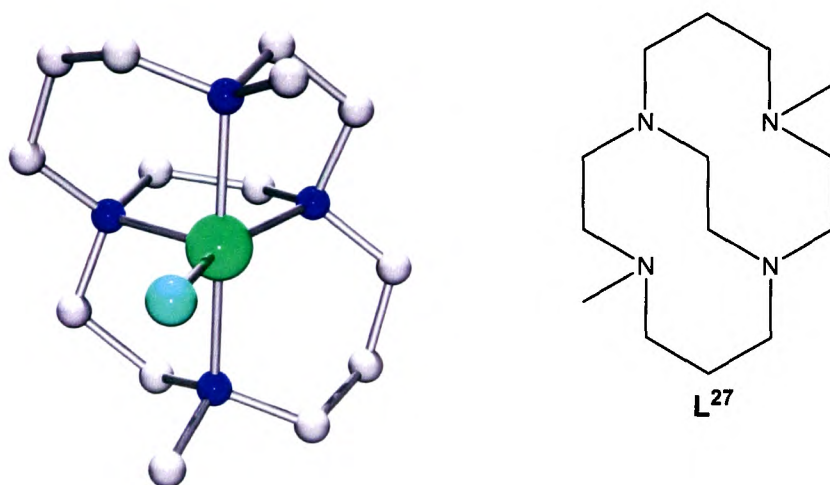


**Figure 62. X-ray crystal structure of  $[\text{CuL}^{27}\text{Cl}]^+$ .**

### 3.1.3 Synthetic Development of Cross-bridged Cyclen

The first cross-bridged example of the smaller macrocycle cyclen was reported by Bencini *et al.* in the early 1990s.<sup>180</sup> The preparation involves the prior synthesis of the bis-methylated cyclen derivative, **L**<sup>38</sup>, which was reported by Ciampolini *et al.* a decade before.<sup>181</sup> This seven step synthesis (Figure 63) involves two separate protection-deprotection steps (firstly with phthaloyl/HCl and secondly with tosyl/H<sub>2</sub>SO<sub>4</sub>) and the formylation of a secondary amine. The protection of **L**<sup>33</sup> with tosyl chloride followed by recrystallisation from ethanol results in the bis-tosyl protected product, **L**<sup>34</sup>, in 82% yield. The sodium salt of deprotonated **L**<sup>35</sup> is then used in situ with bis(2-chloroethyl)-methylamine in dry dimethylformamide to result in the cyclised bis-methylated cyclen, **L**<sup>37</sup>, in 40% yield. Deprotection of the tosyl groups is achieved with concentrated sulphuric acid and the free amine ligand is obtained via extraction from chloroform. The tetrahydrobromide salt of **L**<sup>38</sup> is obtained in 90% yield by the addition of hydrobromic acid to an ethanolic solution of the free ligand.

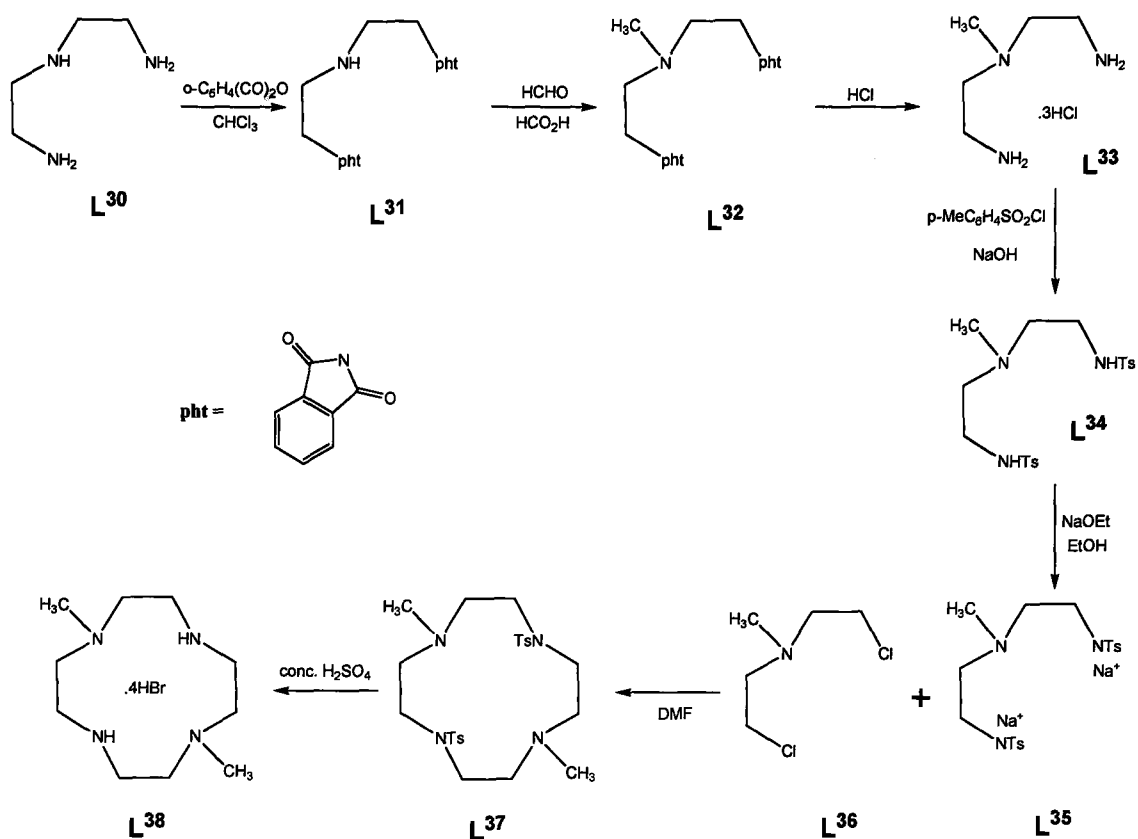


**Figure 63. Synthetic route to bis-methyl cyclen,  $\text{L } 38$ .**

Reaction of  $\text{L } 38$  with oxalyl chloride and triethylamine results in the formation of the bis-amide,  $\text{L } 39$ , in 29% yield following recrystallisation from cyclohexane (Figure 64). The protonated cross-bridged cyclen,  $\text{L } 40$ , is then obtained via reduction with diborane in dry THF and the subsequent addition of HCl. Pure  $\text{L } 40$  is obtained via recrystallisation from an ethanol/water mixture in 65% yield.

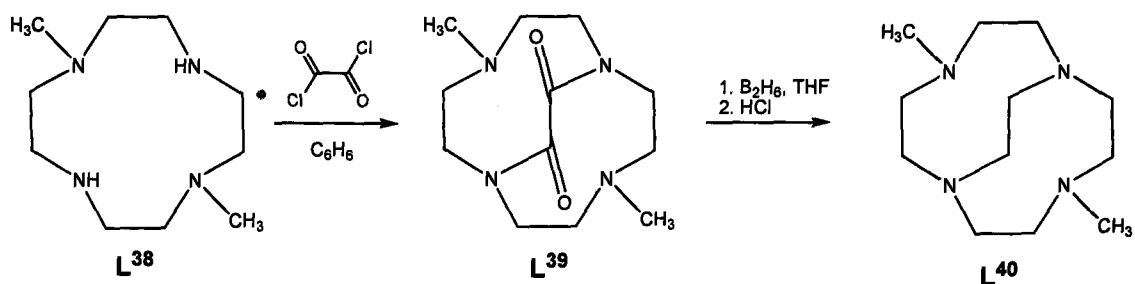


**Figure 64. Synthesis of cross-bridged cyclen, L<sup>40</sup>.**

Weisman *et al.* have reported the preparation of a di-benzyl derivative of cross-bridged cyclen based on their elegant synthesis using bis-aminal methodology.<sup>177</sup> The route is identical to the one shown in Figure 57, except that the starting material is the smaller 12-membered macrocycle. The formation of the bis-aminal, **L<sup>20</sup>**, proceeds in lower yield (63-79%) compared to **3**, presumably as a result of the smaller macrocyclic cavity. The benzylation of the bis-aminal and its subsequent reduction with sodium borohydride proceed in good yields (69-96% and 87-99% respectively). The one disadvantage of this synthesis in comparison to that of Bencini *et al.* is the time the reactions take. The Bencini synthesis can be completed in a few days whereas the Weisman method can take up to 16 days. However, the Weisman method does benefit from the fact that it delivers pure products without the need for any significant purification.

Handel and co-workers have expanded on this work and have published the synthesis of a series of cross-bridged bis-cyclen ligands (Figure 65).<sup>108</sup> They have used xylyl arms in the ortho, meta and para positions as well as a 2,6-pyridine example.

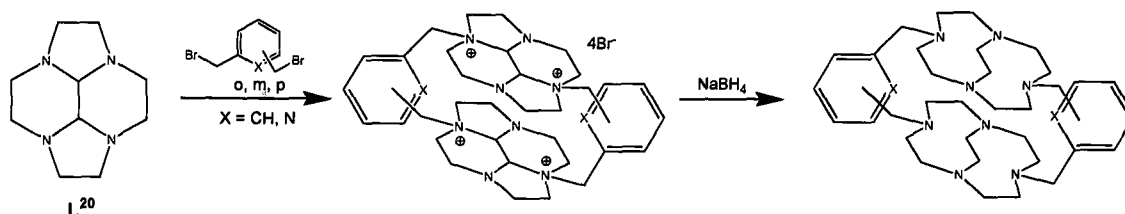


**Figure 65. Synthesis of cross-bridged bis-macrocycle.**

The hydride reduction is dependent on the regioisomer of the xylyl linker group. For example, the ortho and meta compounds give yields of over 90%, whereas the para substituted linker has a yield of only 60%. This is comparable to the yields obtained in this work for hydride reductions on **4**. Just like the cross-bridged cyclam ligands, these compounds exhibit proton sponge properties as evidenced by proton NMR spectroscopy, which reveals a  $\text{NH}^+$  resonance at ca. 12 ppm.

### 3.1.4 Metal Complexes of Cross-bridged Cyclen

There are relatively few transition metal complexes of cross-bridged cyclens in the literature; a search of the CSD reveals there are sixteen crystal structures of cross-bridged cyclen compounds containing benzyl, methyl or no pendent arms. The most common metal complex is iron(III) with four examples, followed by two zinc(II) and two manganese(II) in addition to one each of nickel(II), indium(II), cadmium(II), mercury(II), copper(II), cobalt(II), cobalt(III) and manganese(III). The following section details the reported copper(II) and zinc(II) complexes of cross-bridged cyclen derivatives possessing either methyl or no pendent arms.

There are only two zinc(II) complexes of cross-bridged cyclen in the literature, one possessing two methyl pendent arms and a second without pendent arms, containing two

secondary amine sites.<sup>182, 183</sup> The structure of  $[\text{ZnL}^{40}\text{Cl}_2]$  has been published by Hubin *et al.*<sup>182</sup> Two independent molecules which do not interact with each other are found in the unit cell. Each zinc(II) ion adopts a distorted octahedral coordination environment in the solid state (Figure 66) with zinc(II)-nitrogen bond lengths ranging from 2.217(2) to 2.260(2) Å in one molecule and from 2.222(2) to 2.246(2) Å in the second. There are two bound chloride counter anions present (zinc(II)-chloride distance range 2.3763(7) ← 2.3837(7) Å) completing the six-coordinate geometry.

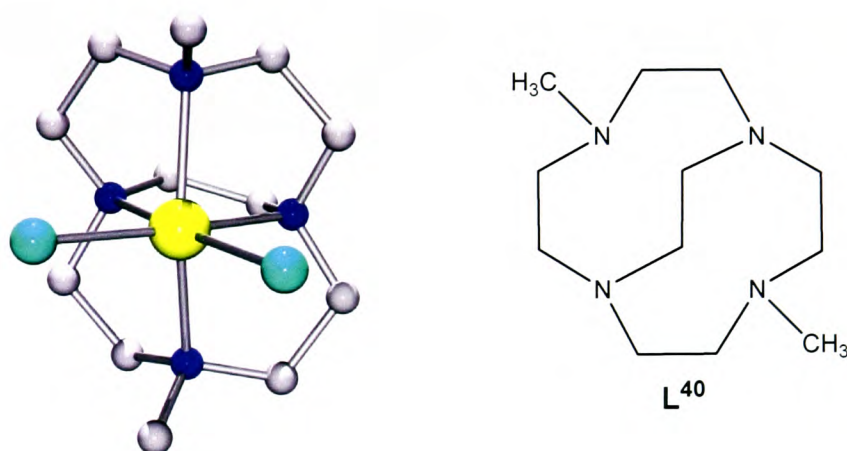


**Figure 66. X-ray crystal structure of  $[\text{ZnL}^{40}\text{Cl}_2]$ .**

In the second example,  $[\text{ZnL}^{41}(\text{OH}_2)_2]^{2+}$ , reported by Niu *et al.*, no pendent arms are present and the zinc(II) metal ion is six-coordinate in the solid state (Figure 67).<sup>183</sup> The zinc(II)-nitrogen bond lengths are shorter (2.133(5)-2.139(4)) Å and the disordered octahedral geometry is completed by two water molecules located cis to each other, the zinc(II)-oxygen bond lengths being 2.123(4) Å. Due to the smaller ligand cleft, the metal ion clearly sits outside of the mean plane of the four macrocyclic nitrogen atoms. This is

evidenced by the angle between the two axial nitrogen atoms and the zinc(II) ion, which is only 156.8(3)°.

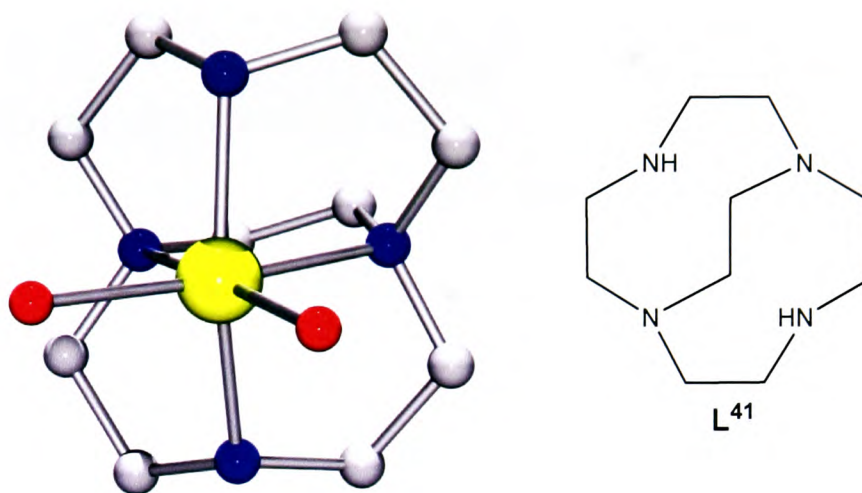


**Figure 67.** X-ray crystal structure of [ZnL<sup>41</sup>(OH)<sub>2</sub>]<sup>2+</sup>.

The only known copper(II) complex of cross-bridged cyclen, [CuL<sup>40</sup>(NCCH<sub>3</sub>)<sub>2</sub>]<sup>2+</sup>, contains two methyl pendent arms.<sup>182</sup> The structure is similar to the zinc(II) example discussed above with the copper(II) adopting a distorted octahedral geometry and the donor atoms are composed of the four macrocyclic nitrogen atoms plus two bound acetonitrile solvent molecules (Figure 68). The copper(II)-nitrogen bond lengths are in the range 2.061(2) to 2.238(4) Å. The presence of the acetonitrile molecules were unexpected as the chloride complex used to grow the crystals was expected to give a five-coordinate structure.

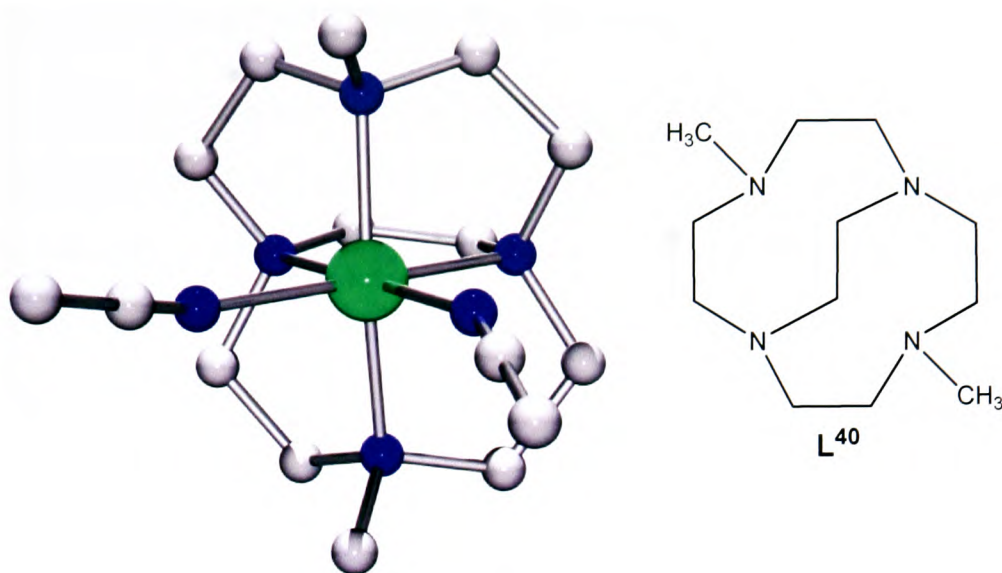


**Figure 68. X-ray crystal structure of  $[\text{CuL}^{40}(\text{NCCH}_3)_2]^{2+}$ .**

Handel and co-workers have reported the synthesis of a series of copper(II) complexes containing the cross-bridged cyclen moiety (Figure 65).<sup>108</sup> These tricyclic macrocycles have been prepared with both mono- and bis-metallic complexes, although no crystal structures have been solved. Interestingly, when the complexation is carried out at low temperature ( $\sim 0^\circ\text{C}$ ), the ratio of copper(II) to ligand never exceeds 1:1, indicating that the second complexation is difficult under these conditions. In fact, no further metallation occurred within a week. Conversely, when the complexation was performed at elevated temperatures (or when a large excess of metal salt was used) the expected bis-metallic complex was obtained. This phenomenon has been attributed to the basic nature of the constrained macrocycles, where one of the rings is protonated and, as a result, electrostatic repulsion lowers reactivity.

### 3.1.5 Kinetic Stability of Cross-bridged Macrocycles

The cross-bridged macrocycles are rigid and therefore have complex stabilities, which are much greater than simple macrocycles. The short cross-bridge gives their transition metal complexes added rigidity constraint. Another characteristic of these ligands is that the bridgehead atoms are also donor atoms. This further increases rigidity, especially in small macrobicycles.

The stability of the resulting transition metal complex can be determined by recording their metal dissociation half lives. This can be achieved via UV-vis spectroscopy for copper(II) complexes or NMR spectrometry for zinc(II) complexes.  $[\text{CuL}^{27}]^{2+}$  is much more stable than  $[\text{CuL}^{40}]^{2+}$  as determined by their respective ligand dissociation half-lives. The half-life of  $[\text{CuL}^{27}]^{2+}$  in 1M  $\text{HClO}_4$  is estimated to be over 6 years (pseudo first order rate constant of dissociation =  $3.5 \times 10^{-9} \text{ s}^{-1}$ ) whereas that of  $[\text{CuL}^{40}]^{2+}$  is only 30 hours (pseudo first order rate constant of dissociation =  $6.4 \times 10^{-6} \text{ s}^{-1}$ ).  $[\text{CuL}^{40}]^{2+}$  is also more rigid than  $[\text{CuL}^{27}]^{2+}$ , due to the decreasing size of the macrocyclic cavity on going from cyclam to cyclen ligands.

## 3.2 Synthetic Aims

In order to prepare a novel cross-bridged cyclam derivative, it was proposed to make a modification of Weisman and co-workers' reduction procedure. The reasoning behind preparing a constrained bis-macrocycle and the synthetic route to compound **4** was highlighted in section 2.2. The proposed route (Figure 69) involves reacting methyl iodide with **4** followed by reduction with sodium borohydride. This synthesis has been designed in collaboration with Dr Tim Hubin (Southwestern State University, Oklahoma, USA).

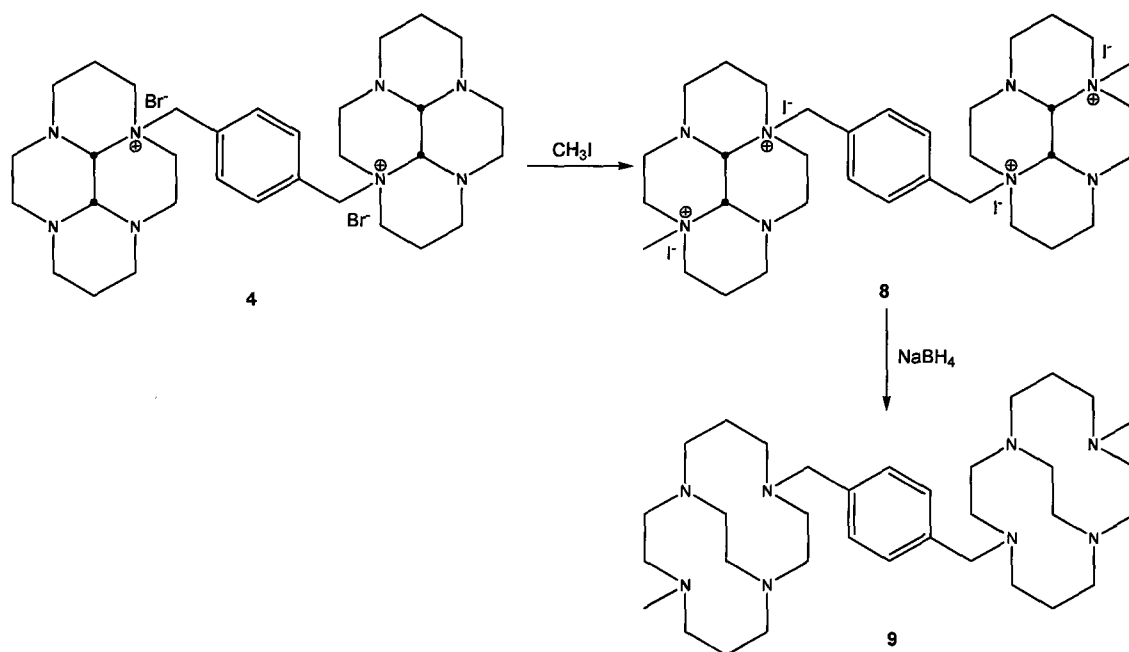


**Figure 69.** Proposed synthetic route to cross-bridged bis-cyclam, **9**.

The synthesis of **9** has proven to be successful and proceeds in an overall yield of just over 50% for the four stage route. This is similar for the route to the side-bridged compounds discussed in the previous chapter even though there is an extra reaction step included. As mentioned previously, the main drawback of this synthetic route is the length

of time needed for the final reduction step. Another problem is the “proton sponge” nature of the final compound, **9**, which means that care must be taken to avoid contact with moisture as the ligand protonates rapidly. However, this problem can be solved by making the HCl salt of the ligand for storage.

### 3.3 Synthetic Discussion

#### 3.3.1 Bis-aminal Precursors

The route to **4** has been covered previously (chapter 2, section 2.3.1). The rigid nature of the macrocycle means that there is only one site for further electrophilic attack. The addition of an alkyl halide is slow and is also complicated as the starting material is insoluble in the reaction solvent. This results in the need for a large excess of a small, reactive, alkyl halide such as methyl iodide and long reaction times. Compound **8** was prepared by adding 100 equivalents (50 per reactive site) of methyl iodide to a suspension of **4** in acetonitrile. This mixture was left for fourteen days at room temperature, and as the reaction proceeds, it is interesting to note that the initial white suspension is replaced by a brown solution. This can be attributed to the anion metathesis of iodide replacing bromide. This is confirmed in the mass spectrum of **8** which reveals a peak at  $m/z$  959 which can be assigned to the loss of iodide.

#### 3.3.2 Reductive Ring Cleavage

The bis-alkylated compound, **8**, can be reduced according to the method previously described by Weisman and co-workers.<sup>173</sup> Our modification of this synthesis proceeded with only twenty equivalents of reducing agent per macrocycle, whereas the literature method required fifty molar equivalents of sodium borohydride. The reduction mechanism has been reported and involves the initial formation of an iminium ion (Figure 70), followed by hydride attack to leave a tricyclic intermediate.<sup>173</sup> This is further attacked by hydride to result in the bicyclo[6.2.2] derivative.

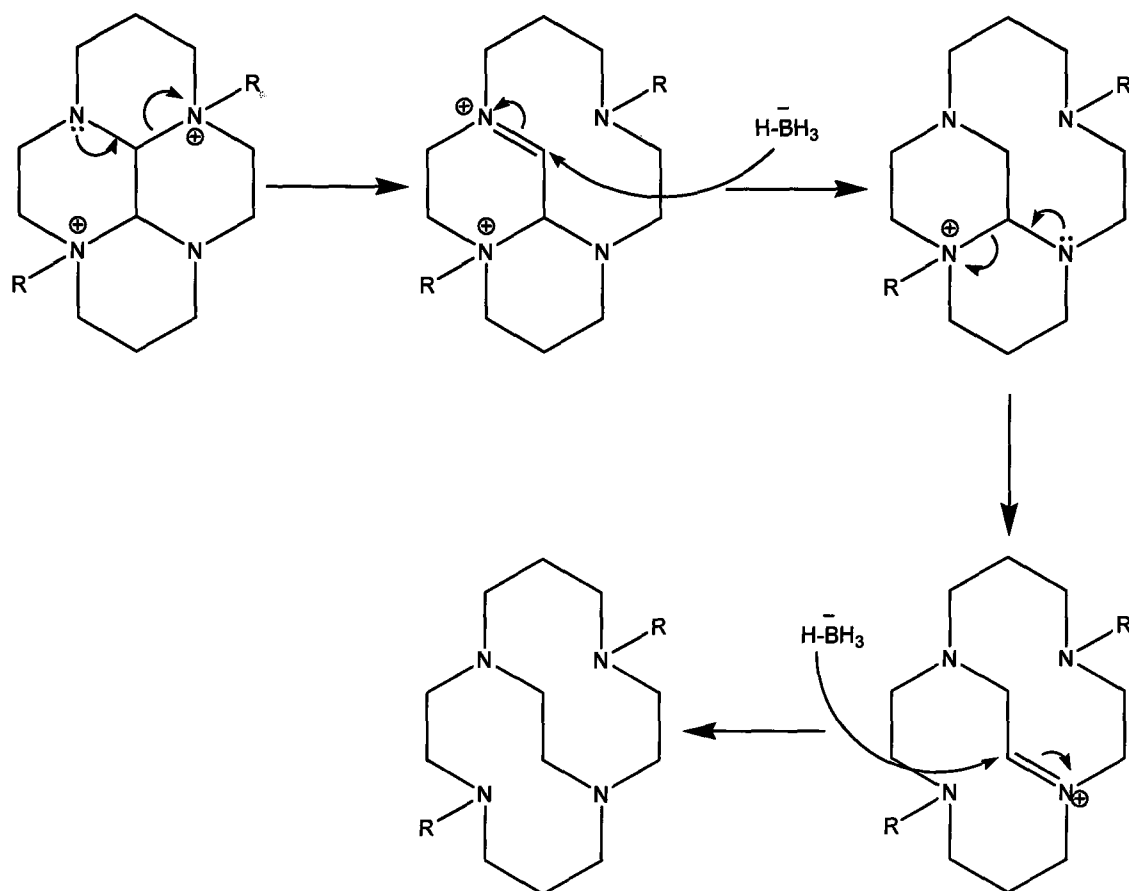


**Figure 70. Mechanism for double ring expansion.**

The yields obtained for **9** are approximately 70%, which is slightly lower than the reported yields; however, this can be attributed to the fact that there are two macrocycles present in our system so a reduced yield would be expected. The free ligand can be protonated by bubbling HCl gas into an ethanolic solution of **9**. The resulting yellow solid was then subjected to elemental analysis which revealed, somewhat surprisingly, that there were seven HCl's present instead of the expected eight.

## 3.4 Transition Metal Complexes

The transition metal complexation of cross-bridged cyclam ligands is significantly more challenging compared to the side-bridged analogues discussed in the previous chapter. Primarily, this is due to the “proton sponge” properties of the cross-bridged ligands. This is a result of the extremely basic nature of the macrocyclic cavity. Protons will compete with metal ions for the macrocyclic cavity and, therefore, rigorously dried solvents are required for the synthesis. The choice of solvent also has a significant effect on the reaction, for example, the zinc(II) complexation will only succeed in DMF. The zinc(II) compounds discussed later in this work (chapter five) have been synthesised by Hubin and his research group, and therefore, the synthesis of these will not be discussed here. The following section details the syntheses of two copper(II) complexes of **9** and their purification. Unfortunately, no single crystals of these complexes were obtained during the course of this work.

### 3.4.1 Copper(II) Complexation

Both copper(II) acetate and copper(II) chloride complexes of **9** were synthesised. Similar to the side-bridged complexes, acetate was chosen as a counter anion as it is a strongly coordinating anion and could also potentially mimic the interaction with aspartate residues on the CXCR4 surface. Chloride was chosen as a counter anion as it has desirable properties for X-ray Absorption Spectroscopy characterisation, which will be discussed later in this work (chapter four).

Complexation was achieved by mixing a dry methanolic solution of **9** with a slight excess of metal salt. The crude products were both purified by size exclusion

chromatography to give the desired complex. The yield obtained for  $[\text{Cu}_2\mathbf{9Cl}_2]\text{Cl}_2$  was a disappointing 36%; however, this was due to the fact that a green impurity came down the sephadex column with the desired blue band. In contrast, the literature yields for copper(II) cross-bridged cyclam derivatives are generally around 65%.<sup>174</sup> This complex was run down the size exclusion column five times in order to maximise the purity of the product. The UV-vis spectrum revealed a very broad d-d transition centred at 622 nm, which is consistent with a five-coordinate geometry. This is expected as it falls in the range of the absorption maxima of  $[\text{Cu}_2\mathbf{L}^{29}]^{2+}$  (675 nm) and  $[\text{Cu}_2\mathbf{L}^{27}]^{2+}$  (596 nm).

The hexafluorophosphate salt can be prepared by adding ammonium hexafluorophosphate.  $[\text{Cu}_2\mathbf{9Cl}_2]^{2+}$  was dissolved in a minimum amount of ethanol and an ethanolic solution containing a 2.2-fold excess of  $\text{NH}_4\text{PF}_6$  was added.  $[\text{Cu}_2\mathbf{9Cl}_2](\text{PF}_6)_2$  rapidly precipitated out of solution and was isolated after filtration and washing with diethyl ether. As expected, no changes in the UV-vis spectrum are observed on replacing two of the unbound chlorides. Mass spectrometry reveals a peak at  $m/z$  390 which corresponds to the loss of two hexafluorophosphate counter anions; however, the compound cannot be seen in the accurate mass spectrum. This can be put down to a common problem with ESI mass spectrometry. The low resolution ESI technique is “soft” and large molecules such as the copper(II) complex in question can readily be identified, whereas the accurate mass collection is a “hard” technique and, as a result, larger molecules are broken up during the course of the experiment and are not observed in the spectrum.

The  $[\text{Cu}_2\mathbf{9}(\text{OAc})_2]^{2+}$  complexation differed from the chloride one above in that it remained in solution during the course of the reaction. Additionally, the colour of the solution was green throughout, as opposed to the blue solution observed for the chloride

species. The crude green product was again purified via size exclusion chromatography. A brown impurity ran down the column before the desired green band was collected. The yield of complexation (54%) is higher than  $[\text{Cu}_2\mathbf{9}\text{Cl}_2]^{2+}$ , which is in agreement with the side-bridged acetate complexes previously discussed. The UV-vis spectra of  $[\text{Cu}_2\mathbf{9}(\text{OAc})_2]^{2+}$  reveals a broad d-d transition, similar to  $[\text{Cu}_2\mathbf{9}\text{Cl}_2]^{2+}$ ; however there is a bathochromic shift in the absorption maxima to 661 nm.

### 3.4.2 EXAFS Analysis

Unfortunately, all attempts to obtain single crystals of these two copper(II) complexes were unsuccessful. Therefore, they have been characterised using X-ray absorption spectroscopy. An in depth look at these results can be found in chapter four; however a brief summary of the EXAFS work is included here.

The EXAFS and XANES spectra of  $[\text{Cu}_2\mathbf{9}\text{Cl}_2]^{2+}$  and  $[\text{Cu}_2\mathbf{9}(\text{OAc})_2]^{2+}$  are essentially identical to each other in the solid state. This suggests that the copper(II) metal ion adopts the same five-coordinate environment in each complex, coordinating to four nitrogen donor atoms and either a chloride or oxygen containing counter anion respectively. Copper(II)-nitrogen bond distances were determined to be just over 2.0 Å. In  $[\text{Cu}_2\mathbf{9}(\text{OAc})_2]^{2+}$ , the copper(II)-oxygen was best fitted to a distance of 1.96(2) Å; however, in  $[\text{Cu}_2\mathbf{9}\text{Cl}_2]^{2+}$  the copper(II)-chloride was further out at 2.26(2) Å. These data are consistent with the crystal structures reported by Hubin and co-workers (Figures 61 and 62), where the copper(II) adopts a square-based pyramidal coordination environment in which the base consists of three nitrogen donors in addition to the counter anion. One of the macrocyclic nitrogen atoms sits in the apical position completing the five-coordinate geometry.

### 3.5 Conclusions

A synthetic route to a bis-macrocyclic compound containing an ethylene cross bridge moiety has been developed. This route proceeds in an overall yield of over 50% for the four step procedure and adds to the ever increasing use of bis-aminal methodology in macrocyclic chemistry. In comparison to the synthetic route to **5**, this route is more time-consuming; however it leads to transition metal complexes of greater kinetic stability. This could be a useful property for *in vivo* studies, as the metal ion will be retained in the macrocyclic cavity for longer and thus potentially being less toxic.

Two copper(II) complexes of **9** have been prepared in relatively low yield. However, the complexes were of sufficient purity to carry out biological testing and also EXAFS analysis. EXAFS suggests that the copper(II) coordination environments in each complex are five-coordinate with a single bond to either chloride or oxygen in addition to the four macrocyclic nitrogen atoms. Given that previously described cross-bridged copper(II) complexes (of **L**<sup>27</sup> and **L**<sup>29</sup>) reported by Hubin *et al.* adopt five-coordinate square-based pyramidal geometries with a longer range axial nitrogen from the macrocycle, it is reasonable to assume that  $[\text{Cu}_2\mathbf{9}\text{Cl}_2]^{2+}$  and  $[\text{Cu}_2\mathbf{9}(\text{OAc})_2]^{2+}$  adopt similar coordination environments.

**Chapter 4. X-RAY ABSORPTION**

**SPECTROSCOPIC ANALYSIS OF**

**COPPER(II) COMPLEXES OF 5 AND 9**

## 4.1 Background

X-ray Absorption Spectroscopy (XAS) can be broken down into two separate entities; X-ray Absorption Near Edge Structure (XANES) and Extended X-ray Absorption Fine Structure (EXAFS) (Figure 71). Although X-ray absorption has been around since the 1930s, EXAFS experiments only became common-place almost forty years later.<sup>184, 185</sup> The first EXAFS experiments using synchrotron radiation were conducted by Kincaid and Eisenberger in the mid 1970s.<sup>186</sup> EXAFS can give structural information on transition metal complexes which are not amenable to X-ray crystallography and for this reason it is the method of choice to study the copper(II) and zinc(II) complexes in this work. Furthermore, EXAFS experiments can be conducted in solution, enabling the coordination environments of the metal complexes to be studied in solution. In addition, the relative affinity of various counter anions to the transition metal ion can be studied. This section details the information which can be obtained from EXAFS, the theory behind the technique and a brief example of how EXAFS data is interpreted in practice.

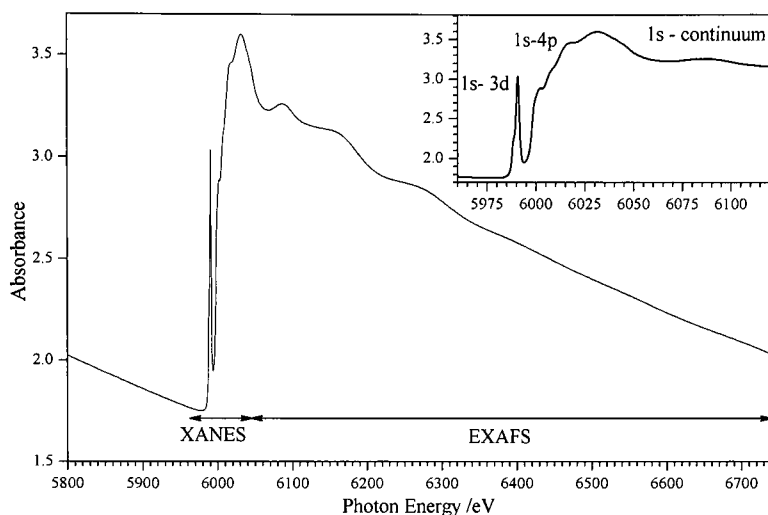


**Figure 71. Cr K-edge XAS spectrum of CrO<sub>2</sub>Cl<sub>2</sub> at 10 K.**

The XANES region (Figure 71) can consist of pre-edge features (e.g. a 1s-3d transition) which can give information on the coordination geometry and oxidation state of the atom of interest. The example in Figure 71 is of CrO<sub>2</sub>Cl<sub>2</sub> which reveals an intense 1s-3d transition due to the tetrahedral environment. For the macrocyclic complexes in this work, the oxidation states of the metal ions are already known so the EXAFS experiment will be more informative. EXAFS gives information about the coordination number of the metal ion, bond distances and the type of the surrounding atoms.

EXAFS is an excellent technique for studying compounds which are not crystalline, and maybe applied to disordered solids and even solutions. When used in transmission or fluorescence mode, the technique is not surface sensitive at the transition metal K-edge as the X-rays can penetrate through the sample if it has been properly prepared. As the metal complexes discussed in chapters two and three have proved difficult to crystallise, EXAFS

was chosen to further study their structural characteristics in the solid state. In addition, EXAFS will give valuable data about the complexes in aqueous solution. EXAFS experiments are relatively trivial to conduct, with the caveat that you have access to an appropriately intense source of tunable X-rays (i.e. synchrotron radiation). Beam-time was applied for and granted to conduct experiments on these complexes at the Daresbury Laboratory Synchrotron Radiation Source (SRS).

## 4.2 XAS Theory

### 4.2.1 X-ray Absorption

An atomic nucleus or a core level electron (e.g. 1s) can absorb X-ray photons of a certain energy according to the photo-electric effect. When the incident X-ray energy is below the binding energy of the core electron (e.g. 1s), the electron can be promoted (photoexcitation) to a higher valence state which will subsequently drop back down to the ground state. When the X-ray energy exceeds the binding energy, the core electron can be ejected into the continuum (photoionisation) (Figure 72).

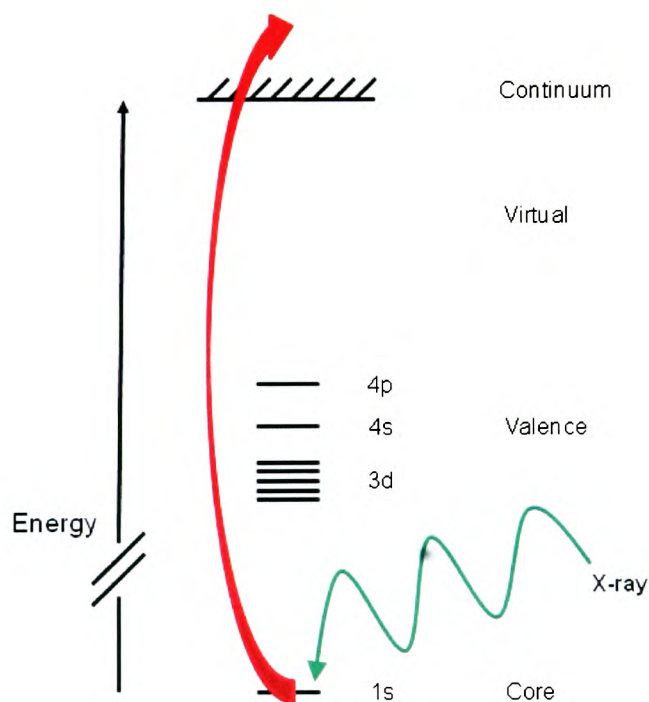


**Figure 72. Schematic representation of the photo-electric effect.**

EXAFS is essentially the measure of  $\mu$  (absorption coefficient) against X-ray energy above the edge.  $\mu$  is a measure of the probability that an X-ray will be absorbed by a core electron and decays exponentially as a function of energy. However, at a specific energy, the core electron will absorb enough energy in order to reach the continuum and a large increase in  $\mu$  is the result (Figure 71). This energy is known as the “edge” and is characteristic of the element in question, which results in another advantage of EXAFS, it being an element specific technique. The oscillations above the “edge” are the result of the interference between the outgoing photo-electron and the part of it that is back-scattered from neighbouring atoms. Therefore, EXAFS can be thought of as a type of electron diffraction; however, the source of electrons is the atom which has absorbed the X-ray photon in the first place.<sup>187</sup> The backscattered wave contains information about the distance, number and type of atoms it has interacted with and so does the EXAFS oscillation. This is the origin of the structural information gathered from EXAFS.

Once the core electron has been excited, the result is a core hole, a photo-electron and the excited atom which then decays by one of two main mechanisms; X-ray fluorescence or the Auger effect (Figure 73). In X-ray fluorescence, a higher energy electron drops down a level to fill the core hole, and in the process, ejecting an X-ray photon of defined energy ( $h\nu$ ) which is characteristic of the atom in question. Therefore, this can be used to identify atoms in solution using fluorescence detection. The Auger effect is a two electron process where one electron drops down to fill the core hole and the second is emitted into the continuum (Figure 73b) with characteristic energy of the orbital from where it has come. In addition, there is a third decay mechanism called secondary electron emission, which deals with the holes left behind by the fluorescence and Auger routes. This can be quite

complicated as it deals with a whole range of processes which may well not have defined energies.

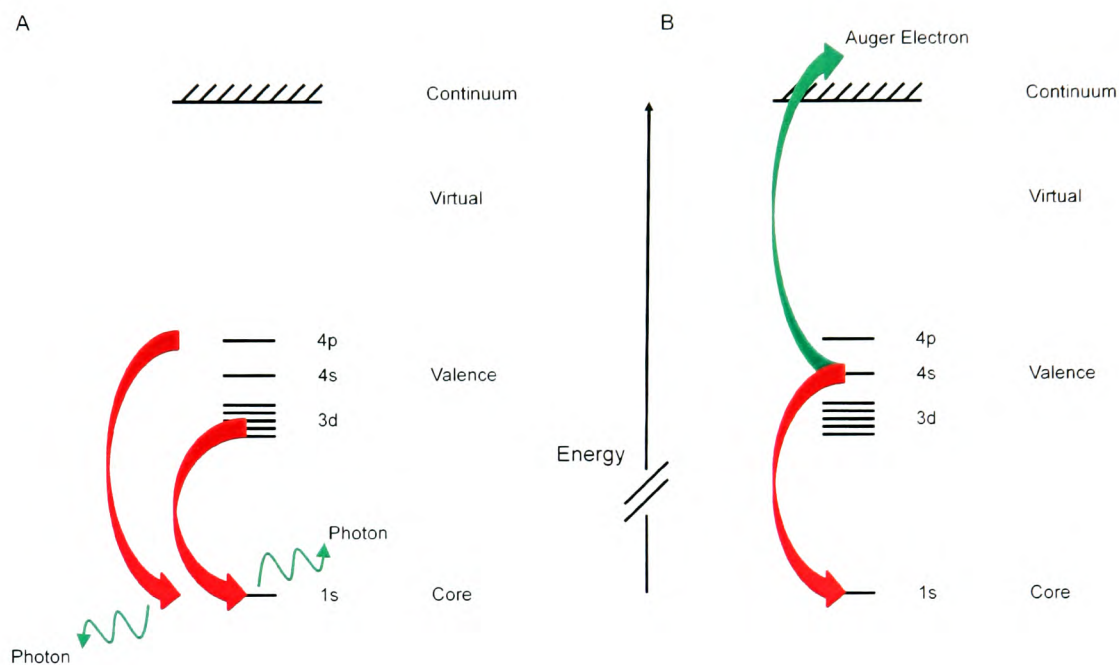


**Figure 73. Schematic representation two decay mechanisms: X-ray fluorescence (A) and the Auger effect (B).**

#### 4.2.2 Data Collection

The EXAFS experiments which were conducted during this work were carried out at the Daresbury SRS on either station 7.1 or 16.5. Solid samples were run in transmission mode using ion chambers with samples diluted in boron nitride and pressed into pellets. Solution samples were run in fluorescence mode, where the sample cells were fitted with kapton windows. The aqueous solutions were frozen in liquid nitrogen before data collection. Both the solid and solution experiments were carried out at 80 K. The spectra were averaged (3 or 4 for solid, ca. 10 for solution) and calibrated (first maximum of the first derivative of the Cu K-edge of copper foil (8979.0 eV)) using PAXAS. The data were

modelled using EXCURVE98. For a more detailed experimental procedure, see experimental section (chapter eight, section 8.1.2)

### 4.2.3 Data Reduction

The raw data collected in an EXAFS experiment is a plot of X-ray photon energy against the absorption coefficient,  $\mu$  (Figure 71) and these data need to be reduced into something more meaningful. This can be divided up into four different sections; pre-edge subtraction, post-edge subtraction,  $k^3$  weighting and finally the Fourier transform (FT) of the EXAFS data. Each step is discussed below.

The pre-edge subtraction can be thought of as removing the background and any instrument function from the data. This is modelled to decay exponentially as if no sample were present (Figure 74), and is usually done by fitting a quadratic expression to  $\mu$  below the “edge” and extrapolating it beyond to higher energies. Following this step, the data are normalised so that the y axis is on a scale of 0-1. This accounts for a single X-ray absorption which is a useful assumption for the data reduction process.

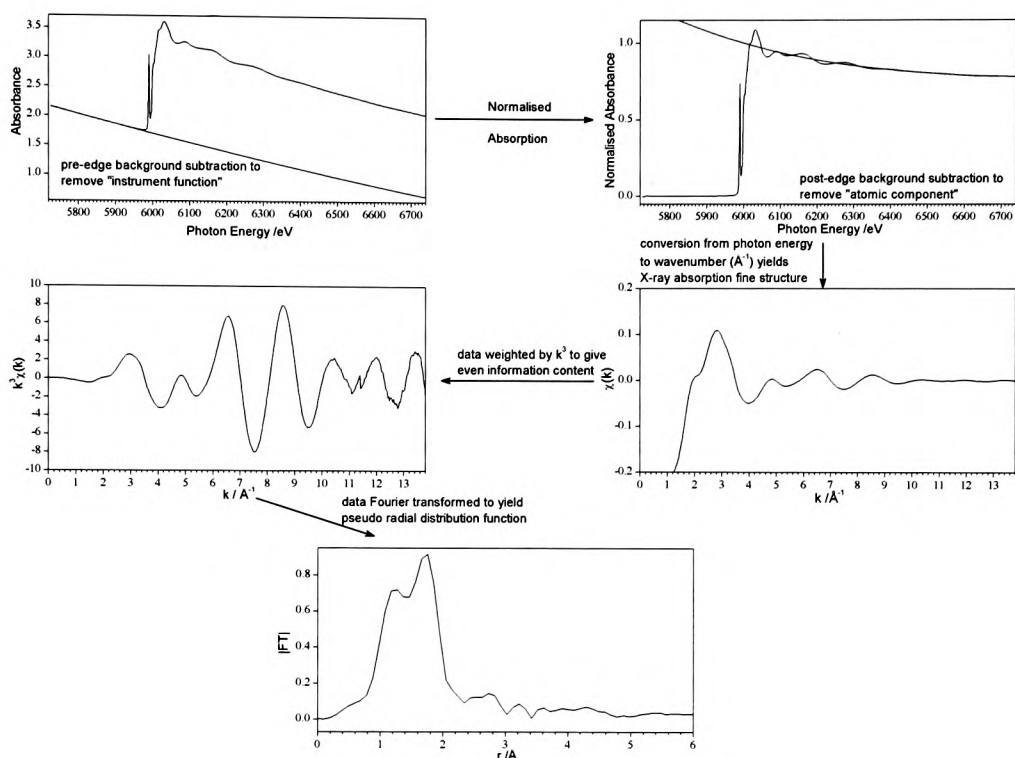


**Figure 74. Summary of the EXAFS data reduction process.**

To extract the EXAFS oscillations from the normalised absorption, what is known as the atomic component is removed. As spectra of free atoms are hard to obtain, this is approximated by either a higher order polynomial or a spline which consists of a series of coupled polynomials (Figure 74). During this process, the abscissa scale is converted from photon energy (eV) to  $k$ -space ( $\text{\AA}^{-1}$ )

As the intensity of the EXAFS signal decreases with energy, the data towards the end of an experiment need to be weighted (Figure 74) so that the fitting uses all of the data. This is conventionally taken to be a  $k^3$  weighting, i.e. all the data-set is multiplied by  $k^3$ , and the result of this treatment is the EXAFS for the complex of interest (Figure 74).

The final step in the analysis of EXAFS data is to take the FT of the EXAFS signal (Figure 74). This involves going from  $k$ -space in  $\text{\AA}^{-1}$  to  $r$ -space in  $\text{\AA}$ . Each peak in the FT corresponds to a coordination sphere of atoms, which allows bond distances to be determined.

#### 4.2.4 Data Modelling

The final step in the EXAFS analysis is fitting a theoretical model to the experimental data. The collected experimental data are initially modelled against a suitable set of structural parameters, such as those obtained from X-ray crystallographic data of related structures or molecular modelling studies. The experimental data are then fitted to the model system by varying the structural parameters until a best least-squares fit is obtained (Figure 75). This gives the experimental data an R value, indicating the quality of the result. In addition, the modelling process leads to statistical uncertainties in the structural parameters being calculated.

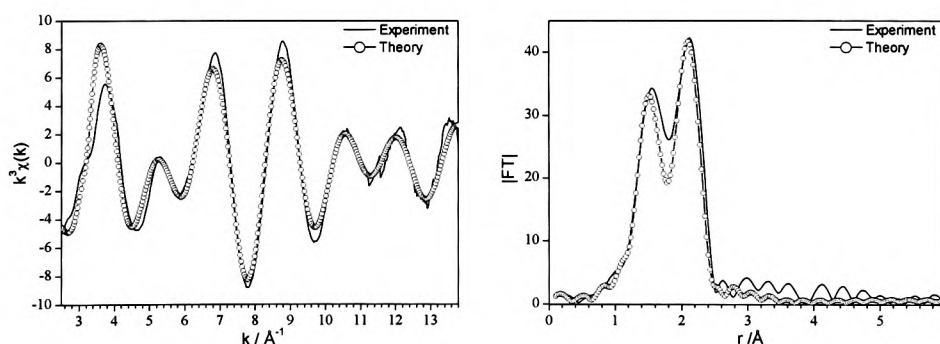


Figure 75. Cr K-edge EXAFS (left) and FT (right) of  $\text{CrO}_2\text{Cl}_2$  at 10 K.

In order to model the data using software such as EXCURVE98, the user defines the number of shells to be included and the atom type. For example, the first coordination shell in this work would be expected to be four nitrogen atoms. This is repeated for the second coordination shell, which could be one or two oxygen atoms or a chloride in the zinc(II) and copper(II) complexes in this study. Provided that the collected data are of sufficient quality, bond distances should be obtained with an accuracy of  $\pm 0.02 \text{ \AA}$  for the first coordination shell. The modelled data will be able to reliably differentiate between atoms whose atomic numbers differ by ten or more. For example, chloride and oxygen could be distinguished, whereas oxygen and nitrogen could not.

### 4.3 Aims of EXAFS Experiments

The aim of the EXAFS work is the characterisation of transition metal complexes in the solid state but also in aqueous solution. The first experimental step would be to confirm that EXAFS would give data that are comparable to the parameters obtained from X-ray crystallographic studies.

Although it is expected that the compound's EXAFS signal would be identical for the solid and solution experiments, EXAFS measurements would be able to confirm this. For the chloride and perchlorate complexes, the solution EXAFS signal would change if they underwent a change in geometry on the addition of acetate, provided that the acetate interacted with the metal ion. Therefore, these experiments could be used as a probe to investigate acetate binding, which has biological significance as the bis-macrocyclic complexes are believed to interact with aspartate residues on the CXCR4 receptor. In addition, short poly-aspartate peptides or a protein with aspartate or glutamate residues on the surface could be used in an EXAFS study to model the binding interaction with the receptor. The recombinant CXCR4 protein is not easy to obtain in sufficient stable quantities to carry out such studies.

## 4.4 XAS Characterisation of Copper(II) Complexes of **5**

For the majority of complexes, three EXAFS experiments were performed. Firstly the solid state data were collected in transmission mode and two aqueous solutions were collected in fluorescence mode. The aqueous solution of complex was split into two and an excess of sodium acetate was added to one and left for twenty-four hours to equilibrate (this was mainly due to beam time considerations as the complexes should reach equilibrium rapidly). This section details the results of the EXAFS studies. There are very few reported X-ray absorption spectroscopic studies of bis-macrocyclic complexes. Only a single example of  $[\text{Cu}_2\mathbf{2}]^{4+}$  has been described which is relevant to this work, although  $[\text{Ni}_2\mathbf{2}]^{4+}$  has also been reported.<sup>188, 189</sup> Both of these complexes have been analysed in the solid state and therefore, there are no reports on solution EXAFS of bis-macrocyclic complexes in the literature.

The zinc(II) complexes of **5** and **9** have been studied, however, due to time constraints, the results are not included in this work. Early analysis of  $[\text{Zn}_2\mathbf{5}(\text{OAc})_2]^{2+}$  suggests that the EXAFS work is in agreement with the solution NMR and X-ray crystallography data.

### 4.4.1 XAS Analysis of $[\text{Cu}_2\mathbf{5}](\text{ClO}_4)_4$

In the absence of any X-ray data on the copper(II) bis-macrocyclic complexes, the appropriate starting point for modelling the data obtained for  $[\text{Cu}_2\mathbf{5}](\text{ClO}_4)_4$  was the single crystal X-ray structure of the mono-copper(II) complex,  $[\text{CuL}^{42}]^{2+}$  (Figure 76), although single crystals of  $[\text{Cu}_2\mathbf{5}\text{Cl}_2]\text{Cl}_2$  and  $[\text{Cu}_2\mathbf{5}](\text{ClO}_4)_4$  were obtained subsequently to the EXAFS studies. On comparison of the modelled EXAFS data with the single crystal X-ray

structure, it is observed that the average copper(II)-nitrogen bond lengths are identical to each other. However, an additional feature is observed in the EXAFS model, which could be a result of water binding to the copper(II) ion.

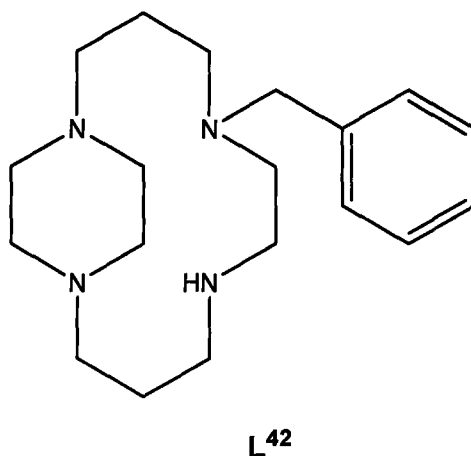


**Figure 76.**  $[\text{CuL}^{42}](\text{ClO}_4)_2$  was used as a starting point for the analysis of  $[\text{Cu}_2\mathbf{5}](\text{ClO}_4)_4$ .

The XANES region of  $[\text{Cu}_2\mathbf{5}](\text{ClO}_4)_4$  (solid, aqueous solution and solution containing an excess of sodium acetate) are essentially the same, the only significant difference being a slight loss in resolution of the solution samples relative to the solid sample (Figures 77 and 78), which is consistent between samples and so appears to be an effect of dissolution. Also included in Figure 77 is the XANES of  $[\text{Cu}_3\mathbf{6}](\text{ClO}_4)_6$  which shows that the trimeric species adopts the same coordination environment as the dimeric complex.

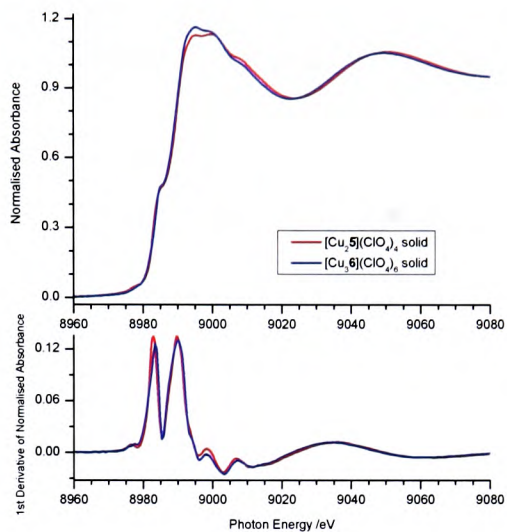


**Figure 77. Cu K-edge XANES spectra of  $[\text{Cu}_{25}](\text{ClO}_4)_4$  and  $[\text{Cu}_6](\text{ClO}_4)_6$  in the solid state at 80 K.**

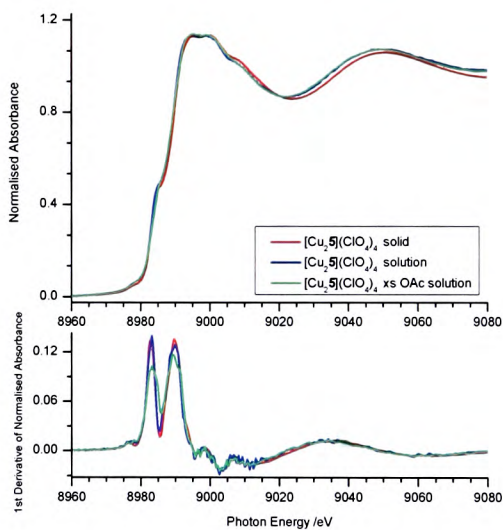


**Figure 78. Cu K-edge XANES spectra of  $[\text{Cu}_{25}](\text{ClO}_4)_4$  derivatives in solution at 80 K.**

Similar to the XANES spectra, the EXAFS and FT data of the solid and two aqueous solutions are essentially identical, although there is a reduction in signal to noise on dissolution (Figure 79).

The solid state data were modelled first and the FT revealed an intense feature at 2.00(2) Å (Table 9), that was assigned to four nitrogen atoms. A copper(II)-oxygen interaction was modelled at a distance of 2.38(2) Å, which was not observed in the X-ray crystal structure. Peaks at longer distances in the FT are due to the carbon atoms from the macrocyclic backbone.

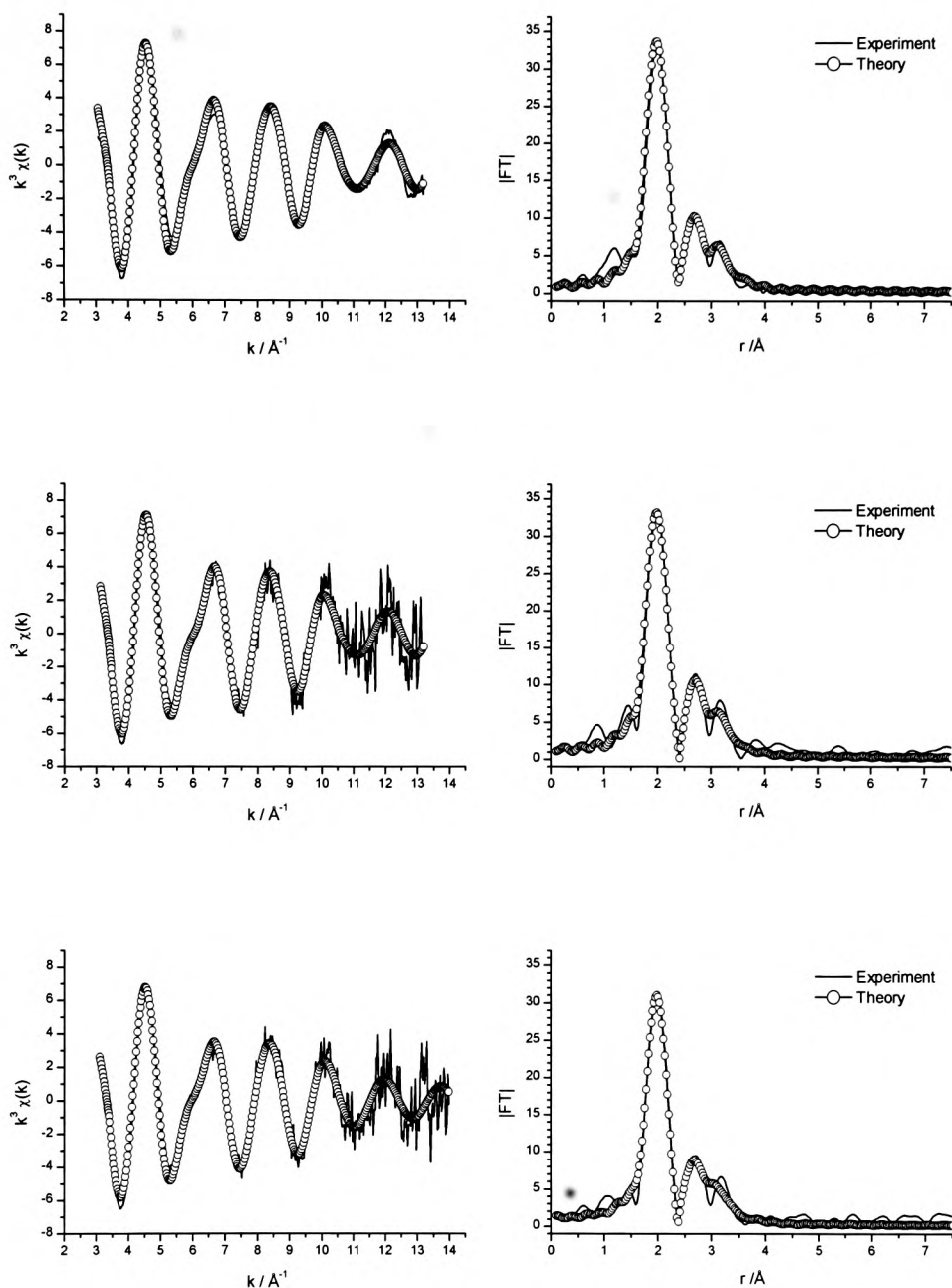


**Figure 79. Cu K-edge EXAFS (left) and FTs (right) of solid  $[\text{Cu}_{25}](\text{ClO}_4)_4$  (top), aqueous solution (middle) and excess acetate solution (bottom) at 80 K.**

On dissolution, there is little change in both the EXAFS and the FTs, indicating that the local environment is very similar in each case. The copper(II)-nitrogen bond distances are essentially the same (2.00(2) Å vs. 2.00(2) Å). There were no significant changes in the EXAFS on adding acetate to the solution. This is in agreement with the UV-vis spectrum which does not alter, even when two hundred molar equivalents of acetate per copper ion were added.

	Cu-N <sub>4</sub>	Cu-O <sub>1</sub>	Cu-C <sub>2</sub>	Cu-C <sub>7</sub>	Cu-C <sub>8</sub>	E <sub>r</sub> <sup>a</sup> / V	R <sup>b</sup> (%)
<b>Solid</b>							
r <sup>c</sup> / Å	1.996(3)	2.375(15)	2.710(8)	2.862(14)	3.347(9)	-0.6(4)	15.7
2σ <sup>d</sup> / Å <sup>2</sup>	0.0091(4)	0.0178(46)	0.0088(21)	0.0347(8)	0.0306(33)		
<b>Aqueous solution</b>							
r / Å	2.000(6)	2.374(21)	2.732(18)	2.868(30)	3.348(18)	0.13(90)	28.1
2σ <sup>2</sup> / Å <sup>2</sup>	0.0093(8)	0.0127(60)	0.0097(50)	0.0396(3)	0.0303(65)		
<b>Excess acetate solution</b>							
r / Å	2.006(5)	2.338(25)	2.721(23)	2.862(30)	3.351(20)	-0.06(88)	28.7
2σ <sup>2</sup> / Å <sup>2</sup>	0.0099(8)	0.0156(64)	0.0153(8)	0.0397(3)	0.0353(76)		

(a) E<sub>r</sub> is single refined parameter to reflect differences in the theoretical and experimental Fermi levels. (b) R = [∫ |χ<sup>T</sup> - χ<sup>E</sup> | k<sup>3</sup>dk / ∫ |k<sup>3</sup>dk|] x 100%. (c) The estimated systematic errors in EXAFS bond lengths are ± 1 % for well-defined coordination shells. (d) 2σ<sup>2</sup> is the Debye-Waller factor. (e) Standard deviations in parentheses.

**Table 9. Refined EXAFS parameters for [Cu<sub>2</sub>5](ClO<sub>4</sub>)<sub>4</sub> in the solid state, aqueous solution and acetate solution.**

#### 4.4.2 XAS Analysis of $[\text{Cu}_2\mathbf{5}(\text{OAc})_2](\text{OAc})_2$

The XANES and EXAFS spectra of  $[\text{Cu}_2\mathbf{5}(\text{OAc})_2](\text{OAc})_2$  (Figure 80) are slightly, but significantly, different from those of  $[\text{Cu}_2\mathbf{5}](\text{ClO}_4)_4$ , the shoulder at ca. 9000 eV disappearing in the acetate complex. The trimeric species  $[\text{Cu}_3\mathbf{6}(\text{OAc})_3](\text{OAc})_3$  is shown to have the same coordination environment as  $[\text{Cu}_2\mathbf{5}(\text{OAc})_2](\text{OAc})_2$  in the solid state.

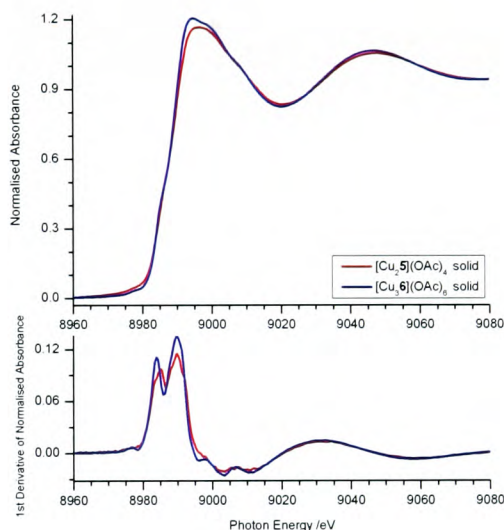


**Figure 80. Cu K-edge XANES spectra of  $[\text{Cu}_2\mathbf{5}(\text{OAc})_2](\text{OAc})_2$  and  $[\text{Cu}_3\mathbf{6}(\text{OAc})_3](\text{OAc})_3$  in the solid state at 80 K.**

In a similar fashion to the perchlorate complex discussed previously, on dissolution there are minimal changes in the XANES spectra (Figure 81). There is, however, a slight loss of resolution in the solution data. The solution containing an excess of sodium acetate is included for completeness and, as expected, no change was observed.

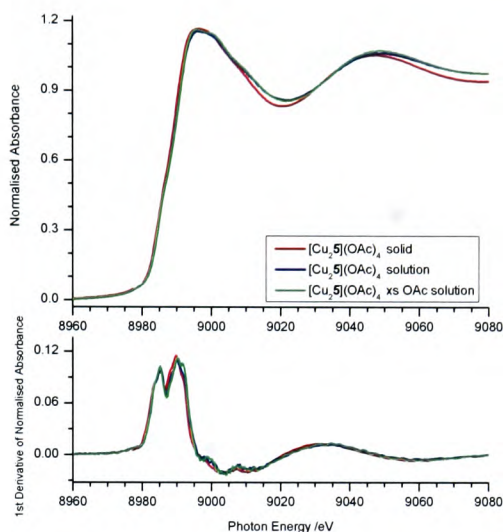


**Figure 81. Cu K-edge XANES spectra of  $[\text{Cu}_{25}(\text{OAc})_2](\text{OAc})_2$  derivatives in solution at 80 K.**

The EXAFS of  $[\text{Cu}_{25}(\text{OAc})_2](\text{OAc})_2$  was best fitted to a model containing four copper(II)-nitrogen bonds at an average distance of 2.02(2) Å in the solid state (Figure 82). The interaction with the acetate counter anion was modelled to a single copper(II)-oxygen at a distance of 2.51(3) Å (Table 10). It is generally considered that axial interactions in copper(II) tetraamine complexes of greater than 2.5 Å should not be considered as bonds.<sup>190</sup> The copper(II)-oxygen distance in  $[\text{Cu}_{25}(\text{OAc})_2](\text{OAc})_2$  falls at the boundary of this distance.

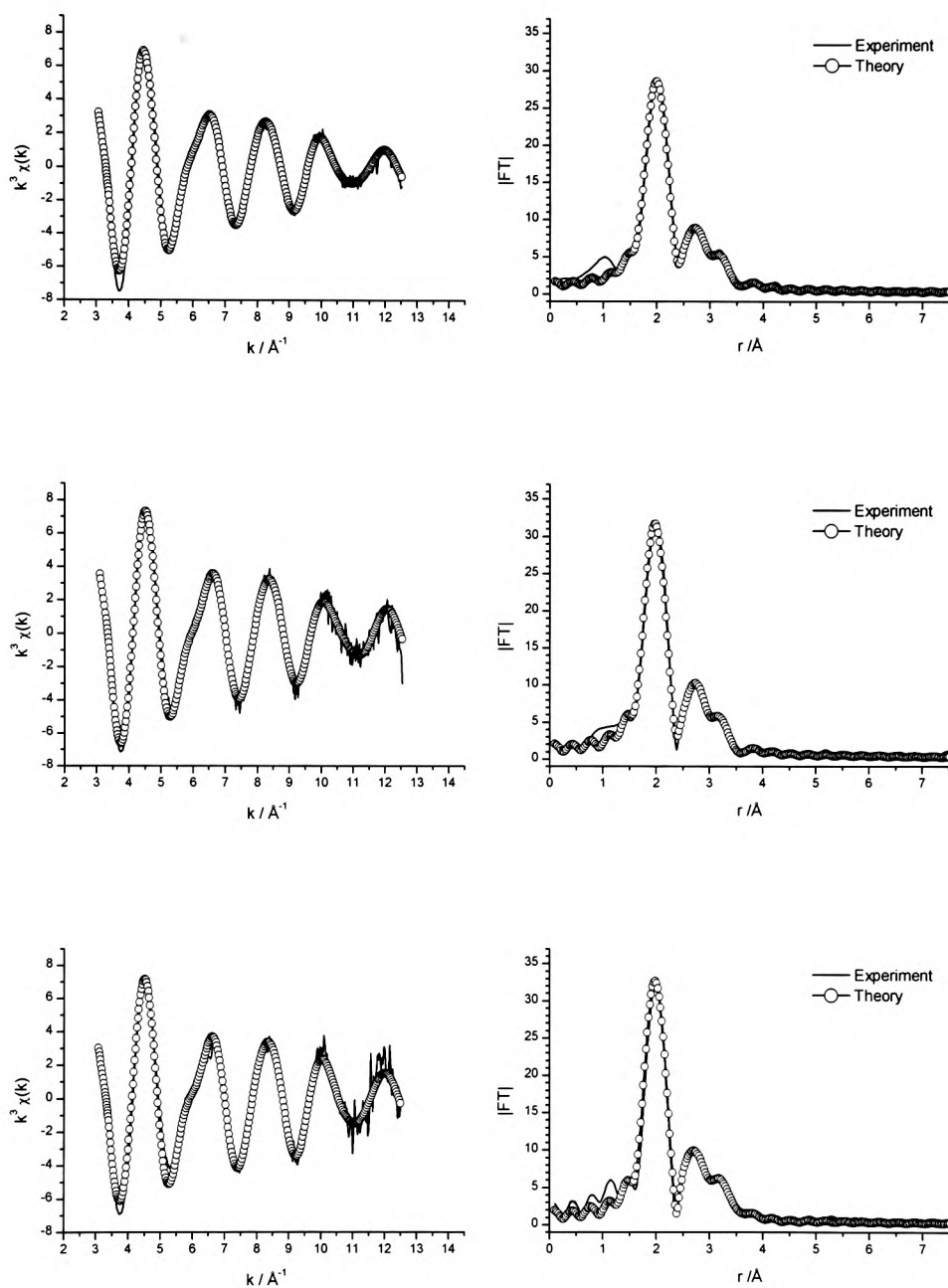


**Figure 82. Cu K-edge EXAFS (left) and FTs (right) of solid  $[\text{Cu}_2(\text{OAc})_2](\text{OAc})_2$  (top), aqueous solution (middle) and solution containing excess acetate (bottom) at 80 K.**

	Cu-N <sub>4</sub>	Cu-O <sub>1</sub>	Cu-C <sub>2</sub>	Cu-C <sub>7</sub>	Cu-C <sub>8</sub>	E <sub>f</sub> <sup>a</sup> / V	R <sup>b</sup> (%)
<b>Solid</b>							
r / Å	2.024(3)	2.507(37)	2.757(13)	2.926(17)	3.375(12)	-0.18 (42)	15.1
2σ <sup>2</sup> / Å <sup>2</sup>	0.0118(5)	0.0362(160)	0.0087(25)	0.0389(62)	0.0359(42)		
<b>Aqueous solution</b>							
r / Å	2.005(3)	2.455(46)	2.749(12)	2.897(13)	3.365(12)	-0.1(42)	17.3
2σ <sup>2</sup> / Å <sup>2</sup>	0.0100(5)	0.0394(48)	0.0081(24)	0.0394(48)	0.0351(46)		
<b>Excess acetate solution</b>							
r / Å	2.011(4)	2.376(38)	2.739(12)	2.893(19)	3.369(12)	-0.50 (63)	20.9
2σ <sup>2</sup> / Å <sup>2</sup>	0.009(5)	0.0296(103)	0.0089(30)	0.0397(2)	0.0300(44)		

(a) E<sub>f</sub> is single refined parameter to reflect differences in the theoretical and experimental Fermi levels. (b) R = [∫ |χ<sup>T</sup> - χ<sup>E</sup> | k<sup>3</sup>dk / ∫ |k<sup>3</sup>dk] x 100%. (c) The estimated systematic errors in EXAFS bond lengths are ± 1 % for well-defined coordination shells. (d) 2σ<sup>2</sup> is the Debye-Waller factor. (e) Standard deviations in parentheses.

**Table 10. Refined EXAFS parameters for [Cu<sub>2</sub>5(OAc)<sub>2</sub>](OAc)<sub>2</sub> in the solid state and aqueous solution.**

#### 4.4.3 XAS Analysis of $[\text{Cu}_2\text{5Cl}_2](\text{PF}_6)_2$

The data obtained from  $[\text{Cu}_2\text{5}(\text{OAc})_2](\text{OAc})_2$  were used as a starting point in the analysis of  $[\text{Cu}_2\text{5Cl}_2](\text{PF}_6)_2$ . Again, the XANES of the tris complex was identical (Figure 83).

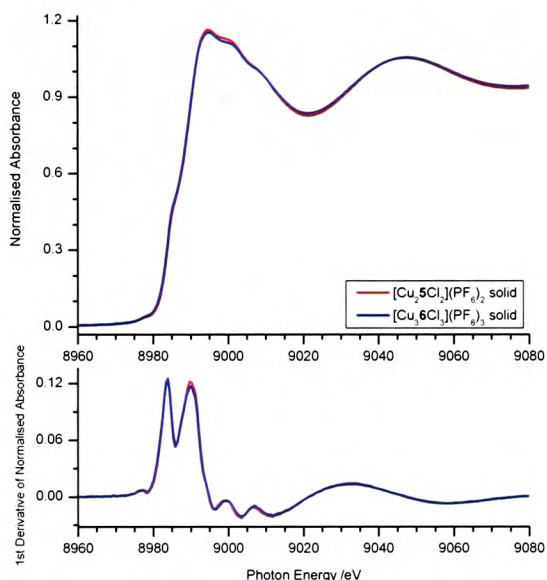


**Figure 83. Cu K-edge XANES spectrum of  $[\text{Cu}_2\text{5Cl}_2](\text{PF}_6)_2$  and  $[\text{Cu}_3\text{6Cl}_3](\text{PF}_6)_3$  in the solid state at 80 K.**

The XANES spectra of  $[\text{Cu}_2\text{5Cl}_2](\text{PF}_6)_2$  and  $[\text{Cu}_2\text{5}(\text{OAc})_2](\text{OAc})_2$  are subtly but significantly different to each other. The chloride and perchlorate complexes are essentially the same, the shoulder at ca. 8978 eV being characteristic of a four coordinate ( $\text{D}_{4\text{h}}$ ) copper(II) geometry.<sup>188, 191, 192</sup> The shoulder is not present in the acetate species, indicating a more five-coordinate character. Later on in the study, the X-ray crystal structure of  $[\text{Cu}_2\text{5Cl}_2](\text{PF}_6)_2$  was determined, which has very similar copper(II)-nitrogen and copper(II)-

chloride bond distances. Once again, on dissolution the XANES spectra were identical as seen in Figures 84 and 85.

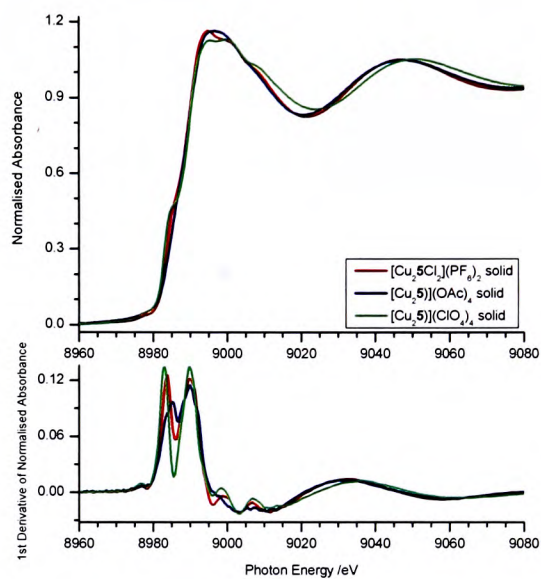


**Figure 84.** Cu K-edge XANES of  $[\text{Cu}_2\text{5Cl}_2](\text{PF}_6)_2$ ,  $[\text{Cu}_2\text{5}(\text{OAc})_2](\text{OAc})_2$  and  $[\text{Cu}_2\text{5}](\text{ClO}_4)_4$  in the solid state at 80 K.

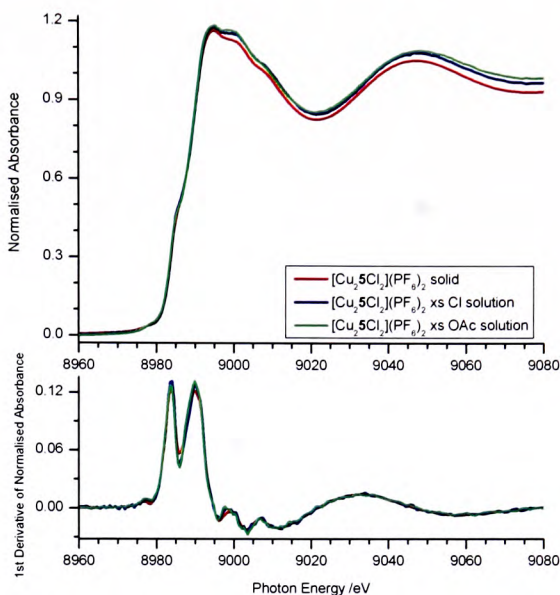


**Figure 85. Cu K-edge XANES of  $[\text{Cu}_25\text{Cl}_2](\text{PF}_6)_2$  derivatives in solution at 80 K.**

The EXAFS of  $[\text{Cu}_25\text{Cl}_2](\text{PF}_6)_2$  was best modelled to a Cu-N<sub>4</sub> interaction at an average of 2.02(2) Å (Figure 86) with a longer copper(II)-chloride distance of 2.54(3) Å (Table 11). On dissolution, the signal to noise decreased as expected and the copper(II)-nitrogen distance (2.01(2) Å) remained essentially the same. Peaks at longer distances were composed of copper(II)-chloride and copper(II) carbon interactions. The addition of acetate to the aqueous solution has no effect on the EXAFS signal, indicating that chloride is not displaced by acetate under these conditions.

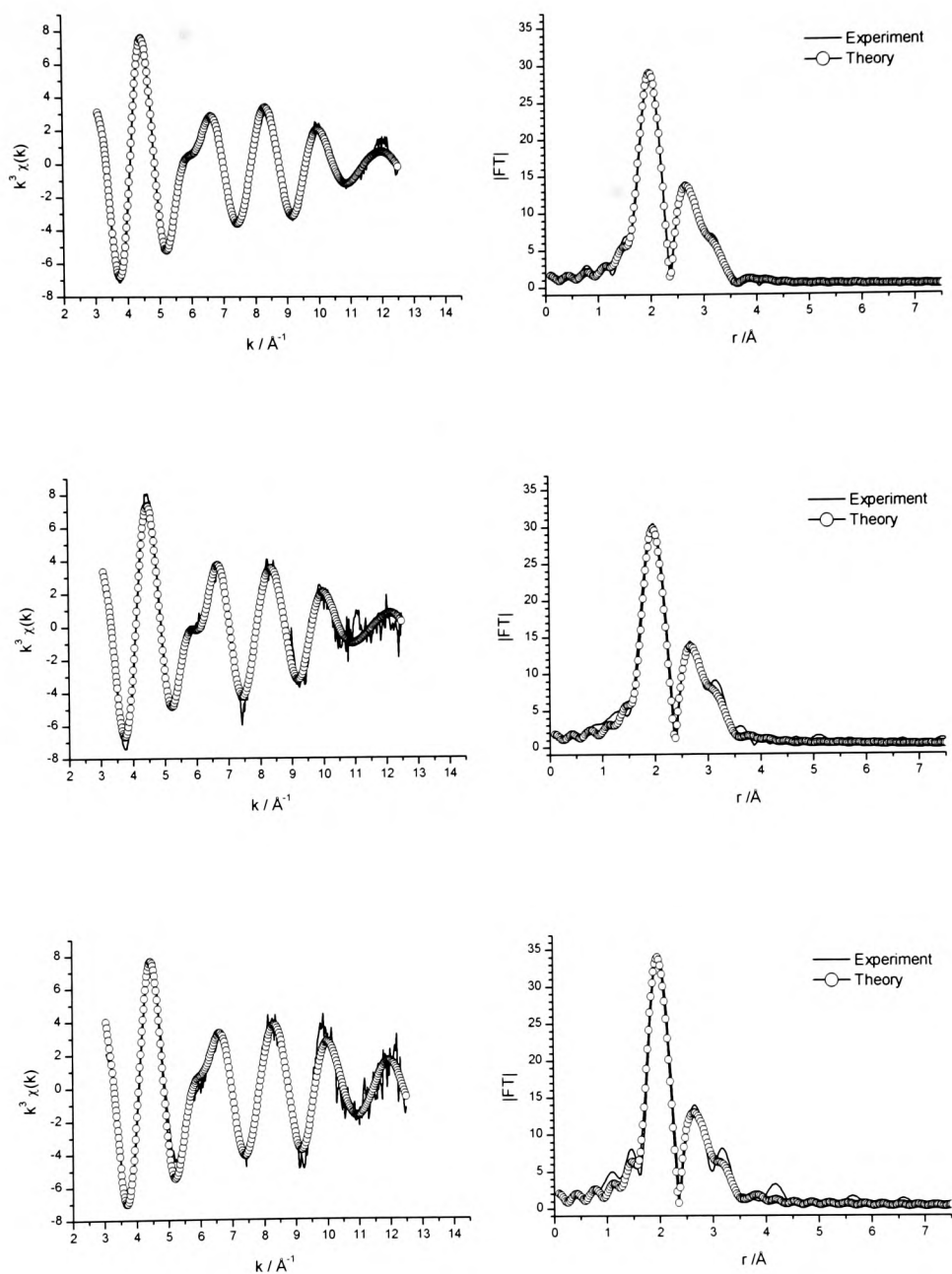


**Figure 86. Cu K-edge EXAFS (left) and FTs (right) of solid  $[\text{Cu}_{25}\text{Cl}_2](\text{PF}_6)_2$  (top) aqueous solution (middle) and solution containing excess acetate (bottom).**

	Cu-N <sub>4</sub>	Cu-Cl <sub>1</sub>	Cu-C <sub>2</sub>	Cu-C <sub>7</sub>	Cu-C <sub>8</sub>	E <sub>f</sub> <sup>a</sup> / V	R <sup>b</sup> (%)
<b>Solid</b>							
r / Å	2.0175(2)	2.544(14)	2.706(12)	2.841(9)	3.395(7)	-0.08	9.7
2σ <sup>2</sup> <sup>d</sup> / Å <sup>2</sup>	0.0112(3)	0.0238(28)	0.0085(23)	0.0325(43)	0.0380(27)	(34)	
<b>Aqueous solution</b>							
r / Å	2.008(4)	2.542(20)	2.695(25)	2.851(19)	3.374(13)	-0.17	21.5
2σ <sup>2</sup> / Å <sup>2</sup>	0.0189(6)	0.0164(41)	0.0084(61)	0.0314(75)	0.0312(47)	(66)	
<b>Excess acetate solution</b>							
r / Å	2.018(4)	2.519(33)	2.735(24)	2.885(27)	3.379(17)	-1.1(6)	22.3
2σ <sup>2</sup> / Å <sup>2</sup>	0.0081(6)	0.0316(104)	0.0085(48)	0.0392(114)	0.0335(65)		

(a) E<sub>f</sub> is single refined parameter to reflect differences in the theoretical and experimental Fermi levels. (b) R = [∫ |χ<sub>T</sub> - χ<sub>E</sub> | k<sup>3</sup>dk / ∫ |k<sup>3</sup>dk] x 100%. (c) The estimated systematic errors in EXAFS bond lengths are ± 1 % for well-defined coordination shells. (d) 2σ<sup>2</sup> is the Debye-Waller factor. (e) Standard deviations in parentheses.

**Table 11. Refined EXAFS parameters for [Cu<sub>2</sub>5Cl<sub>2</sub>](PF<sub>6</sub>)<sub>2</sub> in the solid state, aqueous solution and with excess acetate.**

## 4.5 XAS Characterisation of Copper(II) Complexes of 9

The EXAFS of  $[\text{Cu}_2\mathbf{9}(\text{OAc})_2]^{2+}$  and  $[\text{Cu}_2\mathbf{9}\text{Cl}_2]^{2+}$  have been discussed previously (chapter three, section 3.4.2), however, a detailed account is presented here. The solution data were collected in an analogous fashion to the side-bridged complexes in the previous section.

### 4.5.1 XAS Analysis of $[\text{Cu}_2\mathbf{9}(\text{OAc})_2]^{2+}$

The EXAFS spectrum of  $[\text{Cu}_2\mathbf{9}(\text{OAc})_2]^{2+}$  in the solid state reveals an average copper(II)-nitrogen bond length of 2.10(2) Å and a copper(II)-oxygen bond at 1.96(2) Å (Figure 87). The UV-vis spectrum of  $[\text{Cu}_2\mathbf{9}(\text{OAc})_2]^{2+}$  also suggests a five-coordinate geometry surrounding the copper(II) centre. These data indicate that  $[\text{Cu}_2\mathbf{9}(\text{OAc})_2]^{2+}$  adopts a similar structure to the reported crystal structures of related copper(II) complexes (chapter three section 3.4.1).

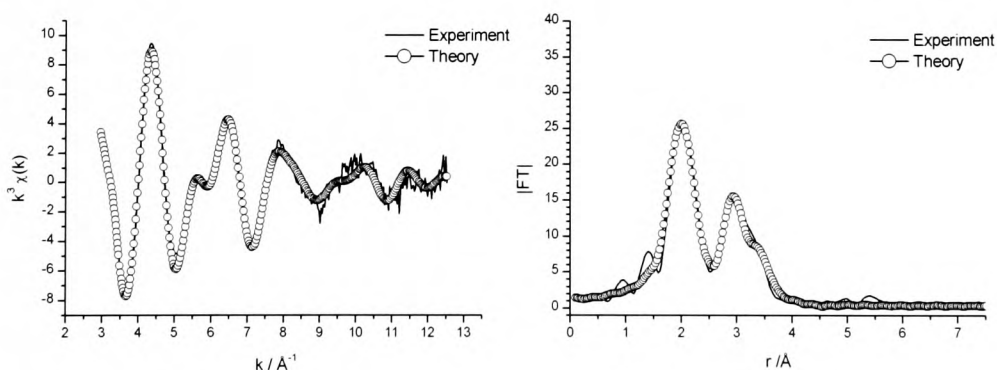


**Figure 87. Cu K-edge EXAFS (left) and FT (right) of  $[\text{Cu}_2\mathbf{9}(\text{OAc})_2]^{2+}$  in the solid state at 80 K.**

On dissolution in water, the EXAFS undergoes minor changes but is still essentially the same when statistical errors are taken into account. The Cu-N<sub>4</sub> bond distances remain the same (2.08(2) Å vs. 2.10(2) Å) (Table 12) and the first coordination sphere is completed by a copper(II)-oxygen interaction at 1.95(2) Å (Figure 88). The bond lengths determined by EXAFS are in good agreement with those of the reported crystal structures of related copper(II) complexes, [CuL<sup>27</sup>]<sup>2+</sup> and [CuL<sup>29</sup>]<sup>2+</sup>.

	Cu-N <sub>4</sub>	Cu-O	Cu-C <sub>2</sub>	Cu-C <sub>7</sub>	Cu-C <sub>8</sub>	E <sub>f</sub> <sup>a</sup> / V	R <sup>b</sup> (%)
<b>Solid</b>							
r <sup>c</sup> / Å	2.096(7)	1.959(13)	2.750(29)	2.940(8)	3.480(8)	0.47(50)	19.0
2σ <sup>2</sup> <sup>d</sup> / Å <sup>2</sup>	0.0157(12)	0.0128(25)	0.0311(90)	0.0150(10)	0.0209(16)		
<b>Aqueous solution</b>							
r / Å	2.079(8)	1.949(32)	2.724(28)	2.934(9)	3.465(10)	0.31(55)	22.3
2σ <sup>2</sup> / Å <sup>2</sup>	0.0116(18)	0.0177(85)	0.0232(110)	0.0132(17)	0.0189(28)		

(a) E<sub>f</sub> is single refined parameter to reflect differences in the theoretical and experimental Fermi levels. (b) R = [∫ |χ<sub>T</sub> - χ<sub>E</sub> | k<sup>3</sup>dk / ∫ |k<sup>3</sup>dk|] × 100%. (c) The estimated systematic errors in EXAFS bond lengths are ± 1 % for well-defined coordination shells. (d) 2σ<sup>2</sup> is the Debye-Waller factor. (e) Standard deviations in parentheses.

**Table 12. Refined EXAFS parameters for [Cu<sub>2</sub>9(OAc)<sub>2</sub>]<sup>2+</sup> in the solid state and aqueous solution.**

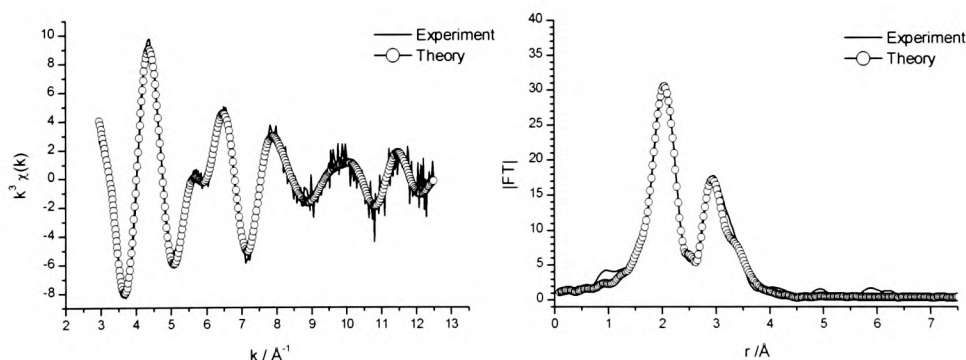


**Figure 88. Cu K-edge EXAFS (left) and FT (right) of [Cu<sub>2</sub>9(OAc)<sub>2</sub>]<sup>2+</sup> in aqueous solution at 80 K.**

#### 4.5.2 XAS Analysis of $[\text{Cu}_2\text{9Cl}_2]^{2+}$

Initial analysis of  $[\text{Cu}_2\text{9Cl}_2]\text{Cl}_2$  suggested that there was a counter anion impurity containing copper(II) chloride (i.e.  $[\text{CuCl}_3]^-$ ). To prevent this impurity affecting the EXAFS analysis, the chloride complex was treated with sodium hexafluorophosphate before the EXAFS studies were undertaken. This was achieved by mixing the chloride complex with 2.2 molar equivalents of sodium hexafluorophosphate in methanol, stirring at room temperature for ten minutes and filtering off the resultant solid. The EXAFS of  $[\text{Cu}_2\text{9Cl}_2]^{2+}$  revealed an intense peak which indicates the presence of a copper(II)-chloride interaction at 2.26(2) Å (Figure 89). This distance is significantly shorter than that observed in  $[\text{Cu}_2\text{5Cl}_2]^{2+}$  which can be explained by the fact that in  $[\text{Cu}_2\text{9Cl}_2]^{2+}$  the chloride occupies an equatorial position and would therefore be expected to form a shorter bond than in  $[\text{Cu}_2\text{5Cl}_2]^{2+}$ , where the chloride occupies an axial position.

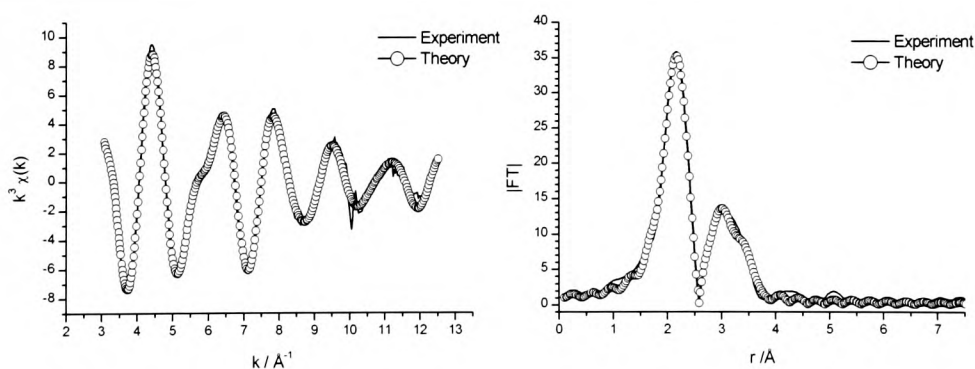


**Figure 89. Cu K-edge EXAFS (left) and FT (right) of  $[\text{Cu}_2\text{9Cl}_2](\text{PF}_6)_2$  in the solid state at 80 K.**

Similar to  $[\text{Cu}_2\text{9}(\text{OAc})_2]^{2+}$ , the best fit of the first coordination shell consisted of a  $\text{Cu-N}_4$  at an average of 2.06(2) Å. The second coordination sphere is completed by two sets of  $\text{Cu-C}$  distances at 2.70(3) Å and 2.93(3) Å respectively (Table 13).

	$\text{Cu-N}_4$	$\text{Cu-Cl}$	$\text{Cu-C}_2$	$\text{Cu-C}_7$	$\text{Cu-C}_8$	$E_f^a / \text{V}$	$R^b (\%)$
<b>Solid</b>							
$r^c / \text{Å}$	2.063(6)	2.260(3)	2.695(27)	2.929(8)	3.449(6)	2.4(4)	11.9
$2\sigma^d / \text{Å}^2$	0.0203(10)	0.0050(5)	0.0341(1)	0.0189(13)	0.0173(14)		
<b>Aqueous solution</b>							
$r / \text{Å}$	2.094(18)	2.246(14)	2.732(66)	2.962(14)	3.455(24)	0.30(13)	30.2
$2\sigma^2 / \text{Å}^2$	0.0146(39)	0.0095(44)	0.0333(360)	0.0086(31)	0.0246(75)		

(a)  $E_f$  is single refined parameter to reflect differences in the theoretical and experimental Fermi levels. (b)  $R = [ \int | \chi_T - \chi_E | K^3 dk / \int | K^3 dk | ] \times 100\%$ . (c) The estimated systematic errors in EXAFS bond lengths are  $\pm 1 \%$  for well-defined coordination shells. (d)  $2\sigma^2$  is the Debye-Waller factor. (e) Standard deviations in parentheses.

**Table 13. Refined EXAFS parameters for  $[\text{Cu}_2\text{9Cl}_2](\text{PF}_6)_2$  in the solid state and aqueous solution.**

If we compare the XANES region of the  $[\text{Cu}_2\text{9}(\text{OAc})_2]^{2+}$  and  $[\text{Cu}_2\text{9Cl}_2]^{2+}$  solid samples (Figure 90), we find that the two are almost identical, indicating that the copper(II) environments are the same in both, apart from the copper(II)-chloride distance is longer than the copper(II)-oxygen distance, as expected. This implies the swapping of chloride with oxygen with no other changes in the copper(II) coordination environment.

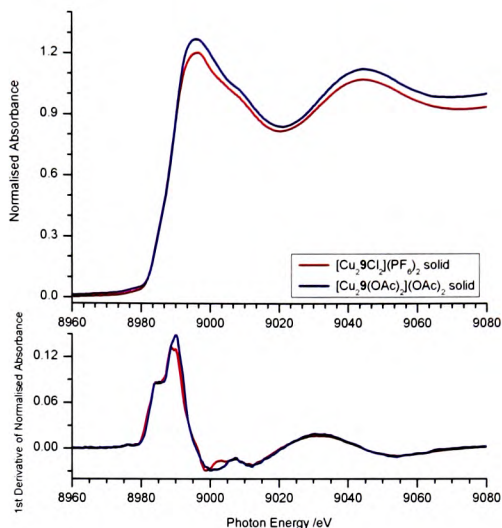


**Figure 90. Cu K-edge XANES of  $[\text{Cu}_2\text{9Cl}_2]^{2+}$  and  $[\text{Cu}_2\text{9(OAc)}_2]^{2+}$  in the solid state at 80 K.**

$[\text{Cu}_2\text{9Cl}_2](\text{PF}_6)_2$  is less soluble in water than  $[\text{Cu}_2\text{9Cl}_2]\text{Cl}_2$  and therefore, an excess of sodium chloride was added to the aqueous solution sample to assist in dissolution of the sample by exchange of the hexafluorophosphate anion for chloride. The solution was filtered through a pad of celite filter aid to remove trace solids before the EXAFS experiment was performed. The solid and solution EXAFS are identical (Figure 91) and are consistent with the XANES analysis.

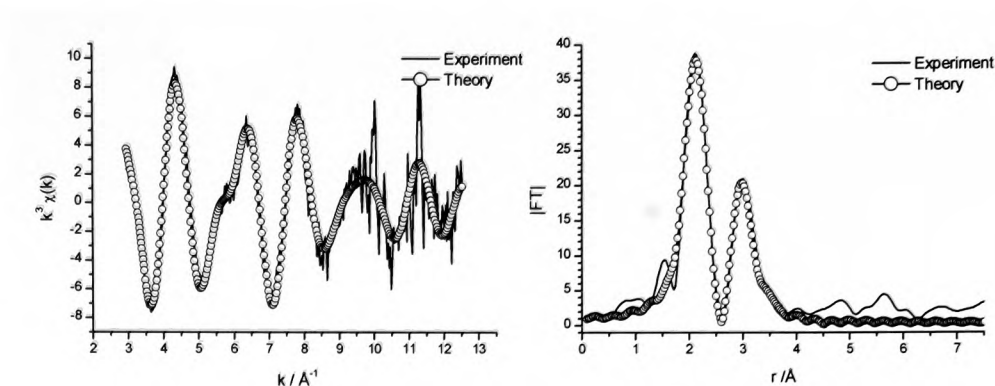


**Figure 91. Cu K-edge EXAFS (left) and FT (right) of  $[\text{Cu}_{29}\text{Cl}_2]\text{Cl}_2$  in aqueous solution at 80 K.**

#### 4.5.3 Anion Displacement Experiments With $[\text{Cu}_{29}\text{Cl}_2]^{2+}$

A second sample was prepared by adding an excess of sodium acetate to  $[\text{Cu}_{29}\text{Cl}_2](\text{PF}_6)_2$  and dissolving in water. After filtering through a pad of celite, the EXAFS experiment was carried out in fluorescence mode. It would be expected that if  $[\text{Cu}_{29}\text{Cl}_2](\text{PF}_6)_2$  interacted with the acetate counter anion, any change in coordination geometry would be observed in the EXAFS data. If the chloride counter anion was replaced by acetate, the EXAFS signal should overlap with that of the acetate complex previously discussed. This is indeed what is observed for this complex (Figure 92).

The solution EXAFS signal is identical to the  $[\text{Cu}_{29}(\text{OAc})_2]^{2+}$  solution EXAFS (Figures 91 and 92), where the first coordination sphere is composed of a Cu-N<sub>4</sub> shell at 2.07(2) Å and a copper(II)-oxygen distance of 1.93(2) Å.

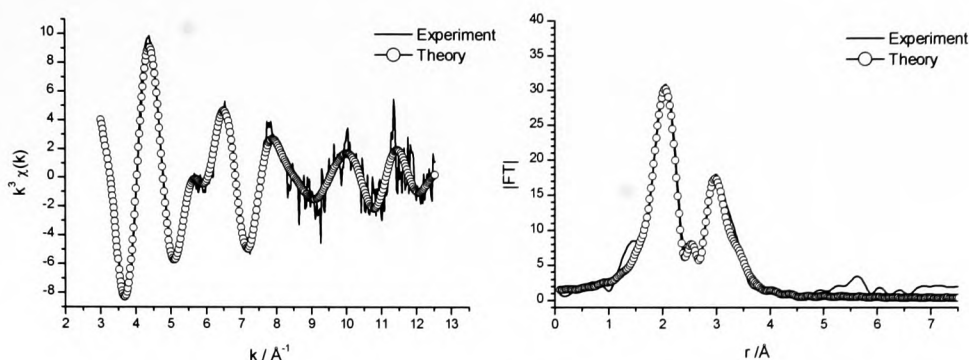


**Figure 92. Cu K-edge EXAFS (left) and FT (right) of  $[\text{Cu}_2\text{9Cl}_2](\text{PF}_6)_2$  in aqueous solution at 80 K with acetate added.**

In the solution containing an excess of sodium acetate, there will still be chloride ions present which could potentially interfere with the results of the EXAFS experiment by scattering the X-ray beam, which has the effect of making the signal to noise ratio worse and therefore, the data less well resolved. In order to negate this potential problem, an excess of silver(II) acetate was added to the solution of  $[\text{Cu}_2\text{9Cl}_2]^{2+}$ . This should have the effect of removing the free chloride counter ions from solution in the form of insoluble silver(II) chloride which can be removed by filtration.

After filtration through a pad of celite filter aid, the EXAFS spectrum was obtained in fluorescence mode (Figure 93). The data are quite noisy, which is attributable to the low concentration of copper(II) in the solution sample. The EXAFS signal is essentially identical to the  $[\text{Cu}_2\text{9(OAc)}_2]^{2+}$  solution previously discussed which confirms that there was no scattering interference in the EXAFS spectrum from any chloride ions.

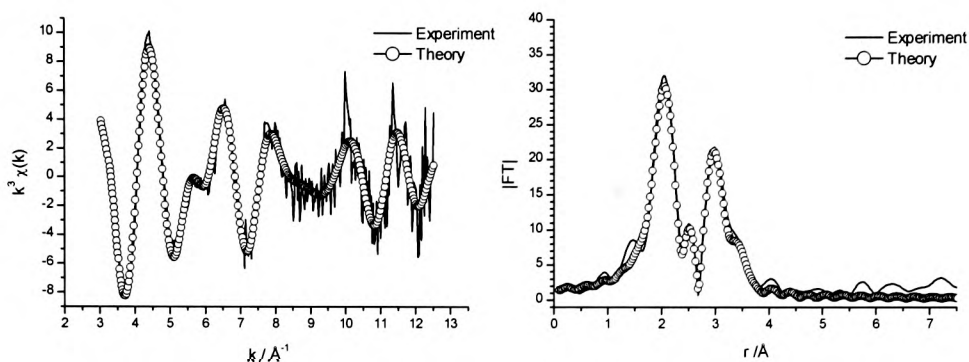


**Figure 93. Cu K-edge EXAFS (left) and FT (right) of  $[\text{Cu}_29\text{Cl}_2](\text{PF}_6)_2$  in aqueous solution at 80 K with silver(II) acetate added.**

	Cu-N <sub>4</sub>	Cu-O	Cu-C <sub>2</sub>	Cu-C <sub>7</sub>	Cu-C <sub>8</sub>	E <sub>f</sub> <sup>a</sup> / V	R <sup>b</sup> (%)
<b><math>[\text{Cu}_29(\text{OAc})_2]^{2+}</math> Solid<sup>f</sup></b>							
r / Å	2.096(7)	1.959(13)	2.750(29)	2.940(8)	3.480(8)	0.47(50)	19.0
2σ <sup>d</sup> / Å <sup>2</sup>	0.0157(12)	0.0128(25)	0.0311(90)	0.0150(10)	0.0209(16)		
<b><math>[\text{Cu}_29(\text{OAc})_2]^{2+}</math> Aqueous solution<sup>f</sup></b>							
r / Å	2.079(8)	1.949(32)	2.724(28)	2.934(9)	3.465(10)	0.31(55)	22.3
2σ <sup>d</sup> / Å <sup>2</sup>	0.0116(18)	0.0177(85)	0.0232(110)	0.0132(17)	0.0189(28)		
<b><math>[\text{Cu}_29\text{Cl}_2]^{2+}</math> with excess NaOAc</b>							
r / Å	2.070(9)	1.929(33)	2.727(22)	2.938(11)	3.452(12)	1.48(6)	25.8
2σ <sup>d</sup> / Å <sup>2</sup>	0.0112(20)	0.0182(99)	0.0092(52)	0.0111(18)	0.0192(37)		
<b><math>[\text{Cu}_29\text{Cl}_2]^{2+}</math> with excess Ag(OAc)<sub>2</sub></b>							
r / Å	2.060(10)	1.912(50)	2.688(17)	2.926(11)	3.448(16)	1.9(7)	31.7
2σ <sup>d</sup> / Å <sup>2</sup>	0.0111(20)	0.0277(182)	0.0034(39)	0.0074(18)	0.0176(45)		

(a) E<sub>f</sub> is single refined parameter to reflect differences in the theoretical and experimental Fermi levels. (b)  $R = [\int |\chi_T - \chi_E| k^3 dk / \int k^3 dk] \times 100\%$ . (c) The estimated systematic errors in EXAFS bond lengths are  $\pm 1\%$  for well-defined coordination shells. (d) 2σ<sup>2</sup> is the Debye-Waller factor. (e) Standard deviations in parentheses. (f) Solid and solution data repeated for completeness and clarity.

**Table 14. Summary of EXAFS parameters for  $[\text{Cu}_29(\text{OAc})_2]^{2+}$  and  $[\text{Cu}_29\text{Cl}_2]^{2+}$  derivatives in the solid state and various aqueous solutions.**

## 4.6 Conclusions

EXAFS has been used in order to study the metal complexes of **5** and **9**. Data for  $[\text{Cu}_2\mathbf{5}](\text{ClO}_4)_4$  in the solid state were found to be identical to the structure determined by X-ray crystallography, confirming that the EXAFS data can be compared to X-ray crystallography.

Interestingly, the copper(II) complexes of **5** were not affected by addition of acetate which is in contrast to literature reports on related zinc(II) complexes of AMD3100.<sup>146</sup> The changes in the AMD3100 complexes are due to the rearrangement of the macrocyclic backbone in the presence of acetate. However, in the configurationally rigid complexes, the EXAFS will only be significantly different if the copper(II) coordination environment is altered in the presence of acetate. UV-vis studies on the copper(II) complexes of **5** support these findings, even with the weakly coordinating perchlorate counter anion. Given that these data suggest the complexes do not bind to acetate, it is still believed that the metal complexes interact with aspartate residues to bind to CXCR4 due to the proximity of acetate residues in the binding cleft and the fact that these complexes do bind to CXCR4 (chapter five).

In the absence of any X-ray crystal structures of complexes of **9**, EXAFS has been employed as the primary structural characterisation technique. The coordination environment of the copper(II) ions in both  $[\text{Cu}_2\mathbf{9}\text{Cl}_2]^{2+}$  and  $[\text{Cu}_2\mathbf{9}(\text{OAc})_2]^{2+}$  is five-coordinate, with an axial interaction with a macrocyclic nitrogen atom. This distance is shorter than would be expected due to the rigidity of the macrocycle. The XANES region of the spectra indicated that the two complexes were identical in structure with oxygen

replacing chloride in the fifth coordination site. The counter anion has been shown to occupy an axial position in the complexes of **5**, at a longer distance than in complexes of **9**, where the counter anion occupies an equatorial position. In contrast to the complexes of **5**, the EXAFS signal of  $[\text{Cu}_2\mathbf{9}\text{Cl}_2]^{2+}$  in aqueous solution underwent a change on the addition of acetate. The solution EXAFS of  $[\text{Cu}_2\mathbf{9}\text{Cl}_2]^{2+}$  with excess acetate present was found to be identical to the  $[\text{Cu}_2\mathbf{9}(\text{OAc})_2]^{2+}$  aqueous solution. This indicates that  $[\text{Cu}_2\mathbf{9}\text{Cl}_2]^{2+}$  shows a greater affinity for acetate exchange than the complexes of **5**, which is somewhat surprising as in the later case, a long range axial anion is being substituted which would be expected to be more favourable than replacing an equatorial counter anion.

**Chapter 5. BIOLOGICAL ASSAYS:  
COMPETITION BINDING, ANTI-VIRAL  
ACTIVITY AND CALCIUM SIGNALLING**

## 5.1 CXCR4 Antagonism

Having synthesised two bis-macrocyclic ligands containing ethylene bridges and a range of their transition metal complexes, characterised them in both the solid state and aqueous solution, the next step in the research was to conduct a variety of assays on these compounds to test their biological properties. To begin, an antibody displacement assay was designed to confirm that the compounds bind to CXCR4 as they are expected to. Jurkat cells were found to express a high level of CXCR4. These assays have been carried out by Abid Khan, a member of the Archibald group in collaboration with Dr John Greenman (Medical Research Laboratory, University of Hull) and a brief summary of the results are presented below. A detailed account of these assays has been published.<sup>193</sup> The anti-viral potency and calcium signalling properties of a selection of compounds has also been determined in collaboration with a group headed by Prof. Erik De Clercq in Leuven, Belgium. The results from these assays are discussed here in addition to a structure-activity relationship analysis.

The strength of antagonist binding to a receptor was analysed by two methods. Firstly, a method of displacing the antagonist from the CXCR4 surface with monoclonal antibodies (mAbs) and secondly, competing the antagonist with mAbs that have been raised to specifically bind to the receptor in question. There have been similar experiments carried out on AMD3100 and its metal complexes.<sup>194</sup> However, these assays were not identical to ours and therefore, AMD3100 and its copper(II) and zinc(II) complexes were synthesised and included in this study as controls (see experimental section for synthetic details). Compounds **5** and **9** and their metal complexes were tested against four different mAbs

which bind to different epitopes of CXCR4; however, only the results from the 12G5 mAb are included here as this binds to CXCR4 in a similar position to AMD3100. The results from these assays have been previously reported, but a brief summary is relevant to this work and as such is included here.<sup>193</sup>

### 5.1.1 Displacement Assay

To summarise the assay itself, it is best to break the procedure down into four steps. To begin with, the Jurkat cells expressing CXCR4 are incubated with a very large excess of antagonist compound (20  $\mu$ M) which saturates the receptor. After half an hour, excess compound is washed off. The cells are then incubated for an hour with a primary mAb which is specific to CXCR4, before a secondary (fluorescently tagged) mAb is added which binds to the primary mAb. The final step in the assay is to quantify the fluorescence intensity via flow cytometry, which can be extrapolated in order to calculate the % binding inhibition of each antagonist compound. An example of a flow cytometry plot is shown in Figure 94. The negative control (purple) represents zero mAb binding and the positive control (red) represents total mAb binding. Therefore, the more effectively a compound competes for receptor binding, the closer it will be to the negative control. In terms of interpreting the results from the assay, the higher the % binding inhibition, the more of the compound binds to CXCR4.

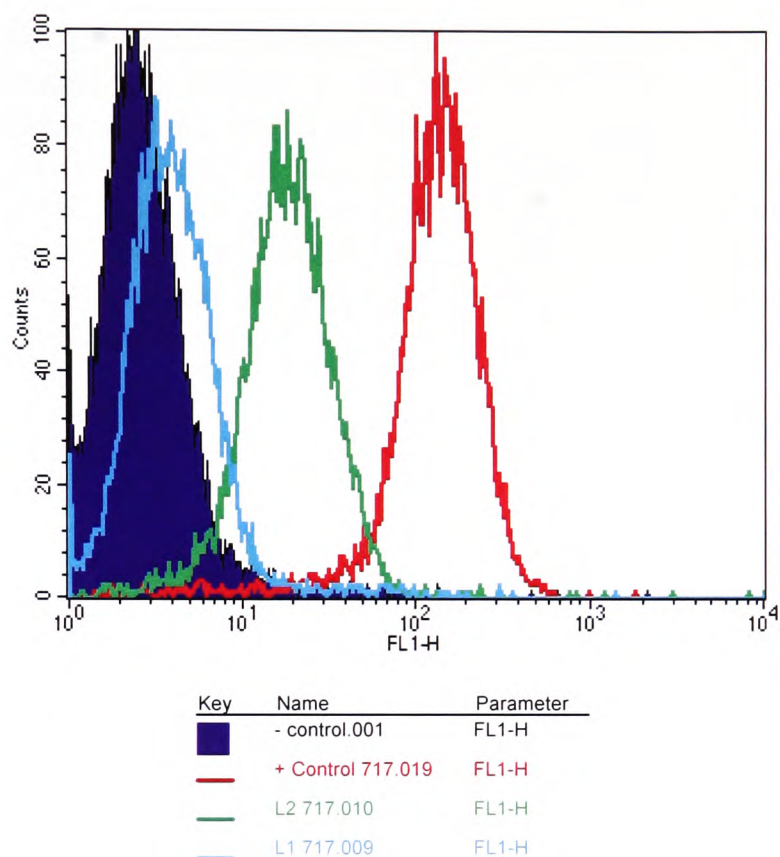


**Figure 94. Typical flow cytometry plot showing negative control (purple), positive control (red) and two different antagonists (blue and green).**

The displacement assay confirms that all of the ligands and their metal complexes bind to CXCR4 under the conditions employed (Figure 95). Each metal complex inhibited 12G5 binding more effectively than AMD3100, except  $[\text{Cu}_2\mathbf{5}]^{4+}$ , which showed similar inhibition to AMD3100. Considering the free ligands (i.e. with no metal present), AMD3100 is significantly more effective than **5** which, in turn, is significantly more effective than **9**.

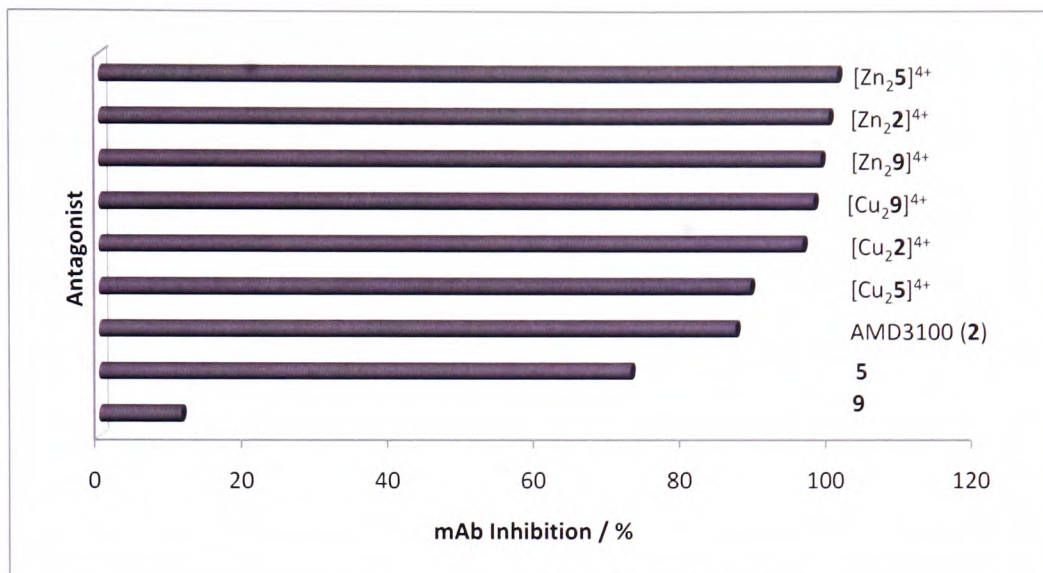


**Figure 95. Summary of mAb 12G5 binding to CXCR4 in the presence of bound antagonists.**

The metal complexes tested all inhibited 12G5 binding at approximately 100% (Figure 95), which means that when statistical errors are considered, they cannot be distinguished from each other. This means that the displacement assay with 12G5 is not ideal as it fails to conclude which complex binds most effectively to CXCR4. In order to probe the binding inhibition further and differentiate between compounds, a competition binding assay was designed.<sup>193</sup>

### 5.1.2 Competition Binding Assay

The competition binding assay was carried out in a similar fashion to the displacement assay described above except that the antagonist was added at the same time as the mAb and a lower concentration (1-10  $\mu\text{M}$ ) of antagonist was used. The antibodies compete with the synthetic compound for receptor binding and the property which is usually reported is the  $\text{IC}_{50}$ , the concentration required to inhibit 50% of mAb binding.

The IC<sub>50</sub> values of the ligands and selected complexes are summarised in Table 15. In agreement with the displacement assay, the IC<sub>50</sub> values reveal that the metal complexes are more effective than the free ligands. Compounds **5** and **9** are less effective than AMD3100 and, in fact, the cross-bridged cyclam, **9**, failed to achieve 50% inhibition at all. It is clear from these data that [Cu<sub>2</sub>**9**]<sup>4+</sup> inhibits mAb binding more effectively than the other complexes tested. Interestingly, [Cu<sub>2</sub>**2**]<sup>4+</sup> shows comparable inhibition to AMD3100 which is in contrast to literature results.<sup>114</sup>

Compound	IC <sub>50</sub> / μM	IC <sub>90</sub> / μM
[Cu <sub>2</sub> <b>9</b> ] <sup>4+</sup>	0.18	0.85
[Zn <sub>2</sub> <b>2</b> ] <sup>4+</sup>	0.25	1.36
[Zn <sub>2</sub> <b>9</b> ] <sup>4+</sup>	0.25	1.35
[Zn <sub>2</sub> <b>5</b> ] <sup>4+</sup>	0.26	1.52
[Cu <sub>2</sub> <b>5</b> ] <sup>4+</sup>	0.33	2.85
[Cu <sub>2</sub> <b>2</b> ] <sup>4+</sup>	0.35	2.39
AMD3100	0.37	4.26
<b>5</b>	17.03	> 17.03
<b>9</b>	n/a	n/a

**Table 15. IC<sub>50</sub> and IC<sub>90</sub> values of compounds tested.**

## 5.2 Anti-HIV Assays

Having confirmed that the complexes bind to CXCR4, it was desirable to send a selection of them to be tested for their anti-HIV properties. These experiments were carried out by Dr Christophe Pannecouque, a member of the research group headed by Prof. Erik De Clercq at the Rega Institute for Medical Research, Katholieke Universiteit in Leuven, Belgium. Compounds **5** and **9** and their complexes have been subjected to a tetrazolium based colorimetric assay for detecting the potency of anti-HIV compounds.<sup>195, 196</sup> This assay has been widely employed over the last twenty years and will be briefly described below in addition to the results obtained in this study.

### 5.2.1 Tetrazolium Based Colorimetric Assay

The assay records the replication of HIV in MT-4 cells over a period of five days. Therefore, the procedure can be separated into three steps; a) infection b) incubation and c) evaluation. The method relies on the HIV-induced cytopathogenic effect and measures the number of cells infected with HIV.

As a control, the HIV is allowed to replicate without adding any anti-viral compound. A stock solution of HIV is added to the cells, which are then incubated at 37°C for five days. The cells are checked every twenty-four hours for the cytopathogenic effect. After five days, the number of infected cells is measured. The accepted measure is known as the CCID<sub>50</sub> (50% cell culture infective dose). This is the amount the HIV stock solution must be diluted by in order to infect 50% of the cells in the assay.

A stock solution containing the anti-viral compound is added to the MT-4 cells in the 96-well plate and the concentration of each well is diluted as required. An excess of HIV (100-300 x CCID<sub>50</sub>) is then added and the cells are left to incubate for five days in a humidified atmosphere at 37°C. After five days, the viability of the cells is examined via the MTT assay.<sup>197</sup>

### 5.2.2 MTT Assay

Left alone, the HIV will multiply rapidly and only a handful of cells, if any, will remain viable after the five day period. The addition of an anti-HIV compound will prevent or reduce viral replication and, as a result, cell survival will be enhanced. This can be measured spectrophotometrically. The yellow 3-(4,5-dimethylthiazol-2-yl)-2,5-diphenyltetrazolium bromide (MTT) is reduced by mitochondrial enzymes to formazan which is a blue colour (Figure 96).

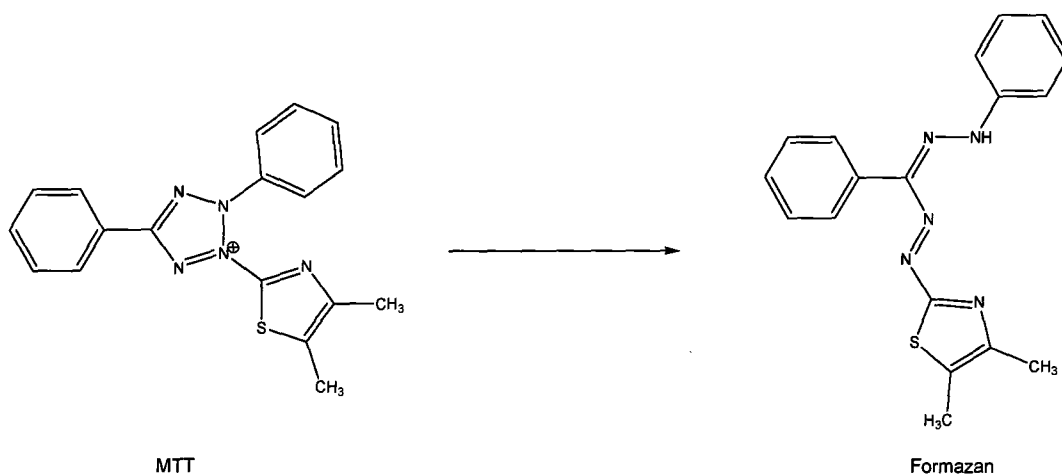


**Figure 96. Reduction of MTT to formazan.**

One disadvantage of using MTT instead of other tetrazolium salts is that organic solvents must be introduced in the analysis due to the fact that the formazan produced is insoluble in cell culture medium. However, this can actually be advantageous as it means that acidified Triton-X 100 has to be added to the cells, which inactivates the HIV. Therefore, people who are carrying out the assay are not at risk of HIV infection.

The IC<sub>50</sub> of the anti-viral compound can then be determined and is defined as the concentration of the compound that is required to reduce the absorbance of the control sample by 50%. For compounds which are themselves coloured (for example the metal complexes in this work), their colour is taken into account when determining their anti-viral properties. Reference compounds are also included in the assays, which include AZT, heparin and dextran sulphate.

AMD3100 and its transition metal complexes have previously been analysed using this assay and found to be in the order:



These complexes have been synthesised and included in this work as reference compounds. Therefore, the IC<sub>50</sub> and CC<sub>50</sub> values reported here may not be exactly the same as reported literature values.

### 5.2.3 Anti-viral Activity of Ligands

The units of IC<sub>50</sub>s and CC<sub>50</sub>s obtained from this assay are µg/mL. Therefore, before compounds can be compared to one another, the units must be converted to µM. The anti-viral potency of the three protonated ligands against a range of viral strains is shown in Table 16. The compounds have been tested against a range of HIV strains, including an AMD3100 resistant virus (JM3100R) and a CCR5 dependent virus (MAC251). MAC251 is an SIV strain and the compounds tested in this assay were all ineffective against this virus (data not included). III<sub>B</sub> and ROD viral strains are examples of HIV-1 and HIV-2 respectively. HIV-2 is a less virulent sub-type than HIV-1; however, HIV-2 predominates in sub-Saharan Africa. Standard deviations are included in the data where two or more experiments have been carried out.

Compound	Strain	Av. IC <sub>50</sub> / µM	SD	Av. CC <sub>50</sub> / µM	SD	Selectivity Index
AMD3100 <sup>113</sup>	JM3100R	0.53	-	-	-	-
	ROD	0.042	-	-	-	-
	III <sub>B</sub>	0.018	-	-	-	-
5	JM3100R	> 100	-	> 100	-	-
	ROD	10.84	3.00	> 100	-	> 10
	III <sub>B</sub>	3.27	0.86	> 100	-	> 32
9	JM3100R	> 100	-	> 100	-	-
	ROD	≥ 94.71	-	> 100	-	≥ 1
	III <sub>B</sub>	9.47	-	> 100	-	> 11

**Table 16. Anti-HIV activity of ligands in MT-4 cells.**

AMD3100 is more potent than both **5** and **9**. The results for **5** and **9** reveal that **5** is more active than **9**, particularly against the ROD viral strain where the cross-bridged compound, **9**, didn't register an IC<sub>50</sub> value under the experimental conditions employed. These data are consistent with the 12G5 mAb competition binding assay in the previous section.

## 5.2.4 Anti-viral Activity of Copper(II) Complexes

A range of copper(II) complexes of the three bis-macrocyclic ligands have been subjected to the anti-HIV assay and these data are detailed in Table 17.

Compound	Strain	Av. IC <sub>50</sub> μM	SD	Av. CC <sub>50</sub> μM	SD	Selectivity Index
[Cu <sub>2</sub> ](ClO <sub>4</sub> ) <sub>4</sub>	JM3100R	1.22	-	> 125	-	> 105
	ROD	0.24	0.13	> 125	-	> 535
	III <sub>B</sub>	0.053	0.010	> 125	-	> 2424
[Cu <sub>2</sub> 2]Cl <sub>4</sub>	JM3100R	0.58	-	50	14.78	86
	ROD	0.08	0.03	50	14.78	624
	III <sub>B</sub>	0.043	0.010	50	14.78	1160
[Cu <sub>2</sub> 5](ClO <sub>4</sub> ) <sub>4</sub>	JM3100R	11.96	2.32	> 125	-	> 11
	ROD	0.1032	0.0373	> 125	-	> 1308
	III <sub>B</sub>	0.0160	0.0024	> 125	-	> 8436
[Cu <sub>2</sub> 5Cl <sub>2</sub> ]Cl <sub>2</sub>	JM3100R	3.75	2.18	> 125	-	> 27
	ROD	0.0403	0.0068	> 125	-	> 2555
	III <sub>B</sub>	0.0190	0.0037	> 125	-	> 5419
[Cu <sub>2</sub> 9Cl <sub>2</sub> ](PF <sub>6</sub> ) <sub>2</sub>	JM3100R	0.0391	0.0086	> 125	-	> 3424
	ROD	0.0183	0.0012	> 125	-	> 7315
	III <sub>B</sub>	0.00491	0.00183	> 125	-	> 27263

**Table 17. Anti-HIV activity of copper(II) complexes in MT-4 cells.**

Apart from [Cu<sub>2</sub>2]Cl<sub>4</sub>, all of the copper(II) complexes were found to be non-toxic to the MT-4 cells in the assay, with CC<sub>50</sub> values in general being greater than 125 μM.

For the two copper(II) complexes of **5**, the choice of counter anion does not affect the anti-HIV activity against the III<sub>B</sub> viral strain. However, [Cu<sub>2</sub>5Cl<sub>2</sub>]Cl<sub>2</sub> shows slightly more potency than [Cu<sub>2</sub>5](ClO<sub>4</sub>)<sub>4</sub> against the ROD strain. These data suggest that the choice of counter anion has little effect on anti-viral activity. In comparison to the copper(II) complexes of AMD3100, the copper(II) complexes of **5** are more potent against III<sub>B</sub> and ROD strains, however, they display poorer activity against the AMD3100 resistant virus.

$[\text{Cu}_2\mathbf{9}\text{Cl}_2](\text{PF}_6)_2$  was found to be the most active copper(II) complex in this assay. For example, against the III<sub>B</sub> strain  $[\text{Cu}_2\mathbf{9}\text{Cl}_2](\text{PF}_6)_2$  is an order of magnitude more potent than  $[\text{Cu}_2\mathbf{5}\text{Cl}_2]\text{Cl}_2$  and against the ROD viral strain,  $[\text{Cu}_2\mathbf{9}\text{Cl}_2](\text{PF}_6)_2$  shows between 2- and 6-fold greater activity in comparison to the copper(II) complexes of **5**. In addition, the selectivity index of  $[\text{Cu}_2\mathbf{9}\text{Cl}_2](\text{PF}_6)_2$  is also greater in comparison to the copper(II) complexes of **5** and AMD3100.

The anti-HIV activity of the copper(II) complexes can be summarised as below:



It is interesting to note that  $[\text{Cu}_2\mathbf{9}\text{Cl}_2](\text{PF}_6)_2$  shows activity against the AMD3100 resistant virus in the nanomolar concentration range ( $\text{IC}_{50}$  39 nM). This is discussed in further detail in the next section.

### 5.2.5 Activity of $[\text{Cu}_2\mathbf{9}\text{Cl}_2](\text{PF}_6)_2$ Against AMD3100 Resistant Virus

$[\text{Cu}_2\mathbf{9}\text{Cl}_2](\text{PF}_6)_2$  was unexpectedly found to be potent against the AMD3100 resistant viral strain JM3100R in the anti-HIV assay. It is known that AMD3100 and its transition metal complexes bind to CXCR4 via interactions with aspartate residues on the receptor surface. Compounds **5** and **9** and their complexes are similar to AMD3100 and would be expected to bind in an analogous manner. Therefore, a further test was carried out against the AMD3100 resistant virus with varying concentrations of antagonist both in the presence and absence of AMD3100 (Figure 97) in order to investigate the binding site competition. As the concentration of AMD3100 increases, less  $[\text{Cu}_2\mathbf{9}\text{Cl}_2](\text{PF}_6)_2$  will be bound to Asp171 and Asp262 and its activity should decrease accordingly. However, if we consider the

activity of  $[\text{Cu}_2\text{9Cl}_2](\text{PF}_6)_2$  at 0.2  $\mu\text{g}/\text{mL}$ , it is clear that it actually increases as the concentration of AMD3100 increases. This suggests that  $[\text{Cu}_2\text{9Cl}_2](\text{PF}_6)_2$  has a slightly different binding site than AMD3100.

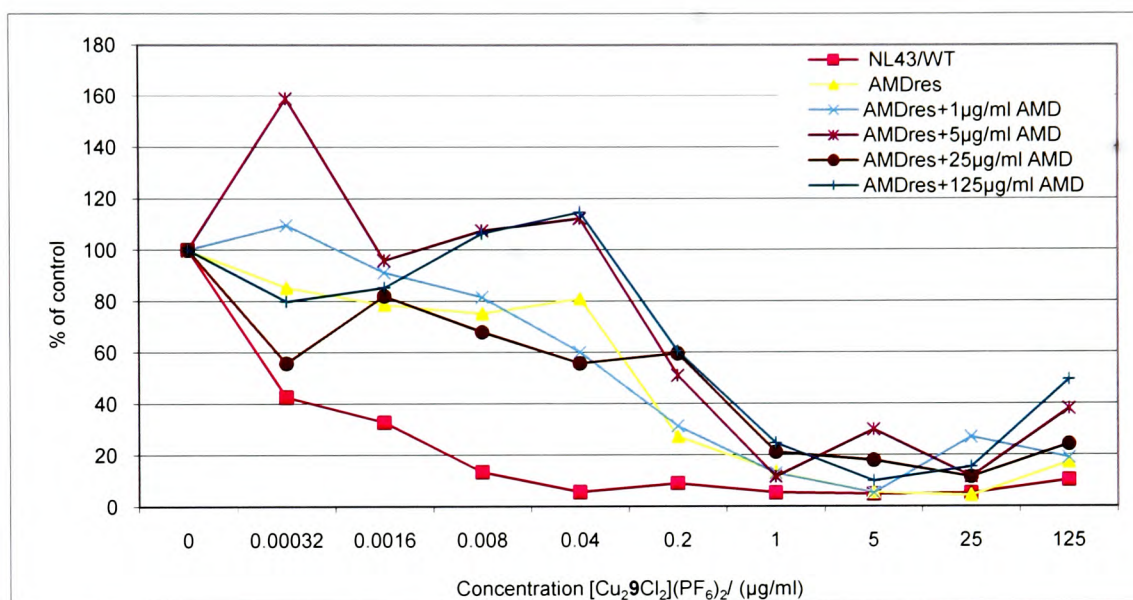


**Figure 97. Inhibition of AMD3100 resistant HIV replication at varying concentrations of both  $[\text{Cu}_2\text{9Cl}_2](\text{PF}_6)_2$  and AMD3100.**

The mechanism by which the AMD3100 resistant virus infects cells is unknown. However, it could be due to its ability to replace AMD3100 already bound to either Asp171 or Asp262. Alternatively, the resistant virus may not be able to displace  $[\text{Cu}_2\text{9Cl}_2](\text{PF}_6)_2$  as easily as AMD3100 due to  $[\text{Cu}_2\text{9Cl}_2](\text{PF}_6)_2$  forming a more stable complex with either Asp171 or Asp262 (or both).

## 5.2.6 Anti-viral Activity of Zinc(II) Complexes

In addition to the copper(II) complexes, a range of zinc(II) complexes of the three bis-macrocyclic ligands have been tested in the anti-HIV assay and these data are detailed in Table 18. Again, all compounds were inactive against the MAC251 virus as expected (data not included).

Compound	Strain	Av. IC <sub>50</sub> / μM	SD	Av. CC <sub>50</sub> / μM	SD	Selectivity Index
[Zn <sub>2</sub> 2]Cl <sub>4</sub>	JM3100R	0.10	-	51.29	-	513
	ROD	0.056	0.050	51.29	-	916
	III <sub>B</sub>	0.012	0.002	51.29	-	4274
[Zn <sub>2</sub> 2](ClO <sub>4</sub> ) <sub>4</sub>	JM3100R	0.102	-	> 100	-	> 1264
	ROD	0.144	0.093	> 100	-	> 895
	III <sub>B</sub>	0.010	0.008	> 100	-	> 12892
[Zn <sub>2</sub> 5(OAc) <sub>2</sub> ](OAc) <sub>2</sub>	JM3100R	0.119	0.038	52.15	4.00	438
	ROD	0.00339	0.00106	52.15	4.00	15383
	III <sub>B</sub>	0.00208	0.00087	52.15	4.00	25072
[Zn <sub>2</sub> 5](ClO <sub>4</sub> ) <sub>4</sub>	JM3100R	0.13	-	62.51	7.16	481
	ROD	0.030	0.015	62.51	7.16	2084
	III <sub>B</sub>	0.0057	0.0034	62.51	7.16	10967
[Zn <sub>2</sub> 9](OAc) <sub>2</sub> (PF <sub>6</sub> ) <sub>2</sub>	JM3100R	3.08	-	≥ 108.02	-	≥ 35
	ROD	0.76	0.22	≥ 108.02	-	≥ 142
	III <sub>B</sub>	0.25	0.20	≥ 108.02	-	≥ 432
[Zn <sub>2</sub> 9](PF <sub>6</sub> ) <sub>2</sub> Cl <sub>2</sub>	JM3100R	0.011	0.002	59.63	2.69	5421
	ROD	0.0059	-	59.63	2.69	10107
	III <sub>B</sub>	0.024	0.020	59.63	2.69	2485

**Table 18. Anti-HIV activity of zinc(II) complexes in MT-4 cells.**

The anti-HIV activity of the zinc(II) complexes of **5** against the ROD and III<sub>B</sub> viral strains were consistent, with an IC<sub>50</sub> of approximately 3 nM being achieved. This is significantly more potent than the zinc(II) complexes of AMD3100 and also an order of magnitude more active than the copper(II) complexes of **5** discussed above. Both [Zn<sub>2</sub>5(OAc)<sub>2</sub>](OAc)<sub>2</sub> and [Zn<sub>2</sub>5](ClO<sub>4</sub>)<sub>4</sub> were found to be toxic to MT-4 cells; however, the selectivity indices were in the order of 15000-25000.

The data obtained from the assay with the two zinc(II) complexes of **9** are somewhat inconsistent. For example,  $[\text{Zn}_2\mathbf{9}](\text{PF}_6)_2\text{Cl}_2$  is active against the ROD viral strain, whereas  $[\text{Zn}_2\mathbf{9}](\text{OAc})_2(\text{PF}_6)_2$  is (relatively) inactive. A discrepancy in the relative toxicities of the two complexes is also observed. For example,  $[\text{Zn}_2\mathbf{9}](\text{OAc})_2(\text{PF}_6)_2$  is non-toxic but  $[\text{Zn}_2\mathbf{9}](\text{PF}_6)_2\text{Cl}_2$  is toxic ( $\text{CC}_{50} \sim 60 \mu\text{M}$ ).

In general, the zinc(II) complexes of **9** are less potent than their side-bridged counterparts.  $[\text{Zn}_2\mathbf{9}](\text{OAc})_2(\text{PF}_6)_2$  and  $[\text{Zn}_2\mathbf{9}](\text{PF}_6)_2\text{Cl}_2$  are also poorer inhibitors of HIV replication than the copper(II) complexes of **9** discussed above. The anti-HIV activity of the zinc(II) complexes can be summarised as below:



### 5.2.7 Anti-viral Properties in PBMCs

In an extension of the anti-HIV studies in MT-4 cells, a selection of antagonists has been tested for their anti-viral activity in peripheral blood mononuclear cells (PBMCs), which have been extracted from human blood samples. PBMCs are found in the immune system and contain  $\text{CD4}^+$  cells. For this reason, they have been widely used in HIV research as they represent the most realistic assay for anti-viral testing.

The  $\text{IC}_{50}$  values of anti-HIV compounds are expected to be higher (i.e. less active) in these cells than in MT-4 cells due to the fact that PBMCs will express a number of receptors on their surfaces which may not, in all cases, include CXCR4. The data from a selection of compounds in this work are shown in Table 19.

Compound	Strain	Av. IC <sub>50</sub> / μM	SD	Av. CC <sub>50</sub> / μM	SD	Selectivity Index
<b>5</b>	III <sub>B</sub>	93.49	-	93.49	-	-
[Zn <sub>2</sub> 2]Cl <sub>4</sub>	III <sub>B</sub>	0.12	0.08	> 96.92	-	> 808
[Zn <sub>2</sub> 5](ClO <sub>4</sub> ) <sub>4</sub>	III <sub>B</sub>	0.52	-	> 135	-	> 260
[Cu <sub>2</sub> 9Cl <sub>2</sub> ](PF <sub>6</sub> ) <sub>2</sub>	III <sub>B</sub>	0.013	0.002	> 133.86	-	> 10297

**Table 19. Anti-HIV activity of selected compounds in PMBCs.**

These data confirm that the IC<sub>50</sub> values are, as expected, higher in PBMCs than in MT-4 cells. For example, [Cu<sub>2</sub>9Cl<sub>2</sub>](PF<sub>6</sub>)<sub>2</sub> is approximately 2.5-fold less active in PBMCs. In agreement with the anti-viral study, **5** is significantly less active than the metal complexes of both AMD3100 and **9**. [Cu<sub>2</sub>9Cl<sub>2</sub>](PF<sub>6</sub>)<sub>2</sub> is the most active compound to be tested in this study, recording an IC<sub>50</sub> value of 13 nM. The most significant difference between the two assays is with [Zn<sub>2</sub>5](ClO<sub>4</sub>)<sub>4</sub> which is two orders of magnitude less potent in PBMCs. The compounds were all found to be ineffective against a CCR5 viral strain (BaL) as expected (data not included).

### 5.3 CXCL12 Induced Ca<sup>2+</sup> Signalling

The intracellular calcium concentration ( $[Ca^{2+}]_i$ ) is maintained at approximately 100 nM by a number of mechanisms. CXCL12 binding to CXCR4 causes a series of events which results in an increase of  $[Ca^{2+}]_i$  to over 1  $\mu$ M. This is an important mechanism for GPCR communication pathways. The presence of an antagonist will prevent CXCL12 binding to CXCR4 and therefore,  $[Ca^{2+}]_i$  will be kept low. This leads to the possibility of calculating the % of bound antagonist. The method used for determining IC<sub>50</sub> values of calcium signalling is briefly described below. These experiments were carried out by Dr Dominique Schols, a member of the research group headed by Prof. Erik De Clercq at the Rega Institute, Katholieke Universiteit in Leuven, Belgium.

#### 5.3.1 Measurement of Intracellular Calcium Concentration

Fura-2 is a commercial indicator which binds to free calcium ions inside cells. The excitation wavelength of Fura-2 is different when bound to calcium and when not. Therefore, the ratio of bound to unbound intracellular calcium can be determined. A method for determining the IC<sub>50</sub> values of antagonist compounds has been reported by Wuyts *et al.*<sup>198</sup>

U87.CD4.CXCR4 cells are loaded with Fura-2 and incubated at 37°C for thirty minutes. Cells are then stimulated with either buffer (control) or varying concentrations of antagonist, followed by CXCL12 at a concentration designed to induce the maximum release of  $[Ca^{2+}]_i$  (100 seconds after first stimulus). The fluorescence of Fura-2 is recorded at two different wavelengths ( $\lambda_{ex}$  340 and 380 nm,  $\lambda_{em}$  510 nm) and the level of  $[Ca^{2+}]_i$  is calculated according to an equation reported by Grynkiewicz *et al.*<sup>199</sup> Similar to the

previously described experiments, the IC<sub>50</sub> is defined as the concentration of antagonist required to inhibit 50% [Ca<sup>2+</sup>]<sub>i</sub> in response to the addition of CXCL12.

### 5.3.2 Calculated IC<sub>50</sub> Values

The IC<sub>50</sub> values of a selection of compounds in cells which express both CXCR4 and CCR5 are shown in Table 20. All of the compounds are inactive against the cells that express CCR5, as expected. Maraviroc, a CCR5 antagonist which has recently been approved for HIV treatment (September 2007), is included as a control sample.

Against the cells that express CXCR4, **9** was found to be essentially inactive, failing to register an IC<sub>50</sub> under the conditions of the experiment. It is interesting to note that AMD3100 is more effective than a number of metal complexes and is significantly more active than its copper(II) complexes.

Compound	IC <sub>50</sub> / μM (U87.CD4.CXCR4)	IC <sub>50</sub> / μM (U87.CD4.CCR5)
<b>9</b>	> 83814	> 838.14
[Cu <sub>2</sub> 2](ClO <sub>4</sub> ) <sub>4</sub>	106.20	> 1027.68
[Cu <sub>2</sub> 2]Cl <sub>4</sub>	56.08	> 771.69
[Cu <sub>2</sub> 5](ClO <sub>4</sub> ) <sub>4</sub>	47.48	> 1079.75
[Zn <sub>2</sub> 9]Cl <sub>4</sub>	4.64	> 855.50
[Cu <sub>2</sub> 9Cl <sub>2</sub> ](PF <sub>6</sub> ) <sub>2</sub>	4.64	> 1070.84
[Zn <sub>2</sub> 5](ClO <sub>4</sub> ) <sub>4</sub>	4.01	> 1083.44
[Zn <sub>2</sub> 2]Cl <sub>4</sub>	2.71	> 775.37
[Zn <sub>2</sub> 2](ClO <sub>4</sub> ) <sub>4</sub>	2.48	> 1031.36
AMD3100	18.67	> 794.47
Maraviroc	> 1000 (μg / mL)	2.09 (μg / mL)

**Table 20. Calcium signalling IC<sub>50</sub>s for a selection of compounds.**

### 5.3.3 Correlation between anti-HIV Activity and Calcium Signalling

The data from the anti-viral assay and the calcium signalling assay can be correlated using linear regression analysis. This involves taking the log of the  $IC_{50}$  of each compound tested and plotting the two assays against one another. Only the transition metal complexes have been included in the correlation as **5** was not run in the calcium signaling assay and **9** failed to register an  $IC_{50}$  in the same assay. The correlation between the complexes is poor due to the fact that  $[Zn_29Cl_2]^{2+}$  does not fit the data (not shown). This could be due to an impurity in one of the samples of  $[Zn_29]^{4+}$ . However, if this complex is removed from the dataset, the correlation is found to be good (Figure 98).

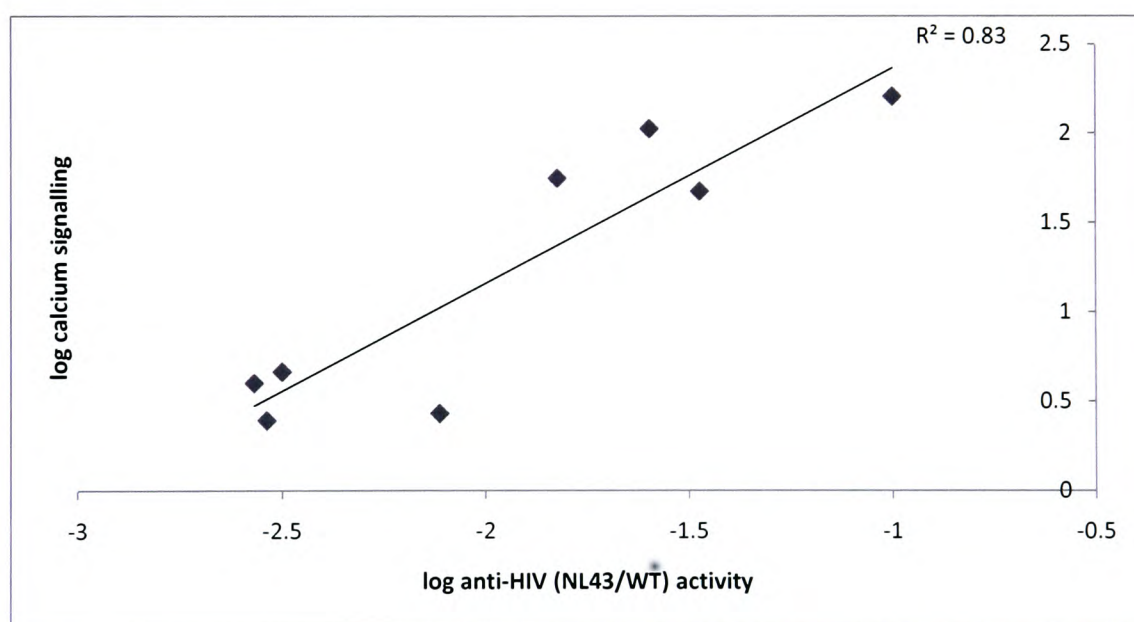


**Figure 98. Correlation between  $IC_{50}$  anti-HIV activity vs  $IC_{50}$  calcium signalling excluding  $[Zn_29]Cl_4$ .**

## 5.4 Structure Activity Relationships

In order to establish the structural relationships between compounds, the mechanism of action of the antagonists must be known. It is widely accepted that AMD3100 and its metal complexes bind to CXCR4 via interaction of the carboxylate arms of the receptor surface amino acids Asp171 and Asp262 with the macrocyclic amine groups.<sup>34</sup> It has also been suggested that an additional interaction with Glu288 is important for receptor binding.<sup>200</sup> As the compounds in this work have similar structures to AMD3100, it is thought that the mechanism of action will be identical. Therefore, it is important to consider the factors which can affect receptor binding. A number of aspects are believed to be important, for example:

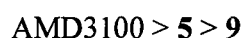
- a) *Stereospecific hydrogen bonding*; it has been shown that cyclam is protonated at physiological pH.<sup>111</sup> As a result, hydrogen bonding can occur between the amine functions on the macrocyclic ring and the carboxylate groups on the receptor surface.
- b) *Electrostatic interactions*; CXCR4 has a surface charge of  $-9$  (section 1.1.4), therefore, the positively charged AMD3100 (+4) and its metal complexes (in general, +4) can interact via direct electrostatic interactions. However, this mechanism appears to be of less importance for metal complexes as the palladium(II) complex of AMD3100 is inactive against HIV.
- c) *Macrocyclic configuration*; the rich configurational chemistry of cyclam has been discussed previously (section 1.5) and the configuration of the macrocycle could play an important role in anti-HIV activity.

- d) *Transition metal coordination environment*; on the complexation of transition metal ions, a coordinate bond between the metal ion and oxygen atoms on the receptor carboxylate groups can be formed. These bonds would be expected to be stronger than any hydrogen bonding interactions. In addition, the coordination preferences of the metal ion itself will play a crucial role in receptor binding.
- e)  *$\pi$ - $\pi$  hydrophobic interactions*; although lower in energy, the stacking of aromatic groups between the aromatic ring of the ligands and the phenyl rings on CXCR4 amino acid residues could potentially occur. Sadler and co-workers have suggested that hydrophobic interactions with tryptophan are important for the binding of copper(II) cyclam to lysozyme.<sup>116</sup>

The rest of this chapter is devoted to a discussion of the structure of the ligands, their copper(II) and zinc(II) complexes and suggested explanations for their anti-viral activities.

#### 5.4.1 Free Ligands

The activity of the three ligands in this work has been tested in an anti-HIV assay and has found to be in the order:



The difference in the activities of the ligands can be rationalised in terms of their varying ability to hydrogen bond to aspartate residues on the CXCR4 surface. AMD3100 has six secondary amine sites and is the most active ligand (Figure 99a). However, on the introduction of an ethylene bridge this number decreases, resulting in fewer secondary amine sites. **5** has only two secondary amine groups and as a result is expected to be less

active than AMD3100 (Figure 99b). This is confirmed in the anti-HIV assay. Furthermore, **9** lacks any secondary amine sites and, therefore, would be expected to be a poorer inhibitor than **5** (Figure 99c). This is particularly evident against the ROD viral strain where **9** is approximately 9-fold less active than **5**. Additionally, in the competition binding assay, **9** failed to achieve 50% inhibition. However, further investigation would be necessary to confirm this theory, taking into account the degree of protonation of each ligand at physiological pH.

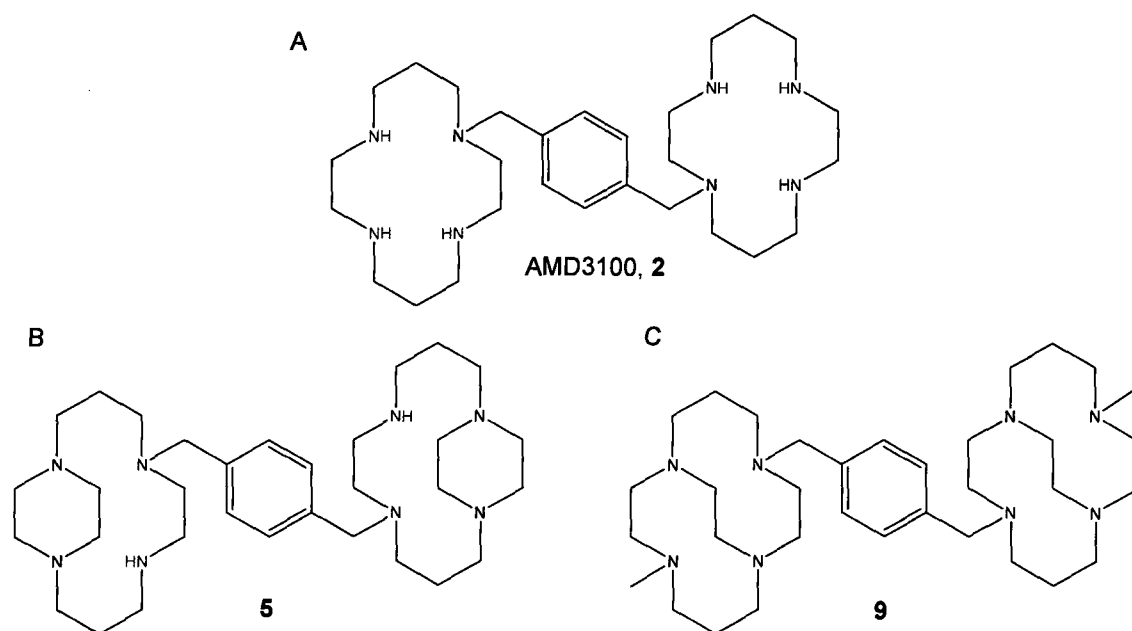


**Figure 99. Ability of bis-macroyclic ligands to H-bond to CXCR4.**

The different activities can also be regarded by the degree of flexibility of the respective macrocyclic units. For example, AMD3100 possesses the most flexible macrocyclic units of the three ligands and is also the most active. This could be due to the ability of the macrocycles to adopt a favourable conformation for receptor binding.

Alternatively, the piperazino moiety formed by an ethylene bridge between two adjacent nitrogen atoms provides some rigidity to **5**; however, the macrocycle as a whole is still reasonably flexible. In contrast, the ethylene bridge between non-adjacent nitrogen atoms physically locks the macrocyclic units in place, meaning that **9** has the least flexible ligand of the three tested.

It has been reported that, upon transition metal complexation, the activity of bis-macrocyclic compounds increases, presumably due to direct coordination bonding being a predominant interaction in place of stereospecific hydrogen bonding.<sup>114</sup> The metal complexes in this study are also more potent inhibitors of HIV replication than their respective ligands. For example, **9** is not very potent, however,  $[\text{Cu}_2\mathbf{9}\text{Cl}_2](\text{PF}_6)_2$  was found to be one of the most active compounds in this study. This highlights the important role that the transition metal plays in the anti-HIV activity of bis-macrocyclic complexes and also suggests that hydrogen bonding may not be essential for receptor binding (of complexes).

#### 5.4.2 Copper(II) Complexes

The anti-HIV activity of the copper(II) chloride complexes in this work has been discussed and has been found to be in the order:



The copper(II) ion in  $[\text{Cu}_2\mathbf{5}\text{Cl}_2]^{2+}$  adopts a five-coordinate, square-based pyramidal coordination environment in the solid state as ascertained by X-ray crystallography (although there is evidence from the EXAFS studies that  $[\text{Cu}_2\mathbf{5}\text{Cl}_2](\text{PF}_6)_2$  is only four-coordinate in the solid state, it is  $[\text{Cu}_2\mathbf{5}\text{Cl}_2]\text{Cl}_2$  that has been tested in the anti-HIV assay).

Although no X-ray structure of  $[\text{Cu}_2\mathbf{9}\text{Cl}_2]^{2+}$  exists, there are examples of mono-macrocyclic copper(II) complexes (e.g.  $\mathbf{L}^{27}$  and  $\mathbf{L}^{29}$ ) that have been structurally characterised (section 3.1.2). The copper(II) ion in these complexes also adopt five-coordinate, square-based pyramidal geometries and it would be expected that  $[\text{Cu}_2\mathbf{9}\text{Cl}_2]^{2+}$  adopts the same coordination environment.

The major difference between the copper(II) chloride complexes of **5** and **9** is the position of the bound counter anion (Figure 100). In  $[\text{Cu}_2\mathbf{5}\text{Cl}_2]^{2+}$ , the square-base consists of the four nitrogen atoms of the macrocycle and the axial position is occupied by the chloride (Figure 100a). In contrast, in  $[\text{Cu}_2\mathbf{9}\text{Cl}_2]^{2+}$ , the square-base consists of three nitrogen atoms and a chloride and the axial position in this case is the fourth macrocyclic nitrogen atom (Figure 100b).

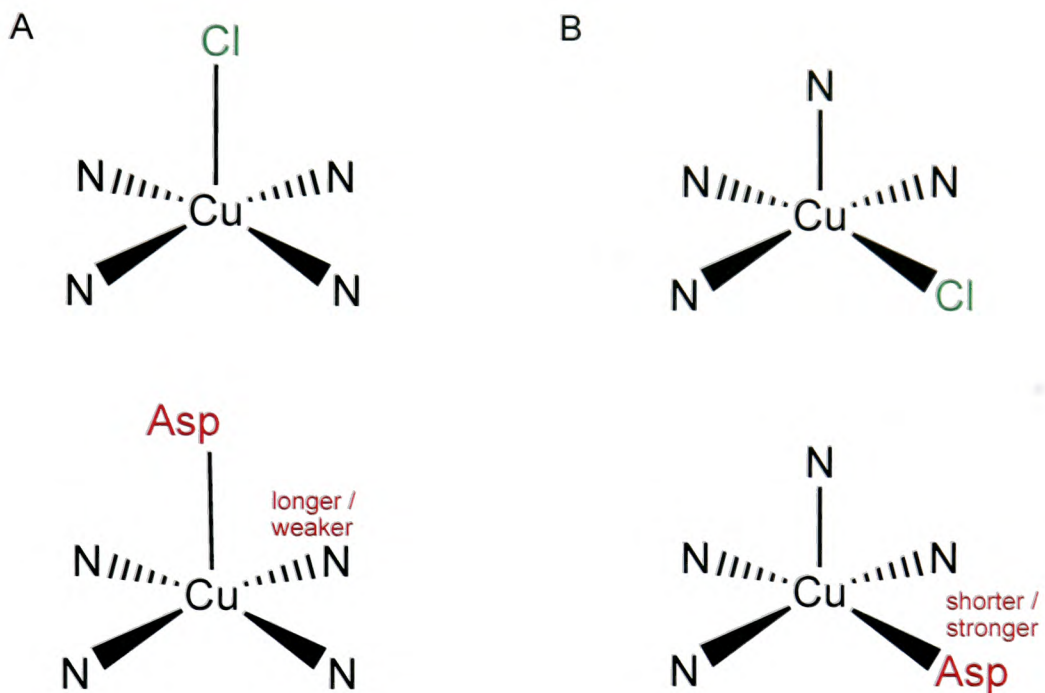


**Figure 100. Schematic representation of copper(II) coordination environments in  $[\text{Cu}_{25}\text{Cl}_2]^{2+}$  (A) and  $[\text{Cu}_{29}\text{Cl}_2]^{2+}$  (B).**

As has already been discussed, it is believed that the ability of the complexes to inhibit HIV replication depends on their respective abilities to bind to CXCR4. Binding of the two complexes to CXCR4 is achieved via the exchange of the bound chloride counter anion for the aspartate residues on the receptor surface. The solution EXAFS of  $[\text{Cu}_2\mathbf{9}\text{Cl}_2]^{2+}$  suggested that, on addition of acetate, the chloride counter anion was directly replaced by an oxygen from acetate. This can be represented as in Figure 100. As copper(II) is a  $d^9$  metal ion, the coordination preferences of the metal result in axial bonds which are weaker than the four equatorial bonds. Therefore, it is anticipated that, once bound to CXCR4,  $[\text{Cu}_2\mathbf{9}\text{Cl}_2]^{2+}$  will be more difficult to displace than  $[\text{Cu}_2\mathbf{5}\text{Cl}_2]^{2+}$  as the complex formed should be thermodynamically more stable due to aspartate being bound to an equatorial site. In addition, the  $[\text{Cu}_2\mathbf{9}]^{4+}$  complex with aspartate will be kinetically more stable than the  $[\text{Cu}_2\mathbf{5}]^{4+}$  aspartate complex. Consequently,  $[\text{Cu}_2\mathbf{9}\text{Cl}_2]^{2+}$  will be the most active complex of the two. The anti-HIV assay confirms that  $[\text{Cu}_2\mathbf{9}\text{Cl}_2](\text{PF}_6)_2$  is more potent than  $[\text{Cu}_2\mathbf{5}\text{Cl}_2]\text{Cl}_2$ .

### 5.4.3 Zinc(II) Complexes

The anti-HIV activity of the zinc(II) acetate complexes in this work has been discussed and has been found to be in the order:



The zinc(II) ion in  $[\text{Zn}_2\mathbf{5}(\text{OAc})_2]^{2+}$  adopts a distorted octahedral coordination environment in the solid state as ascertained by X-ray crystallography. Although the X-ray crystal structure of  $[\text{Zn}_2\mathbf{9}(\text{OAc})_2]^{2+}$  has not been determined, the zinc(II) complex of  $\mathbf{L}^{43}$  (Figure 101) has been structurally characterised. This crystal structure of  $[\text{ZnL}^{43}(\text{OAc})]^+$

shows the zinc(II) ion also adopts a six-coordinate, distorted octahedral geometry with a bidentate acetate counter anion.<sup>201</sup>  $[\text{Zn}_2\mathbf{9}(\text{OAc})_2]^{2+}$  would be expected to adopt the same coordination environment around each zinc(II) ion on binding to the aspartate residues.

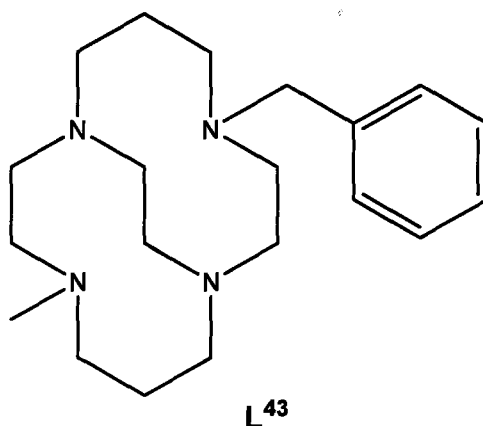


**Figure 101. Cross-bridged ligand L<sup>43</sup>.**

The major difference between the two structures is the position the metal ion occupies in relation to the macrocycle. For example, in  $[\text{Zn}_2\mathbf{5}(\text{OAc})_2]^{2+}$ , the zinc(II) ion sits out of the macrocycle whereas in  $[\text{Zn}_2\mathbf{9}(\text{OAc})_2]^{2+}$  it is held inside the macrocyclic cavity like a shell. Similar to the copper(II) complexes discussed above, another difference between  $[\text{Zn}_2\mathbf{5}(\text{OAc})_2]^{2+}$  and  $[\text{Zn}_2\mathbf{9}(\text{OAc})_2]^{2+}$  is the position of the bound counter anion (Figure 102). In  $[\text{Zn}_2\mathbf{5}(\text{OAc})_2]^{2+}$ , there is essentially a square-base consisting of the four nitrogen atoms of the macrocycle, leaving an open face above the plane for a bidentate acetate counter anion (Figure 102a). In contrast, the metal ion in  $[\text{Zn}_2\mathbf{9}(\text{OAc})_2]^{2+}$  adopts a less distorted octahedral environment where two of the cis sites are available for the bound counter anion (Figure 102b).

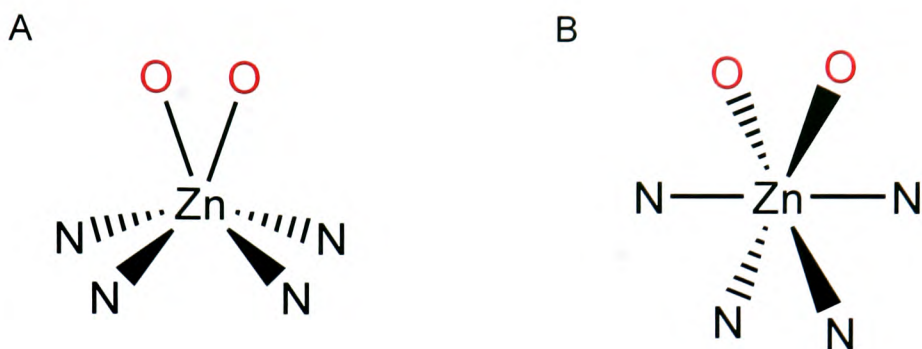


**Figure 102. Schematic representation of the zinc(II) coordination environment in  $[\text{Zn}_{25}(\text{OAc})_2]^{2+}$  (A) and  $[\text{Zn}_{29}(\text{OAc})_2]^{2+}$  (B).**

Unlike copper(II), zinc(II) is a  $d^{10}$  metal ion and as a result has fewer coordination preferences. Therefore, the coordination geometry of the metal ion will be less important in this case. This means that the configuration of the macrocycle will play an important role in the relative activities of the zinc(II) complexes. Another reason why the macrocycle will play an important role is the fact that on receptor binding, the acetate counter anion will be replaced by an aspartate on the CXCR4 surface (i.e. replacing a bidentate oxygen donor with a bidentate oxygen donor). The activity of the zinc(II) complexes could simply be explained on steric grounds. As has already been stated, in  $[\text{Zn}_{25}(\text{OAc})_2]^{2+}$ , the zinc(II) ion resides outside the mean plane of the macrocycle, and as a result could be in a more accessible position to bind to CXCR4 aspartate residues in comparison to  $[\text{Zn}_{29}(\text{OAc})_2]^{2+}$  where the zinc(II) is held inside the macrocyclic cavity. The higher activity of  $[\text{Zn}_{25}(\text{OAc})_2]^{2+}$  could also be attributed to thermodynamics, where the zinc(II) complex of **5** could form a stronger coordination bond to CXCR4 than the zinc(II) complex of **9**. This hypothesis needs to be investigated further, possibly using molecular modelling calculations.

## 5.5 Conclusions

Compounds **5** and **9** and their copper(II) and zinc(II) complexes have been found to bind to CXCR4 as shown in an antibody displacement and competition binding assay. The transition metal complexes are significantly more effective in binding than AMD3100. Additionally, the ligands and complexes are potent inhibitors of HIV replication as shown by a tetrazolium-based assay.

The anti-HIV activity of three ligands has been explained by their relative ability to hydrogen bond to CXCR4. As expected from prior work, potency is vastly improved on the complexation of transition metal ions such as copper(II) or zinc(II).<sup>114</sup> This highlights the importance of coordination bonding to anti-HIV potency.  $[\text{Zn}_2\mathbf{5}(\text{OAc})_2](\text{OAc})_2$  was found to be the most active compound tested in this work, followed by  $[\text{Cu}_2\mathbf{9Cl}_2](\text{PF}_6)_2$ . The much greater activity of  $[\text{Cu}_2\mathbf{9Cl}_2](\text{PF}_6)_2$  compared to **9** suggests that hydrogen bonding plays little role in the binding to CXCR4 for the metal complex, as **9** is the least active compound tested in this study whereas  $[\text{Cu}_2\mathbf{9Cl}_2](\text{PF}_6)_2$  is one of the most active.  $[\text{Cu}_2\mathbf{9Cl}_2]^{2+}$  and  $[\text{Zn}_2\mathbf{5}(\text{OAc})_2]^{2+}$  both show greater activity than their AMD3100 equivalents which confirms that the strategy of configurationally restricting the macrocycle has improved the binding interaction of the complex with the receptor.

# **Chapter 6. TOWARDS THE SYNTHESIS OF ASYMMETRICAL BIS-MACROCYCLES**

## 6.1 Background

The configurationally restricted bis-macrocycles discussed in the previous chapters are symmetrical and relatively facile synthetic routes to each compound have been developed. This work could be extended to the synthesis of asymmetrical ligands; for example a bis-macrocycle containing one side-bridged macrocycle and one cross bridge ring. The synthesis of these ligands is much more challenging in comparison to the ones discussed previously. This chapter presents a synthetic route to one example of an asymmetrical bis-macrocyclic derivative, the synthetic methodology developed during the course of this work and crystal structures of intermediate compounds which have been obtained.

### 6.1.1 Asymmetrical Bis-macrocycles

A synthetic route to a selection of asymmetric bis-macrocyclic compounds using bis-aminal chemistry has been reported by Handel and co-workers.<sup>164</sup> Figure 103 details the synthesis of one example containing a cyclam ring and a cyclen ring tethered by a 1,4-aromatic linker. The attack of **3** by the bis-electrophile is controlled as the ammonium salt has low solubility in solvents such as benzene or THF. The asymmetric bis-macrocycle, **L**<sup>45</sup>, can then be prepared by reacting the ammonium salt, **L**<sup>44</sup>, with a slight excess of a second bis-aminal (Figure 103) followed by deprotection with hydroxylamine to give **L**<sup>46</sup>. This method has been shown to work well provided that the less reactive bis-aminal is used in the first step.

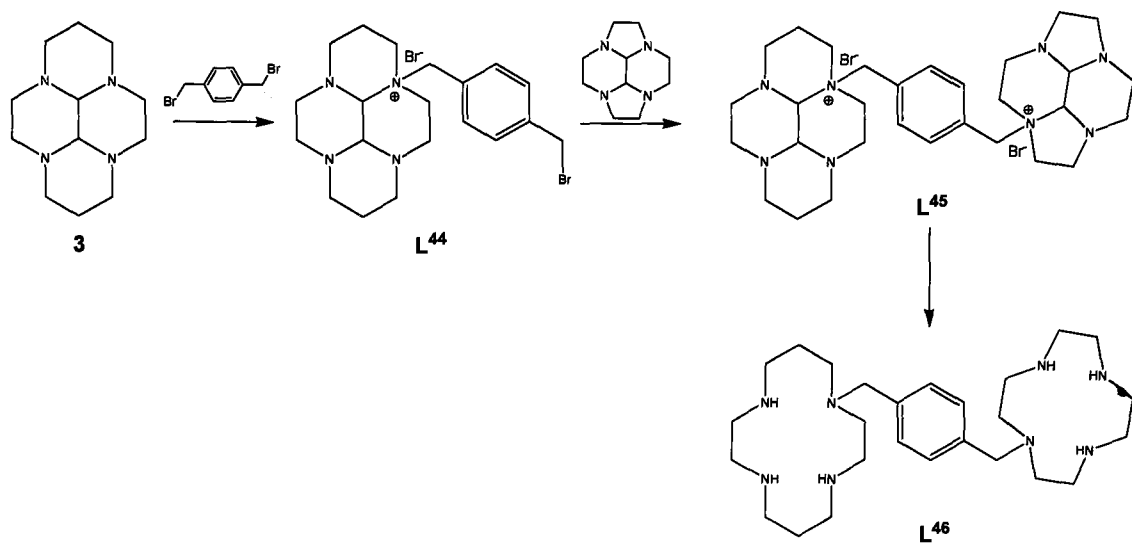


**Figure 103.** Synthesis of asymmetrical bis-macrocycle, L<sup>46</sup>.

## 6.2 Synthetic Rationale

In order to synthesise an asymmetrical configurationally restricted bis-macroyclic ligand, the route shown in Figure 104 was proposed. The initial compound in this scheme is a side-bridged macrocyclic derivative containing an alkyl bromide pendent arm. The route to this compound is proposed in Figure 105. The addition of a primary alkyl bromide to **3** has been discussed in chapter two (section 2.3.1) and would be expected to proceed smoothly. The next step could be varied in different ways in order to create the desired macrocycle. For example, the bis-aminal bridge could be removed entirely to leave a cyclam ring, or it could be directly reduced with sodium borohydride to give another side-bridged unit. The route shown in Figure 104 highlights the cross-bridged macrocycle and consists of an initial reaction with methyl iodide followed by reduction to give a bis-macrocycle containing both a side and a cross-bridged ring.

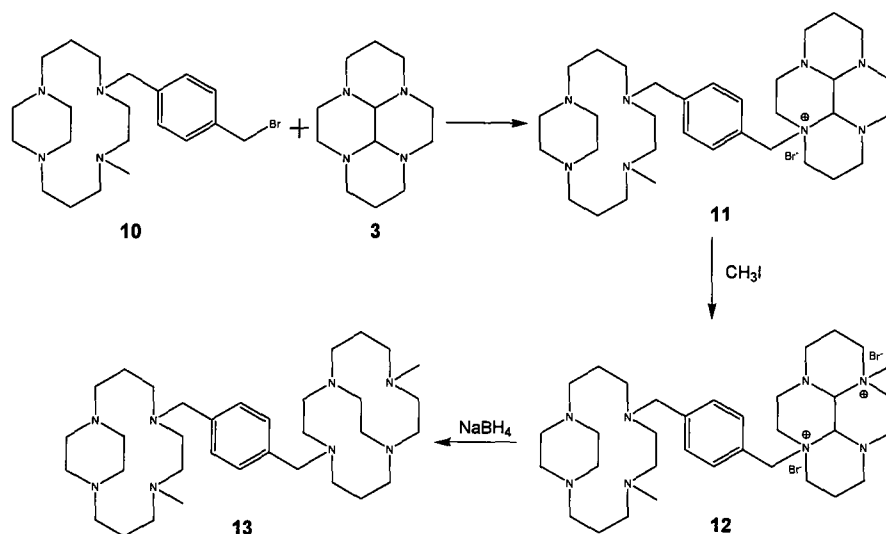
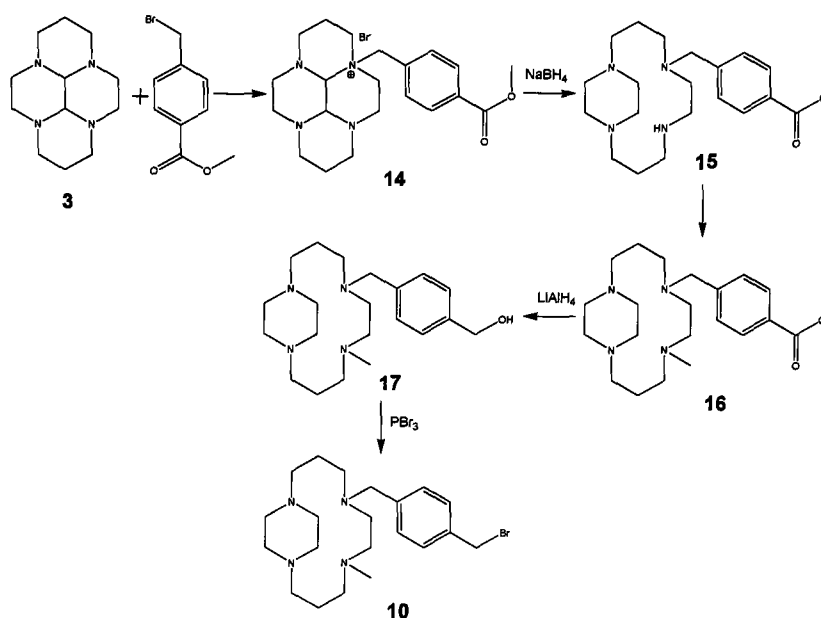


Figure 104. Proposed synthetic route to an asymmetrical bis-macrocycle.



**Figure 105. Proposed synthetic route to 10.**

The route to **10** starts off with the addition of 4-(methylbromo)benzoate to **3** followed by reduction with sodium borohydride according to our established method. One aspect that needs consideration is the remaining secondary amine on the macrocyclic backbone of compound **15**. This group could potentially undergo an intramolecular reaction at a later stage with the bromo pendent arm and, as a result, needs to be protected. Subsequent reduction of the ester to give **17** followed by bromination should result in the desired compound.

Although the first two steps of the proposed route proceeded as expected, the alkylation of **15** has proven to be more difficult than initially anticipated; the following section details the various methods that have been attempted to prepare **16** during the course of this work and discusses other methods that could be employed in order to prepare the desired compound.

## 6.3 Synthetic Discussion

### 6.3.1 Attempted Preparation of 16

During the course of this work, several methods of alkylating compound **15** have been attempted. The routes which have been tried are summarised in Figure 106. This section includes a discussion of these syntheses, summarises failed reactions and finally reports the successful synthesis of **16** via a nickel(II) template reaction.

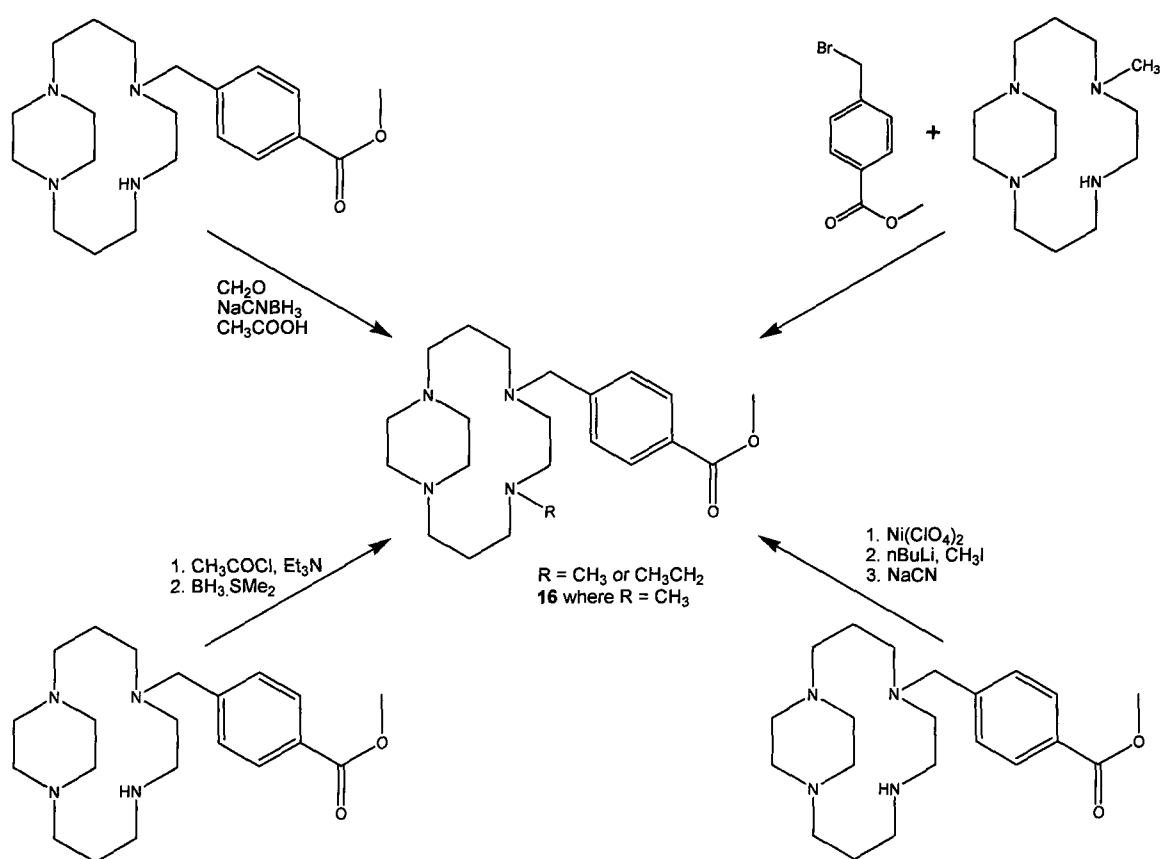


Figure 106. Summary of the attempted preparation of **16**.

### 6.3.1.1 Direct Alkylation I

There are numerous literature procedures for the alkylation of secondary amines with primary alkyl halides.<sup>100, 202, 203</sup> Therefore, initial attempts to alkylate **15** with methyl iodide followed these methods, using potassium carbonate as base and a good solvent for  $S_N^2$  reactions such as acetonitrile (Figure 107).

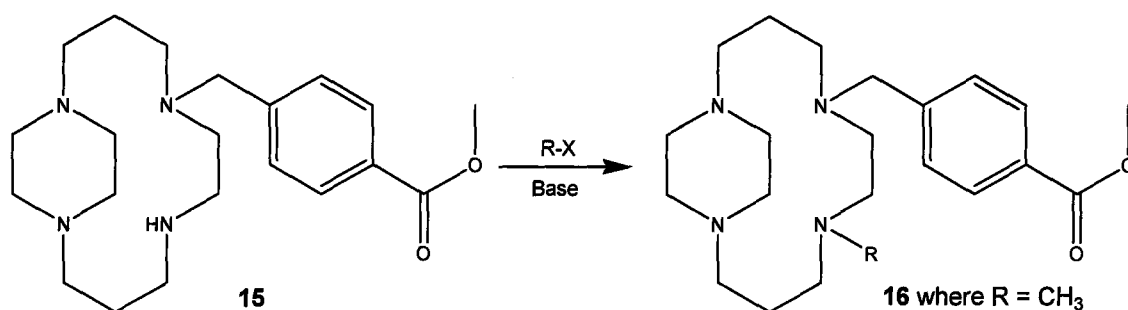


Figure 107. Alkylation of **15**.

Unfortunately, all attempted syntheses following these methods proved to be unsuccessful in terms of isolating a pure product. Varying the amount and the nature of the base, the concentration of the reactants, the reaction temperature and the choice of solvent (to DMF and DCM) had no effect on the purity of the product obtained. The likely problem with direct alkylation is the formation of alkylated ammonium species. This is observed in the mass spectrum of impure **16**, where a peak of  $m/z$  403 indicates an extra methyl group is present.

One of the major problems encountered with these side-bridged macrocycles is purification. For example, they are not mobile on silica or alumina plates and therefore, cannot be separated by  $SiO_2$  or  $Al_2O_3$  column chromatography. The oily nature of the

products results in difficulty in recrystallisation and finally, their high boiling points prevent vacuum distillation being a viable option.

The problem of alkylated ammonium species has also been encountered by Kotek and co-workers who have reported the synthesis of **L<sup>49</sup>** (Figure 108).<sup>204</sup> The direct alkylation of **L<sup>47</sup>** with either ethyl bromoacetate or *tert*-butyl bromoacetate under similar conditions to those described above led to the formation of the mono-quaternised derivative **L<sup>49</sup>** after acidic hydrolysis. This has been attributed to the fact that the secondary amine is involved in a hydrogen bonding network with the two unreactive tertiary amines, leaving the third tertiary amine to be the reactive site towards electrophilic attack as this lone pair either points away from the macrocyclic cavity or is too far away to participate in the hydrogen bonding network.

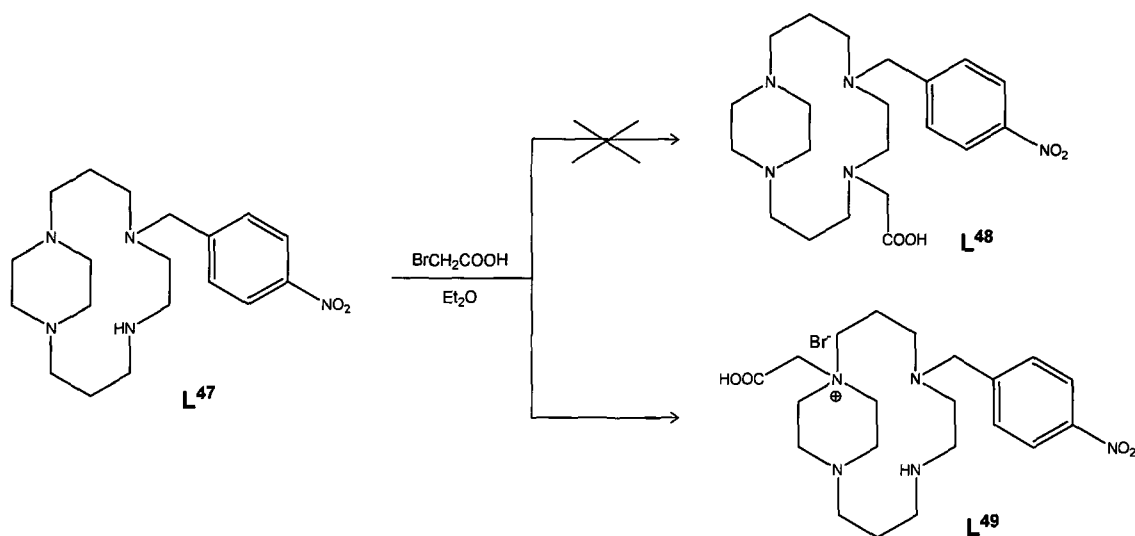


**Figure 108.** Alkylation of **L<sup>47</sup>** results in the unexpected compound, **L<sup>49</sup>**.

### 6.3.1.2 Reductive Amination

The addition of a methyl arm to the alkylated side-bridged macrocycle **L**<sup>13</sup> has been reported by Kolinski (chapter two, section 2.1.1).<sup>160</sup> This involved the reductive amination of the secondary amine with formaldehyde and sodium cyanoborohydride. This method has been followed on the systems in this work (Figure 109) but, as with the direct alkylation method previously discussed, a pure product could not be isolated.

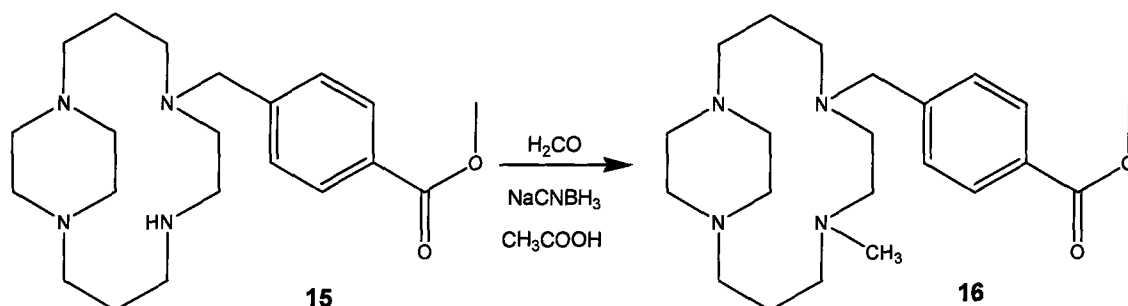
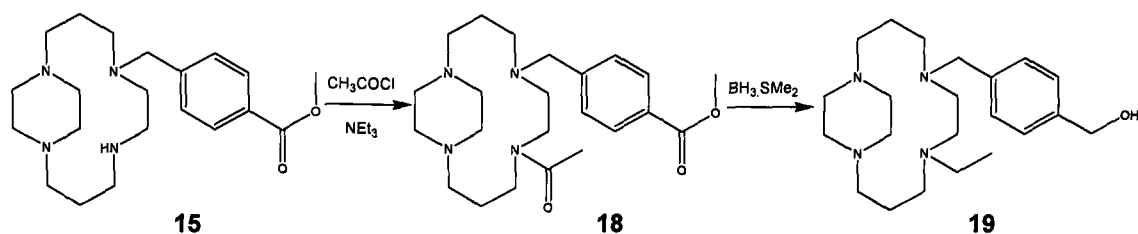


Figure 109. Reductive amination of **15**.

### 6.3.1.3 Acylation & Reduction

Kaden has reported the synthesis of the alkylated bis-side-bridged cyclam, **L**<sup>17</sup>, (chapter two, section 2.1.1).<sup>161</sup> It was envisaged that this methodology could be applied to our system (Figure 110) in order to avoid the previously discussed problems which had been encountered in the attempts to prepare compound **16**.



**Figure 110. Acylation of 15 and subsequent reduction of intermediate 18.**

This route also has the potential advantage that the reduction of the intermediate amide derivative, **18** (which was not isolated), would also reduce the ester functionality of the pendent arm, thus negating the need for a further reduction step in the route. Unfortunately, the attempts at this reaction were unsuccessful and all that could be isolated was a crude mixture of multiple products as shown by proton NMR spectrometry. Attempts at purification of **19** were again ineffective due to the reasons mentioned above.

#### 6.3.1.4 Direct Alkylation II

The previously discussed methods for alkylating **15** have all relied on the ester containing pendent arm being present from the outset. As these reactions proved to be unsuitable it was decided to alter our strategy and try to append the ester functionality to a side-bridged cyclam already containing a methyl group. The proposed route is shown in Figure 111. The mono-methyl side-bridged compound, **21**, has been reported by Kolinski.<sup>160</sup> The published synthetic route to this compound was followed and crystal structures of **20** and **21** have been obtained.

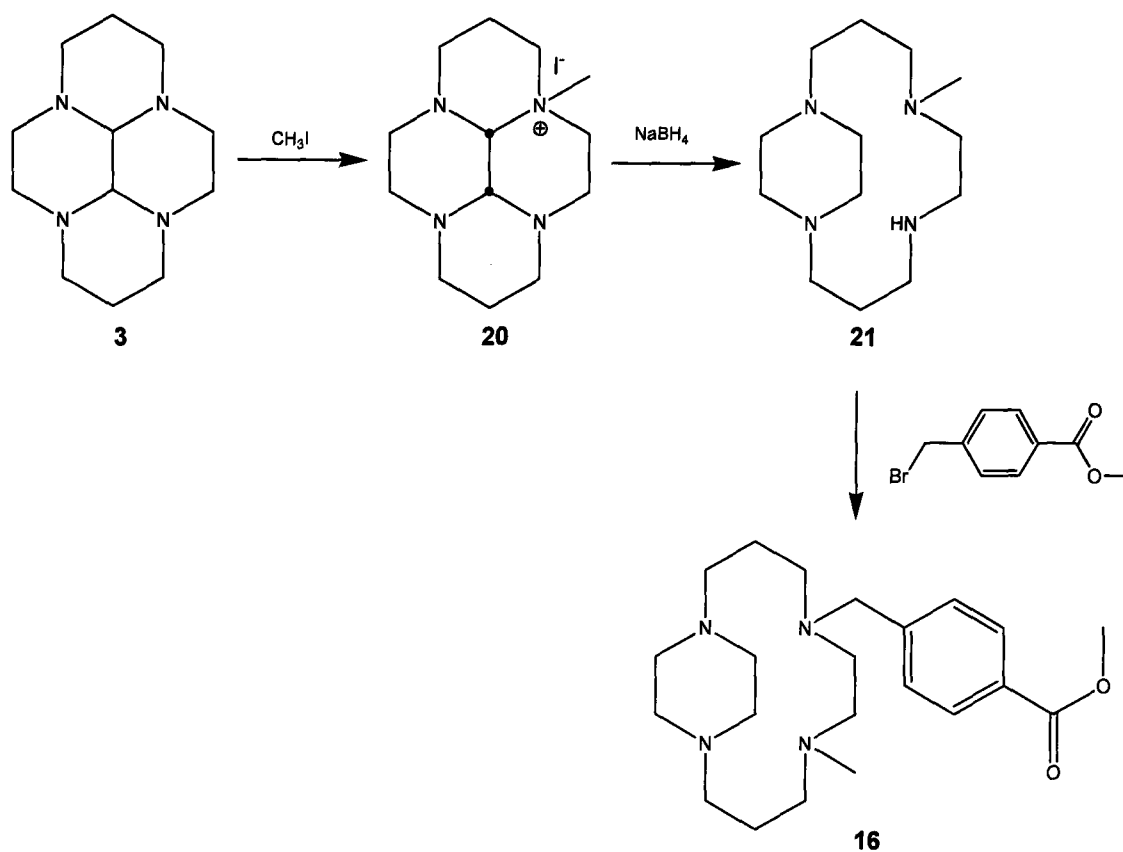


**Figure 111. Proposed alternative synthetic route to 16.**

Methylation of **3** was achieved in almost quantitative yield by dripping methyl iodide into an acetone solution of **3**. The ammonium salt, **20**, precipitates out of solution and can be collected by filtration. Single crystals of **20** (Figure 112) were grown from a methanolic solution and, as expected, the four six-membered rings are in the chair conformation. The overall structure is very similar to the two structures of **3** previously discussed (chapter two, section 2.3.1), which is not entirely unexpected as there is only the addition of a methyl group between the two compounds.

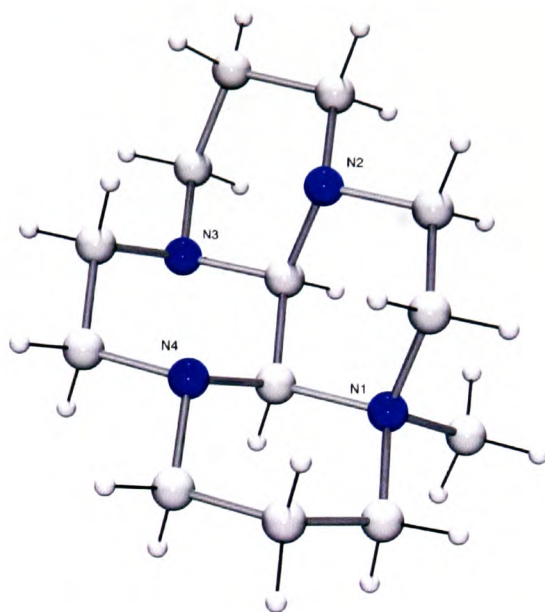


**Figure 112. X-ray crystal structure of 20.**

Reduction of **20** with an excess of sodium borohydride was successful and resulted in the isolation of **21** in excellent yield (81%). Interestingly, it was noted that **21** can be purified in a two-stage process with the addition of nickel(II) and its subsequent removal using sodium cyanide. Single crystals of purified **21** were grown from methanol and its X-ray crystal structure has been determined (Figure 113). The unit cell consists of the macrocycle and two solvent molecules of crystallisation. The piperazino moiety adopts a chair conformation, in contrast to the related compound, **L**<sup>17</sup>, which was crystallised by Kaden and co-workers and adopts a boat conformation.<sup>161</sup> Additionally, **21** is neutral in the solid state.

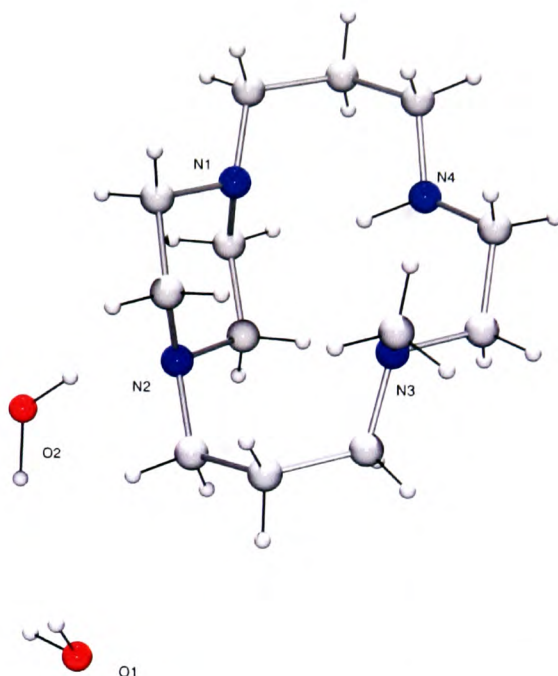


**Figure 113. X-ray crystal structure of 21.**

The reactivity of the sterically bulky ester containing alkyl bromide would be expected to be lower than that of methyl iodide and leads to the possibility that further quaternisation of the macrocycle would not occur as had happened previously. However, the addition of 4-(methylbromo)benzoate using similar conditions as described earlier proved to be ineffective in giving a clean product. The fact that the side-bridged compound does not run on TLC plates means that reaction progress cannot be monitored by these means. The proton NMR spectrum of **16** reveals a messy aromatic region instead of the desired rooftop effect for the 1,4-di substituted phenyl ring.

### 6.3.2 Cross-bridged Cyclam

Having explored several proposed routes to the desired mono-macrocyclic compound, **16**, it was decided to change synthetic strategy and attempt to prepare a cross-bridged mono-macrocycle, **23**. The secondary amine position can be alkylated in a two step process utilising bis-aminal methodology (Figure 114). The ester salt, **14**, can be alkylated with an excess of methyl iodide to give the bis-salt, **22**. This could then be reduced to give the cross bridge compound, **23**, which contains the ester pendent arm together with a methylated tertiary amine. It is also possible that the ester arm would be reduced over the fourteen day reduction time to result in **24**. This would actually be advantageous to this scheme as it would cut down on the number of steps and lead to an increase in the overall yield.

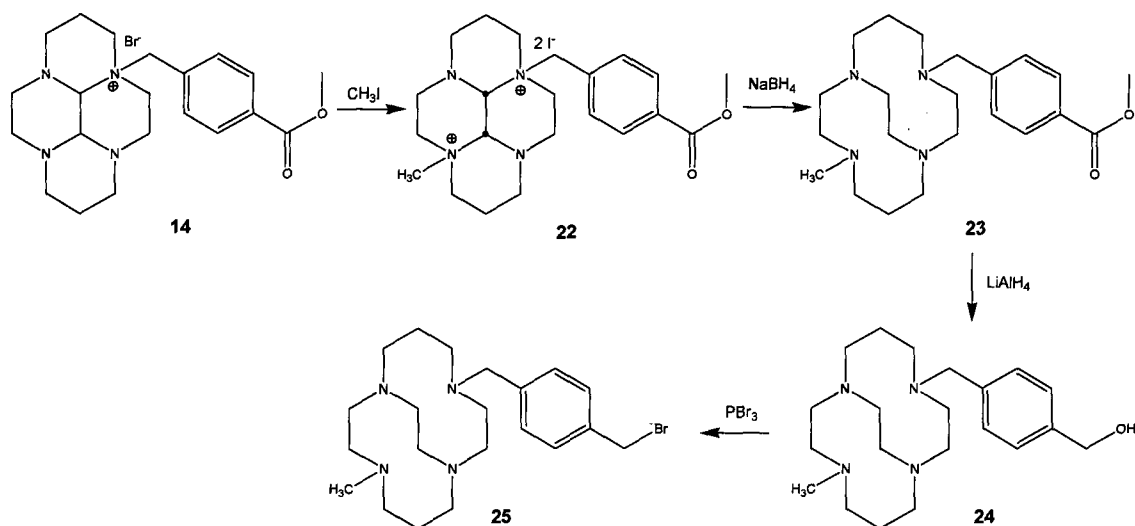
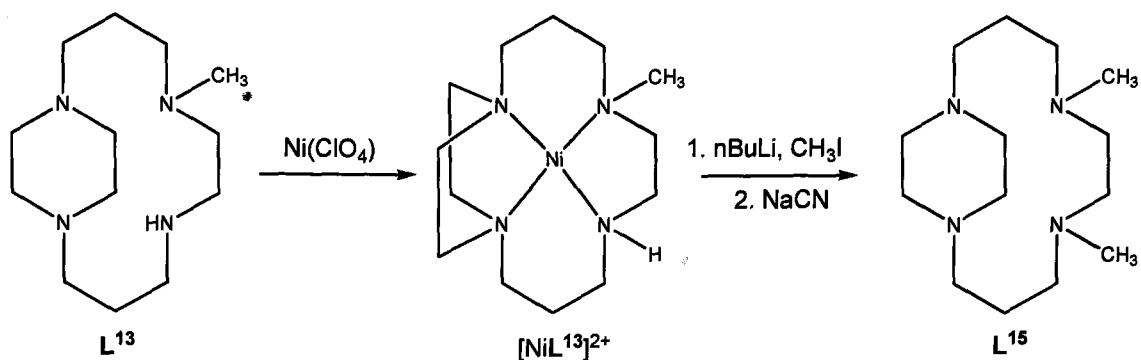


Figure 114. Proposed synthetic route to **25**.

The first step of this sequence involving the addition of methyl iodide to **22** proceeds over a seven day period in quantitative yield. As with the addition of methyl iodide to **3** (chapter three, section 3.3.1), the initial milky suspension is replaced by an orange solution as the reaction progresses, which is attributed to the counter anion metathesis of iodide and bromide. This is confirmed in the mass spectrum of **22**, where the observed molecular ion peak ( $m/z$  386) is the di-cation with the loss of two iodides. Reduction of **22** with an excess of sodium borohydride over fourteen days should lead to the formation of **23**; however, the attempts resulted in a crude product which could not be purified further. Further reduction of the impure product with lithium aluminium hydride had no effect in isolating pure **24** either. In conclusion, further work is required to optimise this synthetic route.

### 6.3.3 Nickel Template Reactions

Whilst searching for synthetic procedures for the alkylation of secondary amines, an alternative preparation of **16** was found in the literature. Kaden and co-workers, following a modification of a reaction initially reported by Barefield *et al.*, prepared the side-bridged macrocycle, **L<sup>15</sup>**, in a three step process via the nickel(II) complex (Figure 115).<sup>161, 205</sup>



**Figure 115. Kaden's synthesis of L<sup>15</sup>.**

The initial nickel(II) complexation of L<sup>13</sup> proceeds in reasonable yield (65%), resulting in a complex which can be deprotonated by nBuLi in dry DMSO solvent. The reported orange solution undergoes a colour change to blue after the addition of nBuLi. Addition of methyl iodide results in the reappearance of the orange solution which was added into a saturated ethanolic solution of ammonium hexafluorophosphate to aid the precipitation of an orange solid. After recrystallisation, the reported yield of L<sup>15</sup> is 62%.

In this work, the method could be adapted in one of two ways in order to synthesise **16**. Firstly, the nickel(II) complex of **21** could be alkylated with 4-(bromomethyl)benzoate or, alternatively, the side-bridged macrocycle containing the ester functional pendent arm (**15**) could be methylated (Figure 116).

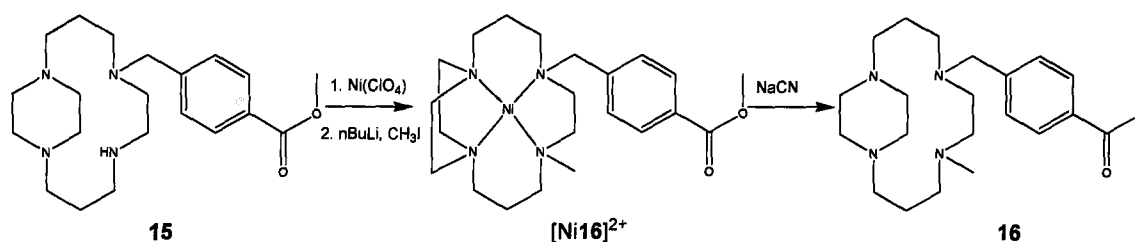


**Figure 116. Proposed synthetic route to 16**

The alkylation of  $[\text{Ni21}]^{2+}$  with 4-(bromomethyl)benzoate was attempted first as the starting material was available. The addition of  $\text{nBuLi}$  to the orange DMSO solution gave the expected blue solution; however, the addition of a DMSO solution of the alkyl bromide had no effect whatsoever and the second suggested route was tried. In fact, the blue colour persisted for approximately three months before an orange solution developed.

The nickel(II) complex of **15** was prepared by mixing the ligand with a slight excess of nickel(II) perchlorate in acetonitrile for two hours. The crude orange solid can be purified via size exclusion chromatography to remove the excess metal salt. The yields for the complexation are excellent (80-90%). Although attempts to grow single crystals of  $[\text{Ni15}]^{2+}$  were unsuccessful, the nickel(II) metal centre would be expected to coordinate to each of the four nitrogen atoms of the macrocyclic ring in a square planar geometry. This would have the effect of disrupting the hydrogen bonding network in the macrocycle which has been reported by Kotek *et al.* This should result in the secondary amine position becoming the most reactive site and it could, therefore, be deprotonated by a strong base, such as  $\text{nBuLi}$ .

On dissolution in dry DMSO,  $[\text{Ni15}]^{2+}$  gives an orange colour which on addition of  $\text{nBuLi}$ , changes to a blue solution as expected. Addition of excess methyl iodide to the blue

solution results in the formation of an orange solution which was dripped into ethanol in order to aid precipitation. Both the ammonium hexafluorophosphate and perchlorate salts of  $[\text{Ni16}]^{2+}$  have been isolated with varying yields.  $[\text{Ni16}](\text{ClO}_4)_2$  is obtained in excellent yield (90%) by dripping the DMSO solution into neat ethanol and filtering off the resulting orange precipitate.  $[\text{Ni16}](\text{PF}_6)_2$  is obtained by dripping the orange solution into a saturated solution of ammonium hexafluorophosphate in ethanol and filtering off the orange precipitate. However,  $[\text{Ni16}](\text{PF}_6)_2$  delivered lower yields (< 70%) in comparison to  $[\text{Ni16}](\text{ClO}_4)_2$ , but without the benefit of a purer product. Both complexes are soluble in acetonitrile and are identical by proton NMR spectrometry. The aromatic region of the spectrum reveals a 1,4-disubstituted rooftop effect and the  $\text{CH}_2$  group of the pendent arm reveals two sets of doublets, indicating that they are diastereotopic as a result of the rigidity imparted by the addition of the nickel(II) metal ion. Although, the new N-methyl group is not clearly seen in the proton NMR spectrum, its presence is confirmed in the carbon NMR spectrum with a peak at 31.2 ppm.

### 6.3.3.1 Decomposition with Cyanide

The decomposition of nickel(II) macrocyclic complexes with sodium cyanide is well known.<sup>206, 207</sup> These reactions have traditionally been carried out in aqueous media; however, poor yields (~ 20%) were recovered in the case of  $[\text{Ni16}]^{2+}$  due to difficulties in extracting **16** from either benzene or DCM. The choice of reaction solvent is dictated by the solubility of the starting material,  $[\text{Ni16}]^{2+}$ , which has been found to be only really soluble in acetonitrile. It was envisaged that the reaction could be carried out in this solvent and then worked up using a soxhlet extraction apparatus. However, sodium cyanide is not soluble in acetonitrile and the reaction will not proceed in neat solvent. After carrying out

the reaction in various media, the optimum conditions have been found to be heating at reflux for two hours in acetonitrile containing ca. 5% water, followed by purification via soxhlet extraction. This results in the isolation of the bis-alkylated side-bridged compound **16** in approximately 50% yield.

The proton NMR spectrum of **16** reveals a pair of doublets in the aromatic region as well as the disappearance of the diastereotopic CH<sub>2</sub> doublets seen in the nickel(II) complex. The alkyl region is, as expected, difficult to interpret fully; however the carbon NMR spectrum reveals the expected number of environments (20) with the N-methyl peak being observed at 31.1 ppm.

#### 6.3.4 Preparation of **26**

The reduction of the macrocyclic ester compound, **16**, with lithium aluminium hydride proceeded smoothly in dry THF. A yield of over 70% was obtained after extraction of the crude reactant. Once again, **17** was not mobile on silica or alumina TLC plates, however, the proton and carbon NMR spectra indicated a pure product.

Bromination of **17** with PBr<sub>3</sub> in pyridine results in the desired precursor, **18**, in a decent yield of ca. 50%. The proton and carbon NMR spectra of **18** are quite difficult to interpret due to the weakness of the sample, even after scans of over an hour for the proton and over 16 hours for the carbon. However, a clean 1,4-aromatic peak was observed in the aromatic region. Furthermore, the mass spectrum of **18** revealed the expected molecular ion peak.

Having prepared the precursor to asymmetrical bis-macrocycles, **18**, the next stage in the research was to attach the second ring. There are various strategies that could be employed in order to append the second macrocycle. However, due to time constraints, it was decided to simply react **18** directly with cyclam (Figure 117). Compound **18** was dissolved in a dilute solution of acetonitrile and a solution of cyclam was added dropwise in order to prevent any polymeric species forming. Again, the proton NMR spectrum was difficult to fully interpret. The mass spectrum of this bis-macrocyclic compound revealed a molecular ion peak indicating that the desired compound had been synthesised.

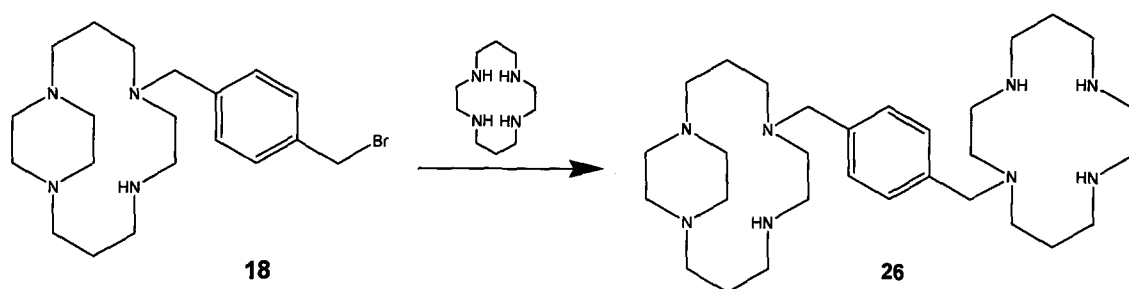


**Figure 117. Synthesis of asymmetrical bis-macrocycle, 26.**

## 6.4 Conclusions

A synthetic route to an asymmetrical bis-macrocyclic compound, **26**, has been designed. The alkylation of the secondary amine of **15** has proven to be unexpectedly challenging and a number of alternative routes have been attempted. A successful strategy involving a nickel(II) template has been found to result in a good yield. The isolation of the protected macrocycle, **16**, also proved difficult but optimum reaction conditions have been found to result in yields of approximately 50%. Reduction of the ester functionality leads to **17**, which has been fully analysed and brominated with  $\text{PBr}_3$  to give **18**. Unfortunately, due to time constraints, this compound could not be characterised completely; however, its mass spectrum contained the expected molecular ion peak.

## **Chapter 7. CONCLUSIONS**

Synthetic routes to two rigidified bis-macrocyclic ligands have been designed and implemented resulting in the preparation of **5** and **9** in good overall yields. In addition, these syntheses benefit from not requiring any lengthy purification steps. A range of transition metal complexes of **5** and **9** have been prepared and tested for their CXCR4 binding potency and anti-HIV activity using a variety of assays. All of the compounds tested are effective CXCR4 antagonists and are highly active against HIV. For example,  $[\text{Zn}_2\mathbf{5}(\text{OAc})_2]^{2+}$  and  $[\text{Cu}_2\mathbf{9Cl}_2]^{2+}$  are more potent than complexes of AMD3100 and have proven to be the most active bis-macrocyclic complexes found to date.

The X-ray crystal structure of  $[\text{Zn}_2\mathbf{5}(\text{OAc})_2]^{2+}$  reveals that the metal ion resides outside the macrocyclic cavity (0.74 Å) and, as a result, could potentially strengthen the coordination interaction with aspartate residues on the CXCR4 surface. This is reflected in the anti-HIV assay which confirms that  $[\text{Zn}_2\mathbf{5}(\text{OAc})_2]^{2+}$  is a more potent antagonist than the analogous zinc(II) AMD3100 complex. The coordination preferences of the copper(II) metal ion could explain the higher activity of  $[\text{Cu}_2\mathbf{9Cl}_2]^{2+}$  compared to  $[\text{Cu}_2\mathbf{5Cl}_2]^{2+}$ . For example,  $[\text{Cu}_2\mathbf{9Cl}_2]^{2+}$  interacts with CXCR4 aspartate residues via an equatorial coordination site whereas  $[\text{Cu}_2\mathbf{5Cl}_2]^{2+}$  coordinates via a weaker axial coordination site. Furthermore,  $[\text{Cu}_2\mathbf{9Cl}_2]^{2+}$  is effective against an AMD3100 resistant viral strain which suggests that it may have a different mode of action to AMD3100, or at the very least there is some variation in the binding site. It would be of interest to further probe this finding by developing a resistant viral strain to  $[\text{Cu}_2\mathbf{9Cl}_2]^{2+}$  to see which regions of the HIV RNA are altered.<sup>124</sup>

It is suggested that the high anti-HIV activity observed for  $[\text{Zn}_2\mathbf{5}(\text{OAc})_2]^{2+}$  and  $[\text{Cu}_2\mathbf{9Cl}_2]^{2+}$  is due to a combination of the binding kinetics to aspartate residues on the

CXCR4 surface and the stability of the interaction. For example, the metal ion in  $[\text{Zn}_2\mathbf{5}(\text{OAc})_2]^{2+}$  is accessible for aspartate binding, resulting in a thermodynamically stable complex once bound to the CXCR4 surface. These kinetic aspects could be investigated further by designing an assay to determine how long the complex remains bound to the receptor.

It would be desirable to investigate the binding of  $[\text{Zn}_2\mathbf{5}(\text{OAc})_2]^{2+}$  and  $[\text{Cu}_2\mathbf{9}\text{Cl}_2]^{2+}$  to CXCR4 further in conjunction with site directed mutagenesis of the receptor.<sup>34</sup> It would also be interesting to conduct *in vivo* studies. Ultimately, these complexes are unlikely to be successful anti-HIV drugs due to the fact that they are not orally bioavailable. However, they could still find use in the clinic for treating other disease states. For example, AMD3100 has found success as a stem cell mobiliser and many other potential uses of CXCR4 antagonists are currently under investigation.<sup>82, 208, 209</sup> Oral bioavailability, according to Lipinski's "Rule of five" could be increased in a number of ways.<sup>210</sup> For example, by lowering the molecular weight to below 500 Daltons. This means that a monocyclam derivative such as **L**<sup>42</sup> or **L**<sup>43</sup> could be orally bioavailable but this would be at the expense of the compound's potency.

X-ray absorption spectroscopy has been used to characterise the coordination environments of the novel metal complexes discussed in this work and also probe their interactions with various counter anions. EXAFS experiments on  $[\text{Cu}_2\mathbf{9}\text{Cl}_2]^{2+}$  have shown that the metal coordination geometry changes on the addition of acetate. These data suggest that the copper(II) complexes of **9** will bind to aspartate residues on the CXCR4 surface. It is interesting to compare the differences between the complexes of **5** and **9**. For example, both complexes adopt a square-based pyramidal geometry; however, the complexes of **5**

have a long range interaction with an axial counter anion, whereas the complexes of **9** have an equatorial counter anion which is shorter as expected. The axial position is occupied by a macrocyclic nitrogen atom which has a short bond length as a result of the configurationally restricted nature of the ethylene cross bridge.

The opening of the new Diamond Synchrotron Radiation Source promises an exciting future for EXAFS in the UK and could lead to the possibility of doing experiments at even lower concentrations than is presently possible. This offers the opportunity to conduct EXAFS experiments directly with the isolated (recombinant) CXCR4 receptor immobilised in a synthetic membrane on an appropriate surface. A method of preparing recombinant CXCR4 on a milligram scale has recently been reported.<sup>211</sup>

The synthesis of asymmetrical bis-macrocyclic compounds proved to be more challenging than was imagined when the work was started. This was due primarily to difficulty in the N-alkylation of the side-bridged derivative, **15**. A number of methods were attempted in order to prepare the methylated compound, **16**, which was eventually successfully synthesised using a nickel(II) template reaction followed by decomplexation with cyanide using a modification of the procedure described by Curtis<sup>207</sup>. The nickel(II) template reaction could also potentially be utilised on **5** to synthesise the bis-macrocycle **27** (Figure 118). Transition metal complexes of this compound would be expected to adopt a trans-IV configuration.

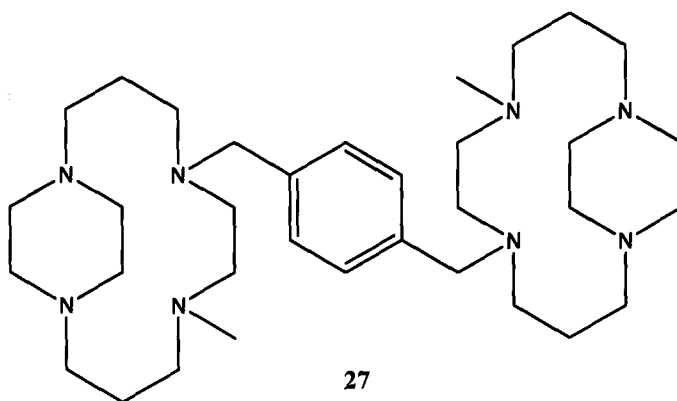


**Figure 118. Proposed bis-macroyclic compound, 27; transition metal complexes should adopt a trans-IV configuration.**

Reduction of **16** results in the alcohol derivative, **17**, which has been fully characterised. The bromination of **17** has been achieved but requires further work to provide a robust procedure. A preliminary reaction of crude **10** with cyclam was attempted, and the resulting mass spectrum indicated that the desired compound was present.

The brominated compound, **10**, is the precursor to a number of bis-macroyclic ligands. The preparation of **10** allows the synthesis of a range of asymmetrical bis-macroyclic compounds which could potentially be prepared by a variety of strategies. For example, compounds containing either a trans-II, trans-IV or cis-V configurationally restricted macrocycle could be prepared (Figure 119). One preliminary example, **26**, with a trans-IV and a cyclam ring has been prepared and requires further study.

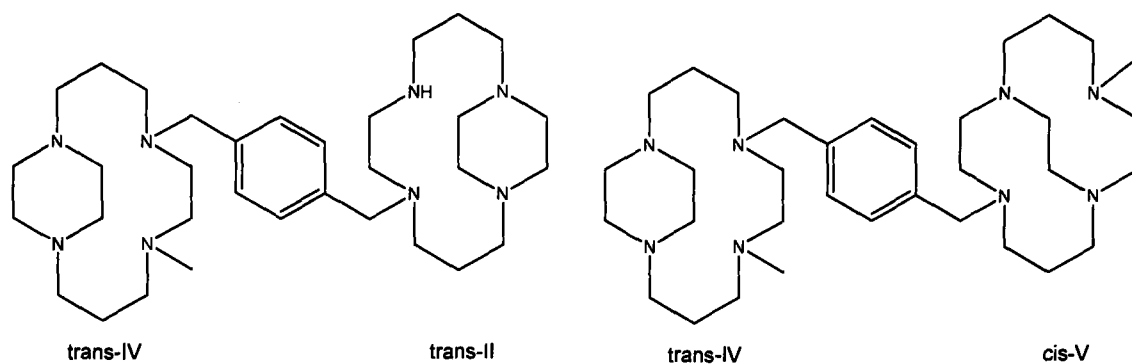


**Figure 119. Two examples of asymmetrical bis-macrocylic compounds.**

The asymmetry of the bis-macrocylic systems could be extended to a complex containing one zinc(II) ion and one copper(II) centre. One possible method would be to carry out the first complexation with half an equivalent of metal salt at low temperature, which has been successfully achieved for bis-macrocylic cyclen compounds.<sup>108</sup>

## **Chapter 8. EXPERIMENTAL**

## 8.1 General Methods

### 8.1.1 Solvents and Reagents

All solvents and reagents were purchased from either Sigma-Aldrich Ltd., Lancaster Chemicals Ltd. (Alfa-Aesar) or Fisher Chemicals Ltd. and were used as supplied unless otherwise stated. Drying of reaction solvents was achieved according to literature methods.<sup>212</sup> Organic solvent extracts were dried with magnesium or sodium sulphate and bulk solvent was removed via rotary evaporation under reduced pressure. Trace solvent was removed using an Edwards RV5 oil pump connected to a standard Schlenk line. Reactions involving dry solvents were carried out under an inert (nitrogen or argon) atmosphere using standard Schlenk line techniques.

### 8.1.2 Analytical Techniques

All <sup>1</sup>H NMR and proton decoupled <sup>13</sup>C NMR spectra were collected on a JEOL JNM-LA400 spectrometer (400 and 100 MHz respectively) at the University of Hull, except that of [Zn<sub>2</sub>5(OAc)<sub>2</sub>]<sup>2+</sup>, which was carried out at the University of Edinburgh using a Bruker Avance 4-channel 800 MHz spectrometer with cryoprobe. Chemical shifts are referenced against residual solvent signals and are designated as: s, singlet; d, doublet; t, triplet; q, quartet; p, pentent; m, multiplet; br, broad. Deuterated solvents were purchased from either Cambridge Isotopes Ltd. or Goss Chemicals Ltd.

Mass spectrometry was carried out via electrospray ionisation (ESI) on a Finnigan LCQ spectrometer. Accurate mass spectra were collected on a Thermofisher LTQ Orbitrap XL spectrometer by the EPSRC National Mass Spectrometry Service at the University of

Wales, Swansea. All calculated models for accurate mass analysis are based on the predominant natural isotopes of C, N, H, and O, and on  $^{63}\text{Cu}$ ,  $^{65}\text{Zn}$ ,  $^{35}\text{Cl}$  and  $^{79}\text{Br}$  isotopes. The molecular ion peak ( $M^+$ ) is defined as the total mass of the compound. Some of the metal complexes show the major peaks with the loss of one or more of the counter anions.

UV-vis spectra were obtained using an Agilent 8453 diode array spectrometer.

Single crystal X-ray diffraction data sets were collected on a Stöe IPDS-II imaging plate diffractometer at the University of Hull using MoK $\alpha$  X-rays ( $\lambda = 0.71073 \text{ \AA}$ ). Crystals were cooled to ca. 150 K during data collection, with the temperature controlled by an Oxford Systems Cryostream Cooler. Diffraction data were solved using direct methods or Patterson syntheses (ShelXS), and the refinement was by the full-matrix least squares against  $F^2$  (ShelXL-97) method.<sup>213, 214</sup> The WinGX program was used for refinement and production of data tables.<sup>215</sup> ORTEP-3 was used for structural visualisation.<sup>216</sup> Hydrogen atoms were fixed in idealised positions and refined against a riding model, with C-H distances of 0.97  $\text{\AA}$ , N-H distances of 0.91  $\text{\AA}$  and  $U_{\text{iso}}$  1.5 times  $U_{\text{eq}}$  of the carrier atom. All ORTEP representations show ellipsoids at the 50% probability level.<sup>216</sup>

Copper(II) and zinc(II) K-edge XAS were collected on either station 7.1 or 16.5 of the Daresbury Laboratory SRS (2 GeV, 100-200 mA). The experimental setup on station 7.1 used either a sagittally focusing or flat crystal Si(111) double crystal monochromator with 70% harmonic rejection in conjunction with a collimating mirror. The data from the solid samples were collected in transmission mode using ion chambers whilst for the solution samples the data were acquired using a nine-element solid state fluorescence detector. On station 16.5 the experimental setup was the same as 7.1 except that a flat

crystal Si(220) monochromator was used with a 30 element detector. The spectra were averaged (ca. 3 for solids, ca. 10 for solutions) and calibrated (first maximum of the derivative of the Cu-K edge of Cu foil, 8979.0 eV, Zn-K edge of Zn foil, x eV) using PAXAS.<sup>217</sup> The data were modelled using curved wave theory in EXCURV98.<sup>218</sup> Preliminary analysis was carried out; however, due to the complex nature of the macrocyclic complexes, full analysis was completed by Dr Nigel Young.

Solid samples were prepared by grinding ca. 5 mg of metal ion (i.e. 20-40 mg sample) and ca. 100 mg boron nitride and pressing at a pressure of 10 tonnes. The pellets were held in a sample holder using sellotape and cooled to ca. 80 K for data collection. Solution samples (ca. 20 mM on station 7.1, ca. 10 mM on station 16.5) were prepared by dissolving the metal complex in deionised water (1 mL) and placing in an aluminium solution cell with kapton windows. The solutions were carefully cooled to ca. 80 K for data collection. The solutions containing an excess of acetate were prepared 24 h before data collection and left to stand at room temperature.

## 8.2 Synthesis of Organic Compounds

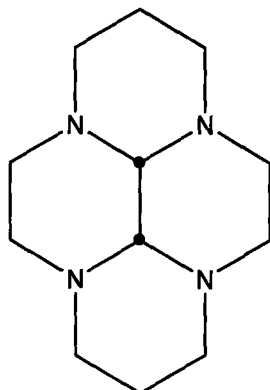
### 8.2.1 Synthesis of 1,4,8,11-tetraazacyclotetradecane, cyclam, 1

The synthesis of cyclam was carried out according to a literature procedure.<sup>219</sup> 1,5,8,12-tetrazadodecane (26 g, 0.15 mol) was added to a solution of nickel (II) perchlorate (54.7 g, 0.15 mol) in water (400 mL). An aqueous solution of glyoxal (40%, 22.5 mL, 0.15 mol) was added and the resulting purple solution was left to stand for 4 h. The solution was cooled to  $\sim 5^{\circ}\text{C}$  and sodium borohydride (11 g, 0.3 mol) was added slowly. The solution was heated to  $90^{\circ}\text{C}$  for 20 minutes and filtered whilst hot. Sodium cyanide (29 g, 0.6 mol) was added to the filtrate and heated at reflux for 2 h. On cooling, sodium hydroxide (15 g, 0.38 mol) was added to the yellow-brown mixture and then concentrated *in vacuo* to a semi solid. The semi solid was washed with chloroform (4 x 100 mL) and the resulting biphasic system was extracted from further chloroform (3 x 100 mL). The combined organic layers were dried ( $\text{Na}_2\text{SO}_4$ ), filtered and concentrated *in vacuo*. The crude material was recrystallised from chlorobenzene (350 mL) and washed with diethyl ether (100 mL) to yield a white crystalline product (11 g, 37%).

$^1\text{H}$  NMR: ( $\text{CDCl}_3$ )  $\delta$  1.62-1.68 (p, 4H, 5.33 Hz, N- $\beta$ - $\text{CH}_2$ ), 2.27 (br s, 4H, NH), 2.60 (s, 8H, N- $\alpha$ - $\text{CH}_2$ ), 2.66-2.68 (t, 8H, 5.33 Hz, N- $\alpha$ - $\text{CH}_2$ ).

$^{13}\text{C}$  NMR: ( $\text{CDCl}_3$ )  $\delta$  29.35 (N- $\beta$ - $\text{CH}_2$ ), 49.38 (N- $\alpha$ - $\text{CH}_2$ ), 50.80 (N- $\alpha$ - $\text{CH}_2$ ).

## 8.2.2 Synthesis of decahydro-3a,5a,8a,10a-tetraaza-pyrene, **3**



The synthesis of **3** was carried out following a minor modification of a literature procedure.<sup>164</sup> Cyclam (5 g, 25 mmol) was dissolved in methanol (100 mL) and cooled to -10°C. A cold (0°C) aqueous solution of glyoxal (40%, 3.63 g) was added over 90 minutes. The clear solution was stirred at -10°C for 30 minutes and at room temperature for 3 h. The solvent was concentrated *in vacuo* and the crude solid was redissolved in diethyl ether (200 mL). The filtrate was dried (MgSO<sub>4</sub>), filtered and evaporated *in vacuo* to yield a white solid (5.45 g, 98%).

<sup>1</sup>H NMR: (CDCl<sub>3</sub>) δ 1.12-1.16 (m, 2H), 2.03-2.26 (m, 8H), 2.64-2.67 (d, 2H), 2.86-2.96 (m, 6H), 3.00 (s, 2H), 3.35-3.52 (m, 2H).

<sup>13</sup>C NMR: (CDCl<sub>3</sub>) δ 19.53 (N-β-CH<sub>2</sub>), 44.68 (N-α-CH<sub>2</sub>), 52.41 (N-α-CH<sub>2</sub>), 54.27 (N-α-CH<sub>2</sub>), 55.97 (N-α-CH<sub>2</sub>), 76.98 (C<sub>aminal</sub>).

MS: (ESI) *m/z* 222 [M]<sup>+</sup>.

### 8.2.2.1 Crystal data and structural refinement for 3.2HClO<sub>4</sub>

Empirical formula	C <sub>12</sub> H <sub>24</sub> Cl <sub>2</sub> N <sub>4</sub> O <sub>8</sub>
Formula weight	423.25
Temperature	150(2) K
Wavelength	0.71073 Å
Crystal system	Monoclinic
Space group	P21/n
Unit cell dimensions	a = 14.4745(10) Å     α = 90°. b = 8.9214(8) Å     β = 114.166(5)°. c = 14.6706(10) Å     γ = 90°.
Volume	1728.4(2) Å <sup>3</sup>
Z	4
Density (calculated)	1.627 Mg/m <sup>3</sup>
Absorption coefficient	0.428 mm <sup>-1</sup>
F(000)	888
Crystal size	0.3 x 0.3 x 0.2 mm <sup>3</sup>
Theta range for data collection	2.57 to 34.80°.
Index ranges	-22 ≤ h ≤ 18, -14 ≤ k ≤ 14, -20 ≤ l ≤ 23
Reflections collected	29524
Independent reflections	7063 [R(int) = 0.0370]
Completeness to theta = 34.80°	94.1 %
Absorption correction	None
Refinement method	Full-matrix least-squares on F <sup>2</sup>
Data / restraints / parameters	7063 / 0 / 242
Goodness-of-fit on F <sup>2</sup>	0.964
Final R indices [I > 2σ(I)]	R1 = 0.0550, wR2 = 0.1459
R indices (all data)	R1 = 0.0844, wR2 = 0.1588
Extinction coefficient	0.0041(12)
Largest diff. peak and hole	0.905 and -0.808 e.Å <sup>-3</sup>

Crystals of  $3.2\text{HClO}_4$  were grown following evaporation of the methanol from the reaction mixture in the presence of  $\text{Zn}(\text{ClO}_4)_2$ .

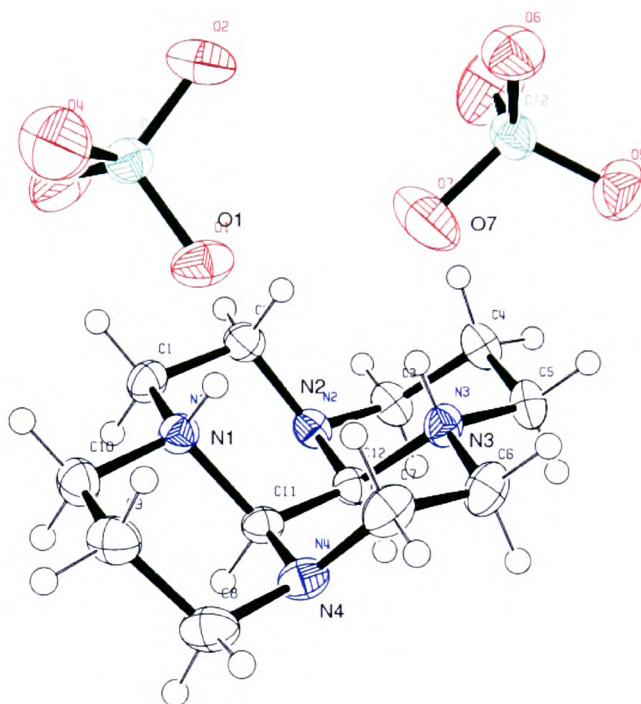


**Figure 120.** ORTEP representation of  $3.2\text{HClO}_4$ .

**Table 21. Bond lengths (Å) and angles (°) for 3.2HClO<sub>4</sub>.**

C(1)-N(1)	1.504(2)	O(5)-Cl(2)	1.4294(17)	C(1)-N(1)-C(11)	111.09(12)
C(1)-C(2)	1.506(3)	O(6)-Cl(2)	1.4291(15)	C(10)-N(1)-C(11)	109.05(14)
C(2)-N(2)	1.458(2)	O(7)-Cl(2)	1.4342(19)	C(12)-N(2)-C(2)	114.55(13)
C(3)-N(2)	1.471(2)	O(8)-Cl(2)	1.417(2)	C(12)-N(2)-C(3)	111.95(13)
C(3)-C(4)	1.523(2)			C(2)-N(2)-C(3)	114.62(15)
C(4)-C(5)	1.517(3)			C(6)-N(3)-C(5)	112.77(14)
C(5)-N(3)	1.510(2)	N(1)-C(1)-C(2)	108.51(13)	C(6)-N(3)-C(12)	110.70(15)
C(6)-N(3)	1.494(2)	N(2)-C(2)-C(1)	109.36(15)	C(5)-N(3)-C(12)	108.55(12)
C(6)-C(7)	1.508(3)	N(2)-C(3)-C(4)	112.31(14)	C(11)-N(4)-C(7)	113.93(16)
C(7)-N(4)	1.467(3)	C(5)-C(4)-C(3)	109.93(17)	C(11)-N(4)-C(8)	112.02(15)
C(8)-N(4)	1.468(3)	N(3)-C(5)-C(4)	109.97(14)	C(7)-N(4)-C(8)	114.78(15)
C(8)-C(9)	1.529(3)	N(3)-C(6)-C(7)	108.89(14)	O(4)-Cl(1)-O(2)	109.82(12)
C(9)-C(10)	1.522(3)	N(4)-C(7)-C(6)	109.08(15)	O(4)-Cl(1)-O(3)	111.78(15)
C(10)-N(1)	1.508(2)	N(4)-C(8)-C(9)	113.01(17)	O(2)-Cl(1)-O(3)	109.73(14)
C(11)-N(4)	1.424(2)	C(10)-C(9)-C(8)	110.38(15)	O(4)-Cl(1)-O(1)	109.41(13)
C(11)-C(12)	1.528(2)	N(1)-C(10)-C(9)	109.86(15)	O(2)-Cl(1)-O(1)	108.40(11)
C(11)-N(1)	1.538(2)	N(4)-C(11)-C(12)	112.75(14)	O(3)-Cl(1)-O(1)	107.61(10)
C(12)-N(2)	1.419(2)	N(4)-C(11)-N(1)	112.35(13)	O(8)-Cl(2)-O(6)	111.59(14)
C(12)-N(3)	1.538(2)	C(12)-C(11)-N(1)	112.10(14)	O(8)-Cl(2)-O(5)	108.34(13)
O(1)-Cl(1)	1.4471(15)	N(2)-C(12)-C(11)	112.54(13)	O(6)-Cl(2)-O(5)	110.41(11)
O(2)-Cl(1)	1.4242(18)	N(2)-C(12)-N(3)	112.35(14)	O(8)-Cl(2)-O(7)	107.97(18)
O(3)-Cl(1)	1.4253(16)	C(11)-C(12)-N(3)	112.35(12)	O(6)-Cl(2)-O(7)	108.97(12)
O(4)-Cl(1)	1.418(2)	C(1)-N(1)-C(10)	111.99(13)	O(5)-Cl(2)-O(7)	109.51(13)

### 8.2.2.2 Crystal data and structural refinement for 3.H[ZnCl<sub>3</sub>(OH<sub>2</sub>)]

Empirical formula	C <sub>12</sub> H <sub>25</sub> Cl <sub>3</sub> N <sub>4</sub> O Zn	
Formula weight	413.08	
Temperature	150(2) K	
Wavelength	0.71073 Å	
Crystal system	Monoclinic	
Space group	P21/c	
Unit cell dimensions	a = 7.0552(5) Å	α = 90°.
	b = 12.3597(11) Å	β = 99.386(6)°.
	c = 20.2463(14) Å	γ = 90°.
Volume	1741.8(2) Å <sup>3</sup>	
Z	4	
Density (calculated)	1.575 Mg/m <sup>3</sup>	
Absorption coefficient	1.874 mm <sup>-1</sup>	
F(000)	856	
Crystal size	0.2 x 0.2 x 0.2 mm <sup>3</sup>	
Theta range for data collection	2.93 to 35.13°.	
Index ranges	-11 ≤ h ≤ 8, -19 ≤ k ≤ 19, -32 ≤ l ≤ 32	
Reflections collected	21853	
Independent reflections	7597 [R(int) = 0.0497]	
Completeness to theta = 35.13°	98.0 %	
Absorption correction	None	
Refinement method	Full-matrix least-squares on F <sup>2</sup>	
Data / restraints / parameters	7597 / 1 / 206	
Goodness-of-fit on F <sup>2</sup>	1.045	
Final R indices [I > 2σ(I)]	R1 = 0.0383, wR2 = 0.0946	
R indices (all data)	R1 = 0.0592, wR2 = 0.1048	
Extinction coefficient	0.0094(8)	
Largest diff. peak and hole	0.684 and -1.031 e.Å <sup>-3</sup>	

Crystals of  $3.H[ZnCl_3(OH_2)]$  were grown following evaporation of a methanolic solution of **3** in the presence of  $ZnCl_2 \cdot 6H_2O$ .

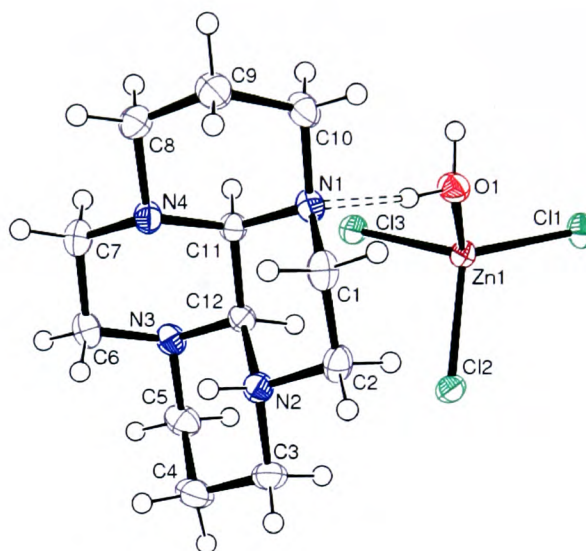


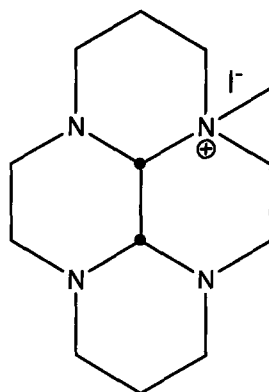
**Figure 121.** ORTEP representation of  $3.H[ZnCl_3(OH_2)]$ .

**Table 22. Bond lengths (Å) and angles (°) for 3.H[ZnCl<sub>3</sub>(OH<sub>2</sub>)].**

C(1)-N(1)	1.477(2)	N(1)-C(1)-C(2)	109.44(15)	C(11)-N(1)-C(10)	109.50(15)
C(1)-C(2)	1.504(3)	N(2)-C(2)-C(1)	109.43(15)	C(1)-N(1)-C(10)	111.31(16)
C(2)-N(2)	1.496(3)	N(2)-C(3)-C(4)	110.41(16)	C(2)-N(2)-C(3)	111.45(15)
C(3)-N(2)	1.511(2)	C(3)-C(4)-C(5)	110.71(16)	C(2)-N(2)-C(12)	111.44(13)
C(3)-C(4)	1.518(3)	N(3)-C(5)-C(4)	112.35(18)	C(3)-N(2)-C(12)	110.87(15)
C(4)-C(5)	1.527(3)	N(3)-C(6)-C(7)	108.90(16)	C(12)-N(3)-C(5)	111.16(16)
C(5)-N(3)	1.469(3)	N(4)-C(7)-C(6)	110.59(16)	C(12)-N(3)-C(6)	113.60(16)
C(6)-N(3)	1.475(3)	N(4)-C(8)-C(9)	111.26(17)	C(5)-N(3)-C(6)	113.32(16)
C(6)-C(7)	1.511(3)	C(8)-C(9)-C(10)	109.46(18)	C(7)-N(4)-C(11)	109.52(15)
C(7)-N(4)	1.462(3)	N(1)-C(10)-C(9)	111.30(15)	C(7)-N(4)-C(8)	108.91(16)
C(8)-N(4)	1.477(2)	N(1)-C(11)-N(4)	112.39(15)	C(11)-N(4)-C(8)	110.10(14)
C(8)-C(9)	1.519(3)	N(1)-C(11)-C(12)	110.21(14)	O(1)-Zn(1)-Cl(1)	110.03(4)
C(9)-C(10)	1.530(3)	N(4)-C(11)-C(12)	110.29(14)	O(1)-Zn(1)-Cl(3)	107.44(5)
C(10)-N(1)	1.484(2)	N(3)-C(12)-C(11)	111.97(14)	Cl(1)-Zn(1)-Cl(3)	117.34(2)
C(11)-N(1)	1.467(2)	N(3)-C(12)-N(2)	111.63(13)	O(1)-Zn(1)-Cl(2)	103.01(4)
C(11)-N(4)	1.472(2)	C(11)-C(12)-N(2)	109.82(14)	Cl(1)-Zn(1)-Cl(2)	112.284(18)
C(11)-C(12)	1.533(2)	C(11)-N(1)-C(1)	112.17(14)	Cl(3)-Zn(1)-Cl(2)	105.65(2)
C(12)-N(3)	1.426(2)				
C(12)-N(2)	1.545(2)				
Zn(1)-O(1)	2.0009(15)				
Zn(1)-Cl(1)	2.2227(5)				
Zn(1)-Cl(3)	2.2574(5)				
Zn(1)-Cl(2)	2.2873(5)				

### 8.2.3 Synthesis of 3a-[methyl]-decahydro-3a,5a,8a,10a-tetraaza-pyrenium bromide,

20



The synthesis of **20** was carried out following a minor modification of a literature procedure.<sup>160</sup> Methyl iodide (0.5 mL, 8 mmol) was added to a solution of decahydro-3a,5a,8a,10a-tetraaza-pyrene (1.77 g, 8 mmol) in acetone (50 mL) and the clear solution was stirred at room temperature for 6 h. A white precipitate was filtered off, washed with acetone (50 mL) and dried *in vacuo* to yield a white powder (2.53 g, 96%).

<sup>1</sup>H NMR: (D<sub>2</sub>O)  $\delta$  1.32-1.35 (m, 1H), 1.74-1.78 (m, 1H), 2.15-2.43 (m, 6H), 2.78-2.97 (m, 8H), 3.23 (s, N- $\alpha$ -CH<sub>3</sub>), 3.36-3.61 (m, 4H), 3.94-3.95 (d, 1H), 4.14-4.19 (m, 1H).

<sup>13</sup>C NMR: (D<sub>2</sub>O)  $\delta$  18.17 (N- $\beta$ -CH<sub>2</sub>), 18.91 (N- $\beta$ -CH<sub>2</sub>), 42.27 (N- $\alpha$ -CH<sub>2</sub>), 46.58 (N- $\alpha$ -CH<sub>2</sub>), 48.83 (N- $\alpha$ -CH<sub>2</sub>), 51.39 (N- $\alpha$ -CH<sub>2</sub>), 51.39 (N- $\alpha$ -CH<sub>2</sub>), 52.24 (N- $\alpha$ -CH<sub>2</sub>), 53.16 (N- $\alpha$ -CH<sub>2</sub>), 54.04 (N- $\alpha$ -CH<sub>2</sub>), 64.80 (N- $\alpha$ -CH<sub>3</sub>), 69.65 (C<sub>aminal</sub>), 83.03 (C<sub>aminal</sub>).

MS: (ESI)  $m/z$  237 [M-I]<sup>+</sup>. HRMS: Calcd. for C<sub>13</sub>H<sub>25</sub>N<sub>4</sub><sup>+</sup>: 237.2074; Found: 237.2075.

**8.2.4 Crystal data and structural refinement for 3a-[methyl]-decahydro-  
3a,5a,8a,10a-tetraaza-pyrenium bromide, 20**

Empirical formula	C <sub>13</sub> H <sub>25</sub> I N <sub>4</sub>	
Formula weight	364.27	
Temperature	150(2) K	
Wavelength	0.71073 Å	
Crystal system	Monoclinic	
Space group	P21/n	
Unit cell dimensions	a = 11.3340(11) Å	α = 90°.
	b = 7.0850(5) Å	β = 103.617(7)°.
	c = 19.1840(18) Å	γ = 90°.
Volume	1497.2(2) Å <sup>3</sup>	
Z	4	
Density (calculated)	1.616 Mg/m <sup>3</sup>	
Absorption coefficient	2.130 mm <sup>-1</sup>	
F(000)	736	
Crystal size	0.15 x 0.10 x 0.10 mm <sup>3</sup>	
Theta range for data collection	3.08 to 34.79°.	
Index ranges	-18 ≤ h ≤ 18, -11 ≤ k ≤ 8, -30 ≤ l ≤ 29	
Reflections collected	17011	
Independent reflections	6373 [R(int) = 0.0770]	
Completeness to theta = 34.79°	98.2 %	
Absorption correction	Numerical	
Max. and min. transmission	0.7979 and 0.6149	
Refinement method	Full-matrix least-squares on F <sup>2</sup>	
Data / restraints / parameters	6373 / 0 / 164	
Goodness-of-fit on F <sup>2</sup>	0.956	
Final R indices [I > 2σ(I)]	R1 = 0.0744, wR2 = 0.1813	
R indices (all data)	R1 = 0.0997, wR2 = 0.1929	
Extinction coefficient	0.0090(13)	
Largest diff. peak and hole	13.045 and -1.746 e.Å <sup>-3</sup>	

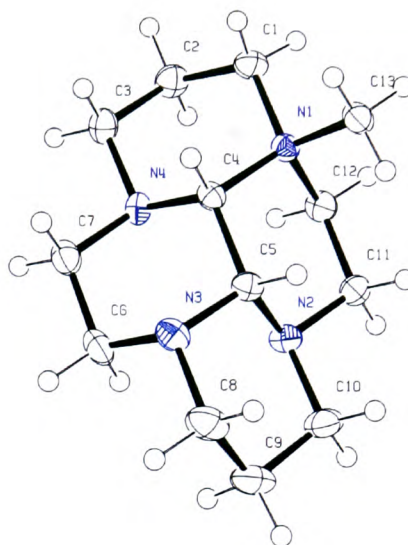
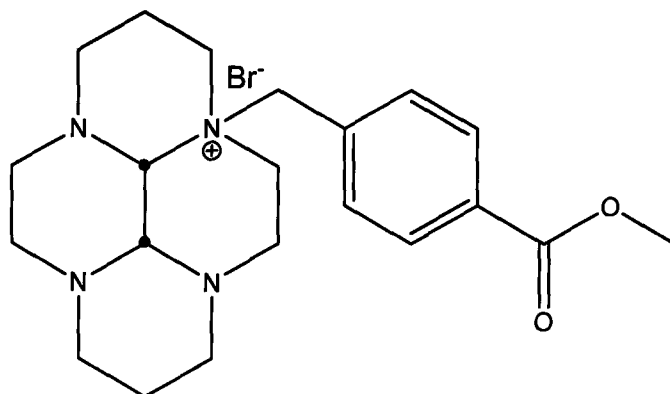


**Figure 122. ORTEP representation of 20.**

**Table 23. Bond lengths (Å) and angles (°) for 3a-[methyl]-decahydro-3a,5a,8a,10a-tetraaza-pyrenium bromide.**

C(1)-C(2)	1.516(7)	C(2)-C(1)-N(1)	112.3(4)	C(13)-N(1)-C(12)	110.8(3)
C(1)-N(1)	1.520(6)	C(3)-C(2)-C(1)	109.6(4)	C(13)-N(1)-C(1)	105.1(4)
C(2)-C(3)	1.507(7)	N(4)-C(3)-C(2)	109.6(4)	C(12)-N(1)-C(1)	110.7(4)
C(3)-N(4)	1.473(6)	N(4)-C(4)-N(1)	110.0(3)	C(13)-N(1)-C(4)	110.3(3)
C(4)-N(4)	1.452(5)	N(4)-C(4)-C(5)	111.5(4)	C(12)-N(1)-C(4)	109.4(3)
C(4)-N(1)	1.525(6)	N(1)-C(4)-C(5)	109.3(3)	C(1)-N(1)-C(4)	110.5(3)
C(4)-C(5)	1.543(6)	N(3)-C(5)-N(2)	111.6(4)	C(11)-N(2)-C(5)	111.3(4)
C(5)-N(3)	1.456(6)	N(3)-C(5)-C(4)	108.2(4)	C(11)-N(2)-C(10)	108.4(4)
C(5)-N(2)	1.473(6)	N(2)-C(5)-C(4)	112.0(3)	C(5)-N(2)-C(10)	109.3(4)
C(6)-N(3)	1.460(6)	N(3)-C(6)-C(7)	109.1(4)	C(5)-N(3)-C(6)	111.8(4)
C(6)-C(7)	1.507(8)	N(4)-C(7)-C(6)	110.7(4)	C(5)-N(3)-C(8)	109.6(4)
C(7)-N(4)	1.475(6)	N(3)-C(8)-C(9)	111.6(5)	C(6)-N(3)-C(8)	113.3(4)
C(8)-N(3)	1.481(7)	C(10)-C(9)-C(8)	109.5(5)	C(4)-N(4)-C(3)	112.1(4)
C(8)-C(9)	1.521(9)	N(2)-C(10)-C(9)	111.1(5)	C(4)-N(4)-C(7)	109.5(3)
C(9)-C(10)	1.520(9)	N(2)-C(11)-C(12)	110.6(4)	C(3)-N(4)-C(7)	108.6(4)
C(10)-N(2)	1.485(7)	C(11)-C(12)-N(1)	111.7(4)		
C(11)-N(2)	1.464(6)				
C(11)-C(12)	1.506(7)				
C(12)-N(1)	1.512(6)				
C(13)-N(1)	1.502(6)				

### 8.2.5 Synthesis of 3a-[phenylenemethylene benzoate]-decahydro-3a,5a,8a,10a-tetraaza-pyrenium bromide, 14



Decahydro-3a,5a,8a,10a-tetraaza-pyrene (4.93 g, 22 mmol) and 4-(methylbromo)benzoate (5.08 g, 22 mmol) were dissolved in dry acetonitrile (100 mL) under nitrogen and stirred at room temperature for 7 days. A white precipitate was collected by filtration, washed with acetonitrile (50 mL) followed by tetrahydrofuran (100 mL) and dried *in vacuo* to yield a white powder (9.48 g, 95%).

$^1\text{H NMR}$ : ( $\text{D}_2\text{O}$ )  $\delta$  1.38-1.42 (d, 1H), 1.70-1.73 (d, 1H), 2.13-2.24 (m, 3H), 2.39-2.45 (m, 2H), 2.54-2.59 (td, 1H), 2.94-3.09 (m, 7H), 3.17-3.29 (m, 3H), 3.41-3.51 (m, 2H), 3.64 (s, 1H), 3.89 (s, 3H, O- $\text{CH}_3$ ), 4.12-4.19 (td, 1H), 4.29-4.30 (d, 1H, 12.91 Hz,  $\text{N}^+\text{-CH}_2$ ), 5.10-5.13 (d, 1H, 12.91 Hz,  $\text{N}^+\text{-CH}_2$ ), 7.59-7.61 (d, 2H, 8.42 Hz,  $\text{CH}_{\text{aromatic}}$ ), 8.06-8.08 (d, 2H, 8.42 Hz,  $\text{CH}_{\text{aromatic}}$ ).

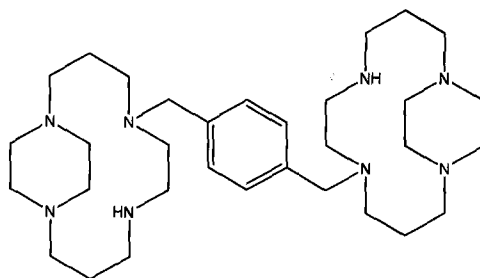
$^{13}\text{C NMR}$ : ( $\text{D}_2\text{O}$ )  $\delta$  18.13 (N- $\beta\text{-CH}_2$ ), 18.53 (N- $\beta\text{-CH}_2$ ), 42.11 (N- $\alpha\text{-CH}_2$ ), 46.73 (N- $\alpha\text{-CH}_2$ ), 48.79 (N- $\alpha\text{-CH}_2$ ), 51.50 (N- $\alpha\text{-CH}_2$ ), 52.10 (N- $\alpha\text{-CH}_2$ ), 53.10 ( $\text{CH}_3\text{-O}$ ), 53.46 (N- $\alpha\text{-CH}_2$ ), 54.12 (N- $\alpha\text{-CH}_2$ ), 60.32 (N- $\alpha\text{-CH}_2$ ), 61.94 (N- $\alpha\text{-CH}_2$ ), 69.74 ( $\text{C}_{\text{aminal}}$ ), 82.53 ( $\text{C}_{\text{aminal}}$ ), 130.28 ( $\text{CH}_{\text{aromatic}}$ ), 131.02 ( $\text{C}_{\text{aromatic}}$ ), 132.02 ( $\text{C}_{\text{aromatic}}$ ), 133.69 ( $\text{CH}_{\text{aromatic}}$ ) 168.63 (C=O).

MS: (ESI)  $m/z$  371 [M-Br]<sup>+</sup>. HRMS: Calcd. for C<sub>21</sub>H<sub>31</sub>N<sub>4</sub>O<sub>2</sub>: 371.2442; Found 371.2442.

Elemental Analysis: (%) Calcd. for C<sub>21</sub>H<sub>31</sub>N<sub>4</sub>O<sub>2</sub>Br: C:55.88 H:6.92 N:12.40; Found C:55.78 H:7.24 N:12.27.



### 8.2.7 Synthesis of 5,5'-[1,4-phenylenebis(methylene)]-bis(1,5,8,12-tetraaza-bicyclo-[10.2.2]hexadecane), 5



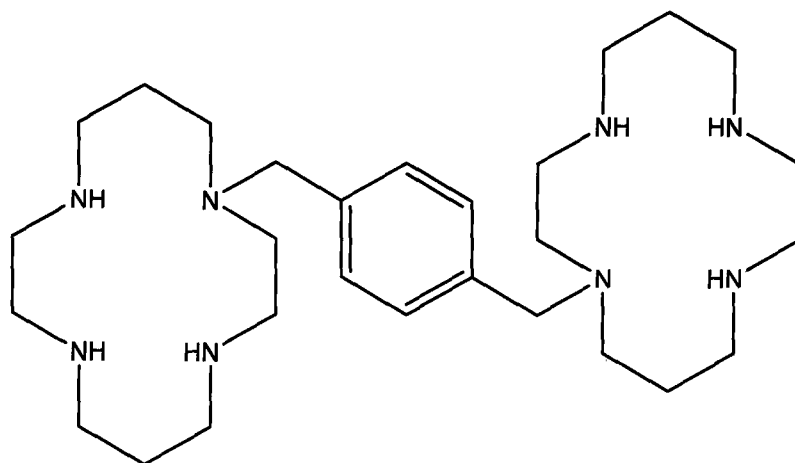
3a,3a'-[1,4-Phenylenebis(methylene)]-bis(decahydro-3a,5a,8a,10a-tetraazapyrenium) dibromide (5.00 g, 7 mmol) was dissolved in methanol (100 mL) and cooled to 0°C. Sodium borohydride (10.72g, 282 mmol) was added slowly and the clear solution was stirred under nitrogen at room temperature for 4 h. The solution was concentrated *in vacuo* and water (50 mL) was added. The pH was adjusted to 14 (KOH pellets) and the basic solution was extracted into dichloromethane (5 x 50 mL). The combined organic fractions were dried (MgSO<sub>4</sub>), filtered and evaporated *in vacuo* to yield a clear oil (2.28 g, 58%).

<sup>1</sup>H NMR: (CDCl<sub>3</sub>) δ 1.72 (m, 4H, NCH<sub>2</sub>), 1.81 (s, 4H, NCH<sub>2</sub>), 2.26 (m, 4H, NCH<sub>2</sub>), 2.56 (m, 12H, NCH<sub>2</sub>), 2.63 (m, 8H, NCH<sub>2</sub>), 2.70 (m, 4H, NCH<sub>2</sub>), 2.93 (m, 4H, NCH<sub>2</sub>), 3.02 (m, 4H, NCH<sub>2</sub>), 3.27 (m, 4H, NCH<sub>2</sub>), 3.65 (s, 4H, NCH<sub>2</sub>Ar), 7.20 (s, 4H, CH<sub>aromatic</sub>).

<sup>13</sup>C NMR: (CDCl<sub>3</sub>) δ 23.52, (N-β-CH<sub>2</sub>), 26.43 (N-β-CH<sub>2</sub>), 48.17 (N-α-CH<sub>2</sub>), 48.26 (N-α-CH<sub>2</sub>), 50.62 (N-α-CH<sub>2</sub>), 51.30 (N-α-CH<sub>2</sub>), 54.73 (N-α-CH<sub>2</sub>), 55.15 (N-α-CH<sub>2</sub>), 55.51 (N-α-CH<sub>2</sub>), 56.24 (N-α-CH<sub>2</sub>), 57.07 (N-α-CH<sub>2</sub>), 129.36 (C<sub>aromatic</sub>), 136.40 (CH<sub>aromatic</sub>).

MS: (ES): *m/z*: 555 [MH]<sup>+</sup>. HRMS: Calcd. for C<sub>32</sub>H<sub>59</sub>N<sub>8</sub><sup>+</sup>: 555.4857; Found 555.4856.

### 8.2.8 Synthesis of 1,1'-[1,4-phenylenebis(methylene)]bis[1,4,8,11-tetraazacyclotetradecane],<sup>164</sup> AMD3100, **2**



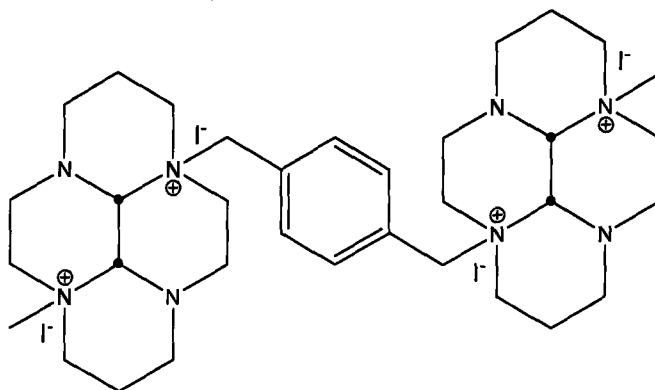
The synthesis of **2** was carried out following a minor modification of a literature procedure.<sup>164</sup> 3a,3a'-[1,4-Phenylenebis(methylene)]-bis(decahydro-3a,5a,8a,10a-tetraazapyrenium) dibromide (320 mg, 0.45 mmol), sodium ethoxide (1.24 g, 18 mmol) and hydroxylamine hydrochloride (1.26 g, 18 mmol) were dissolved in dry methanol (100 mL) and stirred at reflux under nitrogen for 4 h and then at room temperature overnight. The clear solution was concentrated *in vacuo* and a sodium hydroxide solution (10 M, 25 mL) was added. The crude product was extracted from dichloromethane (8 x 50 mL). The combined organic fractions were dried (MgSO<sub>4</sub>), filtered and evaporated *in vacuo* to yield a white powder (200 mg, 87%).

<sup>1</sup>H NMR: (D<sub>2</sub>O) δ 1.83-1.88 (m, 5H), 2.04-2.21 (m, 7H), 2.76-2.80 (m, 9H), 2.92-2.97 (12H), 3.10-3.21 (m, 13H), 3.29-3.32 (t, 4H) 5.44 (s, 1H), 7.35 (s, 4H, CH<sub>aromatic</sub>).

$^{13}\text{C}$  NMR: ( $\text{D}_2\text{O}$ )  $\delta$  21.97 (N- $\beta$ - $\text{CH}_2$ ), 24.80 (N- $\beta$ - $\text{CH}_2$ ), 44.90 (N- $\alpha$ - $\text{CH}_2$ ), 46.75 (N- $\alpha$ - $\text{CH}_2$ ), 47.58 (N- $\alpha$ - $\text{CH}_2$ ), 49.52 (N- $\alpha$ - $\text{CH}_2$ ), 49.66 (N- $\alpha$ - $\text{CH}_2$ ), 51.15 (N- $\alpha$ - $\text{CH}_2$ ), 52.78 (N- $\alpha$ - $\text{CH}_2$ ), 54.70 (N- $\alpha$ - $\text{CH}_2$ ), 54.83 (N- $\alpha$ - $\text{CH}_2$ ), 130.74 ( $\text{CH}_{\text{aromatic}}$ ), 134.60 ( $\text{C}_{\text{aromatic}}$ ).

MS: (ESI)  $m/z$  503  $[\text{MH}]^+$ .

**8.2.9 Synthesis of 8a,8a'-(bismethyl)-3a,3a'-[1,4-phenylenebis(methyl-ene)]bis-(decahydro-3a,5a,8a,10a-tetraazapyrenium) dibromide, 8**

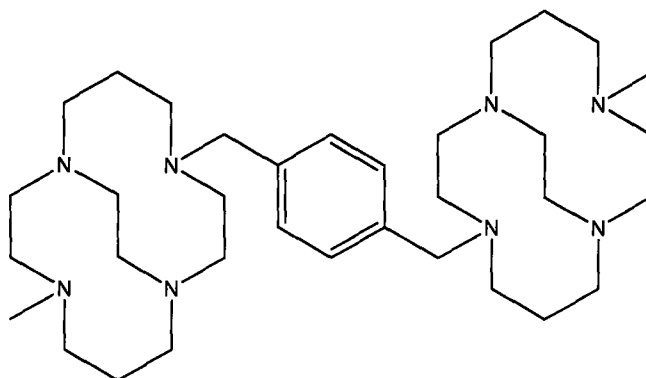


3a,3a'-[1,4-Phenylenebis(methylene)]-bis(decahydro-3a,5a,8a,10a-tetraazapyrenium) dibromide (2.60 g, 3.7 mmol) was suspended in dry acetonitrile (150 mL) under nitrogen and methyl iodide (20 mL, 320 mmol) was added dropwise. The white suspension was stirred at room temperature for 10 days. A second portion of methyl iodide (10 mL, 160 mmol) was added to the now yellow suspension after 5 days. Excess methyl iodide was removed by flowing nitrogen through the suspension for 30 minutes. The yellow solid was collected by filtration, washed with diethyl ether (200 mL) and dried *in vacuo* (3.45 g, 87%).

$^{13}\text{C}$  NMR: (DMSO- $d_6$ ) 18.28 (N- $\beta$ -CH $_2$ ), 18.59 (N- $\beta$ -CH $_2$ ), 37.95 (N- $\alpha$ -CH $_2$ ), 38.17 (N- $\alpha$ -CH $_2$ ), 38.37 (N- $\alpha$ -CH $_2$ ), 46.58 (N- $\alpha$ -CH $_2$ ), 46.64 (N- $\alpha$ -CH $_2$ ), 48.45 (N- $\alpha$ -CH $_3$ ), 51.39 (N- $\alpha$ -CH $_2$ ), 60.89 (N- $\alpha$ -CH $_2$ ), 61.52 (N- $\alpha$ -CH $_2$ ), 65.46 (N- $\alpha$ -CH $_2$ ), 76.98 ( $C_{\text{aminal}}$ ), 77.27 ( $C_{\text{aminal}}$ ), 128.29 ( $C_{\text{aromatic}}$ ), 134.57 ( $\text{CH}_{\text{aromatic}}$ ).

MS: (ESI)  $m/z$  959 [ $\text{M-I}]^+$ . HRMS: Calcd. for  $\text{C}_{34}\text{H}_{58}\text{N}_8\text{I}_3$ : 959.1913; Found 959.1914.

**8.2.10 Synthesis of 12,12'-(bismethyl)-5,5'-[1,4-phenylenebis(methyl-ene)]bis-(1,5,8,12-tetraaza-bicyclo-[6.6.2]hexadecane).7 HCl, 9**

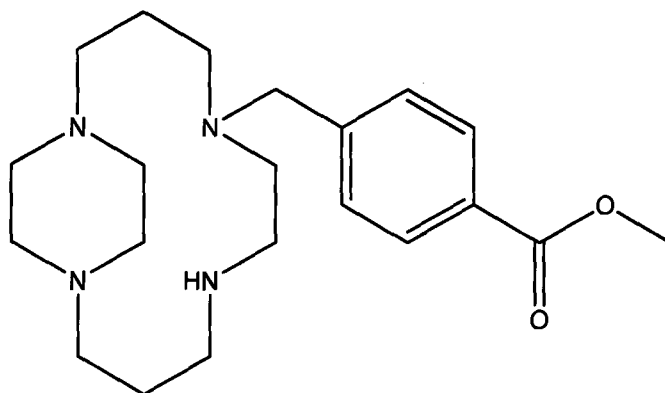


8a,8a'-(Bismethyl)-3a,3a'-[1,4-Phenylenebis(methylene)]-bis(decahydro-3a,5a,8a,10a-tetraazapyrenium) dibromide (3.03 g, 2.8 mmol) was dissolved in ethanol (150 mL) and sodium borohydride (4.25 g, 112 mmol) was added slowly. The clear solution was stirred at room temperature for 14 days and concentrated *in vacuo*. Water (100 mL) was added, the pH was adjusted to 14 (KOH pellets) and the basic solution was extracted with dichloromethane (5 x 100 mL). The combined organic fractions were dried (MgSO<sub>4</sub>), filtered and evaporated *in vacuo* to yield a clear oil. The HCl salt was prepared by bubbling HCl gas into a methanolic solution of the ligand and concentrating the yellow solution *in vacuo* to a yellow powder (1.15 g, 71%).

<sup>13</sup>C NMR: (D<sub>2</sub>O) δ 18.84 (N-β-CH<sub>2</sub>), 19.23 (N-β-CH<sub>2</sub>), 40.05 (N-α-CH<sub>3</sub>), 45.02 (N-α-CH<sub>2</sub>), 49.16 (N-α-CH<sub>2</sub>), 49.34 (N-α-CH<sub>2</sub>), 49.43 (N-α-CH<sub>2</sub>), 50.40 (N-α-CH<sub>2</sub>), 52.96 (N-α-CH<sub>2</sub>), 53.25 (N-α-CH<sub>2</sub>), 56.37 (N-α-CH<sub>2</sub>), 58.72 (N-α-CH<sub>2</sub>), 59.52 (N-α-CH<sub>2</sub>), 128.65 (C<sub>aromatic</sub>), 133.13 (CH<sub>aromatic</sub>).

MS: (ESI) *m/z* 584 [MH]<sup>+</sup>, HRMS: Calcd. for C<sub>34</sub>H<sub>63</sub>N<sub>8</sub><sup>+</sup>: 583.5170; Found 583.5180.

**8.2.11 Synthesis of 5-(4-phenylmethyl benzoate)-1,5,8,12-tetraazabicyclo[10.2.2]-hexadecane, 15**



4-(Decahydro-3a,5a,8a,10a-tetraaza-pyren-3a-ylmethyl)-benzoic acid methyl ester bromide (4.93 g, 11 mmol) was dissolved in methanol (250 mL) and cooled to 0°C. Sodium borohydride (7.40g, 200 mmol) was added slowly and the clear solution was stirred at room temperature for 3 h. The solvent was concentrated *in vacuo* and water (75 mL) was added. The pH was adjusted to 14 (KOH pellets) and the basic solution was extracted with dichloromethane (5 x 75 mL). The combined organic fractions were dried (MgSO<sub>4</sub>), filtered and evaporated *in vacuo* to yield a clear oil (2.45 g, 60%).

<sup>1</sup>H NMR: (CDCl<sub>3</sub>) δ 1.60-1.66 (p, 2H, 11.23 Hz, N-β-CH<sub>2</sub>), 1.68-1.73 (p, 2H, 10.67 Hz, N-β-CH<sub>2</sub>), 2.16-2.21 (m, 2H, N-α-CH<sub>2</sub>), 2.44-2.61 (m, 12H, N-α-CH<sub>2</sub>), 2.84-2.87 (m, 2H, N-α-CH<sub>2</sub>), 2.92-2.97 (m, 2H, N-α-CH<sub>2</sub>), 3.13-3.20 (m, 2H, N-α-CH<sub>2</sub>), 3.61 (s, 2H, N-α-CH<sub>2</sub>), 3.86 (s, 3H, O-CH<sub>3</sub>), 7.28-7.30 (d, 2H, 8.14 Hz, CH<sub>aromatic</sub>), 7.91-7.30 (d, 2H, 8.14 Hz, CH<sub>aromatic</sub>).

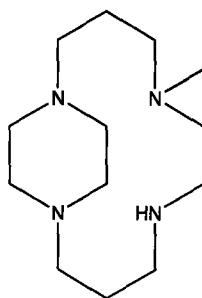
<sup>13</sup>C NMR: (CDCl<sub>3</sub>) δ 23.65 (N-β-CH<sub>2</sub>), 26.07 (N-β-CH<sub>2</sub>), 48.21 (N-α-CH<sub>2</sub>), 48.37 (N-α-CH<sub>2</sub>), 50.46 (N-α-CH<sub>2</sub>), 51.24 (N-α-CH<sub>2</sub>), 52.18 (O-CH<sub>3</sub>), 55.32 (N-α-CH<sub>2</sub>), 55.65 (N-α-CH<sub>2</sub>).

CH<sub>2</sub>), 57.03 (N- $\alpha$ -CH<sub>2</sub>), 57.77 (N- $\alpha$ -CH<sub>2</sub>), 128.97 (C<sub>aromatic</sub>), 129.33 (CH<sub>aromatic</sub>), 129.46 (CH<sub>aromatic</sub>), 144.24 (C<sub>aromatic</sub>), 167.09 (C=O).

MS: (ESI)  $m/z$  375 [MH]<sup>+</sup>. HRMS: Calcd. for C<sub>21</sub>H<sub>35</sub>N<sub>4</sub>O<sub>2</sub><sup>+</sup>: 375.2755; Found 375.2758.

## 8.2.12 Synthesis of 5-(methyl)-1,5,8,12-tetraaza-bicyclo[10.2.2]hexadecane, **21**

### (Method I)



The synthesis of **21** was carried out following a minor modification of a literature procedure.<sup>160</sup> 3a-Methyl-decahydro-3a,5a,8a,10a-tetraaza-pyrenium bromide (2.50 g, 69 mmol) was dissolved in methanol (150 mL) and cooled to 0°C. Sodium borohydride (5.24 g, 1.5 mol) was added slowly and the clear solution was stirred at room temperature for 24 h. The solvent was concentrated *in vacuo* and water (75 mL) was added. The pH was adjusted to 14 (KOH pellets) and the basic solution was extracted with dichloromethane (5 x 75 mL). The combined organic fractions were dried (MgSO<sub>4</sub>), filtered and evaporated *in vacuo* to yield a clear oil (1.33 g, 81%).

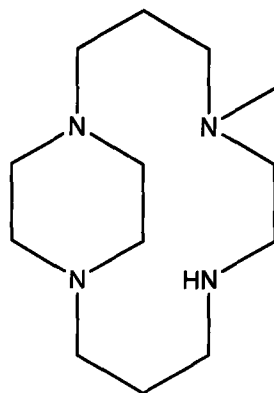
<sup>1</sup>H NMR: (CDCl<sub>3</sub>) δ 1.57-1.67 (m, 4H, N-β-CH<sub>2</sub>), 2.05 (s, 3H, N-α-CH<sub>3</sub>), 2.13-2.21 (m, 2H, N-α-CH<sub>2</sub>), 2.39-2.53 (m, 10H, N-α-CH<sub>2</sub>), 2.61-2.63 (m, 2H, N-α-CH<sub>2</sub>), 2.77-2.80 (m, 2H, N-α-CH<sub>2</sub>), 2.91-2.94 (m, 2H, N-α-CH<sub>2</sub>), 3.17-3.24 (m, 2H, N-α-CH<sub>2</sub>), 4.46 (br s, 1H, NH).

<sup>13</sup>C NMR: (CDCl<sub>3</sub>) δ 23.86 (N-β-CH<sub>2</sub>), 26.32 (N-β-CH<sub>2</sub>), 39.38 (N-α-CH<sub>3</sub>), 47.50 (N-α-CH<sub>2</sub>), 48.47 (N-α-CH<sub>2</sub>), 51.10 (N-α-CH<sub>2</sub>), 51.93 (N-α-CH<sub>2</sub>), 56.50 (N-α-CH<sub>2</sub>), 57.02 (N-α-CH<sub>2</sub>), 59.71 (N-α-CH<sub>2</sub>), 59.89 (N-α-CH<sub>2</sub>).

MS: (ESI)  $m/z$  241  $[\text{MH}]^+$ .

### 8.2.13 Synthesis of 5-(Methyl)-1,5,8,12-tetraaza-bicyclo[10.2.2]hexadecane, 21

#### (Method II)



Nickel(II) 5-(methyl)-1,5,8,12-tetraaza-bicyclo[10.2.2]hexadecane perchlorate (0.69 g, 1.39 mmol) was dissolved in a mixture of water and acetonitrile (30:5 mL). Sodium cyanide (0.27 g, 5.5 mmol) was added to the orange solution in one portion. The orange solution immediately became less intense and was heated at 80°C for 24 h. The resulting clear solution was cooled in an ice bath, filtered to remove any nickel(II) cyanide salts and the acetonitrile was removed *in vacuo*. The pH of the aqueous layer was adjusted to 14 (KOH pellets) and extracted with dichloromethane (5 x 50 mL). The combined organic fractions were dried (MgSO<sub>4</sub>), filtered and concentrated *in vacuo* to yield a yellow oil product (0.24 g, 72%).

<sup>1</sup>H NMR: (CDCl<sub>3</sub>) δ 1.57-1.67 (m, 4H, N-β-CH<sub>2</sub>), 2.05 (s, 3H, N-α-CH<sub>3</sub>), 2.13-2.21 (m, 2H, N-α-CH<sub>2</sub>), 2.39-2.53 (m, 10H, N-α-CH<sub>2</sub>), 2.61-2.63 (m, 2H, N-α-CH<sub>2</sub>), 2.77-2.80 (m, 2H, N-α-CH<sub>2</sub>), 2.91-2.94 (m, 2H, N-α-CH<sub>2</sub>), 3.17-3.24 (m, 2H, N-α-CH<sub>2</sub>), 4.46 (br s, 1H, NH).

$^{13}\text{C}$  NMR: ( $\text{CDCl}_3$ )  $\delta$  23.86 (N- $\beta$ - $\text{CH}_2$ ), 26.32 (N- $\beta$ - $\text{CH}_2$ ), 39.38 (N- $\alpha$ - $\text{CH}_3$ ), 47.50 (N- $\alpha$ - $\text{CH}_2$ ), 48.47 (N- $\alpha$ - $\text{CH}_2$ ), 51.10 (N- $\alpha$ - $\text{CH}_2$ ), 51.93 (N- $\alpha$ - $\text{CH}_2$ ), 56.50 (N- $\alpha$ - $\text{CH}_2$ ), 57.02 (N- $\alpha$ - $\text{CH}_2$ ), 59.71 (N- $\alpha$ - $\text{CH}_2$ ), 59.89 (N- $\alpha$ - $\text{CH}_2$ ).

MS: (ESI)  $m/z$  241 [ $\text{MH}^+$ ].

**8.2.13.1 Crystal data and structural refinement for 5-(methyl)-1,5,8,12-tetraaza-bicyclo[10.2.2]hexadecane, 21**

Empirical formula	C <sub>13</sub> H <sub>32</sub> N <sub>4</sub> O <sub>2</sub>	
Formula weight	276.43	
Temperature	150(2) K	
Wavelength	0.71073 Å	
Crystal system	Triclinic	
Space group	P-1	
Unit cell dimensions	a = 8.838(2) Å	α = 98.47(2)°.
	b = 8.997(2) Å	β = 93.161(19)°.
	c = 11.458(3) Å	γ = 115.029(18)°.
Volume	809.5(4) Å <sup>3</sup>	
Z	2	
Density (calculated)	1.134 Mg/m <sup>3</sup>	
Absorption coefficient	0.077 mm <sup>-1</sup>	
F(000)	308	
Crystal size	0.20 x 0.15 x 0.10 mm <sup>3</sup>	
Theta range for data collection	2.54 to 34.84°.	
Index ranges	-14 ≤ h ≤ 11, -14 ≤ k ≤ 14, -18 ≤ l ≤ 18	
Reflections collected	35577	
Independent reflections	6956 [R(int) = 0.2054]	
Completeness to theta = 34.84°	98.7 %	
Absorption correction	None	
Refinement method	Full-matrix least-squares on F <sup>2</sup>	
Data / restraints / parameters	6956 / 4 / 186	
Goodness-of-fit on F <sup>2</sup>	0.724	
Final R indices [I > 2σ(I)]	R1 = 0.0546, wR2 = 0.0913	
R indices (all data)	R1 = 0.2253, wR2 = 0.1251	
Extinction coefficient	0.022(3)	
Largest diff. peak and hole	0.266 and -0.249 e.Å <sup>-3</sup>	

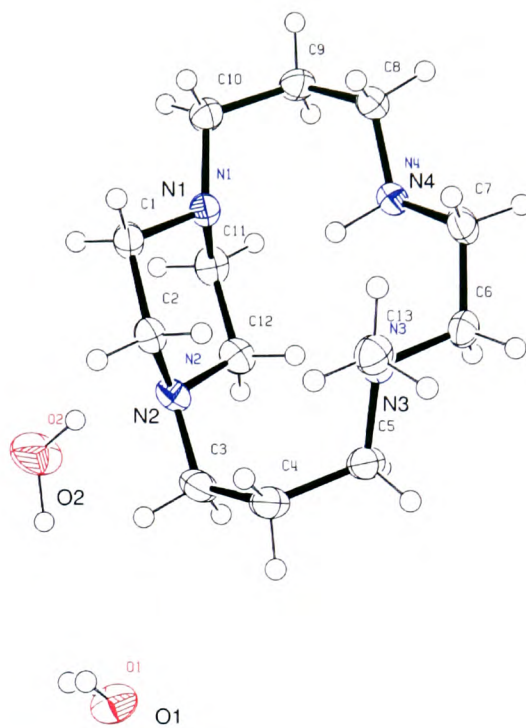


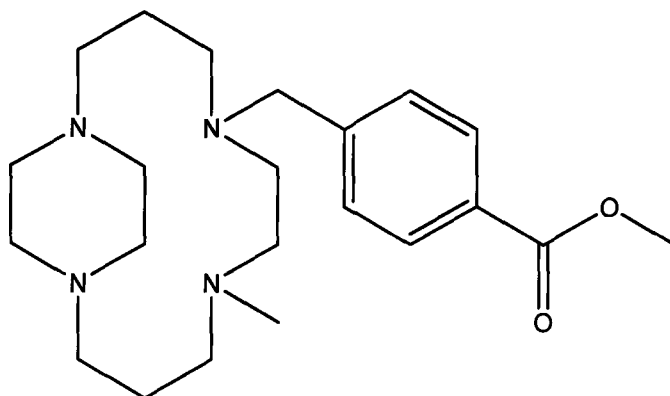
**Figure 123.** ORTEP representation of 21.2H<sub>2</sub>O.

**Table 24. Bond lengths (Å) and angles (°) for 5-(methyl)-1,5,8,12-tetraaza-bicyclo[10.2.2]hexadecane.**

N(1)-C(11)	1.455(2)	O(2)-H(3O)	1.075(18)	C(7)-C(6)-H(6A)	109.1
N(1)-C(1)	1.456(2)	O(2)-H(4O)	1.042(17)	N(3)-C(6)-H(6B)	109.1
N(1)-C(10)	1.465(3)			C(7)-C(6)-H(6B)	109.1
N(2)-C(2)	1.462(2)			H(6A)-C(6)-H(6B)	107.8
N(2)-C(12)	1.465(2)	C(11)-N(1)-C(1)	108.13(15)	N(4)-C(7)-C(6)	109.72(14)
N(2)-C(3)	1.470(3)	C(11)-N(1)-C(10)	114.65(15)	N(4)-C(7)-H(7A)	109.7
N(3)-C(13)	1.459(2)	C(1)-N(1)-C(10)	115.21(14)	C(6)-C(7)-H(7A)	109.7
N(3)-C(6)	1.471(2)	C(2)-N(2)-C(12)	113.06(15)	N(4)-C(7)-H(7B)	109.7
N(3)-C(5)	1.477(2)	C(2)-N(2)-C(3)	112.62(14)	C(6)-C(7)-H(7B)	109.7
N(4)-C(8)	1.463(2)	C(12)-N(2)-C(3)	112.37(15)	H(7A)-C(7)-H(7B)	108.2
N(4)-C(7)	1.464(2)	C(13)-N(3)-C(6)	110.03(14)	N(4)-C(8)-C(9)	111.58(15)
N(4)-H(1N)	1.0206	C(13)-N(3)-C(5)	110.96(15)	N(4)-C(8)-H(8A)	109.3
C(1)-C(2)	1.513(3)	C(6)-N(3)-C(5)	110.96(14)	C(9)-C(8)-H(8A)	109.3
C(1)-H(1A)	0.9700	C(8)-N(4)-C(7)	114.74(14)	N(4)-C(8)-H(8B)	109.3
C(1)-H(1B)	0.9700	C(8)-N(4)-H(1N)	107.9	C(9)-C(8)-H(8B)	109.3
C(2)-H(2A)	0.9700	C(7)-N(4)-H(1N)	105.9	H(8A)-C(8)-H(8B)	108.0
C(2)-H(2B)	0.9700	N(1)-C(1)-C(2)	107.79(14)	C(8)-C(9)-C(10)	114.18(16)
C(3)-C(4)	1.549(3)	N(1)-C(1)-H(1A)	110.1	C(8)-C(9)-H(9A)	108.7
C(3)-H(3A)	0.9700	C(2)-C(1)-H(1A)	110.1	C(10)-C(9)-H(9A)	108.7
C(3)-H(3B)	0.9700	N(1)-C(1)-H(1B)	110.1	C(8)-C(9)-H(9B)	108.7
C(4)-C(5)	1.530(3)	C(2)-C(1)-H(1B)	110.1	C(10)-C(9)-H(9B)	108.7
C(4)-H(4A)	0.9700	H(1A)-C(1)-H(1B)	108.5	H(9A)-C(9)-H(9B)	107.6
C(4)-H(4B)	0.9700	N(2)-C(2)-C(1)	112.44(15)	N(1)-C(10)-C(9)	111.97(15)
C(5)-H(5A)	0.9700	N(2)-C(2)-H(2A)	109.1	N(1)-C(10)-H(10A)	109.2
C(5)-H(5B)	0.9700	C(1)-C(2)-H(2A)	109.1	C(9)-C(10)-H(10A)	109.2
C(6)-C(7)	1.516(3)	N(2)-C(2)-H(2B)	109.1	N(1)-C(10)-H(10B)	109.2
C(6)-H(6A)	0.9700	C(1)-C(2)-H(2B)	109.1	C(9)-C(10)-H(10B)	109.2
C(6)-H(6B)	0.9700	H(2A)-C(2)-H(2B)	107.8	H(10A)-C(10)-H(10B)	107.9
C(7)-H(7A)	0.9700	N(2)-C(3)-C(4)	120.61(16)	N(1)-C(11)-C(12)	108.45(14)
C(7)-H(7B)	0.9700	N(2)-C(3)-H(3A)	107.2	N(1)-C(11)-H(11A)	110.0
C(8)-C(9)	1.527(3)	C(4)-C(3)-H(3A)	107.2	C(12)-C(11)-H(11A)	110.0
C(8)-H(8A)	0.9700	N(2)-C(3)-H(3B)	107.2	N(1)-C(11)-H(11B)	110.0
C(8)-H(8B)	0.9700	C(4)-C(3)-H(3B)	107.2	C(12)-C(11)-H(11B)	110.0

C(9)-C(10)	1.530(3)	H(3A)-C(3)-H(3B)	106.8	H(11A)-C(11)-H(11B)	108.4
C(9)-H(9A)	0.9700	C(5)-C(4)-C(3)	119.40(16)	N(2)-C(12)-C(11)	111.19(15)
C(9)-H(9B)	0.9700	C(5)-C(4)-H(4A)	107.5	N(2)-C(12)-H(12A)	109.4
C(10)-H(10A)	0.9700	C(3)-C(4)-H(4A)	107.5	C(11)-C(12)-H(12A)	109.4
C(10)-H(10B)	0.9700	C(5)-C(4)-H(4B)	107.5	N(2)-C(12)-H(12B)	109.4
C(11)-C(12)	1.505(3)	C(3)-C(4)-H(4B)	107.5	C(11)-C(12)-H(12B)	109.4
C(11)-H(11A)	0.9700	H(4A)-C(4)-H(4B)	107.0	H(12A)-C(12)-H(12B)	108.0
C(11)-H(11B)	0.9700	N(3)-C(5)-C(4)	114.68(15)	N(3)-C(13)-H(13A)	109.5
C(12)-H(12A)	0.9700	N(3)-C(5)-H(5A)	108.6	N(3)-C(13)-H(13B)	109.5
C(12)-H(12B)	0.9700	C(4)-C(5)-H(5A)	108.6	H(13A)-C(13)-H(13B)	109.5
C(13)-H(13A)	0.9600	N(3)-C(5)-H(5B)	108.6	N(3)-C(13)-H(13C)	109.5
C(13)-H(13B)	0.9600	C(4)-C(5)-H(5B)	108.6	H(13A)-C(13)-H(13C)	109.5
C(13)-H(13C)	0.9600	H(5A)-C(5)-H(5B)	107.6	H(13B)-C(13)-H(13C)	109.5
O(1)-H(1O)	1.060(15)	N(3)-C(6)-C(7)	112.45(15)	H(1O)-O(1)-H(2O)	106.9(17)
O(1)-H(2O)	1.075(16)	N(3)-C(6)-H(6A)	109.1	H(3O)-O(2)-H(4O)	121(2)

**8.2.14 Synthesis of 5-(phenylmethyl benzoate)-8-methyl-1,5,8,12-tetra-aza-bicyclo-[10.2.2]hexadecane, 16**



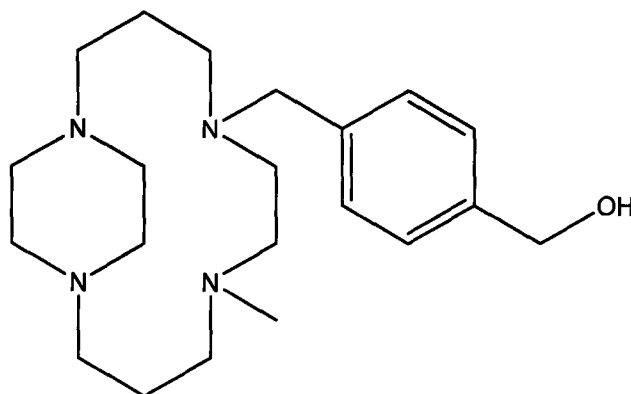
Nickel(II)-5-(phenylmethyl-benzoate)-8-methyl-1,5,8,12-tetraaza-bicyclo[10.2.2]-hexadecane perchlorate (62 mg, 0.10 mmol) was dissolved in acetonitrile (15 mL) and a solution of sodium cyanide (24 mg, 0.49 mmol) in water (1 mL) was added. The mixture was heated to reflux for 2 h and a purple colour developed in the solution after a few minutes. The purple solution changed colour to give an orange solution which was concentrated *in vacuo* to give an orange solid. The crude product was placed in a paper thimble and purified using a soxhlet apparatus with DCM. The remaining solid was dissolved in water (10 mL) and extracted into DCM (5 x 10 mL). The combined organic fractions were dried (MgSO<sub>4</sub>), filtered and evaporated *in vacuo* to yield a yellow oil (21 mg, 54%).

<sup>1</sup>H NMR: (CDCl<sub>3</sub>) δ 1.56-1.75 (m, 4H, N-β-CH<sub>2</sub>), 2.01-2.17 (m, 2H, N-α-CH<sub>2</sub>), 2.48-2.84 (m, 15H, N-α-CH<sub>2</sub> and N-α-CH<sub>3</sub>), 2.85-2.87 (m, 2H, N-α-CH<sub>2</sub>), 2.89-2.97 (m, 2H, N-α-CH<sub>2</sub>), 2.99-3.08 (m, 2H, N-α-CH<sub>2</sub>), 3.69 (s, 2H, N-α-CH<sub>2</sub>), 3.84 (s, 3H, O-CH<sub>3</sub>), 7.44-7.52 (d, 2H, 8.72 Hz, CH<sub>aromatic</sub>), 7.81-7.96 (d, 2H, 8.72 Hz, CH<sub>aromatic</sub>).

$^{13}\text{C}$  NMR: ( $\text{CDCl}_3$ )  $\delta$  23.21 (N- $\beta$ - $\text{CH}_2$ ), 24.75 (N- $\beta$ - $\text{CH}_2$ ), 31.12 (N- $\alpha$ - $\text{CH}_3$ ), 47.16 (N- $\alpha$ - $\text{CH}_2$ ), 48.31 (N- $\alpha$ - $\text{CH}_2$ ), 49.98 (N- $\alpha$ - $\text{CH}_2$ ), 50.02 (N- $\alpha$ - $\text{CH}_2$ ), 51.98 (O- $\text{CH}_3$ ), 55.64 (N- $\alpha$ - $\text{CH}_2$ ), 55.81 (N- $\alpha$ - $\text{CH}_2$ ), 55.97 (N- $\alpha$ - $\text{CH}_2$ ), 57.00 (N- $\alpha$ - $\text{CH}_2$ ), 128.90 ( $\text{C}_{\text{aromatic}}$ ), 129.79 ( $\text{CH}_{\text{aromatic}}$ ), 130.41 ( $\text{CH}_{\text{aromatic}}$ ), 141.92 ( $\text{C}_{\text{aromatic}}$ ), 167.39 (C=O).

MS: (ESI)  $m/z$  389  $[\text{MH}]^+$ . HRMS: Calcd. for  $\text{C}_{22}\text{H}_{37}\text{N}_4\text{O}_2^+$ : 389.2911 ; Found 389.2917.

**8.2.15 Synthesis of 5-(4-phenylmethyl methyl alcohol)-8-methyl-1,5,8,12-tetraaza-bicyclo[10.2.2]hexadecane, 17**



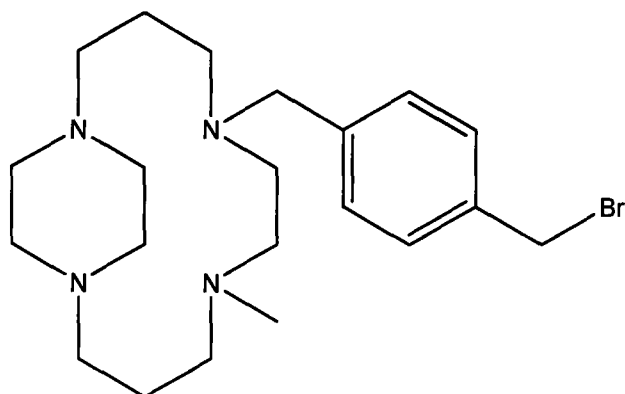
Lithium aluminium hydride (156 mg, 4.11 mmol) was added to a solution of 5-(phenylmethyl benzoate)-8-methyl-1,5,8,12-tetraaza-bicyclo[10.2.2]hexadecane (80 mg, 0.21 mmol) in dry THF (20 mL) under nitrogen and the mixture was stirred at room temperature for 48 h. Methanol (~ 5 mL) followed by water (~ 10 mL) was added dropwise and the solution was concentrated in vacuo. The crude solid was dissolved in water (15 mL) and then extracted with dichloromethane (5 x 20 mL). The pH was adjusted to 14 (NaOH pellets) and re-extracted with dichloromethane (5 x 20 mL). The combined organic fractions were dried (MgSO<sub>4</sub>), filtered and evaporated in vacuo to yield an orange oil (56 mg, 76%).

<sup>1</sup>H NMR: (CD<sub>2</sub>Cl<sub>2</sub>) δ 1.56-1.60 (m, 4H, N-β-CH<sub>2</sub>), 2.08-2.10 (m, 4H, N-α-CH<sub>2</sub>), 2.24-2.60 (m, 12H, N-α-CH<sub>2</sub>), 2.88-2.91 (m, 4H, N-α-CH<sub>2</sub>), 3.07-3.09 (m, 4H, N-α-CH<sub>2</sub>), 3.49-3.50 (br s, 2H, N-α-CH<sub>2</sub>), 4.53-4.54 (s, 2H, ArCH<sub>2</sub>OH), 7.09-7.11 (d, 2H, J = 7.82 Hz, CH<sub>aromatic</sub>), 7.16-7.19 (d, 2H, J = 7.82 Hz, CH<sub>aromatic</sub>)

$^{13}\text{C}$  NMR: ( $\text{CD}_2\text{Cl}_2$ )  $\delta$  23.88 (N- $\beta$ - $\text{CH}_2$ ), 26.32 (N- $\beta$ - $\text{CH}_2$ ), 30.07 (N- $\alpha$ - $\text{CH}_3$ ), 48.08 (N- $\alpha$ - $\text{CH}_2$ ), 48.50 (N- $\alpha$ - $\text{CH}_2$ ), 50.70 (N- $\alpha$ - $\text{CH}_2$ ), 51.34 (N- $\alpha$ - $\text{CH}_2$ ), 54.19 (N- $\alpha$ - $\text{CH}_2$ ), 54.28 (N- $\alpha$ - $\text{CH}_2$ ), 54.34 (N- $\alpha$ - $\text{CH}_2$ ), 54.77 (N- $\alpha$ - $\text{CH}_2$ ), 55.44 (N- $\alpha$ - $\text{CH}_2$ ), 56.30 (N- $\alpha$ - $\text{CH}_2$ ), 57.18 (N- $\alpha$ - $\text{CH}_2$ ), 64.75 (N- $\alpha$ - $\text{CH}_2$ ), 126.80 ( $\text{CH}_{\text{aromatic}}$ ), 129.35 ( $\text{C}_{\text{aromatic}}$ ), 129.99 ( $\text{CH}_{\text{aromatic}}$ ), 141.12 ( $\text{C}_{\text{aromatic}}$ ).

MS: (ESI)  $m/z$  361  $[\text{MH}]^+$ . HRMS: Calcd. for  $\text{C}_{21}\text{H}_{37}\text{N}_4\text{O}^+$ : 361.2962; Found 361.2963.

**8.2.16 Synthesis of 5-(4-phenylmethyl benzyl bromide)-8-methyl-1,5,8,12-tetraaza-bicyclo[10.2.2]hexadecane, 10**

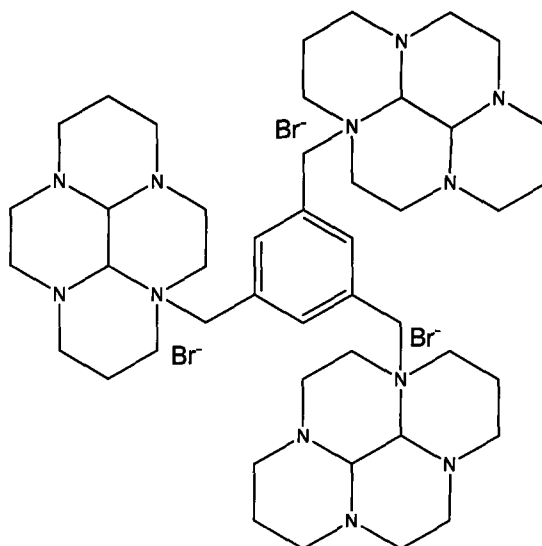


5-(4-Phenylmethyl methyl alcohol)-8-methyl-1,5,8,12-tetraaza-bicyclo[10.2.2]-hexadecane (40 mg, 0.11 mmol) was dissolved in dry pyridine (10 mL) and phosphorus tribromide (8  $\mu$ L, 0.04 mmol) was added in one portion and the orange solution was stirred at room temperature for 4 days. Water (10 mL) was added and the pH adjusted to 14 (NaOH pellets) and the basic solution was extracted with dichloromethane (5 x 10 mL). The combined organic extracts were dried ( $MgSO_4$ ), filtered and evaporated to an orange oil (23 mg, 49%).

$^1H$  and  $^{13}C$  NMR spectra were recorded but not fully characterised due to multiple overlapping signals in the aliphatic region. However, a pair of doublets indicating a 1,4-system was observed in the aromatic region.

MS: (ESI)  $m/z$  361  $[MH]^+$ .

**8.2.17 Synthesis of 3a,3a'3a''-[1,3,5-phenylenetrakis(methylene)]-tris-(decahydro-3a,5a,8a,10a-tetraazapyrenium) tribromide, 7**



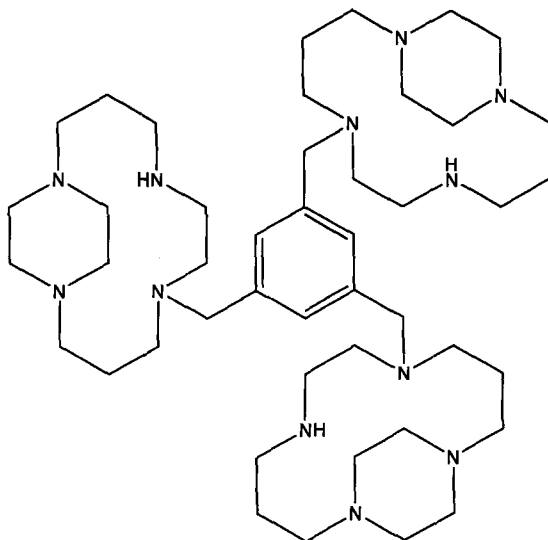
Decahydro-3a,5a,8a,10a-tetraaza-pyrene (3.37 g, 15 mmol) and 1,3,5-tris(bromomethyl)benzene (provided by Dr Steve Archibald) (1.93 g, 5.42 mmol) were dissolved in dry acetonitrile (50 mL) and stirred under nitrogen at room temperature for 5 days. A white precipitate was collected by filtration, washed with acetonitrile (50 mL) followed by diethyl ether (10 x 25 mL) and dried *in vacuo* to yield a white powder (4.63 g, 90%).

$^1\text{H}$  NMR: ( $\text{D}_2\text{O}$ )  $\delta$  1.40-1.43 (m, 3H), 1.75-1.78 (m, 3H), 2.16-2.20 (m, 6H), 2.29-2.34 (m, 2H), 2.42-2.48 (m, 7H), 2.63-2.69 (m, 3H), 2.96-3.10 (m, 24H), 3.19-3.33 (m, 4H), 3.43-3.52 (m, 4H), 3.52-3.60 (m, 2H), 3.66-3.69 (m, 4H), 4.19-4.25 (m, 3H), 4.36-4.37 (m, 3H), 4.90-4.95 (m, 2H), 5.19-5.30 (m, 2H), 7.81-7.83 (br s, 3H,  $\text{CH}_{\text{aromatic}}$ ).

$^{13}\text{C}$  NMR: ( $\text{D}_2\text{O}$ )  $\delta$  18.16 (N- $\beta$ - $\text{CH}_2$ ), 18.63 (N- $\beta$ - $\text{CH}_2$ ), 42.10 (N- $\alpha$ - $\text{CH}_2$ ), 46.74 (N- $\alpha$ - $\text{CH}_2$ ), 51.56 (N- $\alpha$ - $\text{CH}_2$ ), 52.05 (N- $\alpha$ - $\text{CH}_2$ ), 53.48 (N- $\alpha$ - $\text{CH}_2$ ), 54.03 (N- $\alpha$ - $\text{CH}_2$ ), 54.12 (N- $\alpha$ - $\text{CH}_2$ ), 60.15 (N- $\alpha$ - $\text{CH}_2$ ), 61.18 (N- $\alpha$ - $\text{CH}_2$ ), 69.64 ( $\text{CH}_{\text{aminal}}$ ), 82.53 ( $\text{CH}_{\text{aminal}}$ ), 128.88 ( $\text{CH}_{\text{aromatic}}$ ), 140.36 ( $\text{C}_{\text{aromatic}}$ ).

MS: (ESI)  $m/z$  261  $[\text{M}]^{3+}$ . HRMS: Calcd. for  $\text{C}_{45}\text{H}_{75}\text{N}_{12}^{3+}$ : 261.2074; Found 261.2076.

**8.2.18 Synthesis of 12,12',12''-(trismethyl)-5,5',5''-[1,3,5-phenylenetris-(methylene)]-tris(1,5,8,12-tetraaza-bicyclo-[6.6.2]hexadecane), 6**



3a,3a'3a''-[1,3,5-Phenylenetris(methylene)]-tris(decahydro-3a,5a,8a,10a-tetraazapyrenium) tribromide (4.63 g, 4.53 mmol) was dissolved in methanol (150 mL) and cooled to 0°C. Sodium borohydride (10.33 g, 272 mmol) was added slowly and the clear solution was stirred under nitrogen at room temperature for 4 h. The solution was concentrated *in vacuo* and water (100 mL) was added. The pH was adjusted to 14 (KOH pellets) and the basic solution was extracted from dichloromethane (5 x 100 mL). The combined organic fractions were dried (MgSO<sub>4</sub>), filtered and evaporated *in vacuo* to yield a yellow solid (2.78 g, 77%).

<sup>13</sup>C NMR: (CDCl<sub>3</sub>) δ 21.81 (N-β-CH<sub>2</sub>), 22.03 (N-β-CH<sub>2</sub>), 44.68 (N-α-CH<sub>2</sub>), 46.17 (N-β-CH<sub>2</sub>), 47.72 (N-β-CH<sub>2</sub>), 49.30 (N-β-CH<sub>2</sub>), 50.76 (N-β-CH<sub>2</sub>), 54.07 (N-β-CH<sub>2</sub>), 54.27 (N-β-CH<sub>2</sub>), 55.96 (N-β-CH<sub>2</sub>), 56.57 (N-β-CH<sub>2</sub>), 57.23 (N-β-CH<sub>2</sub>), 59.12 (N-β-CH<sub>2</sub>), 129.60 (CH<sub>aromatic</sub>), 130.50 (C<sub>aromatic</sub>).

MS: (ESI)  $m/z$  794  $[MH]^+$ . HRMS: Calcd. for  $C_{45}H_{85}N_{12}^+$ : 793.6942; Found 793.6937.

## 8.3 Synthesis of Transition Metal Complexes

### 8.3.1 General Complexation Procedure

The appropriate ligand (~ 200 mg) was dissolved in methanol (10 mL) and a solution of metal salt (1.1 molar equivalents per macrocycle) in methanol (10 mL) was added dropwise. The mixtures were stirred at room temperature for 3 h and then at reflux for 2 h. The complexes either remained in solution or precipitated out. The solutions were concentrated *in vacuo*, redissolved in a minimum volume of methanol and purified by size exclusion chromatography (Sephadex LH20). Alternatively, the precipitates were collected by filtration, washed with methanol (5 x 20 mL) followed by diethyl ether (2 x 20 mL) and dried *in vacuo*.

#### 8.3.1.1 Size Exclusion Chromatography

Size exclusion chromatography allows the separation of compounds based on molecular weight. For example, high molecular weight metal complexes will run quickly whereas low molecular weight metal salts will run slowly, if at all. Sephadex (LH20) was soaked in methanol for at least 3 h before being used in order for it to swell to its optimum size.

Purification was carried out in two steps. Firstly, a small column in a Pasteur pipette fitted with glass wool was run with methanol eluent to remove the majority of the excess metal salt. Secondly, a column of approximately 15 cm (height) by 1 cm (diameter) was run with methanol eluent to remove trace metal salt. Individually coloured bands were collected and concentrated *in vacuo* to give pure metal complex.

### 8.3.2 Synthesis of $[\text{Zn}_2\mathbf{5}(\text{OAc})_2](\text{OAc})_2$

Ligand **5** (48.3 mg, 0.87 mmol), zinc(II) acetate (0.351 g, 1.91 mmol). The crude product was purified by size exclusion chromatography (Sephadex LH20). The clear oil was triturated with diethyl ether (2 x 20 mL) to give a white crystalline powder (76.9 mg, 77%).

$^1\text{H}$  NMR: (800 MHz, 90%  $\text{H}_2\text{O}$  / 10%  $\text{D}_2\text{O}$ )  $\delta$  1.64 (d,  $J = 16.0$  Hz, 1H, N- $\beta$ - $\text{CH}_2$ ), 1.85 (d,  $J = 16.0$  Hz, 1H, N- $\beta$ - $\text{CH}_2$ ), 2.01 (m, 1H, N- $\beta$ - $\text{CH}_2$ ), 2.14 (m, 1H, N- $\beta$ - $\text{CH}_2$ ), 2.31 (m, 1H, N- $\alpha$ - $\text{CH}_2$ ), 2.39 (m, 1H, N- $\alpha$ - $\text{CH}_2$ ), 2.55 (m, 1H, N- $\alpha$ - $\text{CH}_2$ ), 2.58 (m, 1H, N- $\alpha$ - $\text{CH}_2$ ), 2.60 (m, 1H, N- $\alpha$ - $\text{CH}_2$ ), 2.62 (m, 1H, N- $\alpha$ - $\text{CH}_2$ ), 2.69 (m, 2H, N- $\alpha$ - $\text{CH}_2$ ), 2.86 (m, 1H, N- $\alpha$ - $\text{CH}_2$ ), 2.92 (m, 1H, N- $\alpha$ - $\text{CH}_2$ ), 2.98 (m, 1H, N- $\alpha$ - $\text{CH}_2$ ), 3.04 (m, 1H, N- $\alpha$ - $\text{CH}_2$ ), 3.09 (m, 1H, N- $\alpha$ - $\text{CH}_2$ ), 3.10 (m, 1H, N- $\alpha$ - $\text{CH}_2$ ), 3.11 (m, 1H, N- $\alpha$ - $\text{CH}_2$ ), 3.18 (m, 1H, N- $\alpha$ - $\text{CH}_2$ ), 3.19 (m, 1H, N- $\alpha$ - $\text{CH}_2$ ), 3.35 (m, 1H, N- $\alpha$ - $\text{CH}_2$ ), 3.46 (m, 1H, N- $\alpha$ - $\text{CH}_2$ ), 3.60 (m, 1H, N- $\alpha$ - $\text{CH}_2$ ), 3.89 (d,  $J = 14.5$  Hz, 1H, N- $\alpha$ - $\text{CH}_2\text{Ar}$ ), 4.04 (m, 1H, NH), 4.17 (d,  $J = 14.5$  Hz, 1H, N- $\alpha$ - $\text{CH}_2\text{Ar}$ ), 7.36 (s, 4H,  $\text{CH}_{\text{aromatic}}$ ).

$^{13}\text{C}(^1\text{H})$  NMR: (200 MHz, 90%  $\text{H}_2\text{O}$  / 10%  $\text{D}_2\text{O}$ )  $\delta$  23.40 (N- $\beta$ - $\text{CH}_2$ ), 26.82 (N- $\beta$ - $\text{CH}_2$ ), 45.99 (N- $\alpha$ - $\text{CH}_2$ ), 47.07 (N- $\alpha$ - $\text{CH}_2$ ), 50.88 (N- $\alpha$ - $\text{CH}_2$ ), 51.97 (N- $\alpha$ - $\text{CH}_2$ ), 54.01 (N- $\alpha$ - $\text{CH}_2$ ), 54.66 (N- $\alpha$ - $\text{CH}_2$ ), 54.84 (N- $\alpha$ - $\text{CH}_2$ ), 58.43 (N- $\alpha$ - $\text{CH}_2\text{Ar}$ ), 59.18 (N- $\alpha$ - $\text{CH}_2$ ), 60.55 (N- $\alpha$ - $\text{CH}_2$ ), 132.30 ( $\text{C}_{\text{aromatic}}$ ), 134.70 ( $\text{CH}_{\text{aromatic}}$ ).

MS: (ESI)  $m/z$ : 399  $[\text{M}-(\text{OAc})_2-2\text{H}]^{2+}$ . HRMS: Calcd. for  $\text{C}_{36}\text{H}_{62}\text{N}_8\text{O}_4\text{Zn}_2^{2+}$ : 399.1739; Found 399.1738.

Elemental analysis: (%) Calcd. for  $C_{40}H_{70}N_8O_8Zn_2 \cdot Et_2O \cdot 0.5H_2O$ : C 48.66, H 8.35, N 10.32; Found C 49.00, H 8.07, N 10.07.

### 8.3.2.1 Crystal data and structure refinement for $[\text{Zn}_2\text{5}(\text{OAc})_2]^{2+}$

Empirical formula	$\text{C}_{40} \text{H}_{64} \text{N}_8 \text{O}_{21.30} \text{Zn}_2$	
Formula weight	1128.53	
Temperature	150(2) K	
Wavelength	0.71073 Å	
Crystal system	monoclinic	
Space group	P21/n	
Unit cell dimensions	$a = 12.0978(11) \text{ Å}$ $b = 14.6141(9) \text{ Å}$ $c = 16.4562(14) \text{ Å}$	$\alpha = 90^\circ$ $\beta = 107.824(7)^\circ$ $\gamma = 90^\circ$
Volume	$2769.8(4) \text{ Å}^3$	
Z	2	
Density (calculated)	$1.353 \text{ Mg/m}^3$	
Absorption coefficient	$0.944 \text{ mm}^{-1}$	
F(000)	1181	
Crystal size	$0.15 \times 0.20 \times 0.25 \text{ mm}^3$	
Theta range for data collection	2.60 to $34.78^\circ$ .	
Index ranges	$-19 \leq h \leq 19$ , $-19 \leq k \leq 23$ , $-26 \leq l \leq 21$	
Reflections collected	40408	
Independent reflections	11834 [R(int) = 0.0669]	
Completeness to $\theta = 34.78^\circ$	98.6 %	
Refinement method	Full-matrix least-squares on $F^2$	
Data / restraints / parameters	11834 / 6 / 336	
Goodness-of-fit on $F^2$	0.942	
Final R indices [ $I > 2\sigma(I)$ ]	$R1 = 0.0753$ , $wR2 = 0.2032$	
R indices (all data)	$R1 = 0.1425$ , $wR2 = 0.2293$	
Largest diff. peak and hole	1.120 and $-1.641 \text{ e.Å}^{-3}$	

Crystals were grown via slow evaporation of a methanolic solution.

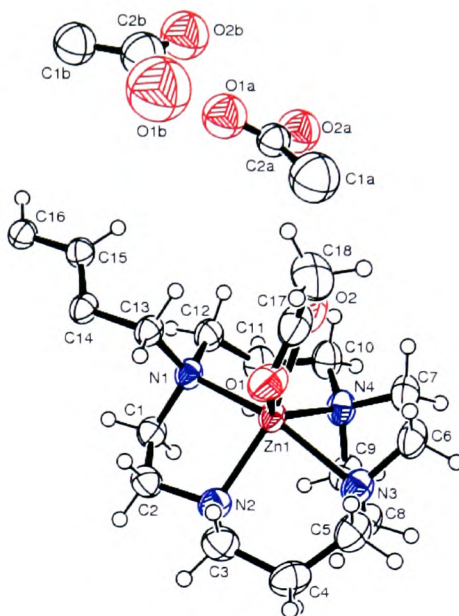


**Figure 124. ORTEP representation of [Zn<sub>25</sub>(OAc)<sub>2</sub>]<sup>2+</sup>. Symmetry transformations used to generate equivalent atoms: -x,-y+1,-z.**

**Table 25. Bond lengths (Å) and angles (°) for [Zn<sub>2</sub>5(OAc)<sub>2</sub>]<sup>2+</sup>.**

Zn(1)-N(4)	2.091(3)	C(1B)-C(2B)	1.503(12)	C(3)-N(2)-C(2)	114.2(3)
Zn(1)-N(2)	2.106(3)	C(2B)-O(2B)	1.193(12)	C(3)-N(2)-Zn(1)	111.9(2)
Zn(1)-O(1)	2.112(3)	C(2B)-O(1B)	1.313(13)	C(2)-N(2)-Zn(1)	105.0(2)
Zn(1)-N(1)	2.166(2)			C(17)-O(1)-Zn(1)	98.5(3)
Zn(1)-N(3)	2.228(3)			N(1)-C(13)-C(14)	115.0(2)
Zn(1)-O(2)	2.407(4)	N(4)-Zn(1)-N(2)	117.91(12)	N(3)-C(5)-C(4)	113.4(3)
N(1)-C(1)	1.483(4)	N(4)-Zn(1)-O(1)	133.57(12)	C(14)#1-C(16)-C(15)	120.9(3)
N(1)-C(12)	1.502(5)	N(2)-Zn(1)-O(1)	102.38(13)	C(9)-N(4)-C(10)	112.7(3)
N(1)-C(13)	1.505(4)	N(4)-Zn(1)-N(1)	100.10(11)	C(9)-N(4)-C(7)	107.0(3)
C(15)-C(14)	1.393(5)	N(2)-Zn(1)-N(1)	84.86(11)	C(10)-N(4)-C(7)	110.4(3)
C(15)-C(16)	1.395(4)	O(1)-Zn(1)-N(1)	105.82(11)	C(9)-N(4)-Zn(1)	104.0(2)
N(3)-C(5)	1.454(5)	N(4)-Zn(1)-N(3)	69.44(12)	C(10)-N(4)-Zn(1)	116.2(2)
N(3)-C(6)	1.464(5)	N(2)-Zn(1)-N(3)	83.85(12)	C(7)-N(4)-Zn(1)	105.9(2)
N(3)-C(8)	1.489(4)	O(1)-Zn(1)-N(3)	94.58(11)	C(16)#1-C(14)-C(15)	118.1(3)
C(1)-C(2)	1.502(5)	N(1)-Zn(1)-N(3)	158.40(10)	C(16)#1-C(14)-C(13)	120.7(3)
C(8)-C(9)	1.548(5)	N(4)-Zn(1)-O(2)	85.97(13)	C(15)-C(14)-C(13)	121.3(3)
N(2)-C(3)	1.481(5)	N(2)-Zn(1)-O(2)	156.11(13)	N(1)-C(12)-C(11)	116.0(3)
N(2)-C(2)	1.489(4)	O(1)-Zn(1)-O(2)	56.31(14)	C(17)-O(2)-Zn(1)	85.1(3)
O(1)-C(17)	1.250(6)	N(1)-Zn(1)-O(2)	90.74(11)	N(2)-C(3)-C(4)	112.4(3)
C(13)-C(14)	1.520(4)	N(3)-Zn(1)-O(2)	106.79(12)	N(4)-C(9)-C(8)	108.5(3)
C(5)-C(4)	1.522(6)	C(1)-N(1)-C(12)	111.7(2)	N(4)-C(10)-C(11)	112.5(3)
C(16)-C(14)#1	1.391(5)	C(1)-N(1)-C(13)	110.8(3)	N(2)-C(2)-C(1)	108.5(3)
N(4)-C(9)	1.475(5)	C(12)-N(1)-C(13)	109.1(3)	C(12)-C(11)-C(10)	114.8(3)
N(4)-C(10)	1.482(5)	C(1)-N(1)-Zn(1)	102.27(19)	O(2)-C(17)-O(1)	119.9(4)
N(4)-C(7)	1.490(4)	C(12)-N(1)-Zn(1)	112.7(2)	O(2)-C(17)-C(18)	119.4(5)
C(14)-C(16)#1	1.391(5)	C(13)-N(1)-Zn(1)	110.13(17)	O(1)-C(17)-C(18)	120.6(5)
C(12)-C(11)	1.521(6)	C(14)-C(15)-C(16)	121.0(3)	N(3)-C(6)-C(7)	107.1(3)
O(2)-C(17)	1.232(7)	C(5)-N(3)-C(6)	113.5(3)	N(4)-C(7)-C(6)	107.6(3)
C(3)-C(4)	1.530(6)	C(5)-N(3)-C(8)	114.3(3)	C(5)-C(4)-C(3)	117.0(3)
C(10)-C(11)	1.528(5)	C(6)-N(3)-C(8)	106.8(3)	O(2A)-C(2A)-O(1A)	125.2(14)
C(17)-C(18)	1.507(5)	C(5)-N(3)-Zn(1)	114.9(2)	O(2A)-C(2A)-C(1A)	116.2(14)
C(6)-C(7)	1.570(6)	C(6)-N(3)-Zn(1)	99.4(2)	O(1A)-C(2A)-C(1A)	117.5(15)
C(1A)-C(2A)	1.568(16)	C(8)-N(3)-Zn(1)	106.6(2)	O(2B)-C(2B)-O(1B)	115.7(12)
C(2A)-O(2A)	1.185(13)	N(1)-C(1)-C(2)	110.3(2)	O(2B)-C(2B)-C(1B)	125.4(11)
C(2A)-O(1A)	1.186(14)	N(3)-C(8)-C(9)	106.7(3)	O(1B)-C(2B)-C(1B)	118.9(11)

### 8.3.3 Synthesis of $[\text{Zn}_2\mathbf{5}\text{Cl}_2](\text{PF}_6)_2$

Ligand **5** (198 mg, 0.36 mmol), anhydrous zinc(II) chloride (97 mg, 0.72 mmol). The white product was collected by filtration (169 mg, 57%).

To a solution of  $[\text{Zn}_2\mathbf{5}\text{Cl}_2]\text{Cl}_2$  (50 mg, 0.06 mmol) in ethanol (20 mL) was added a solution of ammonium hexafluorophosphate (23 mg, 0.14 mmol) in ethanol (5 mL). After stirring at room temperature for 10 minutes the white precipitate was collected by filtration, washed with ethanol (5 x 10 mL) followed by diethyl ether (5 x 10 mL) and dried *in vacuo* to yield a white solid (53 mg, 84%).

MS: (ESI)  $m/z$  376  $[(\text{M}-(\text{PF}_6)_2)^{2+}]$ , 897  $[\text{M}-(\text{PF}_6)]^+$ . HRMS: Calcd. for  $\text{C}_{32}\text{H}_{58}\text{N}_8\text{Cl}_2\text{Zn}_2^{2+}$ : 376.1367; Found 376.1373.

### 8.3.4 Synthesis of $[\text{Zn}_2\mathbf{5}](\text{ClO}_4)_4$

Ligand **5** (198 mg, 0.36 mmol), zinc(II) perchlorate hexahydrate (190 mg, 0.72 mmol), 213 mg, 55%.

MS: (ESI)  $m/z$  779  $[\text{M}-2\text{H}-(\text{ClO}_4)_3]^+$ . HRMS: Calcd. for  $\text{C}_{32}\text{H}_{56}\text{N}_8\text{ClO}_4\text{Zn}_2^+$ : 777.2696; Found 777.2694.

### 8.3.5 Synthesis of $[\text{Cu}_2\mathbf{5}(\text{OAc})_2](\text{OAc})_2$

Ligand **5** (193 mg, 0.35 mmol), copper(II) acetate monohydrate (139 mg, 0.75 mmol). The blue solution was concentrated *in vacuo* and purified by size exclusion chromatography (Sephadex LH20). The resulting solvent was evaporated *in vacuo* to yield a blue crystalline solid (265 mg, 83%).

MS: (ESI)  $m/z$  857  $[M-(OAc)]^+$ . HRMS: Calcd. for  $C_{32}H_{58}N_8(OAc)_3Cu_2^+$ : 857.3770; Found 857.3769.

UV-vis: (H<sub>2</sub>O)  $\lambda_{max}$  562 nm,  $\epsilon$  478 M<sup>-1</sup> cm<sup>-1</sup>.

### 8.3.6 Synthesis of $[Cu_25](ClO_4)_4$

Ligand **5** (198 mg, 0.36 mmol), copper(II) perchlorate hexahydrate (290 mg, 0.78 mmol). A blue solution was observed immediately which developed into a purple precipitate after a few minutes. The purple product was collected by filtration (245 mg, 75%).

MS: (ESI)  $m/z$  777  $[M-2H-(ClO_4)_3]^+$ . HRMS: Calcd. for  $C_{32}H_{58}N_8ClO_4Cu_2^+$ : 777.2700; Found 777.2707.

UV-vis: (H<sub>2</sub>O)  $\lambda_{max}$  554 nm,  $\epsilon$  411 M<sup>-1</sup> cm<sup>-1</sup>.

### 8.3.6.1 Crystal data and structural refinement for [Cu<sub>2</sub>5](ClO<sub>4</sub>)<sub>4</sub>

Empirical formula	C <sub>32</sub> H <sub>56</sub> Cl <sub>4</sub> Cu <sub>2</sub> N <sub>8</sub> O <sub>16</sub>	
Formula weight	1077.73	
Temperature	150(2) K	
Wavelength	0.71073 Å	
Crystal system	Monoclinic	
Space group	P21/n	
Unit cell dimensions	a = 17.257(2) Å	α = 90°.
	b = 15.7102(16) Å	β = 102.416(9)°.
	c = 17.976(2) Å	γ = 90°.
Volume	4759.6(9) Å <sup>3</sup>	
Z	4	
Density (calculated)	1.504 Mg/m <sup>3</sup>	
Absorption coefficient	1.189 mm <sup>-1</sup>	
F(000)	2232	
Crystal size	0.2 x 0.1 x 0.1 mm <sup>3</sup>	
Theta range for data collection	2.59 to 34.91°.	
Index ranges	-27 ≤ h ≤ 27, -24 ≤ k ≤ 25, -28 ≤ l ≤ 24	
Reflections collected	56800	
Independent reflections	20450 [R(int) = 0.1015]	
Completeness to theta = 34.91°	98.3 %	
Absorption correction	None	
Refinement method	Full-matrix least-squares on F <sup>2</sup>	
Data / restraints / parameters	20450 / 60 / 559	
Goodness-of-fit on F <sup>2</sup>	0.874	
Final R indices [I > 2σ(I)]	R1 = 0.1422, wR2 = 0.3621	
R indices (all data)	R1 = 0.3428, wR2 = 0.4444	
Largest diff. peak and hole	1.550 and -0.871 e.Å <sup>-3</sup>	

Crystals were grown by vapour diffusion of diethyl ether at room temperature into a solution of  $[\text{Cu}_2\mathbf{5}](\text{ClO}_4)_4$  in methanol.

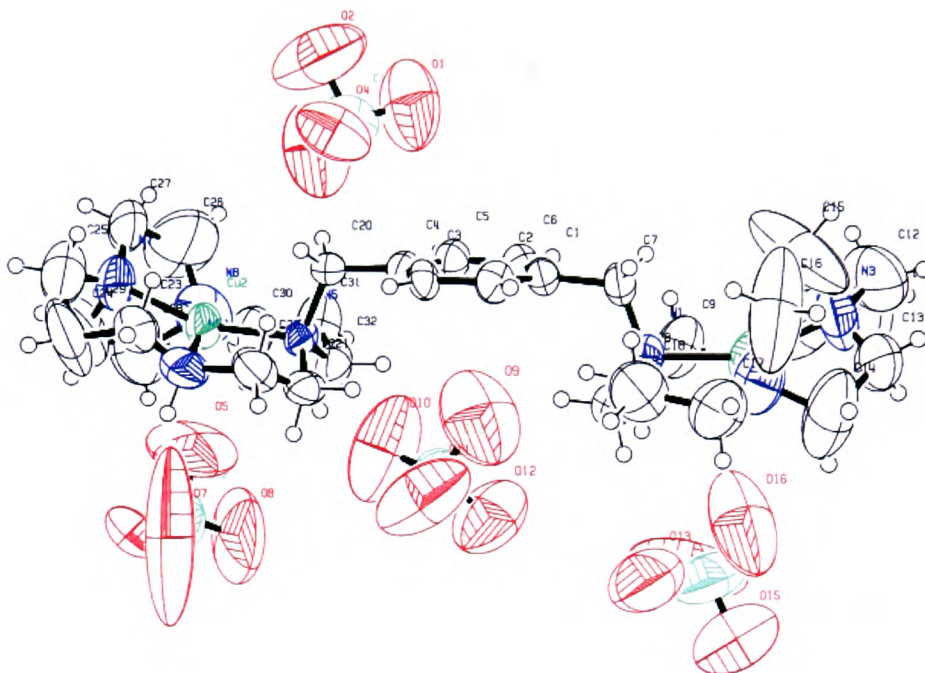


Figure 125. ORTEP representation of  $[\text{Cu}_2\mathbf{5}](\text{ClO}_4)_4$ .

**Table 26. Bond lengths (Å) for [Cu<sub>2</sub>5](ClO<sub>4</sub>)<sub>4</sub>.**

Cu(1)-N(4)	1.855(11)	N(5)-C(20)	1.509(8)	C(21)-C(22)	1.500(13)
Cu(1)-N(3)	1.885(9)	N(6)-C(23)	1.21(2)	C(23)-C(24)	1.50(3)
Cu(1)-N(1)	2.002(5)	N(6)-C(22)	1.472(11)	C(24)-C(25)	1.43(2)
Cu(1)-N(2)	2.048(14)	N(7)-C(27)	1.276(17)	C(26)-C(27)	1.73(3)
Cu(1)-C(15)	2.443(18)	N(7)-C(29)	1.394(19)	C(28)-C(29)	1.68(3)
Cu(1)-C(16)	2.548(16)	N(7)-C(25)	1.620(19)	C(30)-C(31)	1.453(16)
Cu(2)-N(8)	1.849(11)	N(8)-C(30)	1.148(17)	C(31)-C(32)	1.521(15)
Cu(2)-N(7)	1.950(7)	N(8)-C(28)	1.522(19)	Cl(2)-O(8)	1.250(10)
Cu(2)-N(5)	1.988(5)	N(8)-C(26)	1.53(2)	Cl(2)-O(7)	1.336(13)
Cu(2)-N(6)	2.266(11)	C(1)-C(6)	1.352(10)	Cl(2)-O(5)	1.374(10)
Cu(2)-C(30)	2.500(19)	C(1)-C(2)	1.376(10)	Cl(2)-O(6)	1.385(7)
N(1)-C(8)	1.493(11)	C(1)-C(7)	1.528(8)	Cl(1)-O(1)	1.274(11)
N(1)-C(7)	1.496(9)	C(2)-C(3)	1.396(8)	Cl(1)-O(3)	1.295(11)
N(1)-C(19)	1.498(11)	C(3)-C(4)	1.387(9)	Cl(1)-O(4)	1.340(10)
N(2)-C(10)	1.32(2)	C(4)-C(5)	1.397(10)	Cl(1)-O(2)	1.440(11)
N(2)-C(9)	1.654(16)	C(4)-C(20)	1.511(8)	Cl(3)-O(10)	1.293(9)
N(3)-C(13)	1.297(18)	C(5)-C(6)	1.381(9)	Cl(3)-O(12)	1.351(9)
N(3)-C(12)	1.45(2)	C(8)-C(9)	1.490(17)	Cl(3)-O(11)	1.397(11)
N(3)-C(15)	1.61(3)	C(10)-C(11)	1.71(4)	Cl(3)-O(9)	1.400(11)
N(4)-C(17)	1.08(2)	C(11)-C(12)	1.35(4)	Cl(4)-O(16)	1.288(12)
N(4)-C(14)	1.459(16)	C(13)-C(14)	1.71(2)	Cl(4)-O(15)	1.305(11)
N(4)-C(16)	1.47(3)	C(15)-C(16)	1.73(4)	Cl(4)-O(13)	1.368(12)
N(5)-C(32)	1.451(11)	C(17)-C(18)	1.51(2)	Cl(4)-O(14)	1.373(13)
N(5)-C(21)	1.469(10)	C(18)-C(19)	1.505(15)		

**Table 27. Bond angles (°) for [Cu<sub>2</sub>5](ClO<sub>4</sub>)<sub>4</sub>.**

N(4)-Cu(1)-N(3) <sup>iii</sup>	81.4(6)	C(16)-N(4)-Cu(1)	99.5(15)	C(15)-C(16)-Cu(1)	66.5(9)
N(4)-Cu(1)-N(1)	99.4(4)	C(32)-N(5)-C(21)	110.5(6)	N(4)-C(17)-C(18)	123.7(17)
N(3)-Cu(1)-N(1)	154.1(5)	C(32)-N(5)-C(20)	111.9(6)	C(19)-C(18)-C(17)	111.4(15)
N(4)-Cu(1)-N(2)	160.9(5)	C(21)-N(5)-C(20)	112.0(5)	N(1)-C(19)-C(18)	110.9(8)
N(3)-Cu(1)-N(2)	97.1(6)	C(32)-N(5)-Cu(2)	108.3(4)	N(5)-C(20)-C(4)	114.9(5)
N(1)-Cu(1)-N(2)	90.3(4)	C(21)-N(5)-Cu(2)	106.5(4)	N(5)-C(21)-C(22)	111.4(6)
N(4)-Cu(1)-C(15)	74.4(8)	C(20)-N(5)-Cu(2)	107.4(3)	N(6)-C(22)-C(21)	108.8(8)
N(3)-Cu(1)-C(15)	41.1(8)	C(23)-N(6)-C(22)	126.2(16)	N(6)-C(23)-C(24)	117(3)
N(1)-Cu(1)-C(15)	113.9(8)	C(23)-N(6)-Cu(2)	99(2)	C(25)-C(24)-C(23)	101.6(14)
N(2)-Cu(1)-C(15)	116.7(8)	C(22)-N(6)-Cu(2)	102.4(6)	C(24)-C(25)-N(7)	103.7(17)
N(4)-Cu(1)-C(16)	34.6(10)	C(27)-N(7)-C(29)	119.4(18)	N(8)-C(26)-C(27)	102.1(14)
N(3)-Cu(1)-C(16)	61.9(7)	C(27)-N(7)-C(25)	109.7(14)	N(7)-C(27)-C(26)	104.9(15)
N(1)-Cu(1)-C(16)	104.6(4)	C(29)-N(7)-C(25)	101.2(12)	N(8)-C(28)-C(29)	107.0(14)
N(2)-Cu(1)-C(16)	156.5(10)	C(27)-N(7)-Cu(2)	106.5(8)	N(7)-C(29)-C(28)	101.8(11)
C(15)-Cu(1)-C(16)	40.6(10)	C(29)-N(7)-Cu(2)	102.1(9)	N(8)-C(30)-C(31)	130.2(15)
N(8)-Cu(2)-N(7)	79.1(6)	C(25)-N(7)-Cu(2)	118.5(8)	N(8)-C(30)-Cu(2)	43.7(9)
N(8)-Cu(2)-N(5)	104.9(5)	C(30)-N(8)-C(28)	116.3(16)	C(31)-C(30)-Cu(2)	97.3(9)
N(7)-Cu(2)-N(5)	160.3(3)	C(30)-N(8)-C(26)	120.5(17)	C(30)-C(31)-C(32)	107.0(11)
N(8)-Cu(2)-N(6)	162.8(4)	C(28)-N(8)-C(26)	99.2(16)	N(5)-C(32)-C(31)	112.7(7)
N(7)-Cu(2)-N(6)	97.4(4)	C(30)-N(8)-Cu(2)	110.9(12)	O(8)-Cl(2)-O(7)	119.7(16)
N(5)-Cu(2)-N(6)	84.1(3)	C(28)-N(8)-Cu(2)	100.1(12)	O(8)-Cl(2)-O(5)	104.4(12)
N(8)-Cu(2)-C(30)	25.4(5)	C(26)-N(8)-Cu(2)	107.4(15)	O(7)-Cl(2)-O(5)	102.7(14)
N(7)-Cu(2)-C(30)	104.5(5)	C(6)-C(1)-C(2)	118.8(6)	O(8)-Cl(2)-O(6)	110.4(11)
N(5)-Cu(2)-C(30)	81.1(3)	C(6)-C(1)-C(7)	122.3(6)	O(7)-Cl(2)-O(6)	108.9(8)
N(6)-Cu(2)-C(30)	152.1(4)	C(2)-C(1)-C(7)	118.9(7)	O(5)-Cl(2)-O(6)	110.2(8)
C(8)-N(1)-C(7)	110.9(6)	C(1)-C(2)-C(3)	120.4(7)	O(1)-Cl(1)-O(3)	123.9(10)
C(8)-N(1)-C(19)	110.2(7)	C(4)-C(3)-C(2)	120.5(6)	O(1)-Cl(1)-O(4)	113.6(9)
C(7)-N(1)-C(19)	110.7(6)	C(3)-C(4)-C(5)	118.2(5)	O(3)-Cl(1)-O(4)	115.8(9)
C(8)-N(1)-Cu(1)	104.6(5)	C(3)-C(4)-C(20)	120.5(6)	O(1)-Cl(1)-O(2)	102.3(12)
C(7)-N(1)-Cu(1)	109.5(4)	C(5)-C(4)-C(20)	121.3(6)	O(3)-Cl(1)-O(2)	101.4(12)
C(19)-N(1)-Cu(1)	110.8(5)	C(6)-C(5)-C(4)	119.6(7)	O(4)-Cl(1)-O(2)	91.4(9)
C(10)-N(2)-C(9)	111.3(14)	C(1)-C(6)-C(5)	122.4(7)	O(10)-Cl(3)-O(12)	124.4(8)
C(10)-N(2)-Cu(1)	122.5(15)	N(1)-C(7)-C(1)	114.0(5)	O(10)-Cl(3)-O(11)	115.8(9)
C(9)-N(2)-Cu(1)	102.2(7)	C(9)-C(8)-N(1)	111.2(9)	O(12)-Cl(3)-O(11)	110.8(8)

C(13)-N(3)-C(12)	110.4(15)	C(8)-C(9)-N(2)	106.0(10)	O(10)-Cl(3)-O(9)	109.2(12)
C(13)-N(3)-C(15)	126(2)	N(2)-C(10)-C(11)	109.7(16)	O(12)-Cl(3)-O(9)	101.1(9)
C(12)-N(3)-C(15)	101.0(15)	C(12)-C(11)-C(10)	118(2)	O(11)-Cl(3)-O(9)	87.8(9)
C(13)-N(3)-Cu(1)	107.7(11)	C(11)-C(12)-N(3)	109(2)	O(16)-Cl(4)-O(15)	122.8(13)
C(12)-N(3)-Cu(1)	123.6(13)	N(3)-C(13)-C(14)	109.3(10)	O(16)-Cl(4)-O(13)	111.4(11)
C(15)-N(3)-Cu(1)	88.4(10)	N(4)-C(14)-C(13)	101.7(12)	O(15)-Cl(4)-O(13)	108.4(11)
C(17)-N(4)-C(14)	112.8(15)	N(3)-C(15)-C(16)	89.3(18)	O(16)-Cl(4)-O(14)	105.6(12)
C(17)-N(4)-C(16)	113(2)	N(3)-C(15)-Cu(1)	50.5(6)	O(15)-Cl(4)-O(14)	104.6(11)
C(14)-N(4)-C(16)	98.7(15)	C(16)-C(15)-Cu(1)	73.0(9)	O(13)-Cl(4)-O(14)	101.6(15)
C(17)-N(4)-Cu(1)	122.6(17)	N(4)-C(16)-C(15)	110.9(13)		
C(14)-N(4)-Cu(1)	106.4(8)	N(4)-C(16)-Cu(1)	45.9(7)		

### 8.3.7 Synthesis of $[\text{Cu}_2\text{5Cl}_2]\text{Cl}_2$

Ligand **5** (198 mg, 0.36 mmol), copper(II) chloride dihydrate (140 mg, 82 mmol). A green precipitate was observed immediately which redissolved to give a blue solution after a few minutes. The blue solution was purified by size exclusion chromatography (Sephadex LH20). The resulting solvent was evaporated *in vacuo* to yield a blue crystalline solid (178 mg, 60%).

MS: (ESI)  $m/z$  785  $[\text{M}-\text{Cl}]^+$ . HRMS: Calcd. for  $\text{C}_{32}\text{H}_{58}\text{N}_8\text{Cl}_3\text{Cu}_2^+$ : 785.2452; Found 785.2446.

UV-vis: ( $\text{H}_2\text{O}$ )  $\lambda_{\text{max}}$  567 nm,  $\epsilon$  453  $\text{M}^{-1} \text{cm}^{-1}$ .

### 8.3.7.1 Crystal data and structural refinement for [Cu<sub>2</sub>5Cl<sub>2</sub>]Cl<sub>2</sub>

Empirical formula	C <sub>32</sub> H <sub>58</sub> Cl <sub>4</sub> Cu <sub>2</sub> N <sub>8</sub> O <sub>2</sub>
Formula weight	855.74
Temperature	150(2) K
Wavelength	0.71073 Å
Crystal system	Monoclinic
Space group	C2
Unit cell dimensions	a = 17.3370(19) Å      α = 90°. b = 9.1621(8) Å      β = 106.218(9)°. c = 13.5870(18) Å      γ = 90°.
Volume	2072.3(4) Å <sup>3</sup>
Z	2
Density (calculated)	1.371 Mg/m <sup>3</sup>
Absorption coefficient	1.322 mm <sup>-1</sup>
F(000)	896
Crystal size	0.2 x 0.2 x 0.15 mm <sup>3</sup>
Theta range for data collection	2.79 to 34.62°.
Index ranges	-21 ≤ h ≤ 27, -14 ≤ k ≤ 14, -21 ≤ l ≤ 21
Reflections collected	14454
Independent reflections	8175 [R(int) = 0.0498]
Completeness to theta = 34.62°	97.3 %
Absorption correction	None
Refinement method	Full-matrix least-squares on F <sup>2</sup>
Data / restraints / parameters	8175 / 1 / 194
Goodness-of-fit on F <sup>2</sup>	0.870
Final R indices [I > 2σ(I)]	R1 = 0.0797, wR2 = 0.2126
R indices (all data)	R1 = 0.1351, wR2 = 0.2438
Absolute structure parameter	0.40(4)
Extinction coefficient	0.0046(12)
Largest diff. peak and hole	2.851 and -0.822 e.Å <sup>-3</sup>

Crystals were grown by vapour diffusion of diethyl ether at room temperature into a solution of  $[\text{Cu}_2\text{5Cl}_2]\text{Cl}_2$  in methanol.

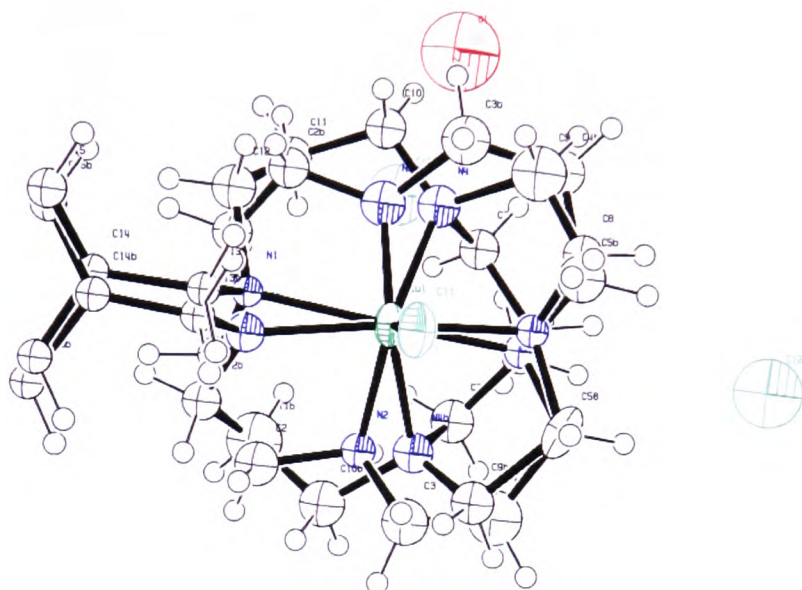


**Figure 126. ORTEP representation of  $[\text{Cu}_2\text{5Cl}_2]^{2+}$  showing the two alternative disordered ring positions. Symmetry transformations used to generate equivalent atoms:  $-x, y, -z+1$ .**

**Table 28. Bond lengths (Å) and angles (°) for [Cu<sub>2</sub>5Cl<sub>2</sub>]Cl<sub>2</sub>.**

Cu(1)-N(2B)	1.891(15)	N(2B)-Cu(1)-N(2)	136.9(4)	C(3)-C(4)-C(58)	119(2)
Cu(1)-N(2)	1.999(11)	N(2B)-Cu(1)-N(3B)	98.4(6)	N(3)-C(6)-C(7)	104.3(11)
Cu(1)-N(3B)	2.004(11)	N(2)-Cu(1)-N(3B)	88.2(5)	N(4)-C(7)-C(6)	110.6(14)
Cu(1)-N(3)	2.088(11)	N(2B)-Cu(1)-N(3)	92.3(6)	N(4)-C(7)-Cl(2A)	100.1(11)
Cu(1)-N(1B)	2.089(14)	N(2)-Cu(1)-N(3)	98.0(5)	C(6)-C(7)-Cl(2A)	143.7(12)
Cu(1)-N(1)	2.112(9)	N(3B)-Cu(1)-N(3)	9.9(4)	C(9)-C(8)-N(3)	112(2)
Cu(1)-N(4B)	2.136(15)	N(2B)-Cu(1)-N(1B)	89.7(6)	C(8)-C(9)-N(4)	106(2)
Cu(1)-N(4)	2.139(16)	N(2)-Cu(1)-N(1B)	73.3(5)	N(4)-C(10)-C(11)	109.6(12)
Cu(1)-Cl(1)	2.4131(11)	N(3B)-Cu(1)-N(1B)	159.5(5)	C(12)-C(11)-C(10)	111.4(12)
N(1)-C(1)	1.332(16)	N(3)-Cu(1)-N(1B)	168.8(5)	C(11)-C(12)-N(1)	116.4(12)
N(1)-C(12)	1.584(18)	N(2B)-Cu(1)-N(1)	74.0(6)	C(14)-C(13)-N(1)	108.7(11)
N(1)-C(13)	1.594(16)	N(2)-Cu(1)-N(1)	88.1(4)	C(15)-C(14)-C(16)	117.2(15)
N(2)-C(3)	1.41(2)	N(3B)-Cu(1)-N(1)	163.9(4)	C(15)-C(14)-C(13)	125.6(15)
N(2)-C(2)	1.50(2)	N(3)-Cu(1)-N(1)	164.8(4)	C(16)-C(14)-C(13)	114.3(14)
N(3)-C(8)	1.39(3)	N(1B)-Cu(1)-N(1)	16.2(3)	C(14)-C(15)-C(15)#1	122.3(12)
N(3)-C(6)	1.476(16)	N(2B)-Cu(1)-N(4B)	132.4(6)	C(14)-C(16)-C(16)#1	116.3(9)
N(3)-C(58)	1.569(15)	N(2)-Cu(1)-N(4B)	23.8(5)	C(12B)-N(1B)-C(13B)	111.8(12)
N(4)-C(10)	1.40(2)	N(3B)-Cu(1)-N(4B)	64.7(6)	C(12B)-N(1B)-C(1B)	107.2(12)
N(4)-C(7)	1.46(2)	N(3)-Cu(1)-N(4B)	74.6(5)	C(13B)-N(1B)-C(1B)	103.8(11)
N(4)-C(9)	1.74(3)	N(1B)-Cu(1)-N(4B)	96.0(6)	C(12B)-N(1B)-Cu(1)	122.0(10)
C(1)-C(2)	1.76(2)	N(1)-Cu(1)-N(4B)	109.6(5)	C(13B)-N(1B)-Cu(1)	113.2(10)
C(3)-C(4)	1.37(4)	N(2B)-Cu(1)-N(4)	24.5(6)	C(1B)-N(1B)-Cu(1)	95.4(8)
C(4)-C(58)	1.63(3)	N(2)-Cu(1)-N(4)	132.3(5)	C(2B)-N(2B)-C(3B)	117.6(13)
C(6)-C(7)	1.49(2)	N(3B)-Cu(1)-N(4)	74.0(5)	C(2B)-N(2B)-Cu(1)	110.0(10)
C(7)-Cl(2A)	2.21(2)	N(3)-Cu(1)-N(4)	68.5(5)	C(3B)-N(2B)-Cu(1)	109.2(11)
C(8)-C(9)	1.36(4)	N(1B)-Cu(1)-N(4)	111.9(6)	C(58)-N(3B)-C(5B)	99.5(12)
C(10)-C(11)	1.52(2)	N(1)-Cu(1)-N(4)	97.2(5)	C(58)-N(3B)-C(6B)	111.4(11)
C(11)-C(12)	1.49(2)	N(4B)-Cu(1)-N(4)	117.0(3)	C(5B)-N(3B)-C(6B)	117.6(14)
C(13)-C(14)	1.56(2)	N(2B)-Cu(1)-Cl(1)	112.8(5)	C(58)-N(3B)-Cu(1)	115.4(8)
C(14)-C(15)	1.30(3)	N(2)-Cu(1)-Cl(1)	108.9(3)	C(5B)-N(3B)-Cu(1)	107.1(13)
C(14)-C(16)	1.42(2)	N(3B)-Cu(1)-Cl(1)	95.2(3)	C(6B)-N(3B)-Cu(1)	106.2(8)
C(15)-C(15)#1	1.31(3)	N(3)-Cu(1)-Cl(1)	90.5(3)	C(9B)-N(4B)-C(7B)	114.2(15)
C(16)-C(16)#1	1.51(3)	N(1B)-Cu(1)-Cl(1)	99.0(4)	C(9B)-N(4B)-C(10B)	116.5(13)
N(1B)-C(12B)	1.39(2)	N(1)-Cu(1)-Cl(1)	100.8(2)	C(7B)-N(4B)-C(10B)	101.9(13)

N(1B)-C(13B)	1.449(19)	N(4B)-Cu(1)-Cl(1)	112.8(4)	C(9B)-N(4B)-Cu(1)	106.6(11)
N(1B)-C(1B)	1.72(2)	N(4)-Cu(1)-Cl(1)	116.5(4)	C(7B)-N(4B)-Cu(1)	102.6(10)
N(2B)-C(2B)	1.47(2)	C(1)-N(1)-C(12)	116.9(11)	C(10B)-N(4B)-Cu(1)	114.3(10)
N(2B)-C(3B)	1.61(2)	C(1)-N(1)-C(13)	117.7(10)	C(2B)-C(1B)-N(1B)	113.0(14)
N(3B)-C(58)	1.419(15)	C(12)-N(1)-C(13)	100.3(9)	C(1B)-C(2B)-N(2B)	110.0(14)
N(3B)-C(5B)	1.48(3)	C(1)-N(1)-Cu(1)	103.7(8)	C(4B)-C(3B)-N(2B)	114.5(14)
N(3B)-C(6B)	1.510(17)	C(12)-N(1)-Cu(1)	110.9(8)	C(3B)-C(4B)-C(5B)	107.6(15)
N(4B)-C(9B)	1.36(2)	C(13)-N(1)-Cu(1)	107.1(7)	N(3B)-C(5B)-C(4B)	113.9(19)
N(4B)-C(7B)	1.56(2)	C(3)-N(2)-C(2)	108.5(12)	C(7B)-C(6B)-N(3B)	104.7(12)
N(4B)-C(10B)	1.62(2)	C(3)-N(2)-Cu(1)	111.5(10)	C(6B)-C(7B)-N(4B)	104.1(14)
C(1B)-C(2B)	1.29(2)	C(2)-N(2)-Cu(1)	107.3(9)	N(4B)-C(9B)-C(58)	105.4(12)
C(3B)-C(4B)	1.53(3)	C(8)-N(3)-C(6)	109.0(13)	C(11B)-C(10B)-N(4B)	112.9(15)
C(4B)-C(5B)	1.68(3)	C(8)-N(3)-C(58)	119.8(12)	C(10B)-C(11B)-C(12B)	106.8(18)
C(6B)-C(7B)	1.45(2)	C(6)-N(3)-C(58)	106.7(10)	N(1B)-C(12B)-C(11B)	117.7(15)
C(9B)-C(58)	1.66(2)	C(8)-N(3)-Cu(1)	113.7(11)	N(1B)-C(13B)-C(14B)	123.6(13)
C(10B)-C(11B)	1.48(3)	C(6)-N(3)-Cu(1)	101.3(8)	C(15B)-C(14B)-C(13B)	127.0(15)
C(11B)-C(12B)	1.54(3)	C(58)-N(3)-Cu(1)	104.5(7)	C(15B)-C(14B)-C(16B)	116.6(14)
C(13B)-C(14B)	1.47(2)	C(10)-N(4)-C(7)	118.4(14)	C(13B)-C(14B)-C(16B)	115.0(15)
C(14B)-C(15B)	1.40(3)	C(10)-N(4)-C(9)	108.6(14)	C(15B)#1-C(15B)-C(14B)	121.6(10)
C(14B)-C(16B)	1.52(2)	C(7)-N(4)-C(9)	99.0(15)	C(16B)#1-C(16B)-C(14B)	119.0(8)
C(15B)-C(15B)#1	1.37(3)	C(10)-N(4)-Cu(1)	123.0(11)	N(3B)-C(58)-N(3)	12.7(7)
C(16B)-C(16B)#1	1.39(2)	C(7)-N(4)-Cu(1)	101.0(10)	N(3B)-C(58)-C(4)	106.4(15)
		C(9)-N(4)-Cu(1)	103.5(12)	N(3)-C(58)-C(4)	118.8(14)
		N(1)-C(1)-C(2)	108.6(11)	N(3B)-C(58)-C(9B)	97.8(10)
		N(2)-C(2)-C(1)	101.5(10)	N(3)-C(58)-C(9B)	109.2(10)
		C(4)-C(3)-N(2)	106.5(18)	C(4)-C(58)-C(9B)	15.2(11)

### 8.3.8 Synthesis of [Cu<sub>2</sub>5Cl<sub>2</sub>](PF<sub>6</sub>)<sub>2</sub>

To a solution of [Cu<sub>2</sub>5Cl<sub>2</sub>]Cl<sub>2</sub> (50 mg, 0.06 mmol) in ethanol (10 mL) was added a solution of ammonium hexafluorophosphate (23 mg, 0.14 mmol) in ethanol (5 mL). After stirring at room temperature for 10 minutes the blue precipitate was collected by filtration, washed with ethanol (5 x 10 mL) followed by diethyl ether (5 x 10 mL) and dried *in vacuo* to yield a pale blue solid (54.98 mg, 87%).

MS: (ESI)  $m/z$  339 [M-2H-2Cl-(PF<sub>6</sub>)<sub>2</sub>]<sup>2+</sup>. HRMS: Calcd. for C<sub>32</sub>H<sub>58</sub>N<sub>8</sub>Cu<sub>2</sub><sup>2+</sup>: 339.1604; Found 339.1612.

UV-vis: (H<sub>2</sub>O)  $\lambda_{\max}$  567 nm,  $\epsilon$  452 M<sup>-1</sup> cm<sup>-1</sup>.

### 8.3.9 Synthesis of [Ni15](ClO<sub>4</sub>)<sub>2</sub>

An acetonitrile solution (50 mL) of nickel (II) perchlorate hexahydrate (15.70 g, 43 mmol) was added dropwise to a solution of 5-(4-phenylmethyl benzoate)-1,5,8,12-tetraazabicyclo[10.2.2]hexadecane (14.59 g, 39 mmol) in acetonitrile (300 mL). An initial green solution was observed which changed to orange after a few minutes and this solution was heated at reflux for 2 h. The orange solution was filtered, concentrated *in vacuo* and purified by size exclusion chromatography (Sephadex LH20). The resulting solvent was evaporated *in vacuo* to yield an orange crystalline solid (16.76 g, 68%).

<sup>13</sup>C NMR: (CD<sub>3</sub>CN)  $\delta$  22.30 (N- $\beta$ -CH<sub>2</sub>), 23.40 (N- $\beta$ -CH<sub>2</sub>), 48.49 (N- $\alpha$ -CH<sub>2</sub>), 48.79 (N- $\alpha$ -CH<sub>3</sub>), 51.03 (N- $\alpha$ -CH<sub>2</sub>), 51.30 (N- $\alpha$ -CH<sub>2</sub>), 52.37 (O-CH<sub>3</sub>), 52.85 (N- $\alpha$ -CH<sub>2</sub>), 52.97 (N- $\alpha$ -CH<sub>2</sub>), 53.47 (N- $\alpha$ -CH<sub>2</sub>), 55.10 (N- $\alpha$ -CH<sub>2</sub>), 56.03 (N- $\alpha$ -CH<sub>2</sub>), 58.38 (N- $\alpha$ -CH<sub>2</sub>), 58.95

(N- $\alpha$ -CH<sub>2</sub>), 130.40 (CH<sub>aromatic</sub>), 130.65 (CH<sub>aromatic</sub>), 132.57 (C<sub>aromatic</sub>), 133.48 (C<sub>aromatic</sub>), 167.12 (C=O).

MS: (ESI)  $m/z$  531 [M-(ClO<sub>4</sub>)]<sup>+</sup>. HRMS: Calcd. for C<sub>21</sub>H<sub>34</sub>N<sub>4</sub>O<sub>6</sub>NiCl<sup>+</sup>: 531.1515; Found 531.1520.

### 8.3.10 Synthesis of [Ni16](ClO<sub>4</sub>)<sub>2</sub>

Nickel(II) 5-(4-phenylmethyl benzoate)-1,5,8,12-tetraazabicyclo-[10.2.2]hexadecane perchlorate (2.00 g, 3.17 mmol) was dissolved in dry DMSO (10 mL) and stirred *in vacuo* for 1 h. The orange solution was purged with argon for 10 minutes and n-butyl lithium (3.5 mL, 1.75 eq) was added dropwise over 30 minutes. A blue colour developed which was stirred at room temperature for 30 minutes. Methyl iodide (0.8 mL, 12.7 mmol) was added dropwise and an orange solution reappeared which was stirred at room temperature for 1 h. The solution was stirred under vacuum again to remove hexanes and excess methyl iodide. The DMSO solution was added dropwise to a saturated solution of ammonium hexafluorophosphate in ethanol (100 mL). The orange precipitate which formed was filtered off and washed with ether (200 mL). The orange solid was dissolved in acetonitrile and evaporated *in vacuo* to yield an orange crystalline solid (1.86 g, 91%).

<sup>13</sup>C NMR: (CD<sub>3</sub>CN)  $\delta$  22.32 (N- $\beta$ -CH<sub>2</sub>), 22.48 (N- $\beta$ -CH<sub>2</sub>), 31.20 (N- $\alpha$ -CH<sub>3</sub>), 50.92 (N- $\alpha$ -CH<sub>2</sub>), 51.43 (N- $\alpha$ -CH<sub>2</sub>), 51.85 (N- $\alpha$ -CH<sub>2</sub>), 52.09 (O-CH<sub>3</sub>), 52.90 (N- $\alpha$ -CH<sub>2</sub>), 53.27 (N- $\alpha$ -CH<sub>2</sub>), 53.76 (N- $\alpha$ -CH<sub>2</sub>), 53.90 (N- $\alpha$ -CH<sub>2</sub>), 58.25 (N- $\alpha$ -CH<sub>2</sub>), 58.54 (N- $\alpha$ -CH<sub>2</sub>), 61.27 (N- $\alpha$ -CH<sub>2</sub>), 62.74 (N- $\alpha$ -CH<sub>2</sub>), 129.65 (CH<sub>aromatic</sub>), 129.82 (CH<sub>aromatic</sub>), 132.73 (C<sub>aromatic</sub>), 141.92 (C<sub>aromatic</sub>), 166.63 (C=O).

MS: (ESI)  $m/z$  223  $[M-(PF_6)_2]^{2+}$ . HRMS: Calcd. for  $C_{22}H_{36}N_4Ni^{2+}$ : 223.1090; Found 223.1088.

### 8.3.11 Synthesis of $[Ni21](ClO_4)_2$

A methanolic solution (10 mL) of nickel (II) perchlorate hexahydrate (1.39 g, 38 mmol) was added dropwise to a solution of 5-(methyl)-1,5,8,12-tetraaza-bicyclo[10.2.2]hexadecane (0.83 g, 35 mmol) in methanol (10 mL). An initial green solution was observed which changed to orange after a few minutes and the solution was heated at reflux for 2 h. The orange solution was filtered off to remove a green precipitate. The resulting orange solution was evaporated *in vacuo* to yield an orange crystalline solid (0.73 g, 42%).

$^{13}C$  NMR: ( $CD_3CN$ )  $\delta$  20.38 (N- $\beta$ - $CH_2$ ), 22.40 (N- $\beta$ - $CH_2$ ), 39.41 (N- $\alpha$ - $CH_3$ ), 45.36 (N- $\alpha$ - $CH_2$ ), 50.81 (N- $\alpha$ - $CH_2$ ), 56.38 (N- $\alpha$ - $CH_2$ ), 56.98 (N- $\alpha$ - $CH_2$ ), 57.02 (N- $\alpha$ - $CH_2$ ), 60.17 (N- $\alpha$ - $CH_2$ ).

MS: (ESI)  $m/z$  397  $[M-ClO_4]^+$ . HRMS: Calcd. for  $C_{13}H_{28}N_4Ni^+$ : 397.1147; Found 397.1149.

### 8.3.12 Synthesis of $[Zn_22(OAc)_2](OAc)_2$

Ligand 2 (56.9 mg, 0.11 mmol), zinc(II) acetate dihydrate (59.7mg, 0.36 mmol) The colourless solution was purified by size exclusion chromatography (Sephadex LH20). The resulting solvent was evaporated *in vacuo* to give a white powder (65.2 mg, 61%).

MS: (ESI)  $m/z$  687  $[M-2H-(OAc)_3]^+$ .

### 8.3.13 Synthesis of $[\text{Cu}_2\text{2}](\text{OAc})_4$

Ligand **2** (81.8 mg 0.16 mmol), copper(II) acetate dehydrate (65.4 mg, 0.36 mmol). The purple solution was purified by size exclusion chromatography (Sephadex LH20). The resulting solvent was evaporated *in vacuo* to give a purple powder (81.5 mg, 58%).

MS: (ESI)  $m/z$  685  $[\text{M}-2\text{H}-(\text{OAc})_3]^+$ .

UV-vis: ( $\text{H}_2\text{O}$ )  $\lambda_{\text{max}}$  513 nm,  $\epsilon$  163  $\text{M cm}^{-1}$ .

### 8.3.14 Synthesis of $[\text{Cu}_2\text{9Cl}_2]\text{Cl}_2$

Ligand **9** (200 mg, 0.34 mmol) was dissolved in dry methanol (20 mL) and a solution of copper(II) chloride dihydrate (130 mg, 1 mmol) in dry methanol (5 mL) was added under an atmosphere of nitrogen. A blue solution developed immediately with a green precipitate forming after a few minutes. The solution was heated at reflux for 2 h, the green precipitate was removed by filtration and the blue filtrate was concentrated *in vacuo*. The crude product was purified by size exclusion chromatography (Sephadex LH20). The resulting solvent was removed *in vacuo* to yield a green crystalline solid (88 mg, 36%).

MS: (ESI)  $m/z$  813  $[\text{M}-\text{Cl}]^+$ , HRMS: Calcd. for  $\text{C}_{34}\text{H}_{62}\text{N}_8\text{Cu}_2\text{Cl}^+$ : 813.2750; Found 813.2743.

UV-vis: ( $\text{H}_2\text{O}$ )  $\lambda_{\text{max}}$  622 nm,  $\epsilon$  109  $\text{M cm}^{-1}$ .

### 8.3.15 Synthesis of $[\text{Cu}_2\text{9Cl}_2](\text{PF}_6)_2$

To a solution of  $[\text{Cu}_2\text{9Cl}_2]\text{Cl}_2$  (50 mg, 0.06 mmol) in ethanol (10 mL), was added a solution of ammonium hexafluorophosphate (23 mg, 0.14 mmol) in ethanol (5 mL). After

stirring at room temperature for 10 minutes a green precipitate had formed and was collected by filtration, washed with ethanol (5 x 10 mL) followed by diethyl ether (5 x 10 mL) and dried *in vacuo* to yield a pale green solid (57 mg, 91%).

MS: (ESI)  $m/z$  390  $[M-(PF_6)_2]^{2+}$ .

UV-vis: (H<sub>2</sub>O)  $\lambda_{max}$  622 nm,  $\epsilon$  109 M cm<sup>-1</sup>.

### 8.3.16 Synthesis of [Cu<sub>2</sub>9(OAc)<sub>2</sub>](OAc)<sub>2</sub>

Ligand **9** (317 mg, 0.54 mmol) was dissolved in dry methanol (20 mL) and a solution of copper acetate monohydrate (239 mg, 1.20 mmol) in methanol (5 mL) was added under an atmosphere of nitrogen. A green colour developed immediately and the solution was heated at reflux for 2 h. The crude product was purified by size exclusion chromatography (Sephadex LH20). The resulting solvent was removed *in vacuo* to yield a green crystalline solid (160 mg, 54%).

MS: (ESI)  $m/z$  813  $[M-(OAc)]^+$ . HRMS: Calcd. for C<sub>34</sub>H<sub>62</sub>N<sub>8</sub>Cu<sub>2</sub><sup>+</sup>: 813.2750; Found 813.2743.

UV-vis: (H<sub>2</sub>O)  $\lambda_{max}$  661 nm,  $\epsilon$  200 M cm<sup>-1</sup>.

### 8.3.17 Synthesis of [Zn<sub>3</sub>6(OAc)<sub>3</sub>](OAc)<sub>3</sub>

Ligand (200 mg, 0.25 mmol), zinc(II) acetate monohydrate (150 mg, 0.83 mmol). The clear solution was concentrated *in vacuo* and purified by size exclusion chromatography (Sephadex LH20). The resulting solvent was evaporated *in vacuo* to yield a white crystalline solid (320 mg, 82%).

MS: (ESI)  $m/z$  1279  $[M-(OAc)]^+$ . HRMS: Calcd. for  $C_{45}H_{80}N_{12}(OAc)_5Zn_3^+$ : 1279.5480; Found 1279.5479.

### 8.3.18 Synthesis of $[Zn_36Cl_3](PF_6)_3$

Ligand **6** (200 mg, 0.25 mmol), anhydrous zinc(II) chloride (113 mg, 0.84 mmol). The white solid product was collected by filtration, washed with methanol (2 x 20 mL) followed by diethyl ether (5 x 20 mL) and dried *in vacuo*. To a solution of  $[Zn_36Cl_3](PF_6)_3$  in ethanol (20 mL) was added a solution of ammonium hexafluorophosphate (135 mg, 0.83 mmol) in ethanol (5 mL). After stirring at room temperature for 10 minutes the white precipitate was collected by filtration, washed with ethanol (5 x 10 mL) followed by diethyl ether (5 x 10 mL) and dried *in vacuo* to yield a white solid (210 mg, 69%).

MS: (ESI)  $m/z$  1089  $[M-(PF_6)_3]^{3+}$ . HRMS: Calcd. for  $C_{45}H_{80}N_{12}Cl_3Zn_3^+$ : 1089.3881; Found 1089.3878.

### 8.3.19 Synthesis of $[Zn_36](ClO_4)_6$

Ligand **6** (200 mg, 0.25 mmol), zinc(II) perchlorate hexahydrate (310 mg, 0.84 mmol). The white solid product was collected by filtration, washed with methanol (2 x 20 mL) followed by diethyl ether (5 x 20 mL) and dried *in vacuo* (310 mg, 78%).

MS: (ESI)  $m/z$  1281  $[M-(ClO_4)_3]^{3+}$ . HRMS: Calcd. for  $C_{45}H_{80}N_{12}(ClO_4)_3Zn_3^{3+}$ : 1281.3272; Found 1281.3270.

### 8.3.20 Synthesis of $[\text{Cu}_3\text{6}(\text{OAc})_3](\text{OAc})_3$

Ligand **6** (200 mg, 0.25 mmol), copper(II) acetate monohydrate (166 mg, 0.83 mmol). The blue solution was concentrated *in vacuo* and purified by size exclusion chromatography (Sephadex LH20). The resulting solvent was evaporated *in vacuo* to yield a blue crystalline solid (265 mg, 79%).

MS: (ESI)  $m/z$  304  $[\text{M}-(\text{OAc})_2]^{4+}$ . HRMS: Calcd. for  $\text{C}_{45}\text{H}_{80}\text{N}_{12}(\text{OAc})\text{Cu}_3^{4+}$ : 304.3843; Found 304.3841.

UV-vis: ( $\text{H}_2\text{O}$ )  $\lambda_{\text{max}}$  565 nm,  $\epsilon$  473  $\text{M}^{-1} \text{cm}^{-1}$ .

### 8.3.21 Synthesis of $[\text{Cu}_3\text{6}](\text{ClO}_4)_6$

Ligand **6** (200 mg, 0.25 mmol), copper(II) perchlorate hexahydrate (310 mg, 0.84 mmol). The purple solid product was collected by filtration, washed with methanol (2 x 20 mL) followed by diethyl ether (5 x 20 mL) and dried *in vacuo* (245 mg, 61%).

MS: (ESI)  $m/z$  1076  $[\text{M}-(\text{ClO}_4)_3]^{3+}$ . HRMS: Calcd. for  $\text{C}_{45}\text{H}_{84}\text{N}_{12}(\text{ClO}_4)_3\text{Cu}_3^{3+}$ : 426.1087; Found 426.1086.

UV-vis: ( $\text{H}_2\text{O}$ )  $\lambda_{\text{max}}$  551 nm,  $\epsilon$  409  $\text{M}^{-1} \text{cm}^{-1}$ .

### 8.3.22 Synthesis of $[\text{Cu}_3\text{6Cl}_3](\text{PF}_6)_3$

Ligand **6** (200 mg, 0.25 mmol), copper(II) chloride dihydrate (142 mg, 0.83 mmol). The blue solution was purified by size exclusion chromatography (Sephadex LH20) and remaining solvent was removed *in vacuo* to yield a blue crystalline solid (not isolated). The blue solid was dissolved in ethanol (10 mL) and a solution of ammonium

hexafluorophosphate (135 mg, 0.83 mmol) in ethanol (5 mL) was added dropwise. After stirring at room temperature for 10 minutes the blue precipitate was collected by filtration, washed with ethanol (5 x 10 mL) followed by diethyl ether (5 x 10 mL) and dried *in vacuo* to yield a pale blue solid (120 mg, 40%).

MS: (ESI)  $m/z$  362  $[M-(PF_6)_3]^{3+}$ . HRMS: Calcd. for  $C_{45}H_{84}N_{12}Cl_3Cu_3^{3+}$ :362.1299; Found 362.1296.

UV-vis: (H<sub>2</sub>O)  $\lambda_{max}$  569 nm,  $\epsilon$  457 M<sup>-1</sup> cm<sup>-1</sup>.

## **Chapter 9. REFERENCES**

- 1 M. Baggiolini, B. Dewald and B. Moser, *Annu. Rev. Immunol.*, 1997, **15**, 675.
- 2 K. Christopherson and R. Hromas, *Stem Cells*, 2001, **19**, 388.
- 3 A. Khan, J. Greenman and S. J. Archibald, *Curr. Med. Chem.*, 2007, **14**, 2257.
- 4 H. E. Broxmeyer, *Curr. Opin. Hematol.*, 2008, **15**, 49.
- 5 R. Horuk, *Cytokine Growth Factor Rev.*, 2001, **12**, 313.
- 6 M. Thelen and J. V. Stein, *Nat. Immunol.*, 2008, **9**, 953.
- 7 S. Abroun, *Yakhteh*, 2008, **10**, 155.
- 8 R. M. Ransohoff and K. B. Bacon, *Expert Opin. Investig. Drugs*, 2000, **9**, 1079.
- 9 J. H. Ruth, J. B. Rottman, K. J. Katschke, S. Qin, L. Wu and G. LaRosa, *Arthritis Rheum.*, 2001, **44**, 2750.
- 10 M. J. Cameron, G. A. Arreaza, M. Grattan, C. Meagher, S. Sharif and M. D. Burdick, *J. Immunol.*, 2000, **165**, 1102.
- 11 C. Gerard and B. J. Rollins, *Nat. Immunol.*, 2001, **2**, 108.
- 12 J. J. Smit and N. W. Lukacs, *Eur. J. Pharmacol.*, 2006, **533**, 277.
- 13 S. T. Holgate, *Clinical & Experimental Allergy*, 2008, **38**, 872.
- 14 E. Oberlin, A. Amara, F. Bachelier, C. Bessia, J. L. Virelizier, F. Arenzana-Seisdedos, O. Schwartz, J. M. Heard, I. ClarkLewis, D. F. Legler, M. Loetscher, M. Baggiolini and B. Moser, *Nature*, 1996, **382**, 833.
- 15 K. Tashiro, H. Tada, R. Heilker, M. Shirozu, T. Nakano and T. Honjo, *Science*, 1993, **261**, 600.
- 16 Z. L. Gao and W. A. Metz, *Chem. Rev.*, 2003, **103**, 3733.
- 17 P. Lusso, *EMBO J.*, 2006, **25**, 447.
- 18 M. Shirozu, T. Nakano, J. Inazawa, K. Tashiro, H. Tada, T. Shinohara and T. Honjo, *Genomics*, 1995, **28**, 495.
- 19 G. Aust, M. Steinert, S. Kiessling, M. Kamprad and C. Simchen, *J. Clin. Endocrinol. Metab.*, 2001, **86**, 3368.
- 20 A. Muller, B. Homey, H. Soto, N. F. Ge, D. Catron, M. E. Buchanan, T. McClanahan, E. Murphy, W. Yuan, S. N. Wagner, J. L. Barrera, A. Mohar, E. Verastegui and A. Zlotnik, *Nature*, 2001, **410**, 50.

- 21 T. Nagasawa, K. Tachibana and T. Kishimoto, *Semin. Immunol.*, 1998, **10**, 179.
- 22 H. J. Yun and D. Y. Jo, *Korean Med. Sci.*, 2003, **18**, 679.
- 23 T. Nagasawa, S. Hirota, K. Tachibana, N. Takakura, S. Nishikawa, Y. Kitamura, N. Yoshida, H. Kikutani and T. Kishimoto, *Nature*, 1996, **382**, 635.
- 24 K. Tachibana, S. Hirota, H. Iizasa, H. Yoshida, K. Kawabata, Y. Kataoka, Y. Kitamura, K. Matsushima, N. Yoshida, S. Nishikawa, T. Kishimoto and T. Nagasawa, *Nature*, 1998, **393**, 591.
- 25 Y. R. Zou, A. H. Kottmann, M. Kuroda, I. Taniuchi and D. R. Littman, *Nature*, 1998, **393**, 595.
- 26 F. Horn, E. Bettler, L. Oliveira, F. Campagne, F. E. Cohen and G. Vriend, *Nucleic Acids Res.*, 2003, **31**, 294.
- 27 T. S. Olson and K. Ley, *Am. J. Physiol. Regul. Integr. Comp. Physiol.*, 2002, **283**, R7.
- 28 T. Jin, X. H. Xu and D. Hereld, *Cytokine*, 2008, **44**, 1.
- 29 M. Baggiolini, *Nature*, 1998, **392**, 565.
- 30 C. C. Bleul, L. J. Wu, J. A. Hoxie, T. A. Springer and C. R. Mackay, *Proc. Natl. Acad. Sci. U. S. A.*, 1997, **94**, 1925.
- 31 S. K. Gupta, P. G. Lysko, K. Pillarisetti, E. Ohlstein and J. M. Stadel, *J. Biol. Chem.*, 1998, **273**, 4282.
- 32 J. Hesselgesser, M. Halks-Miller, V. Del Vecchio, S. C. Peiper, J. A. Hoxie and D. L. Kolson, *Curr. Biol.*, 1997, **7**, 112.
- 33 J. L. He, Y. Z. Chen, M. Farzan, H. Y. Choe, A. Ohagen and S. Gartner, *Nature*, 1997, **385**, 645.
- 34 T. W. Schwartz, L. O. Gerlach, R. T. Skerlj and G. J. Bridger, *J. Biol. Chem.*, 2001, **276**, 14153.
- 35 P. R. Clapham and A. McKnight, *J. Gen. Virol.*, 2002, **83**, 1809.
- 36 N. Cammack, *Antiviral Chem. Chemother.*, 1999, **10**, 53.
- 37 S. Sierra, B. Kupfer and R. Kaiser, *J. Clin. Virol.*, 2005, **34**, 233.
- 38 A. E. I. Proudfoot, *Nat. Rev. Immunol.*, 2002, **2**, 106.
- 39 F. Andre, J. C. Soria, H. Assi, S. Delalogue and M. Spielmann, *Bull. Cancer (Paris)*, 2004, **91**, S254.

- 40 C. Carvalho-Pinto, M. I. Garcia, L. Gomez, A. Ballesteros, A. Zaballos, J. M. Flores, M. Mellado, J. M. Rodriguez-Frade, D. Balomenos and C. Martinez, *Eur. J. Immunol.*, 2004, **34**, 548.
- 41 P. Matthys, S. Hatse, K. Vermeire, A. Wuyts, G. Bridger, G. W. Henson, E. De Clercq, A. Billiau and D. Schols, *J. Immunol.*, 2001, **167**, 4686.
- 42 A. D. Luster, *New. Engl. J. Med.*, 1998, **338**, 436.
- 43 M. M. D'Elcios, G. Del Prete and A. Amedei, *Expert Opin. Ther. Pat.*, 2008, **18**, 309.
- 44 Y. Lavrovsky, Y. A. Ivanenkov, K. V. Balakin, D. A. Medvedeva and A. V. Ivachtchenko, *Mini Rev. Med. Chem.*, 2008, **8**, 1075.
- 45 K. E. Luker and G. D. Luker, *Cancer Lett.*, 2006, **238**, 30.
- 46 C. Murdoch and A. Finn, *Blood*, 2000, **95**, 3032.
- 47 T. K. Tarrant and D. D. Patel, *Pathophysiology*, 2006, **13**, 1.
- 48 J. Vandercappellen, J. Van Damme and S. Struyf, *Cancer Lett.*, 2008, **267**, 226.
- 49 T. Iwamoto, H. Okamoto, Y. Toyama and S. Momohara, *FEBS Journal*, 2008, **275**, 4448.
- 50 K. Kanbe, T. Takemura, K. Takeuchi, Q. Chen, K. Takagishi and K. Inoue, *Bone Joint Surg. Br.*, 2004, **86B**, 296.
- 51 R. Terada, K. Yamamoto, T. Hakoda, N. Shimada, N. Okano, N. Baba, Y. Ninomiya, M. E. Gershwin and Y. Shiratori, *Lab. Invest.*, 2003, **83**, 665.
- 52 C. M. Hogaboam, K. J. Carpenter, J. M. Schuh, A. E. I. Proudfoot, G. J. Bridger and K. F. Buckland, *Pharmacol. Ther.*, 2005, **107**, 314.
- 53 F. Balkwill, *Nat. Rev. Cancer*, 2004, **4**, 540.
- 54 J. A. Burger and T. J. Kipps, *Blood*, 2006, **107**, 1761.
- 55 J. Juarez and L. Bendall, *Histol. Histopathol.*, 2004, **19**, 299.
- 56 T. Murakami, A. R. Cardones and S. T. Hwang, *J. Dermatol. Sci.*, 2004, **36**, 71.
- 57 A. S. Payne and L. A. Cornelius, *J. Invest. Dermatol.*, 2002, **118**, 915.
- 58 F. Balkwill, *Semin. Cancer Biol.*, 2004, **14**, 171.
- 59 M. Arya, H. R. H. Patel and M. Williamson, *Curr. Med. Res. Opin.*, 2003, **19**, 557.

- 60 J. A. Belperio, M. P. Keane, D. A. Arenberg, C. L. Addison, J. E. Ehlert, M. D. Burdick and R. M. Strieter, *J. Leukocyte Biol.*, 2000, **68**, 1.
- 61 C. R. Cooper, C. H. Chay, J. D. Gendernalik, H. L. Lee, J. Bhatia, R. S. Taichman, L. K. McCauley, E. T. Keller and K. J. Pienta, *Cancer*, 2003, **97**, 739.
- 62 A. Ben-Baruch, *Breast Cancer Res.*, 2002, **5**, 31.
- 63 L. P. Su, J. P. Zhang, H. B. Xu, Y. Wang, W. Y. Chu, R. Z. Liu and S. D. Xiong, *Clin. Cancer Res.*, 2005, **11**, 8273.
- 64 T. N. Hartmann, M. Burger and J. A. Burger, *J. Biol. Regul. Homeost. Agents*, 2004, **18**, 126.
- 65 M. Majka, J. Drukala, E. Lesko, M. Wysoczynski, A. B. Jenson and M. Z. Ratajczak, *Folia Histochem. Cytobiol.*, 2006, **44**, 155.
- 66 J. Kim, T. Mori, S. L. Chen, F. F. Amersi, S. R. Martinez, C. Kuo, R. R. Turner, X. Ye, A. J. Bilchik, D. L. Morton and D. S. B. Hoon, *Ann. Surg.*, 2006, **244**, 113.
- 67 S. Brand, J. Dambacher, F. Beigel, T. Olszak, J. Diebold, J. M. Otte, B. Goke and S. T. Eichhorst, *Exp. Cell Res.*, 2005, **310**, 117.
- 68 T. Koshiba, R. Hosotani, Y. Miyamoto, J. Ida, S. Tsuji, S. Nakajima, M. Kawaguchi, H. Kobayashi, R. Doi, T. Hori, N. Fujii and M. Imamura, *Clin. Cancer Res.*, 2000, **6**, 3530.
- 69 T. Mori, R. Doi, M. Koizumi, E. Toyoda, D. Ito, K. Kami, T. Masui, K. Fujimoto, H. Tamamura, K. Hiramatsu, N. Fujii and M. Imamura, *Mol. Cancer Ther.*, 2004, **3**, 29.
- 70 T. Mori, R. Doi, T. Masui, M. Koizumi, E. Toyoda, S. Tulachan, D. Ito, K. Kami, S. Tsuji, S. Namajima, M. Kawaguchi, Y. Fujimoto and M. Imamura, *Gastroenterology*, 2002, **122**, A490.
- 71 S. Singh, U. P. Singh, W. E. Grizzle and J. W. Lillard, *Lab. Invest.*, 2004, **84**, 1666.
- 72 M. Ehtesham, J. A. Winston, P. Kabos and R. C. Thompson, *Oncogene*, 2006, **25**, 2801.
- 73 X. Hong, F. Jiang, S. N. Kalkanis, Z. G. Zhang, X. P. Zhang, A. C. de Carvalho, M. Katakowski, K. Bobbitt, T. Mikkelsen and M. Chopp, *Cancer Lett.*, 2006, **236**, 39.
- 74 S. E. Kuhmann and O. Hartley, *Annu. Rev. Pharmacol. Toxicol.*, 2008, 48425.
- 75 M. Schwarz and T. N. C. Wells, *Curr. Opin. Chem. Biol.*, 1999, **3**, 407.
- 76 Z. Johnson, M. Schwarz, C. A. Power, T. N. C. Wells and A. E. I. Proudfoot, *Trends Immunol.*, 2005, **26**, 268.

- 77 S. Riberio and R. Horuk, *Pharmacol. Ther.*, 2005, **107**, 44.
- 78 J. J. Onuffer and R. Horuk, *Trends Pharmacol. Sci.*, 2002, **23**, 459.
- 79 B. Julg and F. D. Goebel, *Infection*, 2005, **33**, 408.
- 80 A. Vola and A. D. Luster, *Annu. Rev. Pharmacol. Toxicol.*, 2008, 48171.
- 81 E. Galliera, M. M. Corsi, R. Bonecchi, M. Locati and A. Mantovani, *Mini Rev. Med. Chem.*, 2008, **8**, 638.
- 82 H. Tamamura, H. Tsutsumi, W. Nomura, T. Tanaka and N. Fujii, *Expert Opin. Drug Discov.*, 2008, **3**, 1155.
- 83 F. Barresinoussi, J. C. Chermann, F. Rey, M. T. Nugeyre, S. Chamaret, J. Gruest, C. Daugey, C. Axlerblin, F. Vezinetbrun, C. Rouzioux, W. Rozenbaum and L. Montagnier, *Science*, 1983, **220**, 868.
- 84 M. Stevansson, *Nat. Med.*, 2003, **9**, 853.
- 85 A. M. Thayer, *Chem. Eng. News*, 2008, **86**, 29.
- 86 E. De Clercq, *J. Clin. Virol.*, 2004, **30**, 115.
- 87 E. De Clercq, *Int. J. Biochem. Cell Biol.*, 2004, **36**, 1800.
- 88 E. De Clercq, *Antiviral Res.*, 2005, **67**, 56.
- 89 P. Barragan and D. Podzamczar, *Expert Opin. Pharmacother.*, 2008, **9**, 2363.
- 90 A. Hughes, T. Barber and M. Nelson, *J. Infect.*, 2008, **57**, 1.
- 91 S. Martins, M. J. Ramos and P. A. Fernandes, *Curr. Med. Chem.*, 2008, **15**, 1083.
- 92 L. Geeraert, G. Kraus and R. J. Pomerantz, *Annu. Rev. Medicine*, 2008, **59**, 487.
- 93 K. Princen and D. Schols, *Cytokine Growth Factor Rev.*, 2005, **16**, 659.
- 94 E. De Clercq, *Biochim. Biophys. Acta-Mol. Basis Dis.*, 2002, **1587**, 258.
- 95 E. De Clercq, *Nat. Rev. Drug Discov.*, 2003, **2**, 581.
- 96 P. Poignard, E. O. Saphire, P. W. Parren and D. R. Burton, *Annu. Rev. Immunol.*, 2001, **19**, 253.
- 97 P. D. Kwong, R. Wyatt, J. Robinson, R. W. Sweet, J. Sodroski and W. A. Hendrickson, *Nature*, 1998, **393**, 648.

- 98 C. D. Rizzuto, R. Wyatt, N. Hernandez-Ramos, Y. Sun, P. D. Kwong, W. A. Hendrickson and J. Sodroski, *Science*, 1998, **280**, 1949.
- 99 W. Weissenhorn, A. Dessen, S. C. Harrison, J. J. Skehel and D. C. Wiley, *Nature*, 1997, **387**, 426.
- 100 M. Ciampolini, L. Fabbrizzi, A. Perotti, A. Poggi, B. Seghi and F. Zanobini, *Inorg. Chem.*, 1987, **26**, 3527.
- 101 G. J. Bridger, R. T. Skerlj, D. Thornton, S. Padmanabhan, S. A. Martellucci, G. W. Henson, M. J. Abrams, N. Yamamoto, K. De Vreese, R. Pauwels and E. De Clercq, *J. Med. Chem.*, 1995, **38**, 366.
- 102 G. J. Bridger, R. T. Skerlj, S. Padmanabhan, S. A. Martellucci, G. W. Henson, M. J. Abrams, H. C. Joao, M. Witvrouw, K. De Vreese, R. Pauwels and E. De Clercq, *J. Med. Chem.*, 1996, **39**, 109.
- 103 J. Dessolin, P. Galea, P. Vlieghe, J. C. Chermann and J. L. Kraus, *J. Med. Chem.*, 1999, **42**, 229.
- 104 E. K. Barefield, D. Chueng and D. G. Vanderveer, *J. Chem. Soc., Chem. Commun.*, 1981, 302.
- 105 A. Larachelle, A. Krouse, M. Metzger, D. Orlic, R. E. Donahue, S. Fricker, G. J. Bridger, C. E. Dunbar and P. Hematti, *Blood*, 2006, **107**.
- 106 W. C. Liles, H. E. Broxmeyer, E. Rodger, B. Wood, K. Hubel, S. Cooper, G. Hangoc, G. J. Bridger, G. W. Henson, G. Calandra and D. C. Dale, *Blood*, 2003, **102**, 2728.
- 107 W. Yang, C. M. Giandomenico, M. Sartori and D. A. Moore, *Tetrahedron Lett.*, 2003, **44**, 2481.
- 108 N. Bernier, M. Allali, R. Tripier, F. Conan, V. Patinec, S. Develay, M. Le Baccon and H. Handel, *New J. Chem.*, 2006, **30**, 435.
- 109 E. De Clercq, *Proc. Natl. Acad. Sci. U. S. A.*, 1992, **89**, 5286.
- 110 G. J. Bridger and R. T. Skerlj, *Adv. Antiviral Drug Des.*, 1999, **3**, 161.
- 111 R. M. Izatt, K. Pawlak, J. S. Bradshaw and R. L. Bruening, *Chem. Rev.*, 1991, **91**, 1721.
- 112 K. R. Adam, M. Antolovich, I. M. Atkinson, A. J. Leong, L. F. Lindoy, B. J. McCool, R. L. Davis, C. H. L. Kennard and P. A. Tasker, *J. Chem. Soc., Chem. Commun.*, 1994, 1539.

- 113 J. A. Este, C. Cabrera, E. De Clercq, S. Struyf, J. Van Damme, G. Bridger, R. T. Skerlj, M. J. Abrams, G. Henson, A. Gutierrez, B. Clotet and D. Schols, *Mol. Pharmacol.*, 1999, **55**, 67.
- 114 L. O. Gerlach, J. S. Jakobsen, K. P. Jensen, M. R. Rosenkilde, R. T. Skerlj, U. Ryde, G. J. Bridger and T. W. Schwartz, *Biochemistry*, 2003, **42**, 710.
- 115 T. A. Tyson, K. O. Hodgson, B. Hedman and G. R. Clark, *Acta Crystallogr.*, 1990, **C46**, 1638.
- 116 T. M. Hunter, I. W. McNae, X. Y. Liang, J. Bella, S. Parsons, M. D. Walkinshaw and P. J. Sadler, *Proc. Natl. Acad. Sci. U. S. A.*, 2005, **102**, 2288.
- 117 T. M. Hunter, I. W. McNae, D. P. Simpson, A. M. Smith, S. Moggach, F. White, M. D. Walkinshaw, S. Parsons and P. J. Sadler, *Chem. Eur. J.*, 2007, **13**, 40.
- 118 M. C. P. Smith, K. E. Luker, J. R. Garbow, J. L. Prior, E. Jackson, D. Piwnica-Worms and G. D. Luker, *Cancer Res.*, 2004, **64**, 8604.
- 119 C. J. Scotton, J. L. Wilson, K. Scott, G. Stamp, G. D. Wilbanks, S. Fricker, G. Bridger and F. R. Balkwill, *Cancer Res.*, 2002, **62**, 5930.
- 120 F. Marchesi, P. Monti, L. B.E., A. Zerbi, A. Vecchi, L. Piemonti, A. Mantovani and P. Allavena, *Cancer Res.*, 2004, **64**, 8420.
- 121 H. E. Broxmeyer, C. M. Orschell, D. W. Clapp, G. Hangoc, S. Cooper, P. A. Plett, W. C. Liles, X. X. Li, B. Graham-Evans, T. B. Campbell, G. Calandra, G. Bridger, D. C. Dale and E. F. Srouf, *J. Exp. Med.*, 2005, **201**, 1307.
- 122 N. Flomenberg, S. M. Devine, J. F. DiPersio, J. L. Liesveld, J. M. McCarty, S. D. Rowley, D. H. Vesole, K. Badel and G. Calandra, *Blood*, 2005, **106**, 1867.
- 123 E. De Clercq, *Mol. Pharmacol.*, 2000, **57**, 833.
- 124 J. A. Este, K. De Vreese, G. J. Bridger and E. De Clercq, *Antiviral Res.*, 1996, **29**, 209.
- 125 J. A. Este, K. De Vreese, M. Witvrouw, J. C. Schmit, A. M. Vandamme, J. Anne, J. Desmyter, G. W. Henson, G. Bridger and E. De Clercq, *Antiviral Res.*, 1996, **29**, 297.
- 126 D. Schols and E. De Clercq, *J. Gen. Virol.*, 1998, **79**, 2203.
- 127 E. De Clercq, *Med. Res. Rev.*, 2000, **20**, 323.
- 128 E. De Clercq, *Rev. Med. Virol.*, 2000, **10**, 255.
- 129 D. Schols, S. Struyf, J. Van Damme, J. A. Este, G. Henson and E. De Clercq, *J. Exp. Med.*, 1997, **186**, 1383.

- 130 G. A. Donzella, D. Schols, S. W. Lin, J. A. Este, K. A. Nagashima, P. J. Maddon, G. P. Allaway, T. P. Sakmar, G. Henson, E. De Clercq and J. P. Moore, *Nat. Med.*, 1998, **4**, 72.
- 131 B. Schramm, M. L. Penn, R. F. Speck, S. Y. Chan, E. De Clercq, D. Schols, R. I. Connor and M. A. Goldsmith, *J. Virol.*, 2000, **74**, 184.
- 132 S. Glushakova, Y. J. Yi, J. C. Grivel, A. Singh, D. Schols, E. De Clercq, R. G. Collman and L. Margolis, *J. Clin. Invest.*, 1999, **104**, R7.
- 133 H. F. Egberink, E. De Clercq, A. L. W. Van Vliet, J. Balzarini, G. J. Bridger, G. Henson, M. C. Horzinek and D. Schols, *J. Virol.*, 1999, **73**, 6346.
- 134 J. Blanco, J. Barretina, G. Henson, G. Bridger, E. De Clercq, B. Clotet and J. A. Este, *Antimicrob. Agents Chemother.*, 2000, **44**, 51.
- 135 C. W. Hendrix, C. W. Flexner, R. T. MacFarland, C. M. Giandomenico, E. J. Fuchs, E. Redpath, G. J. Bridger and G. W. Henson, *Antimicrob. Agents Chemother.*, 2000, **44**, 1667.
- 136 C. W. Hendrix, A. C. Collier, M. M. Lederman, D. Schols, R. B. Pollard, S. Brown, J. B. Jackson, R. W. Coombs, M. J. Gleshy, C. W. Flexner, G. J. Bridger, K. Badel, R. T. MacFarland, G. W. Henson and G. Calandra, *J. Acquir. Immune Defic. Syndr.*, 2004, **37**, 1253.
- 137 K. Vermeire, S. Hatse, K. Princen, E. De Clercq, G. Calandra, R. Skerlj, G. Bridger and D. Schols, *Antiviral Res.*, 2004, **62**, 38.
- 138 X. Y. Liang and P. J. Sadler, *Chem. Soc. Rev.*, 2004, **33**, 246.
- 139 E. De Clercq, *Metal-Based Drugs*, 1997, **4**, 173.
- 140 E. J. Billo, *Inorg. Chem.*, 1984, **23**, 236.
- 141 L. Y. Martin, L. J. Dehayes, L. J. Zompa and D. H. Busch, *J. Am. Chem. Soc.*, 1974, **96**, 4046.
- 142 B. Bosnich, C. K. Poon and M. L. Tobe, *Inorg. Chem.*, 1965, **4**, 1102.
- 143 M. A. Donnelly and M. Zimmer, *Inorg. Chem.*, 1999, **38**, 1650.
- 144 T. M. Hunter, S. J. Paisey, H. S. Park, L. Cleghorn, A. Parkin, S. Parsons and P. J. Sadler, *J. Inorg. Biochem.*, 2004, **98**, 713.
- 145 S. J. Paisey and P. J. Sadler, *Chem. Commun.*, 2004, 306.
- 146 X. Y. Liang, J. A. Parkinson, M. Weishaupl, R. O. Gould, S. J. Paisey, H. S. Park, T. M. Hunter, C. A. Blindauer, S. Parsons and P. J. Sadler, *J. Am. Chem. Soc.*, 2002, **124**, 9105.

- 147 X. Y. Liang, M. Weishaupt, J. A. Parkinson, S. Parsons, P. A. McGregor and P. J. Sadler, *Chem. Eur. J.*, 2003, **9**, 4709.
- 148 D. H. Busch, *Chem. Rev.*, 1993, **93**, 847.
- 149 J. M. Lehn, *J. Inclusion Phenom.*, 1988, **6**, 351.
- 150 T. J. Hubin, *Coord. Chem. Rev.*, 2003, **241**, 27.
- 151 D. K. Cabbiness and D. W. Margerum, *J. Am. Chem. Soc.*, 1969, **91**, 6540.
- 152 J. M. Lehn and J. P. Sauvage, *J. Am. Chem. Soc.*, 1975, **97**, 6700.
- 153 G. Schwarzenbach, *Helv. Chim. Acta*, 1952, **35**, 2344.
- 154 D. H. Busch, *Chem. Eng. News*, 1970, **23**, 9.
- 155 D. J. Cram, M. P. de Grandpre, C. B. Knobler and K. N. Trueblood, *J. Am. Chem. Soc.*, 1984, **106**, 3286.
- 156 K. P. Balakrishnan, A. Riesen, A. D. Zuberbuhler and T. A. Kaden, *Acta Crystallogr., Sect. C: Cryst. Struct. Commun.*, 1990, **C46**, 1236.
- 157 M. Micheloni, P. Paoletti, S. Burki and T. A. Kaden, *Helv. Chim. Acta*, 1982, **65**, 587.
- 158 K. P. Wainwright, *Inorg. Chem.*, 1980, **19**, 1396.
- 159 H. Yamamoto and K. Maruoka, *J. Am. Chem. Soc.*, 1982, **103**, 4186.
- 160 R. A. Kolinski, *Pol. J. Chem.*, 1995, **69**, 1039.
- 161 R. Kowallick, M. Neuburger, M. Zehnder and T. A. Kaden, *Helv. Chim. Acta*, 1997, **80**, 948.
- 162 A. Ramasubbu and K. P. Wainwright, *J. Chem. Soc., Chem. Commun.*, 1982, 277.
- 163 R. D. Hancock, S. M. Dobson, A. Evers, P. W. Wade, M. P. Ngwenya, J. C. A. Boeyens and K. P. Wainwright, *J. Am. Chem. Soc.*, 1988, **110**, 2788.
- 164 M. Le Baccon, F. Chuburu, L. Toupet, H. Handel, M. Soibinet, I. Dechamps-Olivier, J. P. Barbieri and M. Aplincourt, *New J. Chem.*, 2001, **25**, 1168.
- 165 P. Gluzinski, J. W. Krajewski, Z. Urbanczykowska, J. Bleidelis and A. Kemme, *Acta Crystallogr., Sect. B: Struct. Sci.*, 1982, **38**, 3038.
- 166 M. Kato and T. Ito, *Inorg. Chem.*, 1985, **24**, 509.
- 167 J. D. Silversides, C. C. Allan and S. J. Archibald, *Dalton Trans.*, 2007, 971.

- 168 Y. Dong, L. F. Lindoy, P. Turner and G. Wei, *Dalton Trans.*, 2004, 1264.
- 169 S. Sun, J. Saltmarsh, S. Mallik and K. Thomasson, *Chem. Commun.*, 1998, 519.
- 170 Y. Dong and L. E. Lindoy, *Aust. J. Chem.*, 2001, **54**, 291.
- 171 I. M. Helps, D. Parker, J. R. Morphy and J. Chapman, *Tetrahedron*, 1989, **45**, 219.
- 172 Y. Dong, L. E. Lindoy and P. Turner, *Aust. J. Chem.*, 2005, **58**, 339.
- 173 G. R. Weisman, M. E. Rogers, E. H. Wong, J. P. Jasinski and E. S. Paight, *J. Am. Chem. Soc.*, 1990, **112**, 8604.
- 174 E. H. Wong, G. R. Weisman, D. C. Hill, D. P. Reed, M. E. Rogers, J. S. Condon, M. A. Fagan, J. C. Calabrese, K. C. Lam, I. A. Guzei and A. L. Rheingold, *J. Am. Chem. Soc.*, 2000, **122**, 10561.
- 175 T. J. Wadas, E. H. Wong, G. R. Weisman and C. J. Anderson, *Curr. Pharm. Design*, 2007, **13**, 3.
- 176 W. J. Niu, E. H. Wong, G. R. Weisman, K. C. Lam and A. L. Rheingold, *Inorg. Chem. Comm.*, 1999, **2**, 361.
- 177 G. R. Weisman, E. H. Wong, D. C. Hill, M. E. Rogers, D. P. Reed and J. C. Calabrese, *Chem. Commun.*, 1996, 947.
- 178 T. J. Hubin, N. W. Alcock and D. H. Busch, *Acta Crystallographica Section C-Crystal Structure Communications*, 2000, **56**, 37.
- 179 T. J. Hubin, J. M. McCormick, N. W. Alcock, H. J. Clase and D. H. Busch, *Inorg. Chem.*, 1999, **38**, 4435.
- 180 A. Bencini, A. Bianchi, C. Bazzicalupi, M. Ciampolini, V. Fusi, M. Micheloni, N. Nardi, P. Paoli and B. Valtancoli, *Supramol. Chem.*, 1994, **3**, 141.
- 181 M. Ciampolini, M. Micheloni, N. Nardi and P. Paoletti, *J. Chem. Soc., Dalton Trans.*, 1984, 1357.
- 182 T. J. Hubin, N. W. Alcock, M. D. Morton and D. H. Busch, *Inorg. Chim. Acta*, 2003, **348**, 33.
- 183 W. J. Niu, E. H. Wong, G. R. Weisman, D. C. Hill, D. J. Tranchemontagne, K. C. Lam, R. D. Sommer, L. N. Zakharov and A. L. Rheingold, *Dalton Trans.*, 2004, 3536.
- 184 R. d. L. Kronig, *Z. Phys.*, 1931, **70**, 317.
- 185 R. d. L. Kronig, *Z. Phys.*, 1932, **75**, 190.

- 186 B. M. Kincaid and P. Eisenberger, *Phys. Rev. Lett.*, 1975, **34**, 1361.
- 187 S. J. Gurman, *J. Synchrotron Rad.*, 1995, **2**, 56.
- 188 M. Soibinet, I. Dechamps-Olivier, E. Guillion, J. P. Barbier, M. Aplincourt, F. Chuburu, M. Le Baccon and H. Handel, *Eur. J. Inorg. Chem.*, 2003, 1984.
- 189 M. Soibinet, I. Dechamps-Olivier, E. Guillion, J. P. Barbier, M. Aplincourt, F. Chuburu, M. Le Baccon and H. Handel, *Polyhedron*, 2005, **24**, 143.
- 190 P. Comba, P. Jurisic, Y. D. Lampeka, A. Peters, A. I. Prikhod'ko and H. Pritzkow, *Inorg. Chim. Acta*, 2001, **324**, 99.
- 191 J. Chaboy, A. Munoz-Paez and E. Sanchez Marcos, *J. Synchrotron Rad.*, 2006, **13**, 471.
- 192 J. Chaboy, A. Munoz-Paez, F. Carrera, P. J. Merkling and E. Sanchez Marcos, *Phys. Rev. B*, 2005, **71**, 134208.
- 193 A. Khan, 'Binding Studies of Novel CXCR4 Chemokine Receptor Antagonists', MSc., University of Hull, Hull, 2006.
- 194 S. Hatse, K. Princen, K. Vermeire, L. O. Gerlach, M. M. Rosenkilde, T. W. Schwartz, G. Bridger, E. De Clercq and D. Schols, *FEBS Lett.*, 2003, **546**, 300.
- 195 R. Pauwels, J. Balzarini, M. Baba, R. Snoeck, D. Schols, P. Herdewijn, J. Desmyter and E. De Clercq, *J. Virol. Methods*, 1988, **20**, 309.
- 196 C. Pannecouque, D. Daelemans and E. De Clercq, *Nature Protocols*, 2008, **3**, 427.
- 197 T. Mosmann, *J. Immunol. Methods*, 1983, **65**, 55.
- 198 A. Wuyts, N. Van Osselaer, A. Haelens, I. Samson, P. Herdewijn, A. Ben-Baruch, J. J. Oppenheim, P. Proost and J. Van Damme, *Biochemistry*, 1997, **36**, 2716.
- 199 G. Grynkiewicz, M. Poenie and R. Y. Tsien, *J. Biol. Chem.*, 1985, **260**, 3440.
- 200 A. BreLOT, N. Heveker, M. Montes and M. Alizon, *J. Biol. Chem.*, 2000, **275**, 23736.
- 201 R. E. Mewis, T. J. Hubin and S. J. Archibald, *Unpublished Results*, 2008.
- 202 G. J. Bridger, R. T. Skerlj, S. Padmanabhan, S. A. Martellucci, G. W. Henson, S. Struyf, M. Witvrouw, D. Schols and E. De Clercq, *J. Med. Chem.*, 1999, **42**, 3971.
- 203 K. J. Heroux, K. S. Woodin, D. J. Tranchemontagne, P. C. B. Widger, E. Southwick, E. H. Wong, G. R. Weisman, S. A. Tomellini, T. J. Wadas, C. J. Anderson, S. Kassel, J. A. Golen and A. L. Rheingold, *Dalton Trans.*, 2007, 2150.

- 204 J. Plutnar, J. Havlickova, J. Kotek, P. Hermann and I. Lukes, *New J. Chem.*, 2008, **32**, 496.
- 205 E. K. Barefield, K. A. Foster, G. M. Freeman and K. D. Hodges, *Inorg. Chem.*, 1986, **25**, 4663.
- 206 L. Siegfried and T. A. Kaden, *Helv. Chim. Acta*, 2005, **88**, 380.
- 207 N. F. Curtis, *J. Chem. Soc.*, 1964, 2644.
- 208 E. De Clercq, *Mini Rev. Med. Chem.*, 2005, **5**, 805.
- 209 H. Tamamura and N. Fujii, *Expert Opin. Ther. Targets*, 2005, **9**, 1267.
- 210 C. A. Lipinski, F. Lombardo, B. W. Dominy and P. J. Feeney, *Adv. Drug Del. Rev.*, 1997, **23**, 3.
- 211 A. Dukkupati, J. Vaclavikova, D. Waghray and K. D. Garcia, *Protein Expression & Purification*, 2006, **50**, 203.
- 212 J. Leonard, B. Lygo and G. Procter, '*Advanced Practical Organic Chemistry*', Second Edition, Taylor & Francis, London, 1998.
- 213 G. M. Sheldrick, in 'Program for the Solving of Crystal Structures', 1997.
- 214 G. M. Sheldrick, in 'Program for the Refinement of Crystal Structures', 1997.
- 215 L. J. Farrugia, *J. Appl. Crystallogr.*, 1999, **32**, 837.
- 216 L. J. Farrugia, *J. Appl. Crystallogr.*, 1997, **30**, 565.
- 217 N. Binsted, in 'Program for the analysis of X-ray absorption spectra', 1988.
- 218 N. Binsted, in 'EXCURV98', 1998.
- 219 E. K. Barefield, F. Wagner, A. W. Herlinger and A. R. Dahl, *Inorg. Synth.*, 1976, **16**, 220.